Analytical Development and Biochemical Application of Mass Spectrometry in Combination with Immunoaffinity Methods for Identification and Structural Characterisation of Protein Nitration

Dissertation
zur Erlangung des akademischen Grades eines
Doktors der Naturwissenschaften
an der Universität Konstanz

vorgelegt von

Brînduşa-Alina Petre

Konstanz 2008

Dissertation der Universität Konstanz
Datum der mündlichen Prüfung: **28.05.2008**

1. Referent: Prof. Dr. Dr. h.c. M. Przybylski
2. Referent: Prof. Dr. G. Müller

"The most important function of education at any level is to develop the personality of the individual and the significance of his life to himself and to others. This is the basic architecture of a life; the rest is ornamentation and decoration of the structure."

Grayson Kirk

For my wonderful parents Virginia and Constantin Balan
and for my loving husband Roland

† The present work is also dedicated to the beloved memory of Dr. Viorel Mocanu (1969-2008), my first co-supervisor at the University of Konstanz. His guidance and friendship were invaluable and will never be forgotten.

Acknowledgments

The current work has been performed in the time frame from September 2003 to October 2007 in the Laboratory of Analytical Chemistry and Biopolymer Structure Analysis, Department of Chemistry of the University of Konstanz, under the supervision of Prof. Dr. Dr. h. c. Michael Przybylski.

Besides the very interesting research topic and discussions, crucial in shaping the scientific course of this work, I am grateful to Professor Michael Przybylski for his entire support and the possibility he gave me to attend many international conferences.

I am grateful to Prof. Dr. Gerhard Müller for writing the second evaluation of the dissertation.

I am very thankful to my former professors at the University of Iasi, but most of all to Conf. Dr. Catinca Simion who guide me to study at the Faculty of Chemistry, to Prof. Dr. Alexandru Cecal who gave me the possibility to benefit of an Erasmus-Socrates scholarship and to Prof. Dr. Gabi Drochioiu for his encouragements. They were the ones that understood the necessity of international cooperation in benefit of a productive scientific research at the University of Iasi.

I am grateful to all my collaborators especially to Prof. Dr. Volker Ulrich for providing samples of the Prostacyclin synthase for MS analysis; Prof. Dr. Gerd Döring and Martina Ulrich for providing the Eosinophil samples. Special thanks to Dr. Markus Bachschmitd, Trine Larsen and Dr. med Stefano Barelli. It was a pleasure to work with all these people and to benefit from their knowledge.

A group doesn't mean anything without its members. All members of the group are acknowledged for the nice and sociable atmosphere, but most of all I want to thank to Dr. Nikolay Youhnovski, Dr. Andreas Marquardt, Rheinhold Weber, Dr. Eugen Damoc, Dr. Marilena Manea, Irina Perdivara, Dr. Raluca Stefanescu, Madalina Maftei, and Adrian Moise, for scientific discussions and interesting advices during my work. Special thanks to Mihaela Dragusanu for the dedicated work during her Diploma thesis and for continuing the research on the NITRO-project, and to Bogdan Bernevic who showed me that the ambition is very important in being successful and for his trust in my scientific advices.

I am grateful for many scientific, and not only, discussions I have had with former colleagues Dr. Catalina Damoc, Dr. Roxana Iacob and Dr. Xiaodan Tian to whom I became very closed friends;

Acknowledgments

Special thanks are addressed to all my new friends I found in Konstanz: Teodora and Florin, Ana-Maria and Marius, Luiza and Dr. Robert Gradinaru, Bianca and Dr. Cosmin Pocanschi… in no particular order and all the members of Romanian Orthodox Church in Konstanz for their support and the wonderful time spent together.

Last but not least, my warmest thanks are dedicated to my beloved family. I could never have made it this far without the love and encouragement of my parents, my brother Codrin, Ana-Maria and my loving nephew Stefan. Special thanks to my family-in-law and now, my huge and special thanks to my loving husband. **I thank you Roland**, with my whole heart for your love, encouragement, support and help.

Le multumesc parintilor mei, fratelui meu Codrin, cumnatei mele Ana-Maria si in special nepotului meu Stefan care ma sustin in tot ceea ce fac. Le multumesc deasemenea prietenilor mei din Romania, Simona, Alina, George si Maicutelor de la Varatec care m-au ajutat de multe ori sa ma simt mai aproape de casa.

Finally, I wish to acknowledge that I was not able to complete this thesis on my own, but only with the strength of Providence in me.

The following publications have been resulting from this dissertation:

1. Schmidt P., Youhnovski N., Daiber A., **Balan (Petre) A**., Arsic M., Przybylski M. Ullrich V. (2003) "Specific nitration at tyrosine-430 revealed by high resolution mass spectrometry as basis for redox regulation of bovine prostacyclin synthase", *J. Biol. Chem*, **278**: 12813-12819

2. **Petre B.A**., Youhnovski N., Lukkari J., Weber R., Przybylski M. (2005) "Structural Characterisation of tyrosine-nitrated peptides by ultraviolet and infrared matrix-assisted laser desorption / ionization Fourier transforms ion cyclotron resonance mass spectrometry", *Eur. J. Mass Spectrom*. **11**, 513-518.

3. **Petre B.A**., Drăguşanu M., Przybylski M. (2008) "Molecular recognition specificity of anti-3-nitrotyrosine antibodies revealed by affinity- mass spectrometry and immunoanalytical methods", in: "*Applications of Mass Spectrometry in Life Sciences", Springer - ISBN 978-1-4020-8811-7*

4. Ulrich, M., **Petre B.A**., N. Youhnovski, Prömm F., Schirle M., Schumm M., Pero R.S., Doyle A., Checkel J., Kita H., Thiyagarajan N., Acharya K. R., Schmid-Grendelmeier P., Simon H-U., Lee J.J., Schwarz H., M. Przybylski, G. Döring, (2008) "Post-translational tyrosine nitration of eosinophil granule toxins mediated by eosinophil peroxidase", *J. Biol. Chem. 283 (42) 28629-28640*

5. Dragusanu M., **Petre B.A**., Przybylski M. (2008) "Epitope-motif structure of an anti-nitrotyrosyl-antibody in 3-nitrotyrosine-peptides elucidated by proteolytic excision and affinity-mass spectrometry". *J. Peptide Sci., -* in preparation

6. **Petre B.A**., Ulrich M., Döring G., Przybylski M. (2008) "A molecular and high sensitivity approach for identification of oxidative protein modifications in biological material by affinity-mass spectrometry using epitope-specific antibodies". *Nature Methods, -* in preparation

Conference's oral presentations:

Swiss Proteomics Society (SPS), Lausanne 2007 - "New mass spectrometric approach to molecular characterization of tyrosine nitration in human Eosinophil Proteins"

1st Advanced Research Workshop on Applications of Mass Spectrometry in Life Safety under NATO-auspices, Herculane, Romania *2007* - "Mass spectrometric approaches to molecular characterization of tyrosine nitration in proteins"

European Fourien Transform Mass Spectrometry (EFTMS), Moscow 2007 - "Identification and structure determination of Tyrosine-nitration in proteins using high resolution mass spectrometry"

Oxidative Post-Translational Modifications of Proteins in Cardiovascular Disease (OPTM conference), Boston 2006 - "Identification and characterisation of tyrosine nitration in human eosinophils using FTICR mass spectrometry in combination with immunoanalytical procedure"

Swiss Proteomics Society (SPS), Zürich, 2005 - "Identification and structure determination of Tyrosine nitration in proteins using high resolution mass spectrometry in combination with immunoanalytical methods."

Conference's poster presentations:

Balan (Petre) A., Youhnovski N., Schmidt, P., Ullrich, V., Przybylski, M., (2004) "Specific nitration at tyrosine–430 of bovine prostacyclin synthase revealed by high resolution mass spectrometry", DGMS, Leipzig, Germany

Alina Petre, Nikolay Youhnovski and Michael Przybylski, (2004) "Characterisation of nitrotyrosine - peptides by high resolution electrospray and MALDI mass spectrometry." Peroxynitrite and Reactive Nitrogen Species in Biology and Medicine Conference, Konstanz

Alina Petre, Reinhold Weber, Martina Ulrich, Gerd Doering and Michael Przybylski (2006), "Identification and Structure Determination of Tyrosine Nitration in Human Eosinophils using High Resolution Mass Spectrometry in Combination with Immunoanalytical Methods", American Society for Mass Spectrometry (ASMS), Seattle, USA

Alina Petre, Reinhold Weber and Michael Przybylski (2006) "Structural characterisation of Tyrosine - nitrated peptides by UV and IR MALDI-FTICR mass spectrometry" 17thInternational Mass Spectrometry Conference (IMSC), Prague, Czech Republik

Table of Contents

1 INTRODUCTION

1.1 Biochemistry of oxidative modification in proteins

During the last decades, evidence has been obtained that aging is a function of several closely interrelated parameters, such as metabolic rate, caloric intake, genetics, lifestyle and environmental factors [1]. Therefore, biochemical mechanisms of aging are fundamental to understand many disease processes. Age - related changes in protein functions can be due to both inefficient protein synthesis and an altered pattern of post-translational modifications (PTM). Approximately 200 distinct post-translational protein modifications are known [2] but we are far from a complete understanding of their specific functional and biochemical consequences and a full characterization of possible modifications in aged tissue.

The term *oxidative stress* has been used to indicate when concentrations of reactive oxygen species (ROS) and reactive nitrogen species (RNS) exceed the cellular ability to remove ROS / RNS and repair cellular damage, and ultimately results in the widespread oxidation of biomolecules [3]. This condition known as *oxidative stress* results under certain circumstances when the body's natural defenses are compromise (e.g., following exposure to sunlight in excess, smoking, or in individuals with a genetic predisposition). Consequently, overproduction of ROS and RNS can lead to premature aging and a variety of diseases including cancer, ischemic damage following stroke, arthritis, atherosclerosis, infections, inflammations, and a host of neurodegenerative disorders [4].

Structural alteration introduced into proteins by oxidation can lead to aggregation, fragmentation, denaturation and destruction of secondary and tertiary structure, thereby increasing the proteolytic susceptibility of oxidized proteins. Indeed, *free radicals* can lead to oxidation of amino acids residue side chains, cleavage of peptide bonds and formation of covalently cross-linked protein derivatives [5]. Table 1 summarizes some amino acids modified by oxidation, and their oxidized products.

Table 1: *Some oxidative modification of amino acid residues in proteins* [a]

Amino acid	Oxidized Products
Cysteine	- Oxidation of a sulphydryl group (Cys-SH) to form sulphinic (Cys-SO_2H) or sulphonic (Cys-SO_3H) derivaties
	- Formation of a disulphide bond (Cys-S-S-Cys) as intramolecular or intermolecular cross-linking.
	- Formation of a mixed disulphide (e.g. Cys-S-S-glutathione)
Methionine	- Methionine sulfoxide
Histidine	- 2-oxo-histidine
	- Formation of carbonyl derivatives by direct oxidative attack on amino-acid side chains:
Lysine	- α-aminoadipic semialdehyde from Lys,
Arginine	- Glutamic semialdehyde from Arg,
Proline	- 2-pyrrolidone from Pro,
Threonine	- 2-amino-3-Ketobutyrate from Thr
Phenylalanine	- *o*-tyrosine and *m*-tyrosine
Tryptophan	- *N*-formylkynurenine, kynurenine, 5-hydroxytryptophan
Tyrosine	- 3,4-dihydroxyphenylalanine,
	- 3-chlorotyrosine,
	- 3-nitrotyrosine,
	- dityrosine (Tyr-Tyr cross-links)

[a] *Chemical structures of modified amino acids residues are presented in Appendix 2.*

Oxidation modifications of intracellular proteins can result in functional inactivation or activation through the site-selective oxidative modification of specific amino acids [6, 7] and are not only indicators of toxic and destructive processes in living systems but can also serve to control enzyme activity [8].

Radicals (often referred to as *free radicals*) are atomic or molecular species in biological systems with unpaired electrons on an otherwise open shell configuration, usually highly reactive, but also very unstable. Free amino acids and amino acid residues in proteins are highly susceptible to oxidation by one or more reactive oxygen species (ROS) that (i) are present as pollutants in the atmosphere; (ii) are

generated as by-products of normal metabolic processes; and (iii) are formed during exposure to X-, λ-, or U.V.-irradiation. Oxidative reactions in mitochondria are a major source of biological *oxygen free radicals*. In the normal respiratory pathway oxygen is reduced to water, but in this process partially-reduced oxygen species are produced, the most important being superoxide ($O_2^{\bullet -}$), hydrogen peroxide (H_2O_2), and hydroxyl ions ($^{\bullet}OH$). These radicals are also produced by oxidative enzymes in the endoplasmic reticulum and elsewhere [9]. Usually, a distinction should be made between oxidative stress, generated by reactive oxygen species (ROS), and nitrosative stress, due to an increase in reactive nitrogen species (RNS) production. The major production of RNS such nitric oxide ($NO^{\bullet}$), nitrogen dioxide ($NO_2^{\bullet}$), peroxynitrite ($ONOO^-$) and it derivatives appears to be uncontrolled, and results from what Halliwell describes as “accidents of chemistry” [10]. Nitric oxide ($NO^{\bullet}$), a highly reactive, diffusible, and unstable radical, plays an important role in the regulation of a wide range of physiological processes, including cellular immunity, neurotransmission, and platelet aggregation. Free $NO^{\bullet}$ is a transient species with a half-life of only about five seconds which can diffuse across the cell membrane and react with a variety of targets.

Because free radicals are necessary for the life, the body has a number of mechanisms to minimize free radical induced damage and to repair damage which occurs, such as the enzymes superoxide dismutase, catalase, glutathione peroxidase and glutathione reductase. In addition, a variety of antioxidants play a key role in these defence mechanisms, by reacting with *oxygen free radicals*, nullify their effects [11]. These include α-tocopherol (vitamin E), ascorbic acid (vitamin C), retinoid (vitamin A) sulphydryl containing compound such as cysteine, glutathione, ubiquinone and polyphenols [3]. Oxidative stress denotes a shift in the prooxidant / antioxidant balance in favor of the former.

1.2 Biochemistry of protein nitration

The nitration of tyrosine residue appears to represent a prominent in vivo pathway of protein oxidative modification occurring in many different pathological conditions such as atherosclerosis [12, 13], asthma and lung diseases [14-16], neurodegenerative disease [17-19], chronic hepatitis and cirrhosis [20, 21], diabetes [22] and other disorders. Only a selective number of proteins are modified by nitration in vivo, and this selectivity may be caused by a combination of several factors such as (1), the proteins are in close proximity to the site of generation of nitrating agents; (2), the chemical selectivity of the nitrating reagent; (3), the relative abundance of the target proteins; (4), the accelerated turnover of some of the nitrated proteins; (5), the proteins contain tyrosine residues in a specific primary sequence or in a specific environment and (6), the "repair" of nitrated proteins by a putative enzyme called "denitrase" [23, 24].

The knowledge regarding nitration of proteins is to the most part derived from *in vitro* experiments with well known proteins or with free tyrosine, and the physiological relevance of these findings remains to be defined. The major in vivo mechanisms for protein nitration are summarized in Figure 1 and described in the following [25].

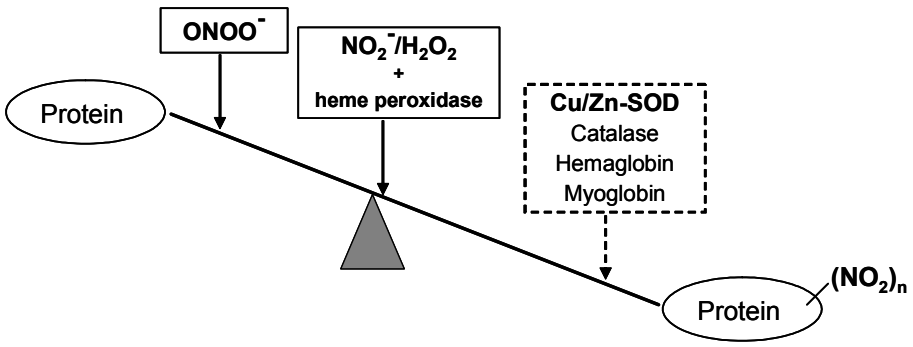

Figure 1: *Different pathways for protein tyrosine nitration. Peroxynitrite ($ONOO^-$) and heme peroxidase-dependent protein nitration are the most likely mechanisms. Other mechanisms, whose physiological relevance remains to be understood, include protein nitration catalyzed by some heme - proteins with pseudo-peroxidase activity.*

Shortly after the discovery of the free radical, nitric oxide ($^{\bullet}NO$) as a cellular messenger, its reaction with superoxide ($O_2^{\bullet-}$) to form peroxynitrite was proposed in order to explain the toxicity linked to their excess formation [26, 27]. Peroxynitrite (PN) can react with a wide range of different biological molecules including lipids [28], DNA [29-31], proteins [32-34] and lead to changes in structure and function. The level of $ONOO^-$ was found to be increased in several disorders such: acute lung injury [35], cystic fibrosis [36], asthma [37], neurodegenerative disease [38, 39], atherosclerosis [40], and diabetes [41].

Figure 2A shows the typical morphology of lung tissue as a control and Figure 2B the immunohystochemisty (using a polyclonal anti 3-NT antibody) indicate the severity of lesions and the formation of 3-nitrotyrosine as a maker of peroxynitrite formation in patients suffering of sever lung infection [42].

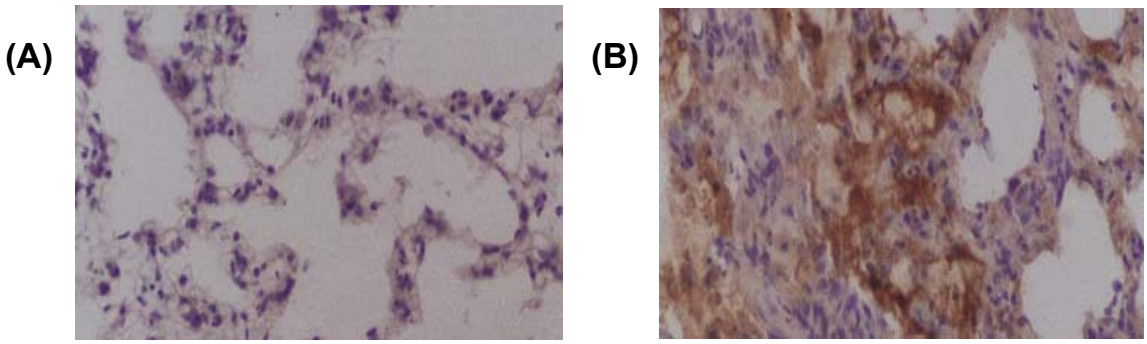

Figure 2: *Immunoreactivity to nitrotyrosine (NT) in lung tissue (A): control group; (B): peroxynitrite induced nitration and implicit damage in the lung cell. [42]*

The main proposed pathway of peroxynitrite (PN) formation is the reaction between nitric oxide and superoxide; the reaction being normally controlled by the action of two enzymes, nitric oxide synthase (NOS) and superoxide dismutase (SOD) (s. Figure 3).

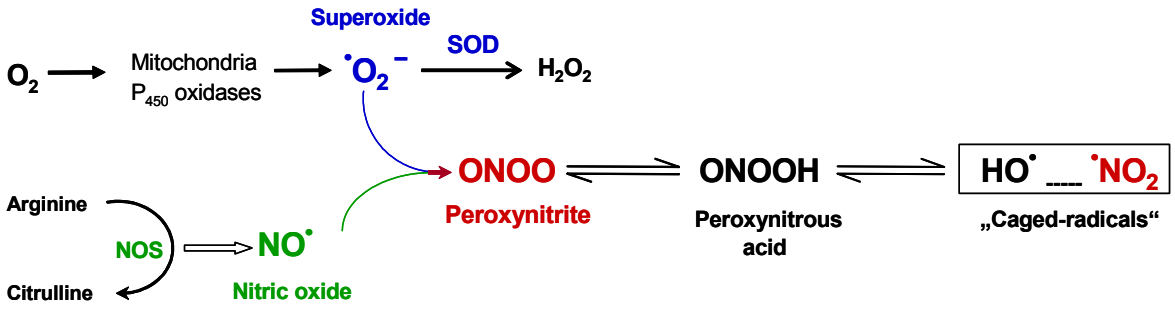

Figure 3: *Formation of peroxynitrite from nitric oxide and superoxide radicals. PN anion it self is unreactive for tyrosine, but protonation to the conjugate acid or Lewis adduct formation with carbon dioxide generates biological nitrating reagent –nitrogen dioxide radical.*

$NO^{\bullet}$ in the cell is synthesised by three isoformes of NO-synthases (NOS), which belong to the P_{450}- protein family. They use L-arginine as substrate and release $NO^{\bullet}$ and L-citruline, via formation of an intermediate, L-hydroxy arginine, according to the equation (1.1)

$$\mathbf{2}\text{L-Arginine} + \mathbf{4}O_2 + \mathbf{3}\text{NADPH} + \mathbf{3}\ H^+ \longrightarrow \mathbf{2}\text{L-Citruline} + 2\ ^{\bullet}NO + \mathbf{4}H_2O + \mathbf{3}\ NADP^+ \quad (\mathbf{1.1})$$

At pH 7, superoxide ($O_2^{\bullet -}$) is a short lived radical with a rather low reactivity. Its short life time is due to its fast self-dismutation in aqueous solutions (s. eq. 1.2). By the reaction with metals and other reactive species superoxide can generate hydroxyl radicals, which may damage nearly all existing biomolecules. *In vivo* there are two enzymatic systems which keep the $O_2^{\bullet -}$ concentration low, the Mn-SOD (only in mitochondria) and Cu, Zn-SOD (in cytosol) releasing hydrogen peroxide as a major decomposition product (s. eq.1.3).

$$\mathbf{2}O_2^{\bullet -} + \mathbf{2}H^+ \longrightarrow O_2 + H_2O_2 \qquad k = 7.3\text{x}10^5\ M^{-1}\ s^{-1} \qquad (\mathbf{1.2})$$

$$\mathbf{2}O_2^{\bullet -} + \mathbf{2}H^+ \xrightarrow{\text{SOD}} O_2 + H_2O_2 \qquad (\mathbf{1.3})$$

Disproportionation of $O_2^{\bullet -}$ occurs with $k = 10^8\ M^{-1}\ s^{-1}$ for the Mn-SOD catalyzed reaction and with $k = 2x10^9\ M^{-1}\ s^{-1}$ under catalysis of Cu, Zn-SOD. Hydrogen peroxide is scavenged in the cell to oxygen and water by catalase. As previously mentioned, PN can be formed *in vivo* by the nearly diffusion controlled reaction of $NO^{\bullet}$ and $O_2^{\bullet -}$:

$$NO^{\bullet} + O_2^{\bullet -} \longrightarrow ONOO^{-} \qquad k = 6.7x10^9\ M^{-1}\ s^{-1} \qquad (\mathbf{1.4})$$

The velocity of the nitric oxide and superoxide reaction (1.4) is a factor of 2-10 faster compared to the velocities of the reactions of Mn- and Cu, Zn-SOD with superoxide. For the suppression of PN formation *in vivo* the $NO^{\bullet}$ concentration is essential. If the nitric oxide concentration gets too high, SOD's cannot complete with it for the superoxide anion and formation of peroxynitrite will be favoured [43].

It is well accepted that peroxynitrite ($ONOO^-$) is stable only in alkaline solution. The unusual stability of $ONOO^-$ is due to its folding into the *cis*-conformation, which can not directly isomerise to the much more stable form, nitrate. After protonation, $ONOO^-$ can isomerise to a *trans*-conformation or *trans*-peroxynitrous acid (ONOOH). Figure 4 shows a compilation of the protonation, conformation equilibrium and pathways for the decomposition of PN, as well as isomerisation and *pKa*-values [44, 45]. T*rans*-peroxynitrous acid (ONOOH) is a strong oxidant and decays rapidly to hydroxyl radical and nitrogen dioxide as a pair of caged radicals [46]. These two radicals undergo electron transfer to form nitronium ion (NO_2^+) and hydroxide (HO^-) or may escape the solvent cage as free radicals. *Trans*-ONOOH is toxic by oxidative mechanisms which result in oxidation of sulphydryls, lipid peroxidation, and nitration of amino acid residues.

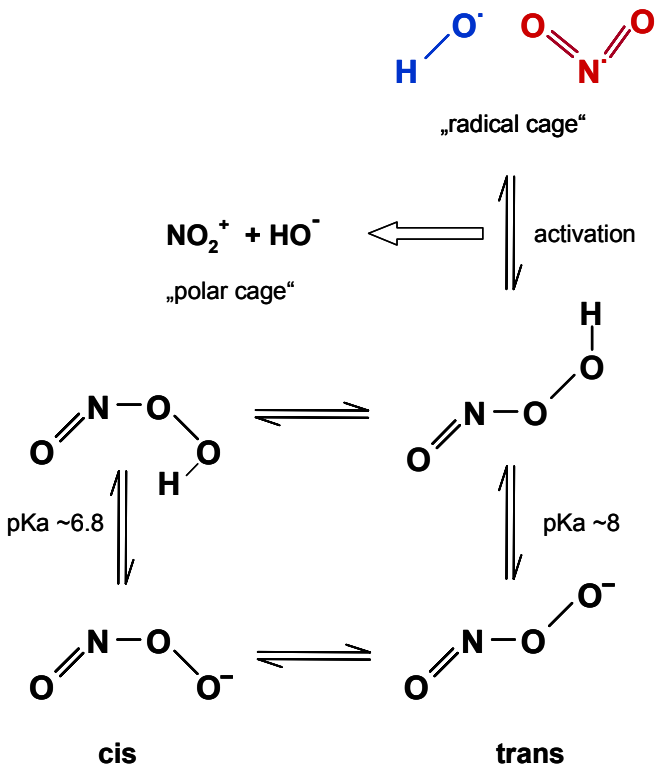

Figure 4: ***Cis-trans*** *isomerisation of peroxynitrite anion (ONOO$^-$) and decomposition of* ***trans****-peroxynitrite conjugate acid (trans-ONOOH) in to hydroxyl radical HO$^\bullet$* and nitric dioxide radical $NO_2^\bullet$ two *highly toxic radicals.*

Nitric oxide is neutral and hydrophobic, capable of traversing membranes, while superoxide is anionic at neutral pH (*pKa* = 4.8), so that PN formation occurs predominantly close to the sites of superoxide formation [47]. In turn, the half-time of peroxynitrite, of ca. 1s, seems to be sufficient to traverse membrane by passive diffusion as its conjugate acid (ONOOH, *pKa* = 6.8) or in the anionic form. Peroxynitrite is more reactive than its precursors nitric oxide and superoxide. First, PN reacts directly with certain amino acid residues such as cysteine and methionine [48]. Second, prosthetic groups, and particularly transition metal centers, are likely to react with peroxynitrite [49, 50]. Third, secondary radicals derived from PN (hydroxyl, carbonate and nitrogen dioxide radicals) can also react with protein residues such as tyrosine, phenylalanine, tryptophan and histidine [7, 51].

For in vitro studies, a solution of peroxynitrite can be prepared by treating acidified hydrogen peroxide with a solution of sodium nitrite, followed by addition of sodium hydroxide. Its concentration is indicated by absorbance at 320 nm (pH 12, λ_{302} = 1670 M^{-1} cm^{-1}) [52]. Preformed PN may be directly used as a nitrating agent for peptides or proteins in 50 mM phosphate solution or even for enzymes in presence of chelating agents (Diethylene-triaminepentaacetic acid, DTPA or Ethylene-dinitrilo-tetraacetic acid, EDTA) that sequesters metal ions so they cannot combine with other compounds. Appreciable amounts of 3-nitro-tyrosine may be produced by peroxynitrite formed *in situ* by a continuous generation of $NO^{\bullet}$ and $O_2^{\bullet\,-}$ using different donors systems such as: PAPA NONOate[1] and xanthine oxidase with pterin as a substrate [53] or directly using SIN-1 (3-morpholinosydnonimine, which is a co-donor of $^{\bullet}NO$ and $O_2^{\bullet-}$) [54].

Another possible mechanism for tyrosine nitration is the oxidation of NO_2^- by peroxidases (horseradish peroxidase, myeloperoxidase or eosinophil peroxidase) in the presence of hydrogen peroxide, leading to $^{\bullet}NO_2$ as a nitrating species. This pathway needs higher concentrations of NO_2^- and H_2O_2 that can be achieved under inflammatory conditions.

Tyrosine nitration is a covalent protein modification resulting from the addition of a nitro- (NO_2) group onto one of the two equivalent carbons CE_1 and CE_2 in the *ortho* position relative to the hydroxyl group of tyrosine residue and is believed to depend on the simultaneous availability of tyrosyl ($Tyr^{\bullet}$) and nitrogen dioxide ($^{\bullet}NO_2$) radicals (s. Figure 5) [55, 56]. The rate-limiting step in tyrosine nitration is its oxidation to $Tyr^{\bullet}$ (Step A in Figure 5), which may proceed more slowly than the rate at which $^{\bullet}NO_2$ reacts with the $Tyr^{\bullet}$ ($k = 3\times10^9\ M^{-1}s^{-1}$, Step B in Figure 5) [57].

[1] Propylamine propylamine NONOate: 1-substituted diazen-1-ium-1,2-diolates; dissociates in a pH-dependent manner to a free amine and nitric oxide.

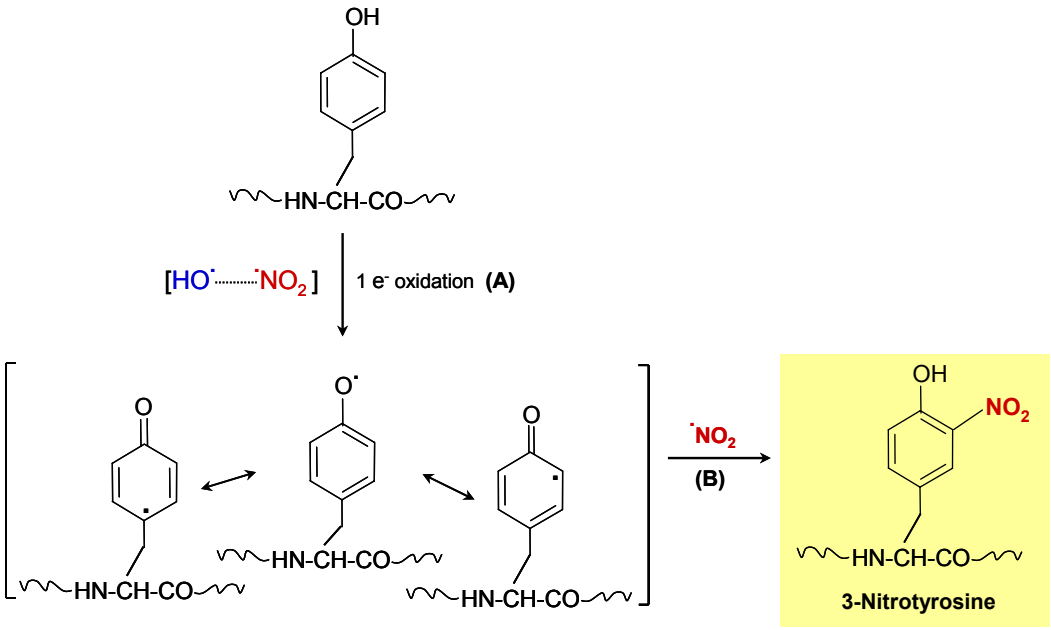

Figure 5: *Proposed reaction mechanism of 3-nitrotyrosine formation by radicals derived from peroxynitrite. The reaction is initiated by one-electron oxidation of tyrosine to the tyrosyl radical which reacts with nitrogen dioxide radical forming a 3-nitro-tyrosine residue.*

A selective targeting of peroxynitite to specific tyrosine residues (site-specific nitration) has been suggested for some proteins, including glutamine synthetase [58], prostacyclin synthase [59], Mn-superoxide dismutase [60], lysozyme, ribonuclease A [61] and tyrosine hydroxylase [62]. One important factor governing nitration seems to be the localization of tyrosine in hydrophobic domains, since the level of nitration of a hydrophobic tyrosine probe located in a lipid bilayer has been reported to be higher than that measured for tyrosine in an aqueous solution [63]. Furthermore, the pH in the external bulk and inside the protein showed to be crucial for nitration, since the oxidative chemistry of peroxynitrite and the nature of radicals formed from its decay are strictly linked to pH [46]. Moreover, the presence of neighbouring negative charges to the tyrosine residue [64], the location of the tyrosine residue in a loop structure and absence of proximal cysteine or methionine residues [61] may increase the yield of nitration. Thus, the specificity of peroxynitrite-dependent tyrosine nitration seems to depend on the secondary and tertiary structure of proteins and the local environment of tyrosine residues.

1.3 Analytical methods for identification and structural characterization of protein nitration

To identify nitrated proteins in environmental and biomedical samples and to assess their relevance for health effects, efficient and sensitive analytical methods are required. The detection, identification and quantification of 3-nitrotyrosine have employed a variety of methods including high-performance liquid chromatography (HPLC) in combination with a variety of detection systems such as UV/VIS [65], fluorescence detection after precolumn derivatisation [66], gas chromatography-mass spectrometry (GC-MS) [67, 68], Liquid chromatography-mass spectrometry (LC-MS) [69-71], proteomics approaches [72-75] and various immunochemical techniques [76-79]. For convenience some of the available methods may be ranked in an approximately increasing order of chemical specificity, from immunochemistry through to mass spectrometry.

A large proportion of studies on 3-nitrotyrosine modifications in tissues and biological fluids has been derived from antibody – based methods, as immunohistochemistry [80], immunoprecipitation, Western blot [81-83], ELISA [76, 84] and immuno-electron microscopy [77]. A polyclonal antibody against 3-nitrotyrosine has been raised first in 1994 by immunization of rabbits using peroxynitrite-treated keyhole limpet hemocyanin, and used to demonstrate the presence of nitro-tyrosine in human atherosclerotic arteries [12]. Today several monoclonal and polyclonal antibodies are commercially available and employed in different studies. Immunohistochemical staining methods have been used to demonstrate increased levels of 3-nitrotyrosine in lung tissue from patients with cystic fibrosis [85], chronic hepatitis and cirrhosis [20, 21], Parkinson's disease [86], Alzheimer's disease [73, 87] and in atherosclerotic plaques [13]. By employing ELISA methods, increased 3-nitrotyrosine formation has been reported in diabetic plasma [22, 84] in birch pollen extract and bovine serum albumin (BSA) samples exposed to air pollutants. Immunohistochemistry and Western blot using 3-NT antibodies have been used to localize nitro-tyrosine within tissue or proteins but are less accurate than chromatographic and ELISA assays. For quantification of protein nitration by ELISA, usually standard curves were constructed by determining the binding of the anti-NT antibody to the immobilized antigen in the

presence of the nitrated BSA. It was noted that the method is only semi-quantitative since affinity of antibodies for nitro-tyrosine residues in various proteins may be different from that on nitrated BSA. A semi-quantitative ELISA can be also performed by studying the antigen-antibody binding using synthetic nitrated peptides. The previous results indicate that the immunoassays developed indeed allow the detection of low amounts of nitrated proteins in complex mixtures but a detailed characterization of the antibodies specificity used in immuno-analysis is essential. Moreover, these methods only provide overall information of nitration, while the specific identification of nitration sites can only be obtained from molecular methods such as mass spectrometry.

Nitro-tyrosine is a stable product and can be easily detected *spectrophotometrically*. Free nitro-tyrosine or nitration of tyrosine residues in purified non-heme proteins is relatively easy to detect by colorimetric techniques owing to the characteristic yellow color. Nitration of tyrosine residues in proteins induces the change of tyrosine into a negatively charged hydrophilic moiety and causes a marked shift of the local pK_a of the hydroxyl group from ca. 10 in tyrosine to 6.8 in nitro-tyrosine. This may modify the protein's conformation and structure, catalytic activity, and/or susceptibility to protease digestion [34]. Nitro-tyrosine is essentially non-fluorescent and absorbs radiation in the wavelength range where tyrosine (Tyr) and tryptophan (Trp) emit fluorescence (300-450 nm), with a Trp-to-nitroTyr Fröster's distance (i.e., the donor-acceptor distance at which the FRET (Fluorescence resonance energy transfer) efficiency is 50%) as large as 26 Å. For this reason, NT has great potential as an energy acceptor in FRET studies, and, indeed, direct chemical nitration of Tyr was used to investigate the structural and folding properties of calmoduline [88] and apomyoglobin [89]. Recently it was demonstrated using the hirudin-thrombin system, that nitro-tyrosine is a suitable spectroscopic probe for investigating ligand-protein interactions, suggesting that its incorporation into proteins may have applications in biotechnology and pharmacological screening [90]. However, little is known about the possibility of exploring the unique spectral properties of NT to study molecular recognition and protein-protein interactions.

1.3.1 Mass spectrometric methods for identification of protein nitration

Mass spectrometry is a powerful analytical tool that offers some unique benefits when applied to the analysis of 3-nitrotyrosine in proteins. The advantages of mass spectrometric analysis are high mass accuracy, high resolution, high sensitivity, short analysis time and low sample consumption. The application of mass spectrometry as an important tool in biochemical and biomedical science has rapidly increased over the last few years. In 2002, the Nobel Prize for Chemistry was awarded to John Fenn and Koichi Tanaka for the development of “gentle ionization” techniques, electrospray ionization (ESI) [91] and matrix-assisted laser desorption/ ionization (MALDI) [92, 93] mass spectrometry. Both methods facilitate the analysis of biomolecules, such as peptides, proteins and other biochemical compounds, without their destruction and thus opened a way to analyse these molecules [94].

Electrospray ionization (ESI) is a method in which the analyte is sprayed at atmospheric pressure into an interface to the vacuum of the mass spectrometric ion source [91]. The sample solution is sprayed across a high potential difference (1-4kV) from a needle tip into an orifice of the mass analyser. Heat and gas flows may assist in the desolvation of the charged droplets containing the analyte molecular-ions. Finally, ion emission (Taylor-cone-model) leads to the formation of multiply protonated or deprotonated ions (s. Figure 6) [95, 96].

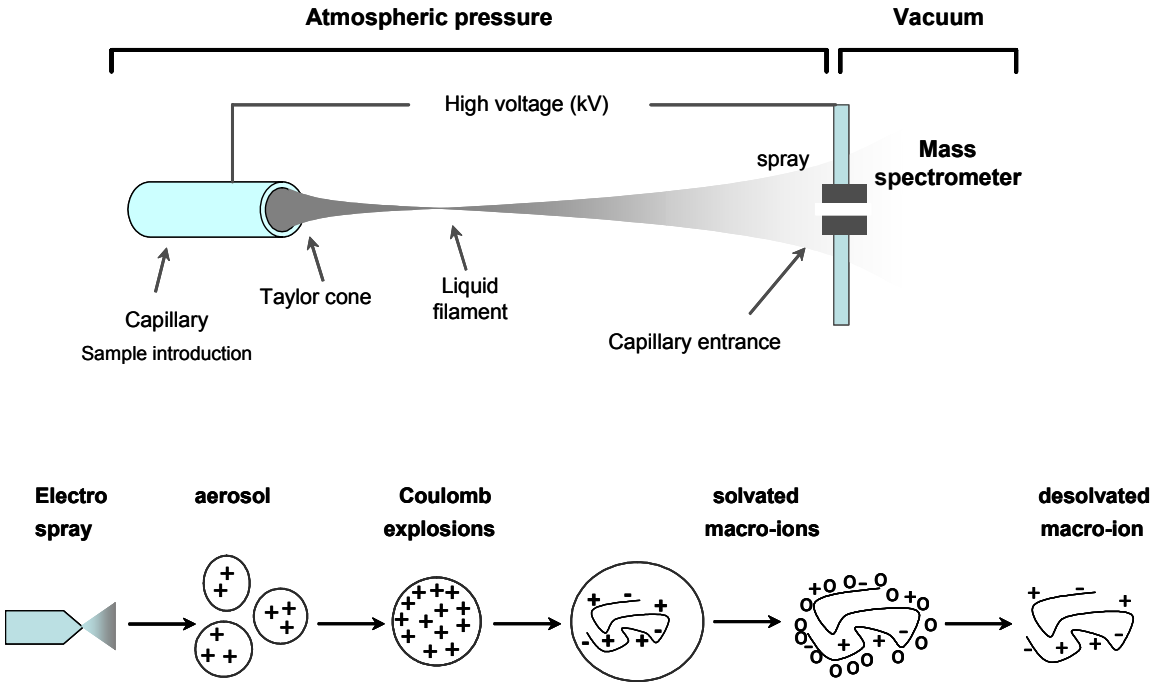

Figure 6: *Principle of ionisation source and mechanism of gaseous ion formation in ESI-MS. The sample solution is admitted through a small capillary from which the spray is formed at atmospheric pressure. The charged aerosol is evaporated due to Coulomb explosions to smaller droplets which finally results in desolvated macro-ions.*

A major advantage of ESI is that it produces multiply charged ions. Multiple charging allows ions to be analysed based on a mass-to-charge (m/z) ratio, which greatly extends the mass range of the mass analyzer. The number of charges varies, depending on several parameters, including analyte size and structure (shape), solvent, pH, and temperature. For positive ion analysis of peptides and proteins, the charges are normally associated with the most basic amino acids of the molecule and the amino terminus [97, 98]. In fact, the maximum number of charges observed can often be estimated from the primary structure.

Solution flow rates can range from microliters to several millilitres making this ionisation method suitable for interfacing to chromatographic separation methods such as capillary electrophoresis or HPLC. In the last few years several microflow devices have been developed to make possible the protein analysis, available only in very low amounts of sample [99, 100]. Especially nano-electrospray has been shown to be feasible for protein analysis and also for the characterisation of non-covalent complexes.

Nano-ESI utilizes borosilicate or fused silica glass capillaries that usually have an opening of only 1-10 µm in diameter. These emitters are usually sputter-coated with a conductive material (gold or silver) to allow the high-voltage contact to be made to the tip. In contrast to normal ESI, no pump is used in nano-ESI, and the flow rate is dictated by the potential that is applied to the emitter. Nano-ESI can easily handle submicroliter volumes of samples at flow rates of about 20-50 nl/min. The low flow rates enable enhanced experimental variation which is especially useful for MS / MS experiments and reaction monitoring [101, 102]. For ESI, analysis can be performed on various types of analysers, including (but not limited) quadrupole time-of-flight (QTOF), triple quadrupole, ion trap, or ion cyclotron resonance (ICR).

Matrix-Assisted- Laser-Desorption-Ionisation (MALDI) For laser desorption methods a pulsed laser is used to desorb species from the target surface The incorporation of an analyte into the crystalline structure of small UV-absorbing molecules provided a vehicle for ions to be created from polar or charged biomolecules [103]. The more recent development of MALDI relies on the absorption of laser energy by a solid, microcrystalline matrix compound such as α-cyano-4-hydroxy cinnamic acid or sinapinic acid [92]. To generate gas phase, protonated molecules, a large excess of matrix material is coprecipitated with analyte molecules by pipetting a submicroliter volume of the mixture onto a metal substrate and allowing it to dry. The resulting solid is then irradiated by nanosecond laser pulses, usually from small nitrogen lasers with a wavelength of 337 nm.
Although the details of energy conversion and sample desorption and ionization continues to be studied, a general understanding of the MALDI mechanism is explained below (s. Figure 7). When the laser strikes the matrix crystals, the energy deposition is thought to cause rapid heating of the crystals brought about by matrix molecules emitting absorbed energy in the form of heat. Photoionization of the matrix molecules is also known to occur [92]. The rapid heating causes sublimation of the matrix crystals and expansion of the matrix and analyte into the gas phase. Ions may be formed through gas-phase proton-transfer reactions in the expanding gas phase plume with photo-ionized matrix molecules.

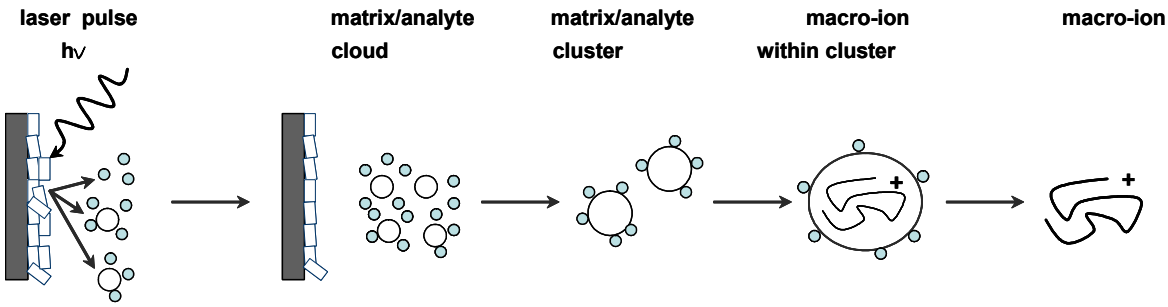

Figure 7: *Principle of ionisation/desorption in MALDI-MS. A matrix/analyte- cloud is desorbed from the microcrystalline matrix/sample preparation by a laser pulse. Proton-transfer from matrix ions is thought to be primarily responsible for the subsequent generation of analyte ions.*

Normally, low charges are generally produced, even in large biopolymers (e.g. singly and doubly protonated ions), in contrast to the multiply-charged ion structures in ESI-MS [104]. Typically, time-of-flight (TOF) analyzers are employed, but several hybrid systems (QTOF), and high resolution Fourier transform ion cyclotron resonance (FT-ICR) analyzers have been successfully adapted.

The ESI-MS analysis of 3-nitrotyrosine-containing peptides yields unambiguous results, where the introduction of the nitro group increases the molecular weight of the original peptide by +45 atomic mass units (amu). Quantitative analysis of 3-nitrotyrosine-containing peptides can be achieved by ESI-MS analysis using the native reference peptide (NRP) method, i.e., relative to the abundance of unmodified peptides of a given protein of interest [105].

In contrast, under standard UV-MALDI –TOF or FTICR mass spectrometer, using a nitrogen laser (337 nm), a set a photochemical decomposition has been observed, which provide a characteristic pattern for peptides containing 3-nitrotyrosine and therefore may provide problems for the identification of tyrosine nitration in biological materials [106, 107]. The newly introduced infrared-MALDI ionisation, have been developed in our laboratory as powerful approaches for unequivocal and sensitive identification of nitrated tyrosine containing peptides, providing more stable ions than in case of using UV-MALDI-ionisation.

In the last few years the combination of 2D-PAGE, western blotting, and mass spectrometry in a powerful proteomic approach was the more typical strategy to analyze a pattern of nitrated proteins in specific conditions. Aulak and co-workers used 2D gel electrophoresis for the resolution and Western blot detection of 3NT-containing proteins, which were subsequently identified in Database by MALDI-TOF MS [72, 108], but no specific 3-nitrotyrosine residues within these proteins have been reported. A similar methodology was applied by Kanski *et al.* to analyze the age-dependent accumulation of 3-nitrotyrosine in rat skeletal muscle [109] and heart [74] and by Turku *et al.* for the identification of 3-NT-containing proteins in the mitochondrial of diabetic mice [79]. Castegna *et al.* characterized by a proteomics approach the nitrated proteins in Alzheimer's disease brain and in the recent paper Sultana *et al.* investigated the tyrosine nitration associated with proteins in brain of subjects with mild cognitive impairment (MIC) as well (AD); where MCI is considered as a transition phase between control and AD. A characteristic feature of these studies is frequently, that only the protein and not the specific Tyr-nitration structure itself was identified.

Recently, new approach based on a chemical modification of the nitro-tyrosine residues that allows specific labeling of the modified proteins with purification tags followed by selective capturing and enrichment of the labeled proteins, were employed to circumvents some of the limitations associated with the existing immunohistochemical, Western blotting, and chromatography-based methods [110, 111]. New proteomic approaches based on the enrichment strategy with improved derivatisation specificity and high efficiency capture of nitro-tyrosine peptides and the availability of new techniques to specifically map the site of nitration will surely yield useful information in studies of oxidative protein modifications in the near future.

1.4 Problems in using analytical methods for identification of protein nitration

The nitration of tyrosine residues in protein represents an important post-translational modification during development, oxidation stress, and biological aging; however it is difficult to be detected. Several years ago Halliwell suggested: "… an under-addressed problem is the reability of assays used to detect and measure 3-nitrtyrosine in tissues and body fluids: immunostaining results vary between laboratories and simple HPLC methods are susceptible to artifacts. Exposure of biological material to low pH (e.g., during acidic hydrolysis to liberate nitro-tyrosine from proteins) or to H_2O_2 might cause artifactual generation of nitro-tyrosine from NO_2^- in the samples. This may be the origin of some of the very large values from tissue nitro-tyrosine levels quoted in the literature" [112]. The ability of methods to specifically measure nitrated substrates; in complex mixture is dependent on a wide range of parameters, including the nature of the nitrating agents for *in vitro* experiments, the nature of the antibody, sample types, amount, other components present and time.

One of the major problems is the site-selectivity of tyrosine nitration in proteins. Schöneich *et al.* showed for creatine kinase, that the selectivity of *in vivo* nitration does not correspond to the product selectivity of *in vitro* studies, where exclusively Tyr^{82} was nitrated when creatine kinase was exposed to peroxynitrite (s. *Table 2*). These studies demonstrated that the *in vitro* exposure of an isolated protein to peroxynitrite may not always be a good model to mimic protein nitration *in vivo*; and is probably depending on the corresponding concentration of RNS. Albumin was modified chemically with tetranitromethane (TNM), and several 3-nitro-tyrosine residues were identified by LC MS/MS analysis of tryptic BSA peptide mixture [108]. Other unspecific tyrosine sites were reported to be nitrated, by treatment of BSA with peroxynitrite [106, 107]. Clearly the nitrating agent and reaction conditions can influence the structure and the extent of chemical modification; however the factors determining the selectivity of tyrosine nitration remain unclear.

The specificity and sensitivity of the different methods in the identification of nitrated proteins and/or nitrated tyrosine sites varies greatly and false positive or negative detection of nitro-tyrosine in proteins may result. Most protein nitrations have been identified by antibodies directed against 3-nitro-tyrosine, and only little information on the properties of these antibodies has been published. Franze *et al*. characterized and compared three monoclonal and three polyclonal 3-NT antibodies with respect to their cross-reactivities and affinities for free 3-nitrotyrosine, synthetic nitrated peptides and nitrated proteins. They observed that a mouse monoclonal antibodies exhibited the highest affinity for free 3-NT, while a polyclonal antibodies exhibited the highest affinities for nitrated proteins [113]. In order to characterize possible false negative or positive responses obtained by using anti 3-NT antibodies, two types of negative control experiments were reported in the literature (i) blockade of 3-NT antibody with pure nitro-tyrosine free amino acid and (ii) reduction to nitro-tyrosine to amino-tyrosine in proteins. Both of these experiments present problems that will be discussed in the next Chapter 2.1.

Both MALDI and ESI mass spectrometry allow the assignment of protein nitration and the nitrated structures in proteins. The fragmentation of nitrated peptides observed by using UV-MALDI laser radiation however, reduces the abundance of the signal for nitrated peptide, resulting in failure to observe such signals in complex peptide mixtures. Therefore, IR-MALDI-FTICR-MS was used first for the characterization of 3-nitro-tyrosine containing peptides and was found as a successfully application for proteome studies of Tyrosine nitration. By using ESI tandem MS/MS for identification of nitro-tyrosine-containing peptides, the characteristic 3-NT immonium ion at m/z 181 does appear to be generally present in the mass spectra of pure standards, but typically at a relatively low intensity, so it is an unreliable indicator of the presence of nitrated tyrosine in the complex mass chromatograms of protein digests.

To rationalize any physiological changes with such modifications, the actual protein nitrated structures must be identified by proteomics methods. While several studies have used proteomics to screen for 3-nitrotyrosine-containing proteins in vivo, most of these studies have failed to prove the nitration structure by mass spectrometry.

The failure of many 2-DE approaches to characterize such nitrated proteins is likely due to multiple causes such as (i) the low steady-state level of 3-NT on specific proteins, (ii) the low abundance of some of the 3-NT-containing proteins, (iii) the solubility, size, hydrophobicity and/or extreme pI values of proteins, which may compromise the isoelectric-focusing in the first step of the 2-DE separation, and (iv) the recovery of 3-NT-containing peptides from the gels and /or HPLC columns during subsequent liquid chromatography-MS analysis.

In conclusion, nitro-tyrosine modification presents particular challenges because of the low levels present in vivo and the potential for artifact formation, therefore require methods which provide a molecular chemical identification are required.

1.5 Scientific goals of the dissertation

The detailed characterisation of nitro-tyrosine containing proteins as well as other post-translational modified proteins is required to fully understand protein function and regulatory events in the cell and organisms. Oxidative modification of proteins may cause substantial biochemical changes as well as pathophysiological consequences, both by chemical reactions and specific enzymatic pathways; however, the identification of corresponding fine-structure modifications is often tedious and requires methods of high sensitivity and molecular specificity. Nitration of Tyrosine residues has been associated to pathophysiological effects in proteins related to neurodegeneration such as in Alzheimer's disease, Parkinson’s disease, atherosclerosis, and broncho-alveolar diseases. While immuno-analytical methods suffer from low detection specificity of antibodies, mass spectrometric methods for identification of Tyrosine nitration are hampered by low stabilities and levels of modification, and by possible changes of structure and proteolytic degradation. In the present work, new mass spectrometric methods have been developed as powerful approaches for unequivocal and sensitive identification of tyrosine-nitrations in proteins.

The major objectives of the dissertation are summarized as follows:

1. Development of a new affinity - mass spectrometric approach for specific identification of nitro- tyrosine sites in proteins.

2. Mass spectrometric applications for the identification of tyrosine nitration sites, (i) in prostacyclin synthase upon peroxynitrite treatment at bovine aortic microsomes, and (ii) of specific endogenous physiological nitration in human eosinophil proteins.

3. Structural modelling investigations of identified 3-nitro-tyrosine residues in proteins, for the elucidation of site selectivity of this modification.

4. Synthesis of nitrated tyrosine-containing targets peptides for developing different analytical strategies such as ESI and MALDI mass spectrometry, Dot blot, ELISA and immuno-affinity – MS methodologies.

5. Evaluation of molecular recognition properties and selectivity of anti 3-nitro-tyrosine antibodies with 3-nitro-tyrosine peptide substrates.

2 RESULTS and DISCUSSION

2.1 Methods for identification of protein nitration

The identification of post-translational modifications (such as nitration, phosphorylation, and carbonylation) of proteins remains one of the most challenging tasks for mass spectrometry. Because such modifications often occur at low levels their detection and structure determination present extreme difficulties. Nitro-tyrosine modification in proteins may cause substantial biochemical changes as well as pathophysiological consequences. The identification of corresponding protein tyrosine nitration sites by both (i) chemical reaction such as peroxynitrite and (ii) specific enzymatic pathways, requires methods of high sensitivity and molecular specificity.

For detection and structure identification of tyrosine nitration in proteins several methods have been employed in the present work and they are summarized in Figure 8 and described in the following paragraphs.

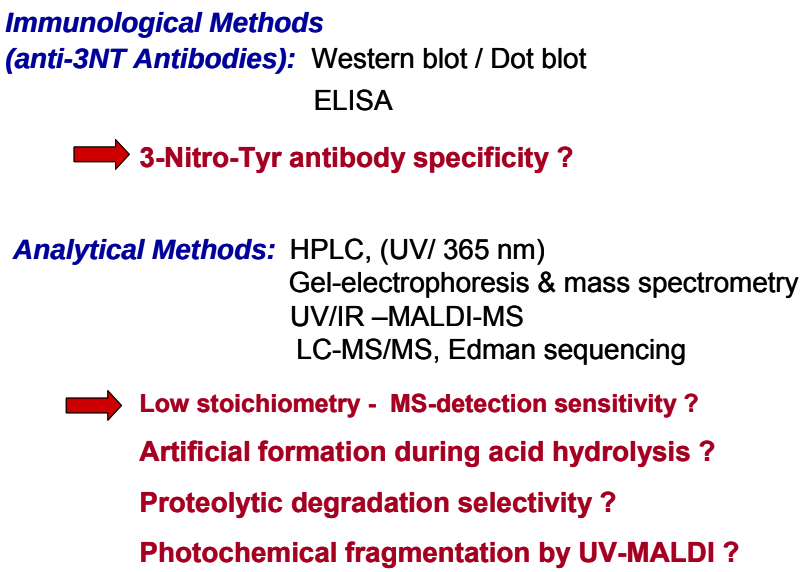

Figure 8: *Methods for detection and structure identification of tyrosine nitration in proteins and (in red) their specific problems and inconveniences*

Immunoanalytical methods such as Dot blot, Western blot and ELISA using different types of antibodies have been use in order to obtain an overall localization of nitrated tyrosine in proteins. Several considerations are important in the use and interpretation of the 3-NT antibodies.

Of primary importance, the protocol must be optimized for the particular tissue and disease state. The dilution of the antibody, the incubation time and blocking condition must be varied. A problem that can arise with immunological detection on nitro-tyrosine is the occasional occurrence of nitration in certain lots of blocking proteins. This can be a particular problem when using commercial milk powder as a blocking agent, since mastitis in milk cows can cause some batches of milk to exhibit nitration. Bovine serum albumin (BSA) which is used very often as blocking buffer may also be endogenously nitrated. Trying to develop negative controls for detection of nitrated proteins in biological samples by Western blot, it was previously shown that the nitro-tyrosine antibodies have a much greater affinity for nitro-tyrosine in peptides and proteins than for the free 3-NT amino acid, i.e., the tripeptide glycyl-*nitro*-tyrosyl-alanine (Gly-Tyr(NO_2)-Ala) has more than one hundredfold better affinity than free nitro-tyrosine [78]. Generally, lower concentration of free 3-nitrotyrosine (1-10 mM) are sufficient to fully block the immunoreactivity of 3-NT with biological samples, although blocking may not be complete for *in vitro* experiments (using high concentration of nitrating reagent) and in inflamed tissue with large amount of tyrosine nitration [114]. Second, the nitro-tyrosine can be reduced to amino-tyrosine (Tyr-NH_2) *in situ* with sodium dithionite [108] and this reaction was applied for the nitrocellulose membrane after electro-blotting. Dithionite reduction should be carried out immediately prior to subsequent analysis as amino-tyrosine will slowly auto-oxidize back to nitro-tyrosine. The reaction conditions (concentration, time) should be optimized for each experiment for a complete reduction; which is difficult to be followed without mass spectrometry analysis.

Nitro-tyrosine containing peptides were successfully detected by HPLC and LC systems due to its characteristic absorption wavelength in UV/VIS spectrum. At basic pH, the UV/VIS spectrum of free NT displays a major band at 422 nm, characteristic of the ionized form, whereas at acidic pH a prominent band appears at 365 nm, assigned to the contribution of the neutral form. The absorbance spectrum of a series of known concentrations of nitro-tyrosine at acidic and basic pH was used as

reference to determine the concentration of nitro-tyrosine in nitrated BSA, IgG and plasma proteins [115, 116]. This method is reliable for the quantification of nitro-tyrosine in proteins or peptides as well as the free amino acid. However, its use is restricted due to its poor sensitivity (~1µM), its interference from prosthetic groups, which absorb in the 350-to 450 nm region (e.g., heme, NADH, and flavins) and the need for relatively pure samples [90, 116].

2.1.1 Mass spectrometric methods for identification of protein nitration

Of the currently available methods, only mass spectrometry and Edman sequencing are able to locate specifically the 3-nitro-tyrosine sites in proteins. Almost all proteins nitration targets have been identified by antibodies directed against to nitro-tyrosine and only a few tyrosine-nitrated sites were precisely identified by mass spectrometry. Several 3-nitrotyrosine specific sites identified by mass spectrometry in both, in vivo and in vitro experiments from (a) the previous investigations are summarized in Table *2*a and (b) the results of the present Dissertation in Table 2b.

Table 2a: *Tyrosine nitration sites identified by mass spectrometry in previous studies*

Nitrated Protein	Mass spectrometric methodology	Nitration site identified	Ref.
Manganese Superoxide Dismutase (MnSOD)	**In vitro /** peroxynitrite ESI-MS / Edman sequencing of digested MnSOD	Tyr^{34}	[117]
	In vitro / peroxynitrite ESI-MS/MS analysis of digested MnSOD	$Tyr^{34}/Tyr^{45}/Tyr^{193}$	[64]
Sarco/endoplasmic Reticulum Ca-ATPase (SERCA)	**In vivo** HPLC-ESI-MS analyis of digested SERCA	Tyr^{294} /Tyr^{295}	[118]
	In vitro / peroxynitrite; LC-MS/MS of in –gel tryptic peptide mixture	Tyr^{122}	[119]
Tyrosine hydrohylase (TH)	**In vitro** / peroxynitrite MALDI-TOF and Tyrosine-scanning mutagenesis	Tyr^{423} /Tyr^{428} /Tyr^{294}	[120]
Creatin Kinase	**In vivo**	Tyr^{82}	[74]
	In vitro / peroxynitrite Proteomic analysis and HPLC-nano-ESI-MS/MS	Tyr^{14} /Tyr^{20}	

A combination of HPLC separation and ESI-MS/MS analysis of proteolytic fragments from MnSOD treated with high concentration of PN (500 μM) revealed that three residues (Tyr^{45}, Tyr^{193}, and Tyr^{34}) were nitrated [64]. In contrast, other group identified by ESI-MS and Edman sequencing at low PN concentration a nitro-tyrosine only at the MnSOD - Tyr^{33} residue. Detection of in vivo nitrated MnSOD in chronic rejection of human renal allograft is based only by Western blot and Immunohistochemistry methods [121] and no nitrated tyrosine site was specified.

By means of partial proteolytic digestion of isolated SERCA-2a from aged slow-twitch skeletal muscle, followed by HPLC-electrospray-MS analysis, Viner *et al.* have detected a single proteolytic fragment with a molecular mass of 90 Daltons higher than expected. This fragment may corresponds to mono-nitration of both Tyr^{294} and Tyr^{295} or di-nitration of either Tyr^{294} or Tyr^{295} [118]. The site selective localization of modified tyrosine residues was not definite by MS/MS, due to low nitration level in biological sample. In contrast, in vitro treatment of SERCA with peroxynitrite results in a different site for tyrosine nitration, at Tyr^{122}, identification supported by tandem MS analysis of the digested peptides fragments [119].

In a further study, tyrosine hydroxylase (TH) was treated by (500 μM) peroxynitrite and following the V8 protease[2] digestion separation, an abundant non-nitrated peptide fragment corresponding to residues V^{410}- E^{436} of TH was obtained by MALDI-TOF mass spectrometry. In addition, the same MALDI-TOF mass spectrum showed very low abundant signals due to peroxynitrite-induced mass shifts of +45, +90, and +135 Daltons; corresponding probably to three nitro-tyrosine sites contained in the TH peptide fragment [120]. Peaks corresponding to photochemical decomposition product ions 16 and 32 units lower than the peak for nitrated species hamper the exact identification of nitrated tyrosine target.

Schöneich *et al*. have used HPLC-nano-ESI-MS/MS to demonstrate for creatine kinase that the selectivity of the in vivo nitration at Tyr^{14} and Tyr^{20} did not correspond to the product of nitration at Try^{82} by treatment with peroxynitrite.

[2] Protease from Staphylococcus aureus strain V8 which cleaves peptide bonds on the carboxyl side of aspartic and glutamic acid residues.

Even when mass spectrometry has been used in all these studies, major problems exist because (i) chemical instability, (ii) resistance to proteolytic degradation, (iii) low levels of 3-nitro-tyrosine containing peptides and (iv) low chemical selectivity of reactive nitrogen species in “in vitro” studies. Clearly, methods which assure the chemical stabilities and a definite sequence determination of nitrated tyrosine peptides in proteins are necessary.

Table 3b: *Tyrosine nitration sites identified by mass spectrometry in the present work*

Nitrated Protein	Mass spectrometric methodology	Nitration site identified
Prostacyclin Synthase	**In vitro** / peroxynitrite nano-ESI-FTICR-MS of digested PGIS and Edman sequencing	Tyr^{430}
Eosinophil peroxidase	**In vivo** HPLC-ESI-MS of digested EPO	Tyr^{349}
Eosinophil cationic protein (ECP) and Eosinophil-derived neurotoxin (EDN)	**In vivo** new PROFINEX-MS approach and Edman sequencing	Tyr^{33} Tyr^{33}

High resolution Fourier-transform ion cyclotron resonance mass spectrometry (FTICR MS), using electrospray (ESI) and infrared-MALDI ionisation, has been developed in this work as powerful approaches for unequivocal and sensitive identification of specific Tyr-nitrations sites in proteins (s. Table 2b). Important features of the mass spectrometric protein analysis are the high selectivity and sensitivity, high mass accuracy, short analysis time and low sample consumption.

The major advantage in using ESI-MS is that the nitro-group is fully stable under ESI and ESI-MS^n conditions, allowing site-specific assignment of nitrated peptides in complex mixtures by a mass shift of + 45 Da from the un-modified peptide. A basic approach to looking at 3-nitro-tyrosine was to isolate the nitro-peptide, perform MS/MS, and to observe the characteristic nitro-tyrosine immonium ion formation (181 Da), which may serves as a signature for a nitro-tyrosine - containing peptide [71, 107]. By coupling capillary HPLC or LC systems to an ESI-mass spectrometer the additional advantage of cleaning up and concentrating the sample to further increase

the sensitivity was obtained. Hence, if only very low amounts of 3-nitro-tyrosine within the biological sample were available (as is often the case in proteomics studies or in identification of PTM's) direct infusion using micro-capillaries by nano – ESI or nano-LC-MS/MS were the methods of choice. The term nano-electrospray is intended to reflect the low flow (nl/min.) and the droplet size (100-200 nm) characteristic to the interface.

Using the newly introduced IR laser radiation on a MALDI – FTICR mass spectrometer the principal findings were that: (i) the resulting IR-and UV –MALDI mass spectra of a given nitrated peptide were strikingly different; (ii) nitrated peptide ions produced by IR-MALDI (with a 2.94 µm NeYAG-laser) undergo less fragmentation and the photochemical adducts produced during UV-MALDI due to nitro-group were absent in IR-MALDI. IR-MALDI will likely become a useful future method for the unambiguous identification of tyrosine nitration sites in complex peptides mixtures. In addition, localization of 3-nitro-tyrosine residues in proteins was obtained from N-terminal peptide sequencing by Edman degradation.

2.1.2 Development of a new affinity-mass spectrometry approach for identification of protein nitration

Recent studies in our laboratory have focused on the development of high selectivity and high resolution MS approaches to the identification of antigen-antibody recognition structure [122]. Affinity – mass spectrometry methods, in combination with proteolytic digestion, have been previously developed and employed (i), for the identification of antigen - epitopes (epitope – excision and – extraction-MS*)* [122, 123]; and (ii), in an affinity- proteomics approach which enables direct protein identification from biological material with unprecedented selectivity [124, 125]. Whereas initial applications of mass spectrometric epitope mapping have been performed on small sequence epitopes such as from a pure polypeptides [126, 127], several studies have shown that large, native proteins including conformational epitopes can also be successfully investigated [123, 128-130] .

The methodology for identification of specific affinity-bound peptide/protein(s) is based on the identification of epitope sequences due to the observations that (i) an

antibody will protect the binding site(s) of a bound antigen-peptide from proteolytic cleavage (epitope-excision), and (ii) an antibody will specifically bind the antigen-peptide comprised in a complex mixture (epitope-extraction).

In the present work, antibodies against 3-nitro-tyrosine has been employed in a proteolytic affinity extraction-MS approach (termed “PROFINEX”) approach for direct identification of specific nitrated sites in biological material (s. Figure 9). The principle is analogous to the epitope extraction-MS method, where the protein containing the antigen motif is digested in solution and the proteolytic peptide mixture is added to the antibody column. The immune complex is allowed to form and the peptides remaining in solution are removed and collected as non-binding fraction (*supernatant fraction*). Due to the high antibody - antigen specificity, only peptides containing the antigenic determinant (3-nitro-tyrosine) will interact with the paratope; the corresponding antibody sequence responsible for interaction with the epitope. In the second step the matrix is washed extensively in order to ensure complete removal of unbound peptides. The last volume of the washing buffer referred to as washing fraction is collected to be analyzed by MS. The peptides remaining bound to the antibody are eluted (elution fraction) under different conditions using 0.1% trifluoroacetic acid (TFA), 4M $MgCl_2$, 0.1M glycine (pH 2.3) [34, 104]. The 0.1% TFA was the solvent of choice in this work due to the compatibility with the mass spectrometric methods of peptide identification. To further use the column, the affinity matrix is regenerated by washing steps with neutral buffer (PBS).

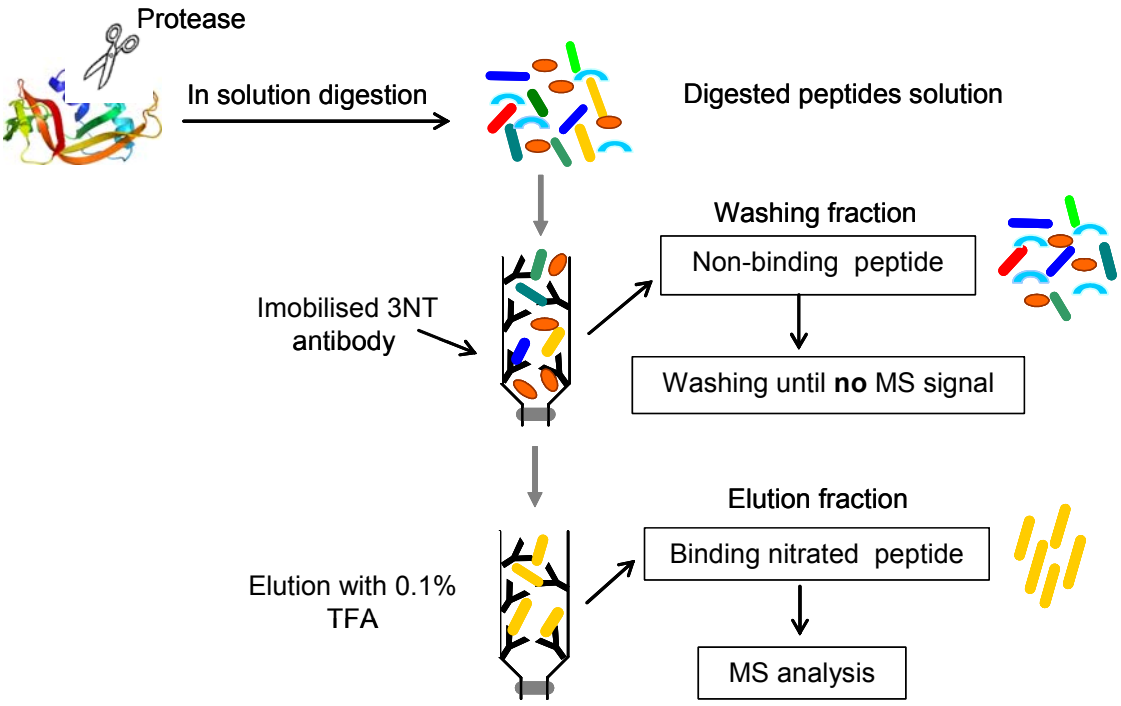

Figure 9 : *The principle of proteolytic affinity extraction - MS with immobilized antibodies. The antigen is digested in solution, and then the resulting peptide mixture is presented to the Sepharose – immobilized antibody column. Washing steps are performed to remove the non-binding peptide fragments; the remaining affinity-bound peptide(s) are eluted and analysed by mass spectrometry.*

The choice of the protease depends on the sequence of the antigen and the length of the cleavage products. By overlapping the fragments identified in the elution fraction upon treatment with various proteases, a precise identification of the epitope amino acid sequence can be achieved.

The combination of the proteolytic affinity-extraction approach with high resolution mass spectrometry was proven to be a precise method which allowed the detection and identification of low protein nitrations *in vivo*. Alternatively, the PROFINEX method may be employed by using an improved immuno-magnetic procedure for the isolation of 3-nitro-tyrosine containing peptides or proteins. The magnetic dynabeads are pre-coated with anti-3NT antibodies before adding the proteolytic peptides mixture or protein solution. A second, anti-IgG antibody is applied and the beads are separated from the immune complex using a magnetic field [131-133]. The eluted nitro-tyrosine- modified peptides are then analysed by mass spectrometry.

2.2 Application of mass spectrometry to the identification of protein nitration

In the present work, mass spectrometry was applied, for the identification of protein nitrations (i), upon peroxynitrite treatment of bovine aortic microsomes contain active prostacyclin synthase, (ii), specific endogenous nitration of human eosinophil-peroxidase (EPO) and (iii) enzymatic nitration of eosinophil cationic proteins (ECP) and eosinophil-derived neurotoxin (EDN) by eosinophil peroxidase EPO.

2.2.1 Identification of tyrosine nitration in Prostacyclin synthase

2.2.1.1 Structure and biological activity of Prostacyclin synthase

Prostacyclin (PGI_2), first discovered in 1976, is one of the major prostaglandins, which is derived from arachidonic acid by the action of the cyclooxygenase (COX) system coupled to prostacyclin synthase (s. Figure 10). Prostacyclin synthase (PCS), is a cytochrome P_{450} – type enzyme with antithrombotic, antiproliferative, and dilatory functions in the normal vasculature, which catalyzes an isomerization of prostaglandin H_2 to prostacyclin, a potent mediator of vasodilatation and anti-platelet aggregation [134].

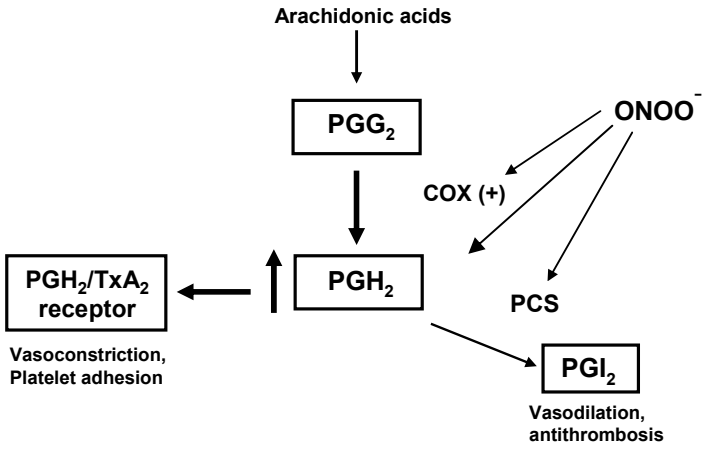

Figure 10: *Prostacyclin pathway and peroxynitrite influences. $ONOO^-$ provides peroxide tone that activates cyclooxygenase (COX), resulting in increased production of prostaglandin G_2 and prostaglandin H_2. $ONOO^-$ also nitrates and inactivates prostacyclin synthase (PCS), exacerbating the build-up of proinflammatory PGH_2.*

The vascular tone critically depends not only on the endothelial release of prostacyclin but also on the endothelial production of nitric oxide [135]. PN is formed as a product of the almost diffusion-limited reaction of NO with superoxide radical [136] and it was demonstrated that inactivation of PCS by (i) micro-molar peroxynitrite concentrations [135, 137], and by a (ii) continuous generation of NO and ($O_2^{\bullet -}$) from SIN-1[3] [54] may favor atherosclerotic processes.

The elucidation of the crystal structure of human prostacyclin synthase demonstrates that PCS exhibits the typical triangular prism-shaped P_{450} fold with only moderate structural differences and notable sequence divergence in location of several helices, *heme* environment and the meander region [138, 139]. Chiang et al. reported the crystal structure of human prostaglandin I_2 synthase at 2.15 Á resolution, which represented the first three-dimensional structure of a class III cytochrome P_{450} (s. Figure 11).

[3] 3-morpholinosydnonimine (SIN-1) generates both nitric oxide and superoxide, causing subsequent production of peroxynitrite.

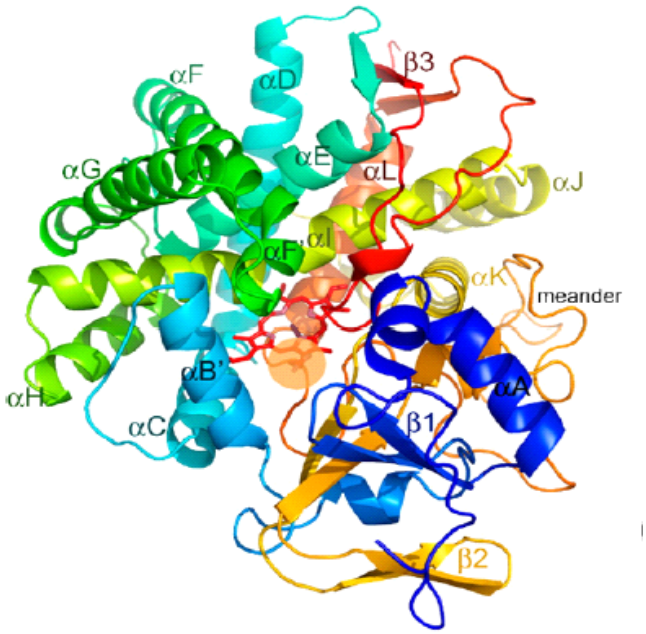

Figure 11: *Ribbon representation of human PCS viewed from substrate entrance channel (beige circle). The structure is rainbow - colored with the N terminus in blue and the C terminus in red. The heme is shown as a stick model in the center of the molecule.*

The human PCS structure reveals an unusual meander region (residues R^{393}-P^{433}) located on the proximal side of the *heme* and protrudes to the protein surface. The *heme* is embedded between I and L helices. The *heme* - thiolate nature of the PCS enzyme and the known reactivity of P_{450} proteins with organic peroxides and $OONO^-$ [140] suggested a catalytic action of the *heme* iron, which could be established by model studies with other *heme* and *heme* - thiolate proteins [59].

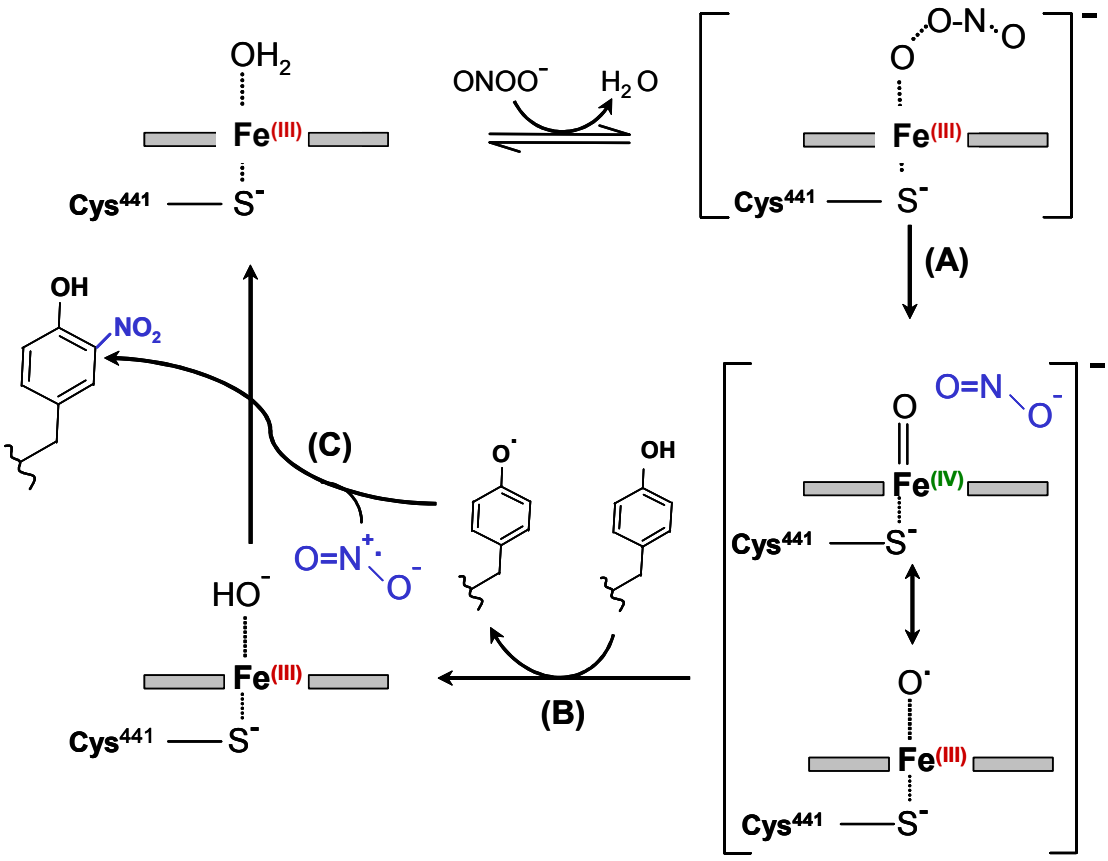

Figure 12: *Proposed mechanism of heme-thiolate catalysed tyrosine nitration by peroxynitrite in prostacyclin synthase. Reaction A: $ONOO^-$ oxidizes the Fe^{III} heme to a Fe^{IV}=O porphyrin cation radical and NO_2^- via a Fe^{III}-ONOO intermediate. Reaction B: Electron transfer from NO_2^- to the porphyrin cation radical intermediate and formation of nitrogen dioxide radical ($^{\bullet}NO_2$). Reaction C: Hydrogen atom transfer from Tyrosine residue leading to Tyr radical which will react with $^{\bullet}NO_2$ to form 3-nitrotyrosine. (Ullrich et al. 2001)*

In the proposed scheme (Figure 12), catalysis is initiated by PN reaction with Fe^{III} *heme*, resulting in the formation of a Fe^{III} – ONOO complex (pathway A) and producing the Fe^{IV} =O porphyrin cation radical intermediate and NO_2^-. Electron transfer from NO_2^- to the porphyrin cation radical intermediate may occur, resulting in nitrogen dioxide ($^{\bullet}NO_2$) formation (pathway B). Hydrogen atom abstraction from tyrosine results in a tyrosyl radical, that can couple with $^{\bullet}NO_2$ to form 3-nitro-tyrosine (pathway C).

Deeb *et al* showed that the inactivation of prostaglandin H_2 synthase-1 by peroxynitrite is due to *heme* catalyses the specific tyrosine-385 residue [141].

Prostacyclin synthase was found to be localized to the caveolae-like endothelial NO synthase [142] and hence PN formation may occur in close vicinity to PGI_2 synthase. This localisation in a “quasi-extracellular” compartment is a further important factor for efficient nitration by low concentration of PN followed by inactivation of the prostacyclin synthase. The studies performed in this thesis was initiated by the finding of Zou *et al.* [40, 143], that PN was able to inhibit PCS already at submicromolar levels, which can be generated under physiological conditions or in early stage atherosclerotic lesions; immunoprecipitation with antibodies raised against 3-nitrotyrosine yielded PCS as the main nitrated protein in blood vessels. Treatment of bovine aortic microsomes containing active prostacyclin synthase with increasing concentrations of peroxynitrite (PN) yielded specific staining of this enzyme on Western blots using antibodies against 3-nitrotyrosine (3-NT). In the following, molecular evidence for the specific nitration of bovine prostacyclin synthase was obtained by high resolution Fourier transform-ion cyclotron resonance (FT-ICR) mass spectrometry. Furthermore, it is shown an unusual slow digestion by thermolysin, presumably because of a tight fold around the heme, to release a tetra-peptide by an unexpected specific cleavage adjacent to the nitrated tyrosine residue.

2.2.1.2 Localisation of nitrated prostacyclin synthase in aortic microsome upon peroxynitrite treatment

Superoxide anions were shown to play a crucial role since they combine rapidly with NO to form peroxynitrite in a nearly diffusion-controlled reaction and therefore indirectly participate in the modulation of vascular tone [136, 144, 145]. The vascular tone critically depends on the endothelial release of nitric oxide and prostacyclin [142]. As previously reported, peroxynitrite is able to inhibit prostacyclin formation in aortic microsomes [135]. Because the postulated mechanism [59, 140] suggested that only active prostacyclin synthase can be nitrated, bovine aortic microsomes, containing active PCS were first nitrated with increasing concentrations of PN and then the enzyme was isolated by gel electrophoresis. After isolation of PCS the protein bands were transferred from the gel to a nitrocellulose membrane (s. Figure 13) which was further stained with different antibodies.

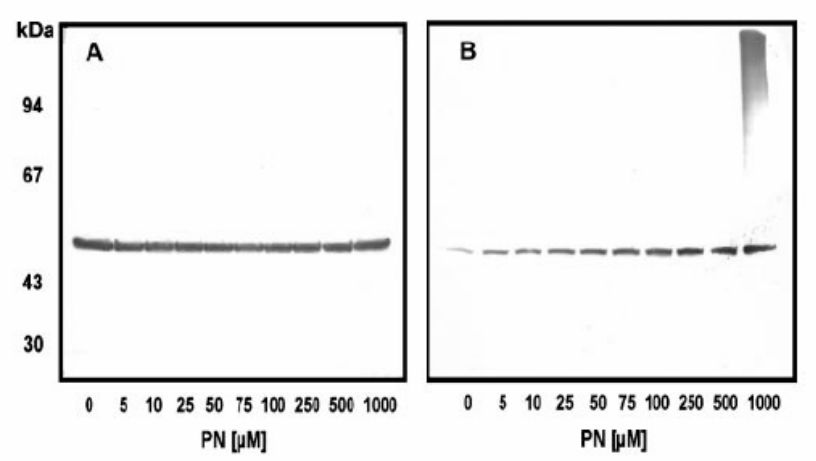

Figure 13: *Western blot of aortic microsomes treated with increasing concentrations of PN. A, immunodetection of prostacyclin synthase (52kDa band) was performed with a polyclonal antibody against PGI_2 synthase. B, immunodetection of 3-NT-positive proteins was achieved with a monoclonal antibody against 3-NT from the same blot. Each lane of the preceding 8% Tris glycine gel contained 20 µg of protein.*

Western blot analyses provided identical, specific bands at approximately 52 kDa when stained by a polyclonal antibody against PCS (s. Figure 13A), and a monoclonal antibody against 3-nitro-tyrosine (s. Figure 13B). A concentration of peroxynitrite higher than 500 µM caused unspecific additional staining of other proteins. An obvious dependence of peroxynitrite concentration on the extent of nitration was found up to 250 µM,, which was at variance with the high affinity seen with the isolated enzyme [135, 137], but may be explained by competitive targets proteins for PN in the microsomal fraction. The control also stained weakly, which probably was because of the presence of some atherosclerotic plaques in bovine arteries [40] or by low specificity of the employed 3-NT antibody. Following treatment of aortic microsomes with 25 µM PN, PCS was about half-maximally nitrated and about half-inhibited. Previous studies with other P_{450} and with model proteins [71, 134, 146] have indicated that multiple tyrosines nitration may occur at high PN concentration; therefore, a PN concentration of 25 µM was selected, and appeared to be the most suitable to yield selective tyrosine modification in PCS.

2.2.1.3 PGI_2 peptide mapping using MALDI-TOF mass spectrometry

Several aliquots of bovine aortic microsomes were treated with PN (final concentration 25 µM) and the nitrated proteins were immunoprecipitated. The precipitates were then separated by SDS-PAGE, obtaining a single band at approximately 52 kDa and the intact IgG molecule band (s. Figure 14A). The gel band at 52 kDa was excised, collected and in-gel-digested using trypsin. Due to only one cysteine (Cys^{441}) residue present in PCS sequence, no reduction and alkylation was performed. The tryptic peptides fragments were extracted and analysed by MALDI-TOF mass spectrometry (s. Figure 14B).

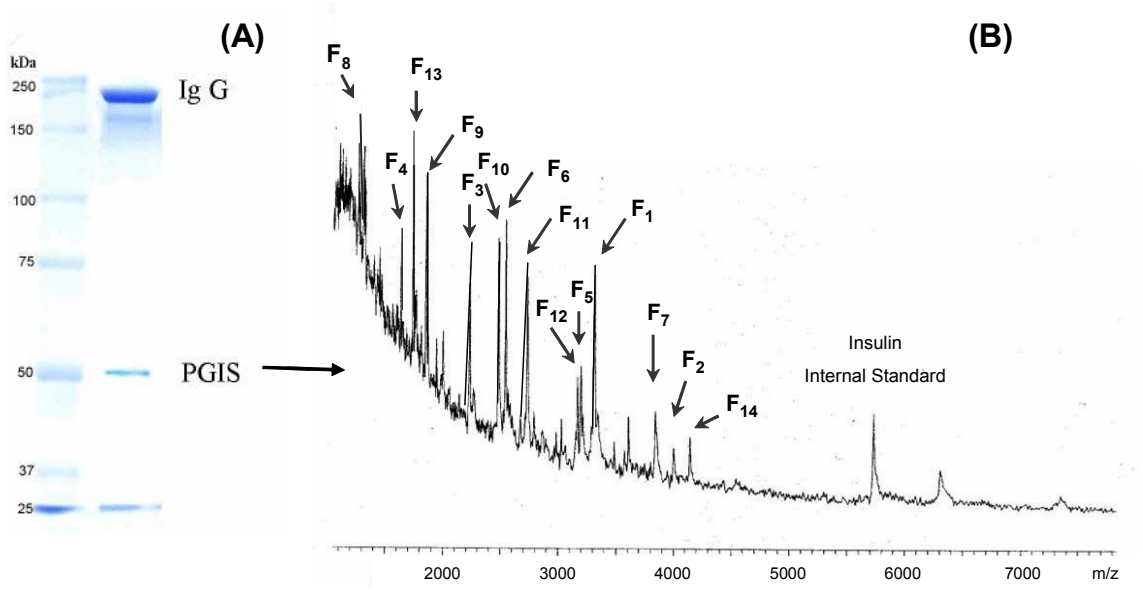

Figure 14: *(A) SDS-PAGE of nitrated microsomes after immunoprecipitation using a monoclonal anti 3-NT antibody and (B) MALDI-TOF mass spectrum of PCS peptides fragment after tryptic digestion*

All m/z values from the MALDI-TOF mass spectra were used for database search using Mascot peptide mass fingerprinting search engine and NCBInr database. The species (Mammalian) and the protease (trypsin) were selected within the entry task. 4 missed cleavages were allowed and the mass tolerance was set to 2 Da. Detailed database search results (s. Figure 15) showed the unambiguous identification of *Prostaglandin I_2 (prostacyclin) synthase [Bos taurus]* with the NCBInr entry number*: gi 27806107* and a top score at 82.

The MALDI-TOF mass spectrometer was internally calibrated using bovine insulin (internal standard) as is shown in the mass spectrum.

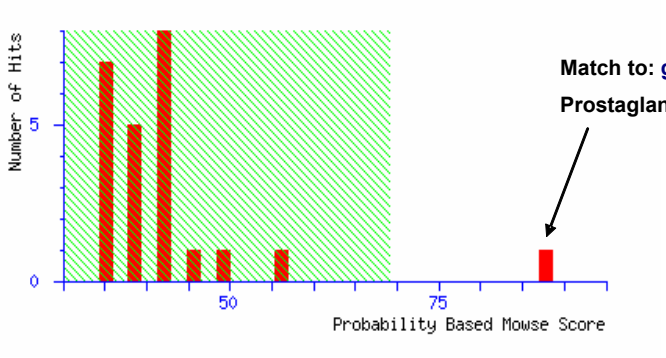

Fragment	Start - End	Observed	Mr(expt)	Mr(calc)	Delta	Miss	Sequence
f_1	26 - 56	3318.3000	3317.2921	3318.7365	-1.4445	1	R.RPGEPPLDLGSIPWLGHALEFGKDAAGFLTR.M
f_2	57 - 91	4004.4000	4003.3921	4002.5569	0.8352	3	R.MKEKHGDIFTVLVGGRHVTVLLDPHSYDAVVWEPR.S
f_3	73 - 91	2233.1000	2232.0921	2233.4807	-1.3886	0	R.HVTVLLDPHSYDAVVWEPR.S
f_4	132 - 145	1638.7000	1637.6921	1638.8399	-1.1479	0	K.ELQALTDAMYTNLR.T
f_5	146 - 174	3199.4000	3198.3921	3198.6013	-0.2093	0	R.TVLLGDTVEAGSGWHEMGLLEFSYGFLLR.A
f_6	175 - 197	2547.8000	2546.7921	2546.6595	0.1325	0	R.AGYLTQYGVEAPPHTQESQAQDR.V
f_7	175 - 208	3846.3000	3845.2921	3844.0803	1.2117	1	R.AGYLTQYGVEAPPHTQESQAQDRVHSADVFHTFR.Q
f_8	198 - 208	1315.3000	1314.2921	1315.4361	-1.1440	0	R.VHSADVFHTFR.Q
f_9	217 - 234	1858.4000	1857.3921	1857.1201	0.2720	4	K.LARGSLSAGDKDRVGKVK.G
f_{10}	311 - 333	2486.0000	2484.9921	2483.8322	1.1598	0	R.GELETVLLGAEQPISQMTTLPQK.V
f_{11}	383 - 405	2737.5000	2736.4921	2737.1479	-0.6559	1	R.LLLFPFLSPQKDPEIYTDPEVFK.Y
f_{12}	383 - 408	3171.2000	3170.1921	3170.6095	-0.4175	2	R.LLLFPFLSPQKDPEIYTDPEVFKYNR.F
f_{13}	429 - 444	1744.3000	1743.2921	1744.9268	-1.6348	0	K.NYSLPWGAGHNQCLGK.G
f_{14}	445 - 480	4146.4000	4145.3921	4143.6879	1.7041	1	K.GYAVNSIKQFVFLVLTQFDLELITPDVDIPEFDLSR.Y

No match to: 1445.5000, 2004.5000

Figure 15: *MASCOT search results showing the identification of Prostaglandin I_2 (prostacyclin) synthase by MALDI-TOF peptide mass fingerprinting using Mascot search engine. 14 tryptic peptides from a total of 16 tryptic peptide obtained in the MALDI-TOF MS were directly identified.*

From 16 total tryptic peptide ions in MALDI-TOF mass spectrum, 14 peptides (annotated as f_1-f_{14}) were directly identified with a total mass accuracy (< 2 Da) and they covered 53% of the PCS protein sequence, percent which covered and showed only 9 unmodified tyrosine residues from a total of 15 tyrosine residues in PCS sequence (s. Figure 16) Several tryptic peptides were identified as containing multiple (< 4) missed cleavages with a mass tolerance (< 1 Da), tolerance accepted in case of using low resolution and low mass accuracy time of flight (TOF) mass analyser. These partially cleaved peptides and the low sequence coverage obtained were caused by a high proteolytic stability of PCS protein, especially in a close vicinity to the catalytic centre (Figure 16).

[1]MSWAVVFGLLAALLLLLLTRRRTR**RPGEPPLDLGSIPWLGHALEFGKDAAGFLTRMKEK**
HGDIFTVLVGGRHVTVLLDPHSYDAVVWEPRSRLDFHAYAVFLMERIFDVQLPHYNPGDE
KSKMKPTLLHK**ELQALTDAMYTNLRTVLLGDTVEAGSGWHEMGLLEFSYGFLLRAGYLTQ**
YGVEAPPHTQESQAQDRVHSADVFHTFRQLDLLLPK**LARGSLSAGDKDRVGKVKGRLWK**L
LSPTRLASRAHRSRWLESLLHLEEMGVSEEMQARALVLQLWATQGNMGPAAFWLLLFLL
KNPEALAAVR**GELETVLLGAEQPISQMTTLPQK**VLDSMPVLDSVLSESLRLTAAPFITRE
VVADLALPMADGREFSLRRGDR**LLLFPFLSPQKDPEIYTDPEVFKYNR**FLNPDGSEKKDF
YKDGKRLK**NYSLPWGAGHNQCLGKGYAVNSIKQFVFLVLTQFDLELITPDVDIPEFDLSR**
YGFGLMQPEHDVPVRYRIRP[500]

Figure 16: *Identification of Prostacyclin synthase (PCS) based on the correlation of the MALDI-TOF mass spectrum and database. The obtained 53% sequence coverage is shown in red. From 15 Tyr residues in PCS sequence 6 Tyr residues (shown in blue) were not matched by the sequence coverage.*

However, no nitrated peptides or other modified peptides were detected by these mass spectrometric data; results which contradict western blot data but may be explained by an extensive photochemical fragmentation of the nitro group in the MALDI source [147], since the resulting ions may obscure the assignment of nitration sites in a complex proteolytic peptide mixtures. To achieve higher yields and a more efficient cleavage, tryptic digestion and MALDI-TOF mass spectrometry were not well suited, and a better protocol was developed.

2.2.1.4 Mass spectrometric identification of nitro-tyrosine residue in Prostacyclin synthase

High resolution mass spectrometric methods using Fourier transform- ion cyclotron resonance (FT-ICR MS) have been developed as powerful tools for the unequivocal and sensitive identification of tyrosine nitration in proteins. Previous studies with other P_{450} proteins and with model proteins [71, 134, 146] had indicated that multiple tyrosines nitration may occur; therefore, in this study a PN concentration of 25 µM was selected that appeared most suitable to yield selective modification of a single tyrosine residue. Treatment and isolation of bovine aortic microsomes (s. Experimental Part) provided ~20 µg of prostacyclin synthase isolated on SDS-PAGE from the 52-kDa band and electroeluted from the gel (Figure 17, lane D). For a better isolation and solubilization of PCS different type of protocols such as using detergent (Triton X-100) or precipitation by $CaCl_2$ were performed.

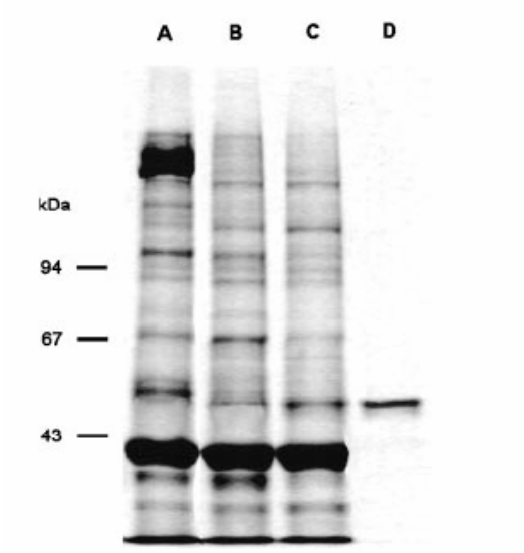

Figure 17: *Isolation and purification steps of prostacyclin synthase on a Coomassie Blue-stained 8% Tris glycine gel; (**A**) microsomal fraction from bovine aorta; (**B**) microsomes after solubilization with 1% Triton X-100; (**C**) microsomes upon precipitation with $CaCl_2$; (**D**) PGI_2 synthase fraction after electroelution. Lanes A–C contained 35 µg of total proteins; lane D, 5 µg of prostacyclin synthase.*

The 52 kDa band was excised from the gel and digested by thermolysin protease under extensive digestion conditions (24 h, 50°C). Thermolysin has low cleavage specificity; therefore, it produces a number of short fragments that are suitable for mass spectrometric and sequencing analysis. At these conditions a distinct, abundant peak was found in the PN treated protein by HPLC at specific wavelength for 3-nitro-tyrosine, λ = 365 nm with a retention time of approximately 31 min (Figure 18C). Typical peptides fractions were obtained at 220 nm, suggesting that a large portion of the protein had been digested (Figure 18B and D). A small peak was also observed in the untreated control enzyme, confirming the presence of a small basal nitration of PGI_2 synthase in bovine aortic microsome (Figure 18A).

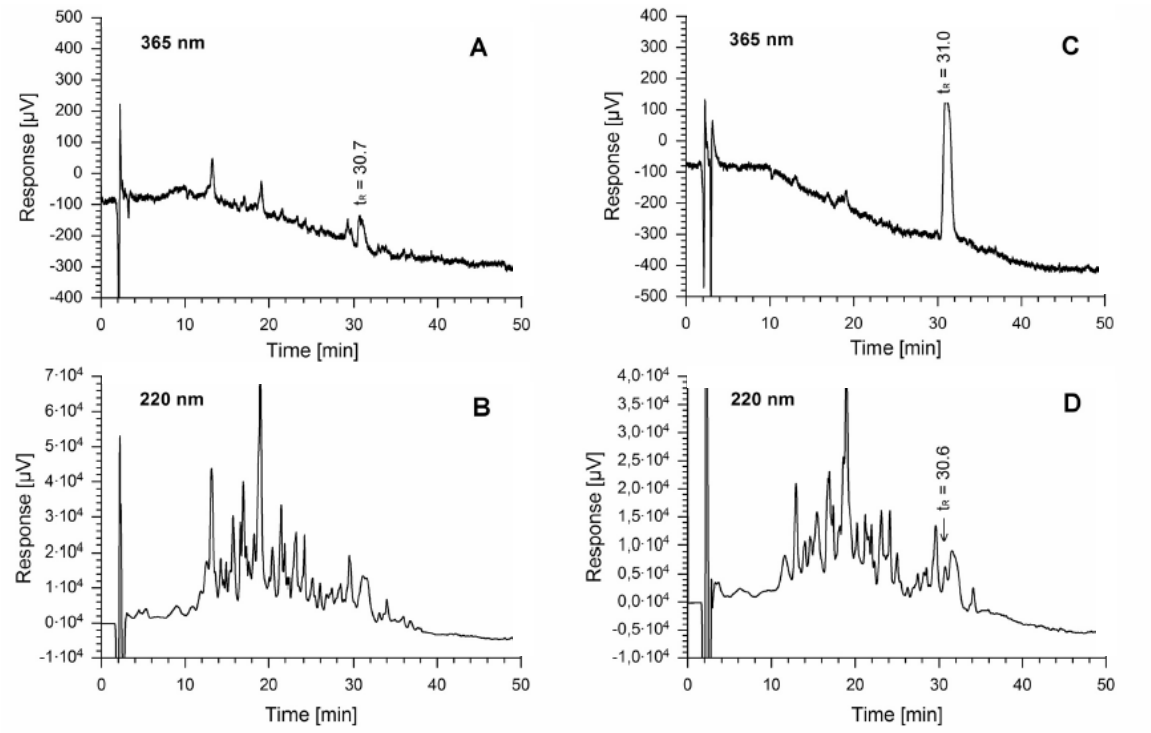

Figure 18: *HPLC detection of NT-positive peptides in thermolysin digests of PN-treated microsomes. A and B, HPLC of thermolysin digested non-nitrated PCS monitored at 365 and 220 nm; C and D, nitrated PCS (25 µM PN) monitored at 365 and 220 nm. The fraction corresponding to the peak at 31.0 min was separated and used for sequencing and mass analysis.*

The HPLC-isolated fraction with the retention time at 31.0 min. was collected and after lyophilisation was analyzed by nano-ESI-FTICR - MS (s. Figure 19A), which resulted in the unequivocal structure determination and identification of the PGI_2 nitration site. The ESI-FT-ICR mass spectrum yielded a single major protonated molecular ion at m/z 582.2907, corresponding to the monoisotopic ion of a short tetra-peptide, H_2N-**LKNY(NO_2)-**OH, (PCS-(427–430) peptide fragment); in addition a less abundant sodium adduct $[M+Na]^+$ was observed. Several less abundant ions were also found indicating some contamination of the HPLC column, but did not interfere with the precise mass determination of the nitrated tetra-peptide.

The specificity of the FT-ICR-MS analysis was ascertained by comparison with all possible thermolysin fragments and their tyrosine-containing products, none of which could account for the MS data of the nitrated peptide. Additional proof for the nitration at Tyr-430 came from Edman microsequencing, which yielded the sequence LKNY(NO_2), using 3-NT pure amino acid as a standard and the FT-ICR mass spectrum of the synthetic tetra-peptide in the carboxamide form (s. Figure 19B).

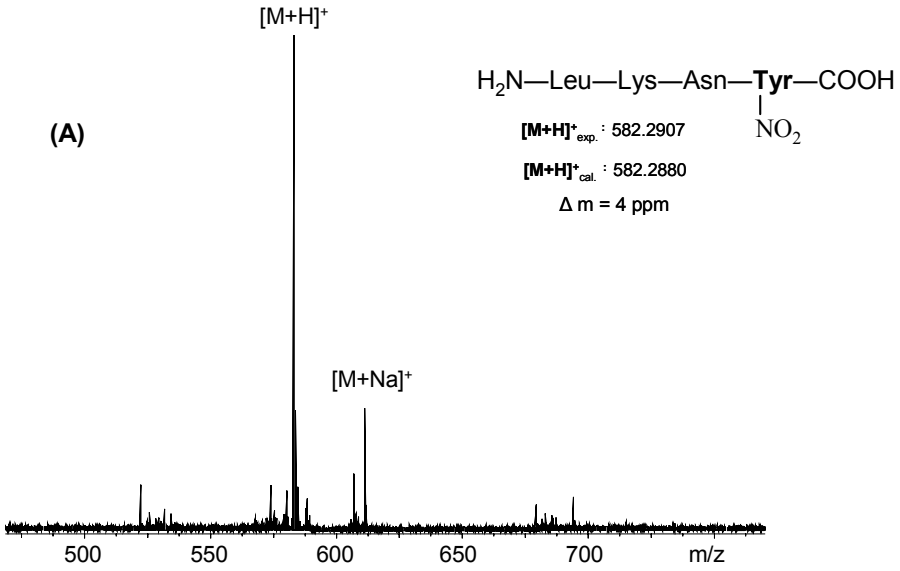

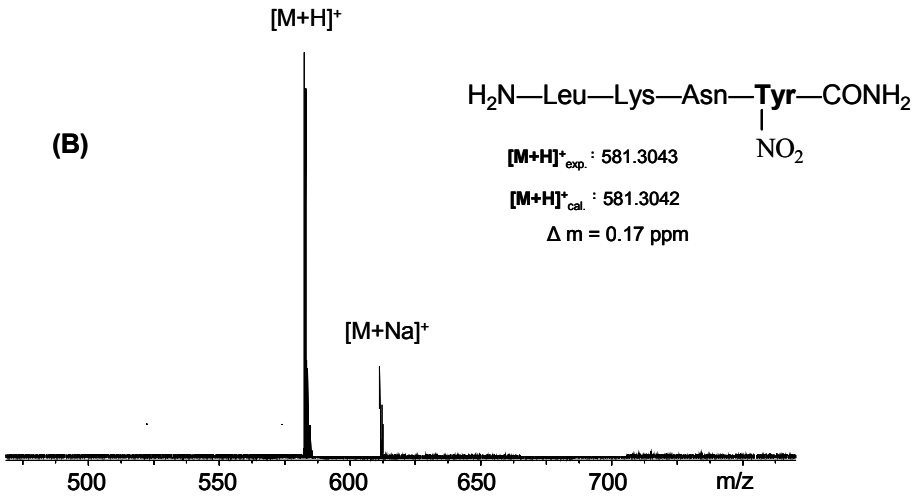

Figure 19: *A, nano-ESI-FT-ICR-MS spectrum of the isolated 365-nm absorbing peptide. The spectrum shows a major peak at 582.2907 atomic mass units. The calculated $[M+H]^+$ of the nitrated LKNY(nitro) peptide (582.2882) fits to the experimental data (Δm = 4 ppm). The peak at 604.2730 corresponds to the sodium adduct of the same nitrated peptide with quasimolecular ion $[M+Na]^+$; B, FT-ICR mass spectrum of the synthetic tetra-peptide in the carboxamide form LKNY(nitro)-CO-NH_2.*

Notable is that the thermolysin protease specificity was modified by tyrosine nitration. Thermolysin preferentially cleaves at N-terminal of bulky and aromatic residues as Ile, Leu, Val, Ala, Met, Phe, Tyr and Trp, as shown in Figure 20. Cleavage N-terminal to Leu is preferred over cleavage of N-terminal to Phe which is preferred over the others. In our case an unusual cleavage occur probably due to the presence of nitro ($^{-}NO_2$) group attached to Tyr residue, cleavage at the C-terminal part of Nitro-Tyr^{340} residue, not at the N-terminal, as expected.

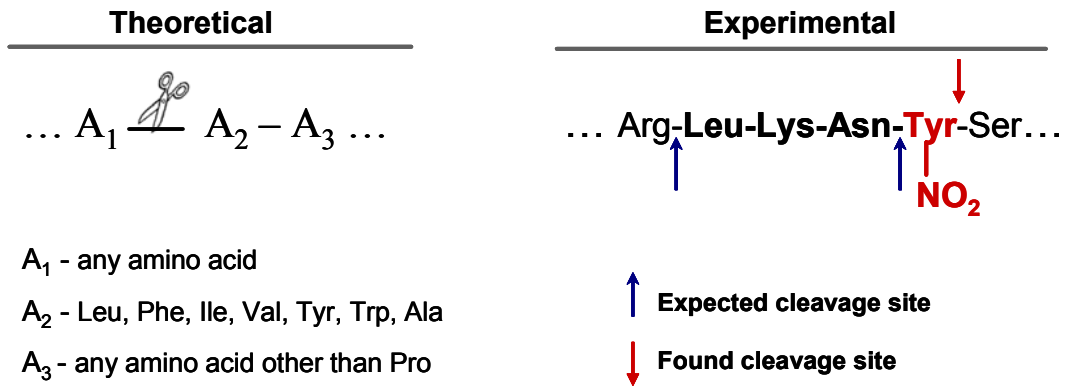

Figure 20: *Expected and observed thermolysin cleavage sites of PCS-(427–430). Arrows are indicating the expected cleavage sites (in blue) and the experimental observed thermolysin cleavage site (in red).*

In previous work with other P450 proteins a nitration with PN resulted in proteolytic peptides with a specific characteristic absorbance at 365 nm, from which the position of the 3-nitro-tyrosine could be identified [134, 146]. The isolated PCS protein was subjected to pronase digestion under conditions that should lead to quantitative release of the 3-NT residue for HPLC analysis. Prolonged digestion for 72 hrs provided the complete liberation and HPLC detection of 3-nitrotyrosine, suggesting a decreased accessibility for degradation in the microenvironment of the nitration site. The localization of nitrated PCS (427-430) tetra-peptide identified by high resolution and high mass accuracy mass spectrometry is shown in Figure 21. The primary amino acid sequence corresponds to prostacyclin synthase (PGI2S_BOVIN with Swiss-Prot primary accession number: Q29626).

[1]MSWAVVFGLLAALLLLLLTRRRTRRPGEPPLDLGSIPWLGHALEFGKDAAG
FLTRMKEKHGDIFTVLVGGRHVTVLLDPHSYDAVVWEPRSRLDFHAYAVFLM
ERIFDVQLPHYNPGDEKSKMKPTLLHKELQALTDAMYTNLRTVLLGDTVEAGS
GWHEMGLLEFSYGFLLRAGYLTQYGVEAPPHTQESQAQDRVHSADVFHTFR
QLDLLLPKLARGSLSAGDKDRVGKVKGRLWKLLSPTRLASRAHRSRWLESYL
LHLEEMGVSEEMQARALVLQLWATQGNMGPAAFWLLLFLLKNPEALAAVRG
ELETVLLGAEQPISQMTTLPQKVLDSMPVLDSVLSESLRLTAAPFITREVVADL
ALPMADGREFSLRRGDRLLLFPFLSPQ[393]KDPEIYTDPEVFKYNRFLNPDGSE
KKDFYKDGKR[427]**LKNY(NO$_2$)**[430]SLP[433]WGAGHNQ**C**[441]LGKGYAVNSIKQFVFL
VLTQFDLELITPDVDIPEFDLSRYGFGLMQPEHDVPVRYRIRP[500]

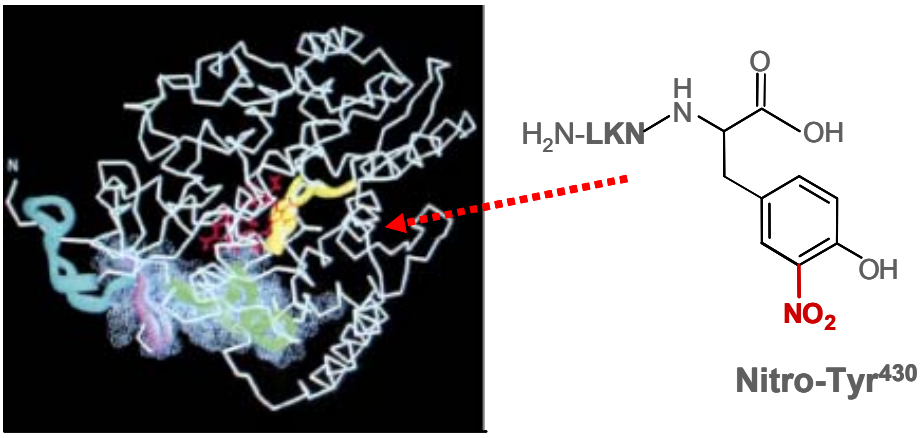

Figure 21: *Up: The amino acid sequence of bovine prostacyclin synthase: (in red) the nitrated tetra-peptide fragment identified by MS and (underline) the meander region (K^{393}-P^{433}), located on the proximal side of the heme. Down: Constructed 3-D structural model of human PCS based on the $P450_{BM-3}$ X-ray structure (according to Dent et al. Biochem. J. 2002). The red structure denotes heme and the arrow indicates the probable localization of nitrated fragment 427-430 in a tight fold around the heme binding site.*

The examination of the crystal structure of human PCS reveals an unusual meander region (residues [393]RDPEIYTDPEVFKYNRFLNPDGSEKKDFYKDGKR**LKNY**NMP[433]) located on the proximal side of the heme structure. A high sequence homology for this fragment was observed for bovine prostacyclin synthase (residue [393]KDPEIYTDPEVFKYNRFLNPDGSEKKDFYKDGKR**LKNY**SLP[433]). This coil region is markedly longer (by more than ten residues) comparable to other P_{450}'s, and the coil structure protrudes to the protein surface.

The specificity of this single post-translational modification, producing inactivation of prostacycline synthase, may be provided by the heme catalysis involved that allows the exclusive nitration of Tyr-430 residue closely located to the heme and in the same time accessible to the reactive nitrogen species. Obviously mutation of the Tyr-430 residue should give further clues to the importance of this amino acid.

2.2.2 Identification of physiological nitration in human eosinophil peroxidase

2.2.2.1 Structure and biochemical nitration of human eosinophils

Eosinophil granulocytes are white blood cells of the immune system which protects the body against disease and infection, control mechanisms associated with allergy, asthma and inflammatory disorders. The eosinophilic response in allergic and inflammatory disease is associated with protein nitration, detected as immunostaining for 3-nitrotyrosine (3NT) [148].

An increase in eosinophils number, i.e. the presence of more than 500 eosinophils/µl of blood is typically seen in people with a parasitic infestation of the intestines, a collagen vascular disease (such rheumatoid arthritis), extensive skin diseases (such as exfoliative dermatitis) and Addison's disease. *Hypereosinophilia* is a disease characterised by a marked increase in the eosinophil count in the bloodstream. Eosinophils develop and mature in the bone marrow before migrating into blood, persist in the circulation for 6-12 hours, and can survive in tissue for an additional 2-3 days in the absence of stimulation. Following activation by an immune stimulus, eosinophils degranulate to release an array of cytotoxic granule cationic proteins that are capable of inducing tissue damage and dysfunction [149].

Human eosinophil granules contain four cationic proteins including: Major basic protein (MBP), Eosinophil cationic protein (ECP), Eosinophil-derived neurotoxin (EDN) and Eosinophil peroxidase (EPO) (s. Figure 22).

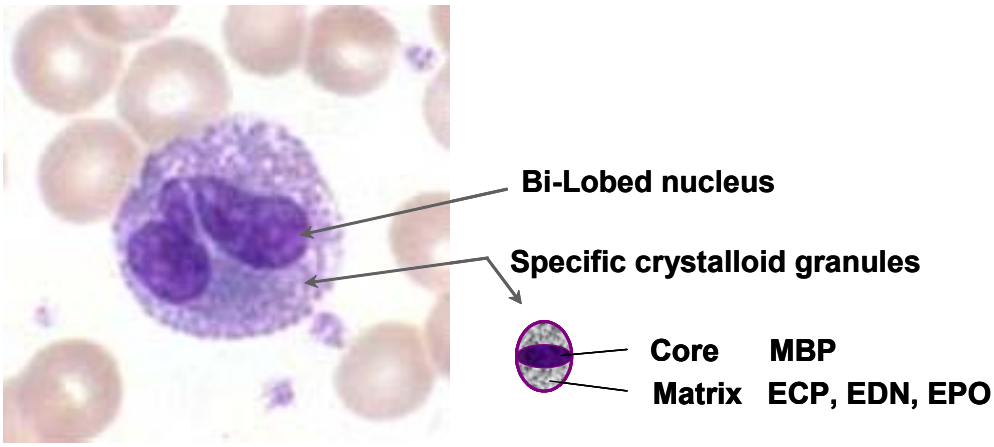

Figure 22: *Structure of the human eosinophil; the crystalloid granule core contain MBP and the matrix contain ECP, EDN and EPO*

Eosinophils are thought to mediate many of their cytotoxic and tissue-destroying effects through their exceptional ability to generate oxidizing species [150]. Indeed, the respiratory burst of eosinophils generates several times as much superoxide anion ($O_2^{\bullet -}$) and hydrogen peroxide (H_2O_2) as the corresponding number of neutrophils [151]. Human eosinophil peroxidase (EPO) an abundant *heme* protein secreted from activated eosinophils plays a central role in oxidant production by eosinophils. It is believed that EPO amplifies the oxidizing potential of H_2O_2 produced during the respiratory burst by using it as co-substrate to generate cytotoxic oxidants. Besides $ONOO^-$, it was noted that other reactions, such as nitrite-dependent *heme* peroxidase reactions also may give a rise to protein tyrosine nitration *in vivo* [152, 153]. It has been shown that *heme* peroxidase enzymes (myeloperoxidases, eosinophil peroxidases, horseradish peroxidases) in the presence of nitrite and hydrogen peroxide can nitrate different proteins in heart homogenates [154], or different pure proteins [152, 155].

Several mechanisms for the peroxidase catalyzed phenol nitration in the presence of nitrite/hydrogen peroxide have been proposed but, the nature of the nitrating species has not been clarified. The favored pathway involves one-electron oxidation of nitrite by the peroxide-generated enzyme intermediates known as a compound I and compound II [156, 157]

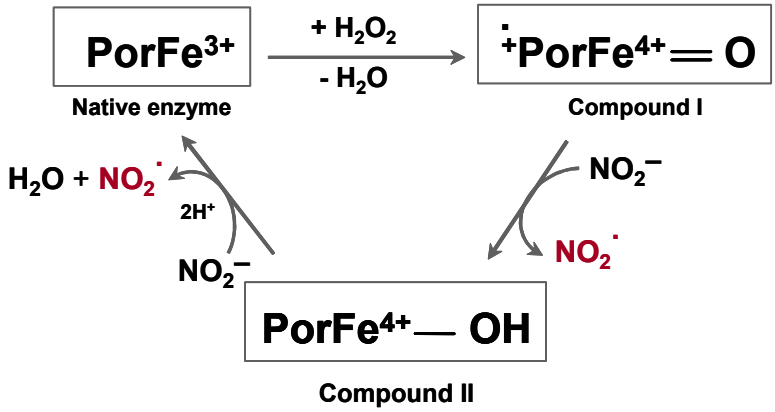

Figure 23: *Schematic representation of RNS generation by eosinophil peroxidase. The cycles utilize hydrogen peroxide to oxidize the native enzyme to compound I. Por denotes porphyrin. NO_2^- and $^{\bullet}NO_2$ represent substrates being oxidized and the formed radical product, respectively.*

Further $NO_2^{\bullet}$ could either nitrate a phenol with a reaction stoichiometry of 2:1 or directly react with a peroxidase-generated phenoxy radical according to reaction 5:

$$NO_2^{\bullet} + PhOH \longrightarrow NO_2^{-} + PhO^{\bullet} + H^+ \quad (2.1)$$

$$NO_2^{\bullet} + PhO^{\bullet} \longrightarrow \mathbf{O_2N\text{-}PhOH} \quad (2.2)$$

Tyrosine nitration under these conditions was specifically inhibited by catalase and azide (a myeloperoxidase inhibitor) but not by SOD; this suggests that the mechanism of tyrosine nitration is $ONOO^-$ - independent. Protein tyrosine nitration could be also achieved by the direct oxidation of nitrite by H_2O_2, but this reaction requires nonphysiological concentrations of hydrogen peroxide.

The contribution of EPO to 3-nitrotyroine formation in vivo may be tissue-specific, even at site of inflammation characterized by eosinophil recruitment and activation. Identifying the mechanisms and products of EPO-dependent oxidative damage is a critical step toward development of targeted interventions designed to interrupt oxidative tissue injury in eosinophilic inflammatory disorders. All three eosinophil granule proteins ECP, EDN, and EPO were isolated and purified from four patients

with hypereosinophilia; abnormal elevate number of eosinophil in blood. Preliminary studies showed only eosinophils exhibiting positive staining to 3-nitro-tyrosine by immuno- double fluorescence micrographs from the total human blood granulocyte [132].

2.2.2.2 Eosinophil peroxidase peptide mapping by mass spectrometry

Eosinophil peroxidase (EPO) (EC 1.11.1.7) is a member of the mammalian heme-containing peroxidase, which also include myeloperoxydase (MPO), lactoperoxidase (LPO), and thyroid peroxidase (TPO). The human coding sequence of EPO and MPO is about 70% homologous at the amino acid level.

Eosinophil peroxidase is a two chains structure which contains an approximately 53 kDa heavy chain and a light chain of approximately 13 kDa bound only by strong non-covalent forces. The two chain structures results from proteolytic processing of precursor molecules [158] of 715 residues in EPO [159]. Based on the N-glycosylation consensus the heavy chain contains four candidates for attachment of glycosamine-base carbohydrate.[4] One intrachain disulphide bridge is found in the light chain, whereas on the heavy chain five disulphide bounds are formed. Due to the presence of two unpaired cysteins (Cys^{291} and Cys^{455}), the heavy chain has a high tendency to aggregate [160]. The light chain contains only two tyrosine residues, whereas the heavy chain contains eleven tyrosine residues. EPO is highly cationic with a pI > 11 attributed to its high content of arginine.

Eosinophil peroxidase was isolated and purified from human eosinophil granule suspension, derived from hypereosinophilic patients with marked eosinophilia, using chromatographic methods [161, 162]. The integrity of the purified eosinophil peroxidase was assessed by separation of the components present in the sample on a 1D-gel performed under denaturing and reducing conditions.

[4] N-glycosylated motiv : Asn-X-Ser/Thr, where X is any amino acid except Pro

The SDS-PAGE gel separation of the purified EPO sample is shown in Figure 24. For gel electrophoresis approximately 10 µg of purified EPO sample were directly used in order to estimate its content (Figure 24, line A). The presence of still intact EPO band at ~ 68 kDa indicates that the strong non-covalent interactions between the two EPO subunits were not completely denaturated by the SDS reducing buffer in a very short time before the gel was run. Two bands corresponding to heavy (~ 53 kDa) and light chain (~13 kDa) could be observed. The fade band that can be distinguished below 37 kDa showed that the sample contain >95 % EPO protein.

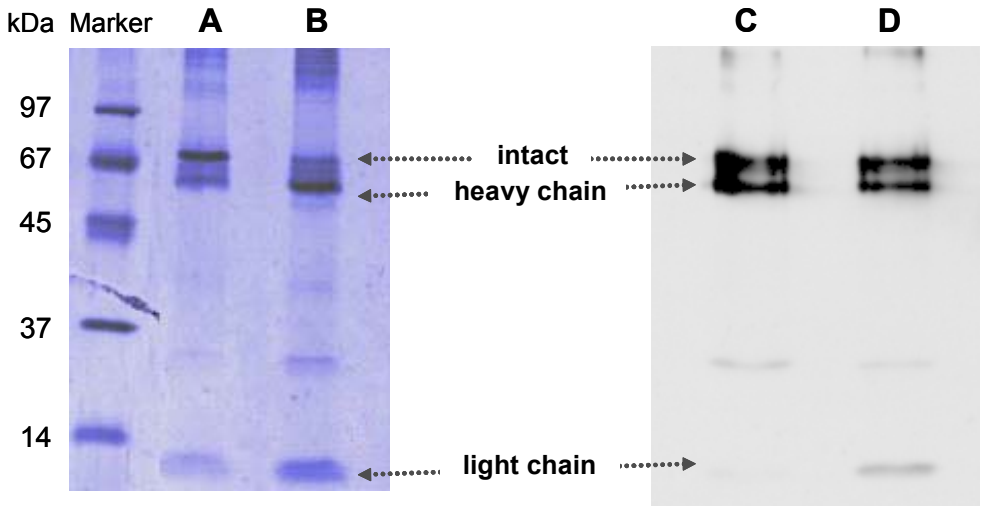

Figure 24: *SDS gel electrophoresis of EPO purified from human eosinophil granules and visualized by colloidal Coomassie (left) and Western blot using a monoclonal 3-nitro-tyrosine antibody.*

Another 10 µg of sample were first reduced with DTT and alkylated using IAA in order to disrupt the intrachain disulphide bounds between cysteine residues and the non-covalent interchain interactions (Figure 24, line B). A better separation was obtained and more intense bands corresponding to the light and heavy chain were observed. The still intact EPO band may result by new interchain disulphide bounds formation due to the unpaired cysteins (Cys^{291} and Cys^{455}) on the heavy chains.

The presence of 3-nitro-tyrosine modification in eosinophil peroxidase was elucidated by western blotting using a monoclonal anti 3NT antibody (**Ab**$_1$). Interestingly, only

the intact and heavy chain band, and not the light chain band, of purified EPO (calculated molecular weight: 12.7 Da) was 3NT-positive. The specificity of the 3NT antibody binding only to 3-nitro-tyroisne containing peptides was previously proved by dot blot analysis and will be discussed later in Chapter 2.4.

The sequence details of EPO light and heavy chain fragments resolved by 1D-gel electrophoresis were identified by mass spectrometry. Upon proteolytic digestion of the protein, peptide mass fingerprinting was used for eosinophil peroxidase identification. This “bottom-up” analysis involves determination of the masses of all peptides resulted in the digest mixture. The most commonly used enzyme for protein digestion is trypsin, which cleaves the protein at the C-terminal side of lysine and arginine (when they are not followed by a proline).

Despite of the 3NT negative response in the Western blot, the light chain was also excised in-gel digested with trypsin, and the resulting peptide fragments were extracted and analysed by MALDI-FT-ICR mass spectrometry. Proteolytic digestion in the gel matrix was carried out according to the procedure of Shevchenko *et al*. [163]. Monoisotopic masses of all singly-charged ions from the MALDI-FT-ICR mass spectra were used for database search using Mascot peptide mass fingerprinting search engine and NCBInr database. Figure 25 presents the MALDI-FT-ICR mass spectrum and the identification with a high probability based on the Top score of Eosinophil preperoxidase (AA-127 to 575) (NCBInr gi l 31183). The identified EPO sequence correspond to the EPO preperoxidase enzyme which contains in addition to light and heavy chains the Propep peptide fragment (1-127) which is removed naturally in the EPO mature form. The intact EPO mature sequence is indicated between residues 128 to 575, with the light chain fragment (128-238) and the heavy chain fragment (239-575). Since the Epo sample employed in this work was isolated from mature eosinophil all the calculation and assignment of the amino acids exclude the Propep fragment and also the signal peptide of the precursor enzyme which is given in UniProt KB (Universal Protein Knowledgebase) [164]. The first light chain amino acid (127) is becoming residue number 1 and the first residue in the heavy chain (239) becomes residue number 112.

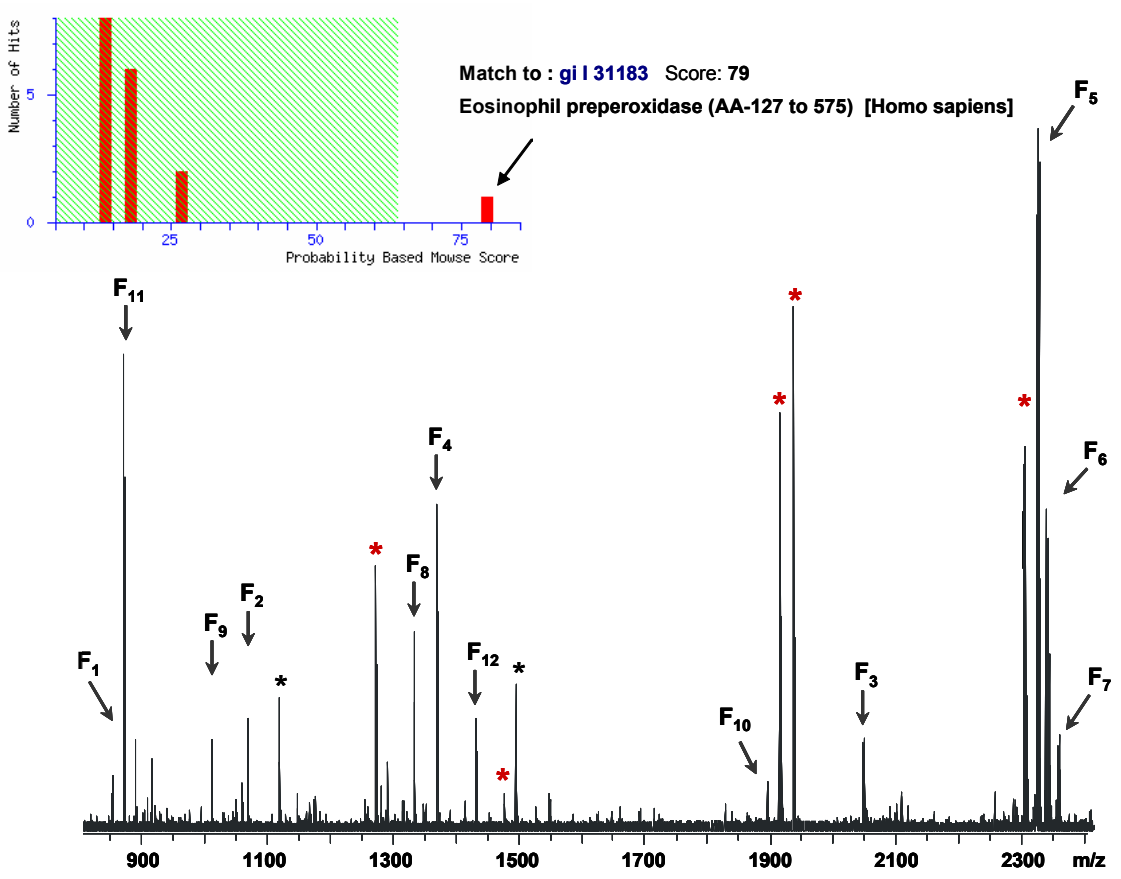

Figure 25: *Identification of light chain peptide fragments from human eosinophil peroxidase by MALDI- FT-ICR peptide mass fingerprinting (labelled by F_1 to F_{12}) and the Mascot database search result provided identification of Eosinophil preperoxidase (AA-127 to 575) with a significant Top score of 79. The tryptic light chain fragments manually assign as carrying oxidized residues are labelled with red stars and the not identified fragments labelled with black stars.*

From 19 peptide ions observed in the MALDI-FT-ICR mass spectrum twelve were identified by peptide mass finger printing using NCBInr Database and they covered 68% of the EPO light chain fragment (s. Figure 26). Two peptide ions could not be identified as being part from the eosinophil peroxidase and five signals were assign as being shifted to higher masses (+ 16 Da or +32 Da) by manually interpretation (Table 4) using the theoretical tryptic peptides fragments given by the GPMAW programme (s. Experimental Part).

	Start - End	Observed	Mr(expt)	Mr(calc)	ppm	Miss	Sequence	
F_1	133 - 139	866.4852	865.4779	865.4770	1	1	K.YRTITGR.C	
F_2	135 - 143	1063.5401	1062.5328	1062.5240	8	1	R.TITGRCNNK.R	
F_3	140 - 157	2039.1187	2038.1114	2038.0966	7	2	R.CNNKRRPLLGASNQALAR.W	
F_4	145 - 157	1366.7931	1365.7858	1365.7840	1	0	R.RPLLGASNQALAR.W	
F_5	158 - 177	2321.1337	2320.1264	2320.1164	4	0	R.WLPAEYEDGLSLPFGWTPSR.R	
F_6	158 - 177	2337.1345	2336.1272	2336.1113	7	0	R.WLPAEYEDGLSLPFGWTPSR.R	Oxidation (HW)
F_7	158 - 177	2353.1357	2352.1284	2352.1063	9	0	R.WLPAEYEDGLSLPFGWTPSR.R	2 Oxidation (HW)
F_8	178 - 188	1340.8366	1339.8293	1339.8201	7	2	R.RRNGFLLPLVR.A	
F_9	180 - 188	1028.6271	1027.6198	1027.6178	2	0	R.NGFLLPLVR.A	
F_{10}	180 - 196	1896.1269	1895.1196	1895.1105	5	1	R.NGFLLPLVRAVSNQIVR.F	
F_{11}	189 - 196	886.5131	885.5058	885.5032	3	0	R.AVSNQIVR.F	
F_{12}	197 - 208	1447.7457	1446.7384	1446.7328	4	2	R.FPNERLTSDRGR.A	

No match to: 1118.5701, 1266.6301, 1479.7501, 1498.6431, 1912.1357, 1928.1362, 2303.1245

Figure 26: *The specific peptide fragments corresponding to EPO light chain identified by peptide mass fingerprinting using MASCOT program and NCBInr database. The calculated and experimental mass, as well as the mass accuracy, miss cleavage sites for each peptide fragment and two oxidative modified fragments are indicated. The underline peptide masses in the no match row were assigning as being oxidized or dehydrated (in box) by comparison with the theoretical tryptic peptides masses (GPMAW programme).*

The tryptic peptide fragment corresponding to (31-50) EPO - light chain sequence was identified in its un-modified state with Mw $_{cal.}$: 2320.1164 and with two additional oxygen atoms (+16 Da) at Mw $_{cal.}$: 2336.1113 and (+32 Da) at Mw $_{cal.}$: 2352.1284 respectively. The oxidative modifications may correspond to tryptophan oxidation as given by Database results or to other amino acids contained in the sequence such as Pro, Tyr, Ser which are susceptible to be oxidised or hydroxylised *in vivo* by reactive oxygen species. The peak corresponding to peptide ion $[M+H]^+_{exp.}$: 2303.1328 represent the dehydration product (loss of one H_2O molecule), due to the neighbouring Asp-Gly amino-acids in (31-50) peptide fragment a well known phenomena which my occur *in vivo* [165, 166] and during the peptide synthesis [167, 168].

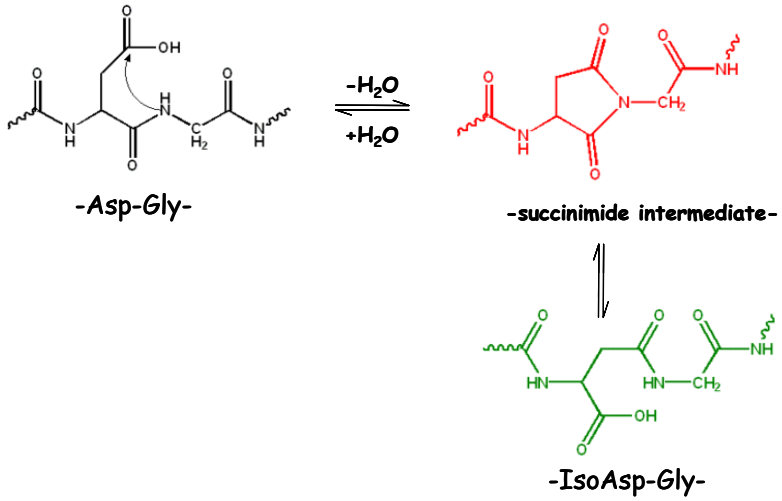

Figure 27: *Schematic representation of pathway for succinimide formation from Asp-Gly sequences. The Asp side chain carboxyl is subject to attack from the α-nitrogen of the flanking residue and is base catalyzed. Hydrolysis of the resulting succinimide leaves a mixture of α-Gly- and -IsoAsp-Gly- products.*

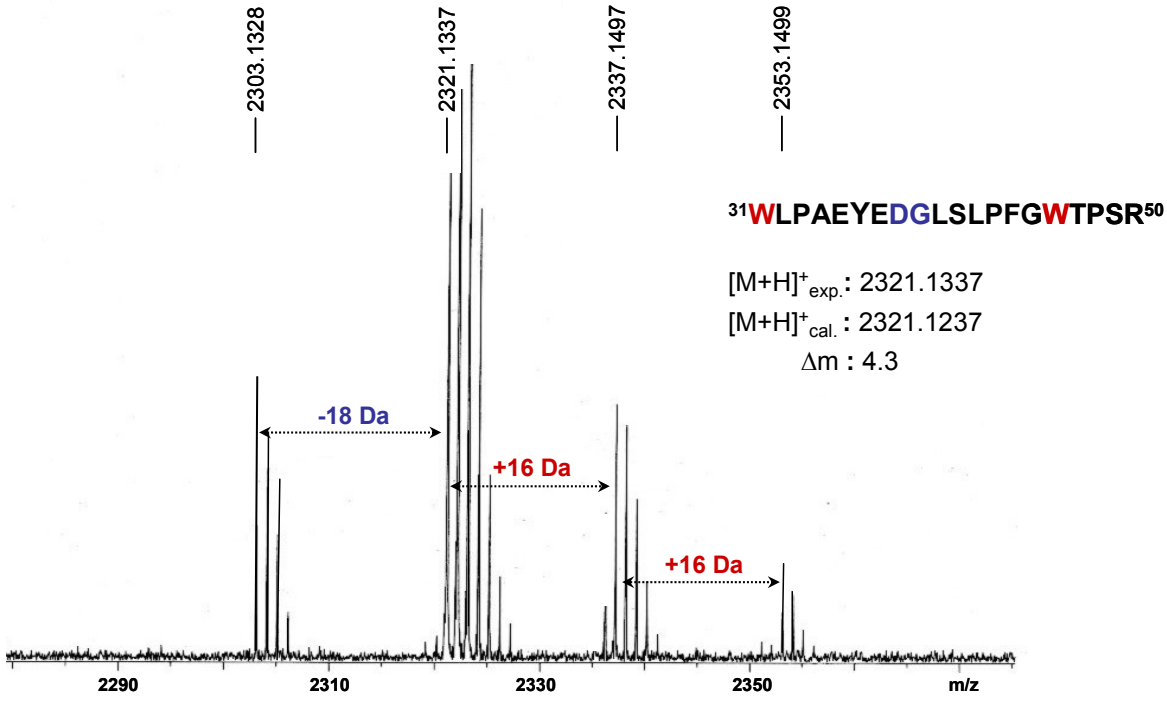

Figure 28: *MALDI-FT-ICR mass spectrum of digested EPO light chain. Zoom of the 2300 Da mass range showing the oxidative products and the dehydrated product of peptide corresponding to 31-50 EPO tryptic fragment (F_5)*

Table 4: *MS details of EPO light chain modified peptides fragments assigned by comparison with theoretical tryptic peptides fragments in GPMAW programme.*

Tryptic Fragment	Sequence	Un-modified $[M+H]^+_{exp.}$	Mass shift	Modified $[M+H]^+_{exp.}$
F_X^*	^{70}**FP**NE**RP**TSD**R**^{79}	1234.6175	F_X^***+32**	1266.6301
F_{12}	^{70}**FP**NE**RP**TSD**R**G**R**^{81}	1447.7457	F_{12}**+32**	1479.7501
F_{10}	^{53}NG**F**LL**P**LV**R**AVSNQIV**R**^{69}	1896.1269	F_{10}**+16**	1912.1397
F_{10}	^{53}NG**F**LL**P**LV**R**AVSNQIV**R**^{69}	1896.1269	F_{10}**+32**	1928.1362

*un-modified tryptic peptide fragment not present in the mass spectra

- **in bold** possible modified residues from Delta Mass: Database of protein PTM [169, 170]

None of the two tyrosine residues within the EPO-light chain and covered by the resulted Database sequence coverage (68%) was identified as being modified by nitration, these results were in agreement with the Western blot experiment.

For a subsequent analysis and a possible identification of 3-nitro-tyrosine containing peptides the heavy chains band was also cut out, in-gel digested with trypsin, and the resulting tryptic peptides were extracted and analyzed by MALDI-FT-ICR mass spectrometry. Figure 29 shows the MALDI-FT-ICR mass spectrum and the identification with a high probability based on the Top score of Eosinophil preperoxidase (AA-127 to 575) (NCBInr gi l 31183)

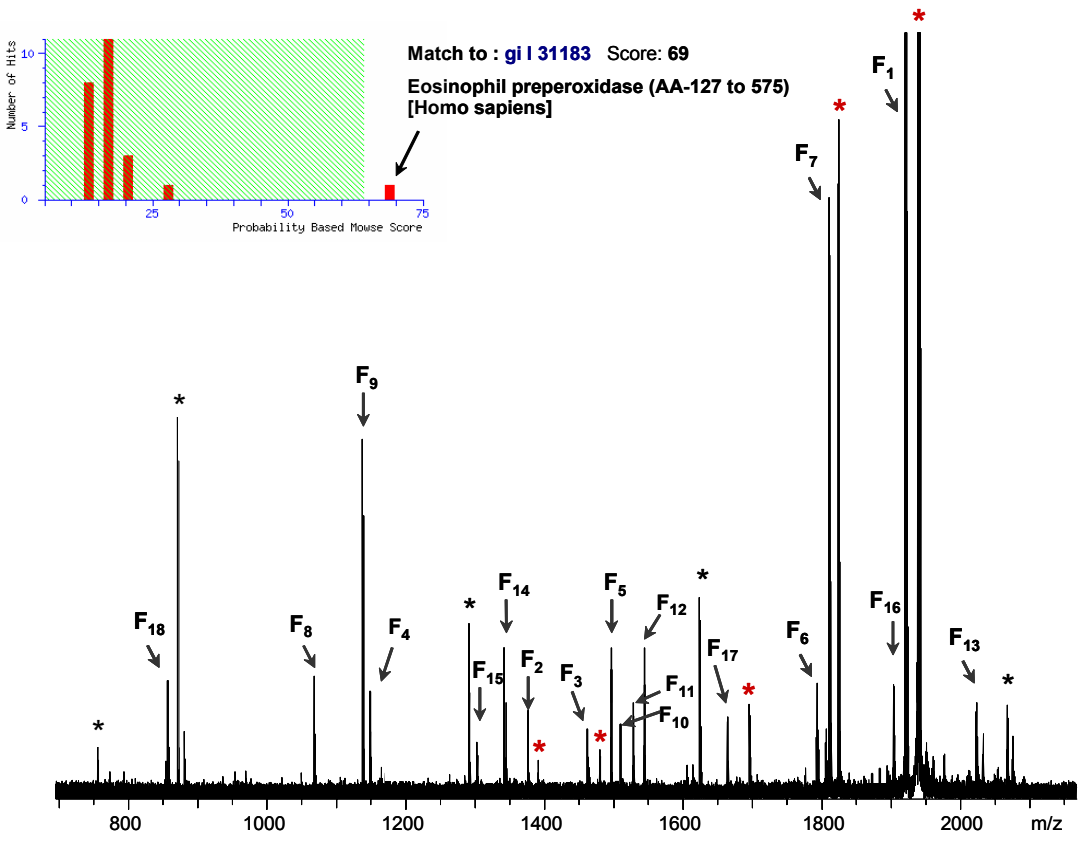

Figure 29: *Identification of heavy chain peptide fragments from human eosinophil peroxidase by MALDI- FT-ICR peptide mass fingerprinting and the Mascot database search result (labelled by F_1 to F_{18}) provided identification of Eosinophil preperoxidase (AA-127 to 575) with a significant Top score of 69. The tryptic heavy chain fragments characterized manually as carrying oxidized residues are labelled with red stars and the not identified fragments labelled with black stars.*

All 18 matched peptides, the corresponding sequences and their modified residues are shown in the Mascot detailed search result (s. Figure 30). The low sequence coverage of 34% and several unmatched signals in the mass spectrum are possible peptides resulting from a higher miss cleavage number (>2, used for database search), and probably to a high level of oxidation in the EPO heavy chain fragment. Some of the observed modifications within the heavy chain such as deamidation and methionine oxidation may usually arise by using high pH > 8 and extended incubation time at 37°C during the in gel tryptic digestion procedure.

	Start - End	Observed	Mr(expt)	Mr(calc)	ppm	Miss	Sequence
F_1	313 - 328	1915.1002	1914.0929	1914.0911	1	2	R.LRNRTNYLGLLAINQR.F
F_2	317 - 328	1375.7808	1374.7735	1374.7619	8	0	R.TNYLGLLAINQR.F
F_3	353 - 365	1463.7437	1462.7364	1462.7351	1	1	R.SARIPCFLAGDTR.S
F_4	356 - 365	1149.5800	1148.5727	1148.5648	7	0	R.IPCFLAGDTR.S
F_5	397 - 408	1495.7201	1494.7128	1494.7103	2	2	R.WNGDKLYNEARK.I 2 Deamidated (NQ)
F_6	435 - 449	1794.8350	1793.8277	1793.8268	1	1	R.TLGHYRGYCSNVDPR.V
F_7	435 - 449	1810.8286	1809.8213	1809.8217	-0	1	R.TLGHYRGYCSNVDPR.V Oxidation (HW)
F_8	441 - 449	1067.4650	1066.4577	1066.4502	7	0	R.GYCSNVDPR.V
F_9	450 - 459	1137.6504	1136.6431	1136.6342	8	0	R.VANVFTLAFR.F
F_{10}	460 - 471	1511.7296	1510.7223	1510.7214	1	0	R.FGHTMLQPFMFR.L
F_{11}	460 - 471	1527.7296	1526.7223	1526.7163	4	0	R.FGHTMLQPFMFR.L Oxidation (M)
F_{12}	460 - 471	1543.7227	1542.7154	1542.7112	3	0	R.FGHTMLQPFMFR.L 2 Oxidation (M)
F_{13}	478 - 496	2032.0212	2031.0139	2030.9962	9	0	R.ASAPNSHVPLSSAFFASWR.I
F_{14}	497 - 508	1344.7611	1343.7538	1343.7449	7	0	R.IVYEGGIDPILR.G
F_{15}	553 - 563	1302.5970	1301.5897	1301.5789	8	0	R.DHGLPGYNAWR.R Deamidated (NQ); Oxidation (HW)
F_{16}	564 - 579	1903.0105	1902.0032	1902.0006	1	2	R.RFCGLSQPRNLAQLSR.V
F_{17}	617 - 630	1663.8775	1662.8702	1662.8552	9	0	R.VGPLLACLFENQFR.R
F_{18}	694 - 700	859.4785	858.4712	858.4712	0	0	R.LNLSAWR.G

Figure 30: *Mascot detailed database search results of unambiguous identification of Eosinophil preperoxidase showing the heavy chain matched peptides and their modification. The calculated and experimental mass, as well as the mass accuracy, miss cleavage sites for each peptide fragment and modified fragments are indicated.*

Within the database search several modification entries such as oxidation at Met, His, Trp and deamidation (Asn, Gln) were used and the corresponding modified sequences are presented in Figure 30. In addition, five peptides signals were manually assigned in the mass spectrum as being oxidized due to their mass shift (+16Da, +32Da); because their possible modified amino acids do not exist in database search as a variable modification entry (s. Table 5).

Table 5: *MS details of EPO heavy chain modified peptides fragments assigned by comparison with theoretical tryptic peptides fragments in GPMAW programme.*

Tryptic Fragment	Sequence	Un-modified $[M+H]^+_{exp.}$	Mass shift	Modified $[M+H]^+_{exp.}$
F_1	^{186}L**R**N**R**TN**Y**LGLLAINQ**R**^{201}	1915.1002	F_1+16	1931.1097
F_2	^{190}TN**Y**LGLLAINQ**R**^{201}	1375.7808	F_2+16	1391.7692
F_3	^{226}SA**R**I**PCF**LAGDT**R**^{238}	1463.7437	F_2+16	1479.7367
F_7	^{308}TLGH**YR**G**YC**SNVD**PR**^{322}	1810.8286	F_7+16	1826.8351
F_{17}	^{490}VG**P**LLA**C**L**F**ENQ**FR**^{503}	1663.8775	F_{17}+32	1695.7760

in bold possible modified amino acids from Delta Mass: a Database of Protein Post Translational Modifications [169, 170]

The structures of possible modified products of eosinophil peroxidase peptides are shown in Table 6. Only MS/MS and Edman sequencing experiments could provide the localization of the oxidation sites

Table 6: *Details of possible amino acids oxidation products*

Amino acid	Oxidized product	Structure	Reference
Arg	5-Hydroxy-2-aminovaleric acid (HAVA)	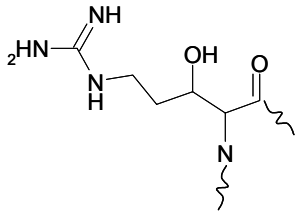	[171]
Cys	Sulfenic acid*	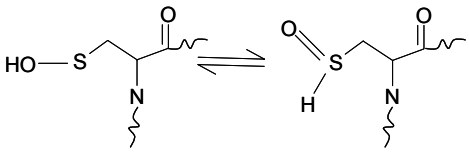	[172-174]
Phe	ortho-tyrosine or meta-tyrosine	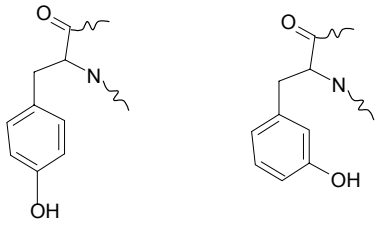	[175, 176]
Pro	3-hydroxyproline or 4-hydroxyproline	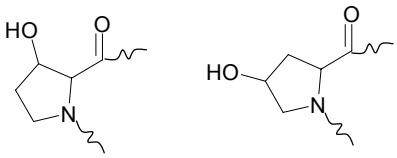	[177],[178]
Trp	5-Hydroxytryptophane	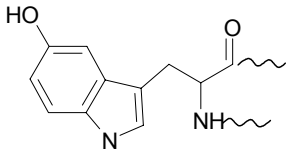	[179]
Tyr	3,4-DihydroxiPhenylalanine (**DOPA**)	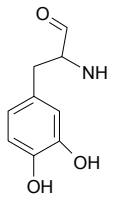	[180-182]

*Sulfenic acids appear to exist as one of two tautomers.

In summary, the results obtained by peptide mass fingerprinting indicates that EPO is intensively oxidized due to its catalytic co-substrate, hydrogen peroxide. In the whole EPO sequence, seven residues were identified as being oxidized and eight further peptides were found by comparison with the theoretical tryptic peptides fragments as being shifted to a higher mass (+16 Da or +32 Da) corresponding to addition of one or two oxygen atoms. However, no nitrated peptides were detected by these mass spectrometric data. These results contradict western blot data but may be explained by an extensive photochemical fragmentation of the nitro group in the MALDI source [147]. Since the eosinophil peroxidase was isolated from native eosinophil granules, the nitration level may be low and the resulting un-modified ions may obscure the assignment of nitration sites in the complex proteolytic peptide mixture.

```
  1 EFRGQDPCQG TDPASPGAVE TSVLRDCIAE AKLLVDAAYN WTQKSIKQRL
 51 RSGSASPMDL LSYFKQPVAA TRTVVRAADY MHVALGLLEE KLQPQRSGPF
101 IVTDVLTEPQ LRLLSQASGC ALRDQAERCS DKYRTITGRC NNKRRPLLGA
151 SNQALARWLP AEYEDGLSLP FGWTPSRRRN GFLLPLVRAV SNQIVRFPNE
201 RLTSDRGRAL MFMQWGQFID HDLDFSPESP ARVAFTAGVD CERTCAQLPP
251 CFPIKIPPND PRIKNQRDCI PFFRSAPSCP QNKNRVRNQI NALTSFVDAS
301 MVYGSEVSLS LRLRNRTNYL GLLAINQRFQ DNGRALLPFD NLHDDPCLLT
351 NRSARIPCFL AGDTRSTETP KLAAMHTLFM REHNRLATEL RRLNPRWNGD
401 KLYNEARKIM GAMVQIITYR DFLPLVLGKA RARRTLGHYR GYCSNVDPRV
451 ANVFTLAFRF GHTMLQPFMF RLDSQYRASA PNSHVPLSSA FFASWRIVYE
501 GGIDPILRGL MATPAKLNRQ DAMLVDELRD RLFRQVRRIG LDLAALNMQR
551 SRDHGLPGYN AWRRFCGLSQ PRNLAQLSRV LKNQDLARKF LNLYGTPDNI
601 DIWIGAIAEP LLPGARVGPL LACLFENQFR RAETETGSGG RTRCFHQRQR
651 KALSRISLSR IICDNTGITT VSRDIFRANI YPRGFVNCSR IPRLNLSAWR
701 GT
```

Figure 31: *Protein sequence of Eosinophil preperoxidase (gi l 31183). In italic the Propep (1-127) fragment which is removed naturally in mature EPO. In bold the light start residue (R^{1}) and heavy chain start residue (V^{112}). NCBInr matched peptides are shown in bold red, all eight non-nitrated tyrosine covered by Database results are in bold blue and oxidative residues identified by Database are indicated in underline bold.*

2.2.2.3 Identification of nitro-Tyrosine in Eosinophil peroxidase by UV-LC-MS/MS mass spectrometry

In order to avoid possible artificial oxidative modification which may occur during the in-gel digestion, the intact EPO was digested in solution by trypsin and the resulting peptide mixture was analysed by nano-ESI MS/MS, using a ESI-QTRAP (Applied Biosystems / MDS SCIEX QTRAPTM), a hybrid triple-quadrupole ion trap mass spectrometer [183]. An ion trap performs several important functions including mass accumulation, selective mass isolation and excitation for collision induced dissociation (MS^n) and sequential mass ejection to produce a mass spectrum. Automated MS/MS analysis was performed utilizing the Information Dependent Acquisition (IDA) software 1.3.2 (s. Experimental Part). All MS/MS data (s. Figure 32) were directly used for a database search procedure using the Mascot MS/MS Ion Search procedure.

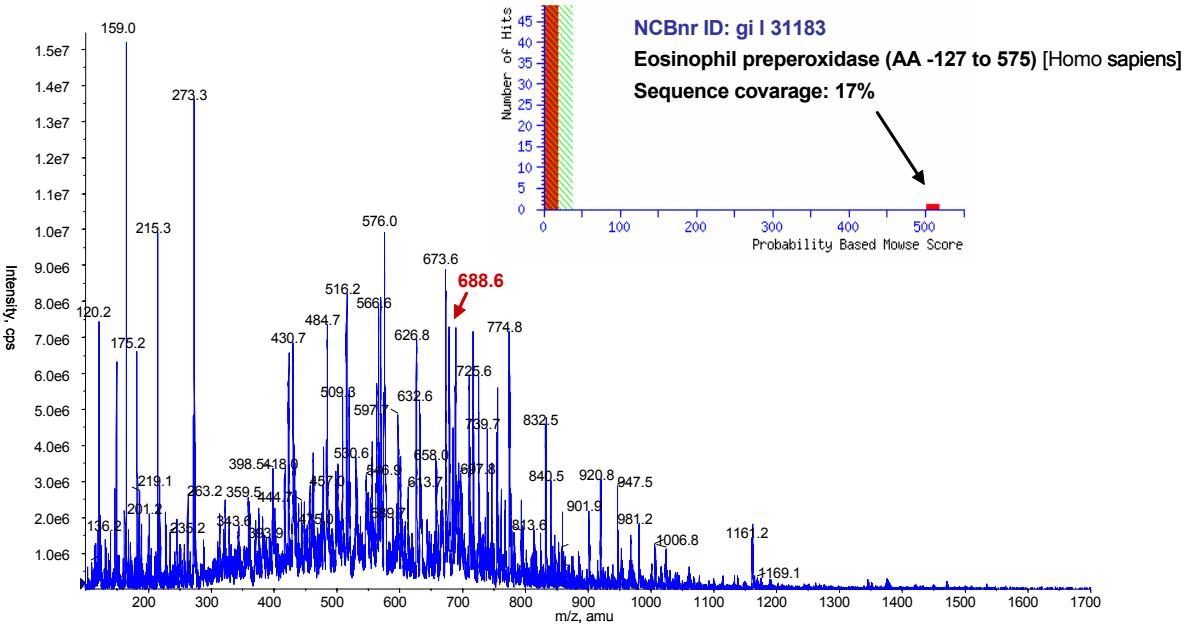

Figure 32: *Nano - LC-ESI-MS mass spectrum of in solution digested EPO. The identification of eosinophil preperoxidase (AA-127 to 575) was done using the Mascot MS/MS Ion Search program and NCBInr Database. The EPO preperoxidase has an apparent molecular weight of ca.80 kDa and a pI of ca. 10.2.*

An example of an automated MS/MS analysis is shown in Figure 33 for the doubly charged $[M+2H]^{2+}$ ion of the heavy chain tryptic peptide fragment (190-201). A characteristic immonium ion for tyrosine resulted by fragmentation of the amide bond releasing (b_2 ion) and (y_9 ion), could be observed at 136.1 Da.

The entire MS/MS data showed no nitro-tyrosine containing peptide in the digested eosinophil peroxidase mixture, suggesting again the low relative concentrations of nitrotyrosine-containing peptides in eosinophil proteins isolated from hypereosinophilic patients.

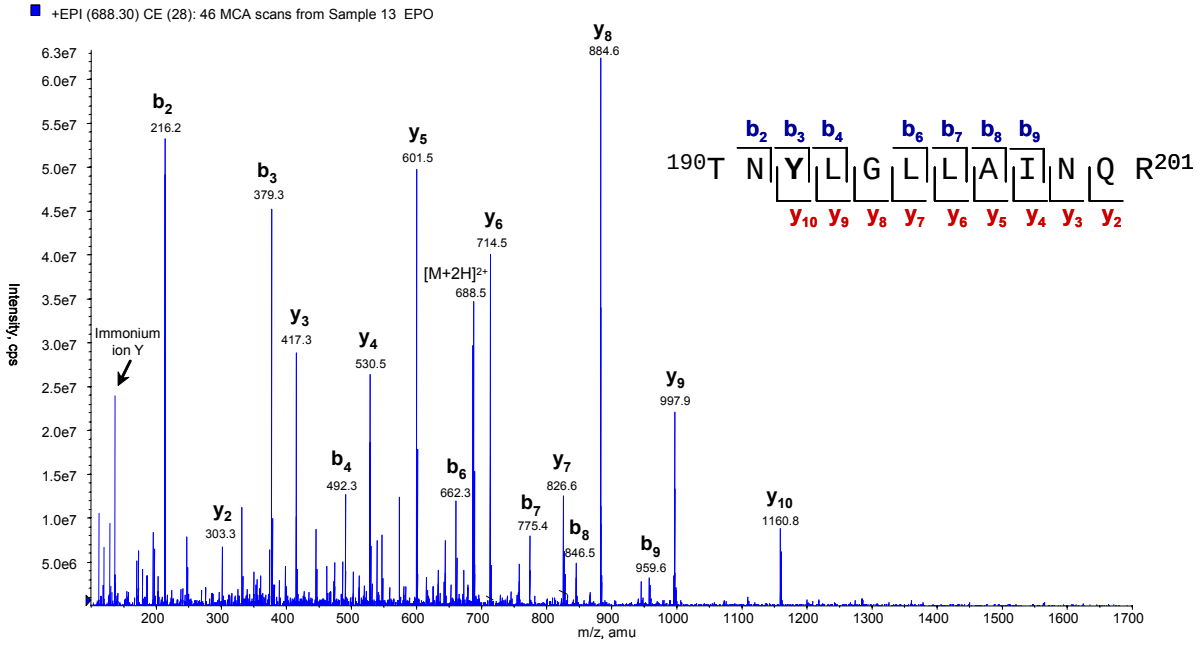

Figure 33: *Nano – ESI – Qtrap MS/MS spectrum of the $[M+2H]^{2+}$ ion of the tryptic peptide (79-90). Fragmentation of the amide bond resulting (b_2 ion) and (y_9 ion) provided the immonium ion for tyrosine residue.*

To identify nitration sites in eosinophil peroxidase an HPLC system with a UV multi-wavelength detector was coupled with the ESI mass spectrometer, using a specific wavelength (365 nm) in order to detect only 3-nitro-tyroisne containing peptides.

Since the EPO light chain fragment was found by Western blot non-nitrated, it was separated from the heavy chain in presence of reducing buffer (50 mM Tris-HCl, 8%

(w/v) SDS, urea, (w/v) 12% glycerol, pH 6.8) using a Microcon centrifugal filter device (s. Experimental part). A low-adsorbing, hydrophilic YM-membrane with a nominal molecular weight limit (NMWL) at 30 kDa was successfully used due to its ability to retain molecules above its specified molecular weight. The solution which passed through the membrane containing the EPO light chain fragment was lyophilised and after desalting and concentration using a ZipTip C_4 was analysed by MALDI-TOF – MS (s. Figure 34). The MALDI-TOF mass spectrum showed the singly and doubly charged ions which correspond to the EPO light chain polypeptide. A mass deviation of ca. 221 Da for the EPO light chain was observed, and the attachment of approximately 14 oxygen atoms was estimated.

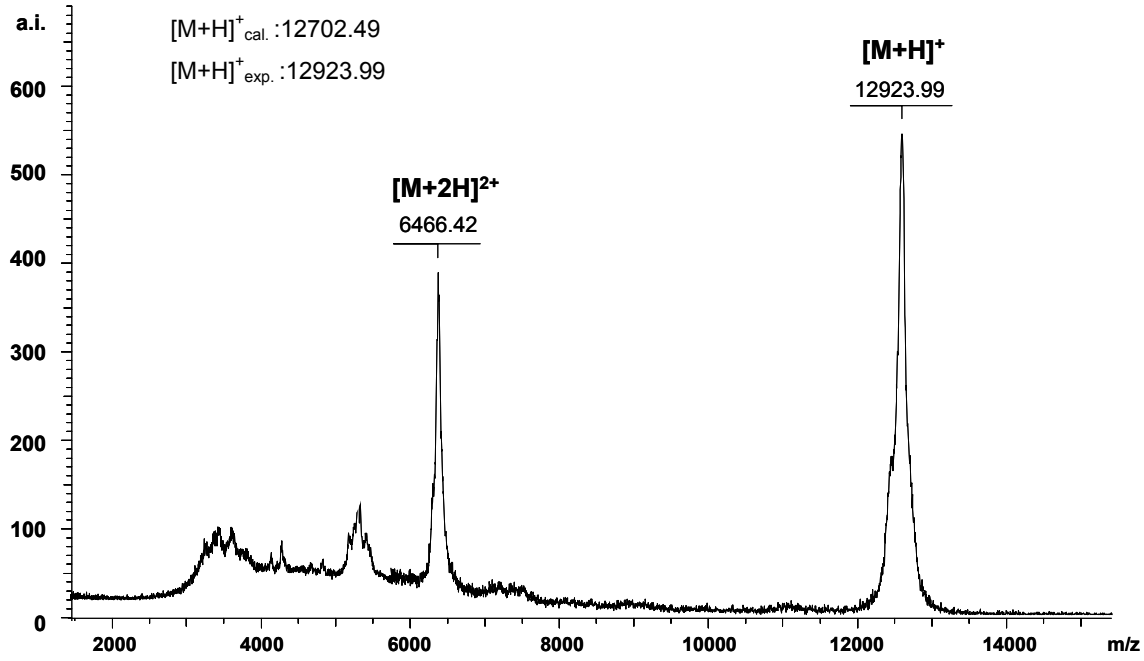

Figu **34:** *MALDI-TOF mass spectrum of separated Eosinophil peroxidase light chain using a 30 kDa mass cut-off Microcon centrifugal filter device.*

The EPO heavy chain fragment (Mw ca. 53.5 kDa) retained on the membrane was washed to remove possible impurities or excess salt, then dissolved in 10 mM NH_4HCO_3, and digested in solution using trypsin. The tryptic peptide mixture was separated by an HPLC system coupled to the ESI instrument. The tryptic peptide mixture was monitored by both a ultraviolet detector and the total ion chromatogram (TIC) as shown in Figure 35. Figure 35 A represents the UV profile with detection at 365 nm (selective for 3-nitro-tyrosine), showing a prominent peak at retention time

23.18 min and a smaller one at 26.63 min. The TIC was produced by measuring the total ion current from the mass analyser, and provided a good summary of all EPO heavy chain ions being separated and detected during the entire experimental time (s. Experimental part). The peak at the retention time of ca. 25 min, (s. Figure 35B) was found to contain the human eosinophil peroxidase heavy chain peptide fragment [^{333}FGHTMLQPFMFRLDSQ**Y(NO$_2$)**R^{350}] with a single nitration site at Tyr-349. In the MS experiment, the intensity of the signal as the peptide elutes from the chromatographic column was plotted over time (s. Figure 35C). The area under this curve is the eXtracted Ion Current or eXtracted Ion Chromatogram (XIC), a measure that is proportional to the peptide's abundance [184].

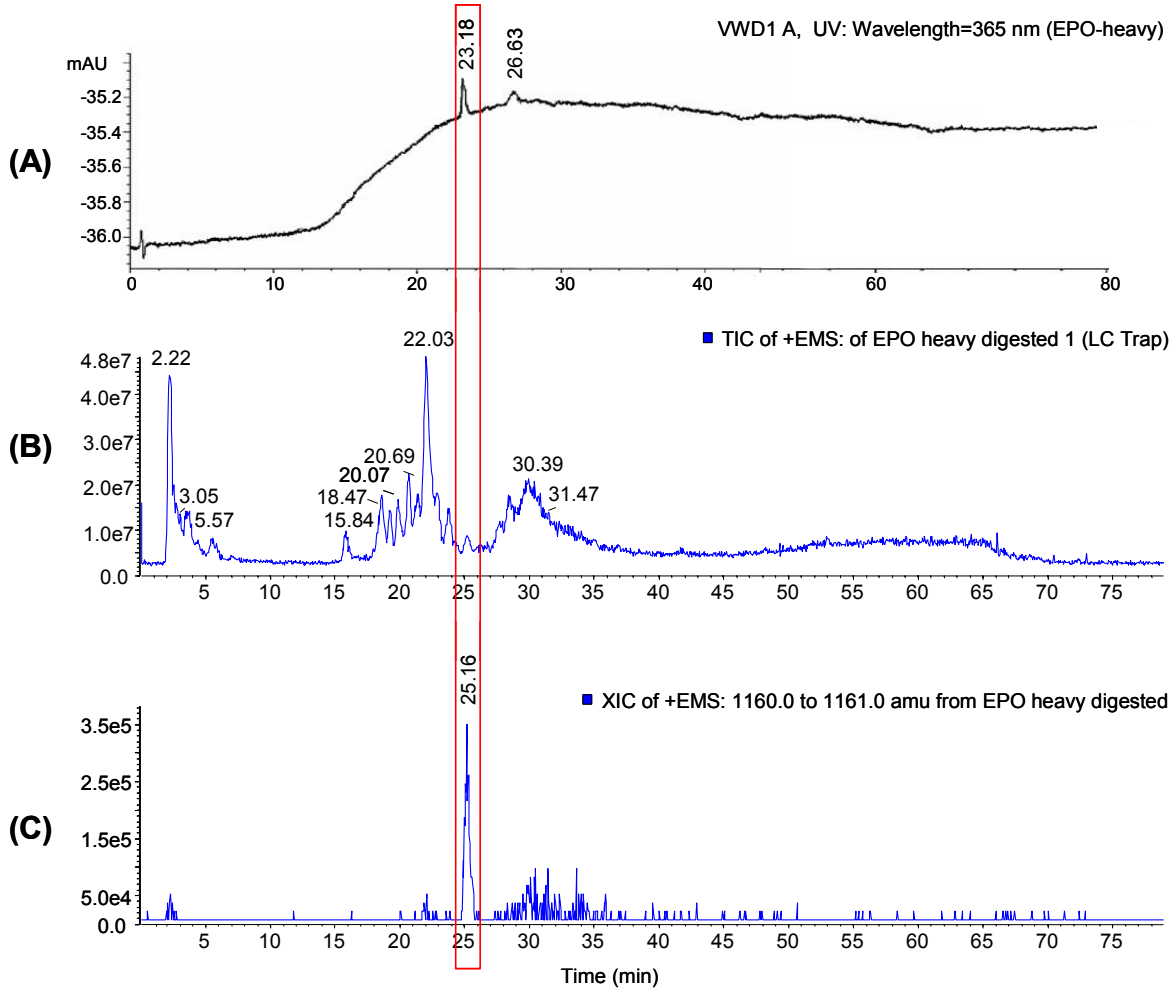

Figure 35: *Summary of HPLC-UV-ESI-MS analysis of EPO-heavy chain tryptic peptides mixture. (A) UV profile monitored at 365 nm. (B) Total ion chromatogram of digested EPO heavy chain. The peak at ~ 25 min was identified as being EPO (333-350) peptide fragment nitrated at Tyr^{349}.(C) The eXtracted ion current (XIC) for m/z 1160, corresponding to EPO (333-350) with a given mass window (± 1Da)*

The nitrated EPO (333-350) peptide fragment contains a miss cleavage site at Arg^{344}, which may be part of a specific substrate sequence after addition of the nitro-group at Tyr ^{349} which possible creates a steric hindrance in the EPO structure (s. paragraph 2.4).

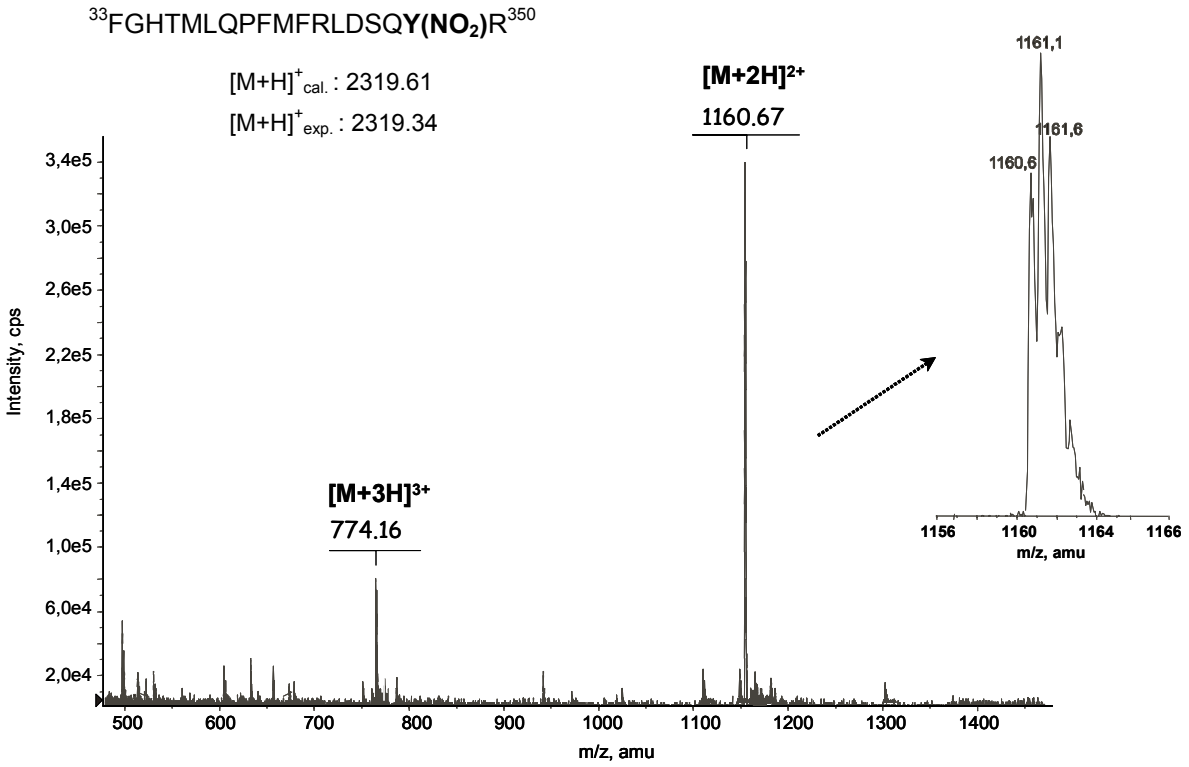

Figure 36: *ESI-mass spectrum of human eosinophil peroxidase- heavy chain (333-350) nitrated fragment from HPLC-UV-MS chromatogram at 25.16 min. The experimental $[M+H]^+$ was compare to all theoretical EPO tryptic peptide fragments containing Tyr residue provided by GPMAW program and was found to correspond to F^{333}-R^{350} peptide fragment shifted with +45 Da providing evidence for the NO_2 group.*

Tandem ESI-MS/MS sequencing of the nitrated tyrosine containing peptide (333-350) fragment was not successful due to (i) the very small amount of nitrated peptide within the biological eosinophil peroxidase, or (ii) its high stability towards MS fragmentation. The types of fragment ions observed in an MS/MS spectrum depend on many factors including primary sequence, the amount of internal energy, how the energy was introduced, charge state, etc.

To confirm the identified nitrated peptide sequence, the nitrated peptide (333-350) was synthesised by SPPS (as described in Experimental part). The peptide was subjected to final purification by preparative RP-HPLC, and characterised by mass spectrometry.

The nano-ESI-FTICR spectra of the EPO Tyr-nitrated peptides (333-350) showed most abundant multiply protonated molecular ions with mass determination accuracies in the low ppm range, as illustrated in Figure 37. The presence of mainly doubly and triply protonated molecular ions indicate the molecular homogeneity of the synthesized EPO peptide.

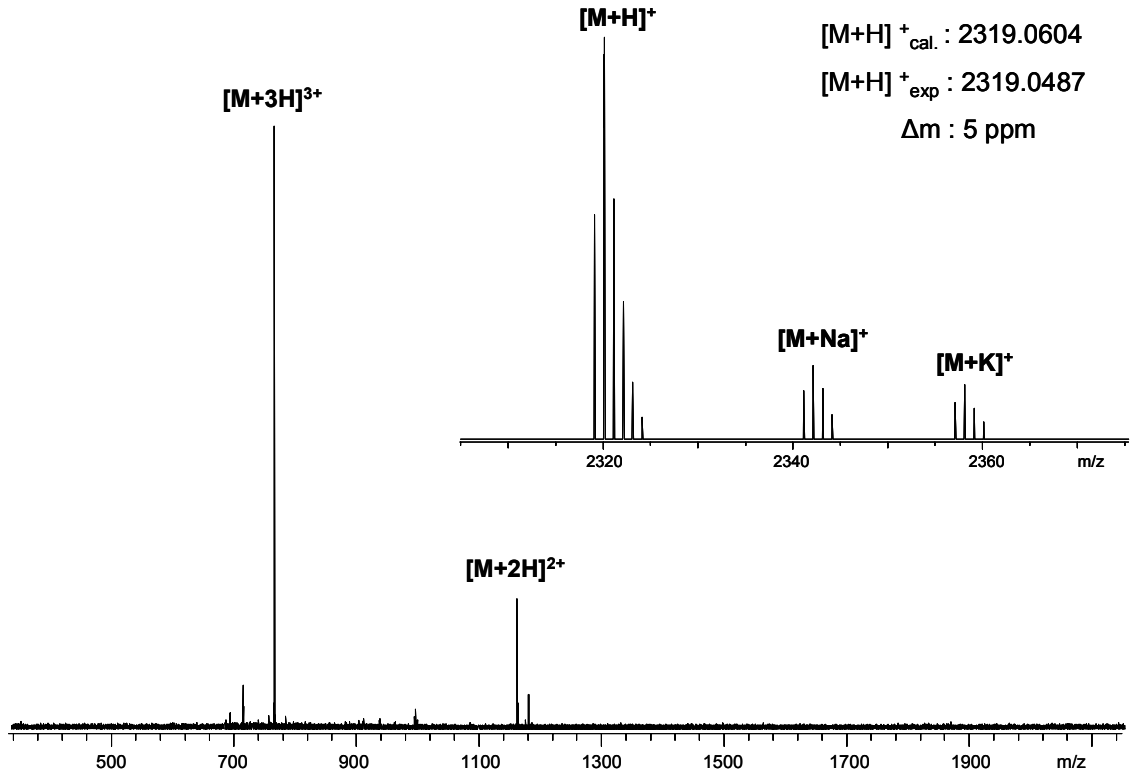

Figure 37: *Nano-ESI-FTICR mass spectrum of synthetic, Tyr^{349}- nitrated peptide, EPO (333-350). The inserts show the isotopic fine structure of the $[M+H]^+$ ion obtained by deconvolution.*

In addition, the synthetic Tyr^{349}-nitrated EPO peptide was analyzed using electrospray ionization on an Esquire 3000plus ion trap mass spectrometer (s. Figure 38). The amino acid sequence was confirmed by isolation and fragmentation of the most abundant quadruply charged precursor ion (or parent ion) of *m/z* 581.0 in the ESI-mass spectrum (Figure 38A). This ion was selectively focused into a collision cell for fragmentation and the resulted daughter ions were analysed by tandem mass spectrometry. As shown in Figure 38B, fragmentation of *m/z* 581.0 produced only a few set of y and b ions confirming the EPO (333-350) peptide fragment. This indicated that due to it secondary structure the nitrated EPO (333-350) peptide

fragment is stable to the collision induced fragmentation. The location of the nitrated Tyr^{349} could be determined from the y ions as illustrated by the insert in Figure 38B.

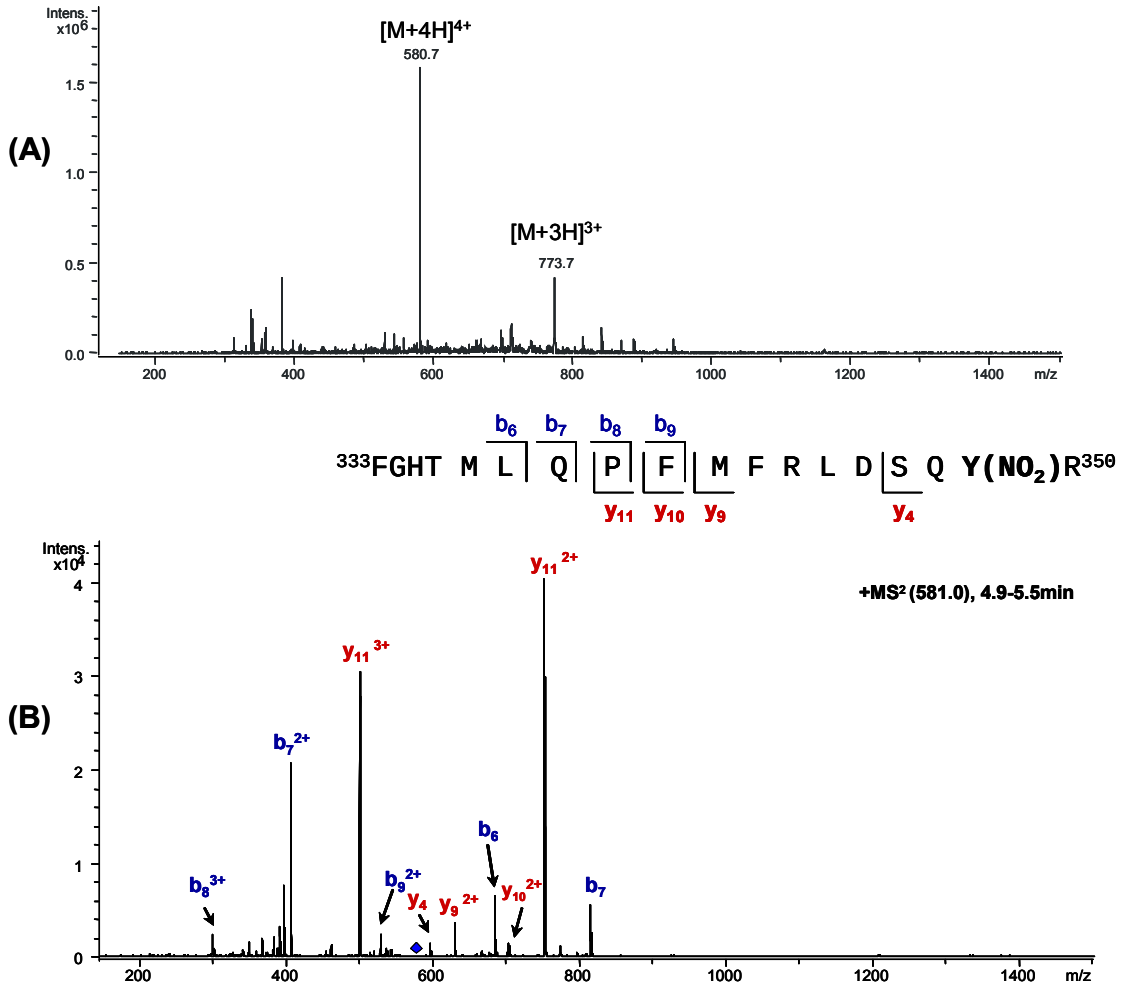

Figure 38: *ESI-Ion trap MS of the synthetic EPO (333-350) peptide. (A) ESI-mass spectrum showing triply and quadruply charged peptide ions. (B) CID mass spectrum of the quadruply protonated precursor ion at m/z 581.0. The observed b and y fragment ions are indicated in blue and red, respectively. The insert shows the nitrated EPO peptide sequence and location of y and b ions resulted by collision induced dissociation.*

The crystal structure of the related myeloperoxidase MPO (PDB ID 1DNU) [185] was used as a template for homology modelling and further comparative studies to assess the spatial orientation of the nitrated Tyr^{349} residue in EPO. EPO and MPO share ~71% sequence identity [159], suggesting that both enzymes have similar

tertiary structures. This comparison showed that non-nitrated Tyr^{350} (Tyr^{349} in EPO) is present in a highly flexible loop region (~23 amino acids in length) in a weak, parallel stacking interaction [186] with Tyr^{557} (Tyr^{555} in MPO) (Fig. 4C). However, upon nitration of Tyr^{350}, the flexibility of this loop is lost due to steric hindrance and the net electronegativity of the nitrated Tyr^{350} residue likely prevents the stacking interactions with Tyr^{557}, forcing the nitro group of Tyr^{350} to be permanently exposed to the surface of the molecule.

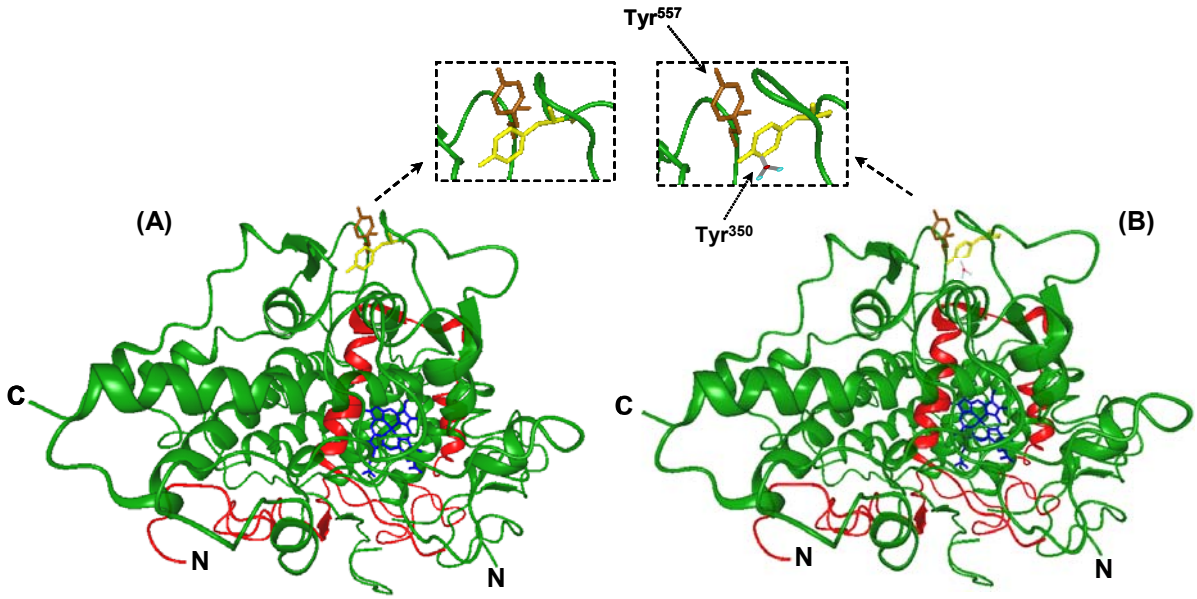

Figure 39: (A) *Ribbon diagram of the human myeloperoxidase (MPO) based on the X-Ray crystal structure (PDB accession number 1DNU). (B) Ribbon diagram of the human MPO after introduction of the nitro group at Tyr^{350}.The MPO light chain is shown in red, the heavy chain fragment in green and the heme in blue. The places of neighbouring Tyr^{350} and Tyr^{557}residues in the MPO structure, before and after nitration at Tyr^{350} are indicated. The figures were rendered using the program BallView 1.1.1.*

The conformational changes introduced by the addition of a nitro group on a Tyr – containing peptide were analysed by CD spectroscopy using nitrated and non-nitrated synthetic peptides. The CD spectrum for nitrated ($EPO_{\underline{1}}$) and non-nitrated ($EPO_{\underline{2}}$) (333-350) peptides were recorded in water and trifluoroethanol (TFE) (s. Figure 40); the latter solvent is known to preferentially stabilize proteins and peptides in ordered conformation [187, 188] The CD spectrum of both peptides in water showed the predominance of a random coil conformation, characterized by a

negative band at 197 nm (n→π*) and a small positive shoulder at approximately 220 nm (π→π*) for $EPO_{\underline{2}}$ and strong negative band shifted to 200 nm and a small negative shoulder at approximately 218 nm for $EPO_{\underline{1}}$ (s. Figure 40A). In TFE the peptides adopt helical conformation and the CD spectrum are characterised by an intensive positive band at 196 nm ($\pi\rightarrow\pi^*_{perpendicular}$) and negative bands at approximate 208 nm ($\pi\rightarrow\pi^*_{parallel}$) and 222 nm (n→π*) for $EPO_{\underline{1}}$ and a less intensive and broad positive band shifted to 199 nm and more intensive negative band at 207 nm and 223 nm for $EPO_{\underline{2}}$ (Figure 40B). A decrease in ellipticity upon Tyr^{349} nitration was observed in both CD spectroscopy analyses, results confirming the structural changes obtained by molecular modelling studies of MPO.

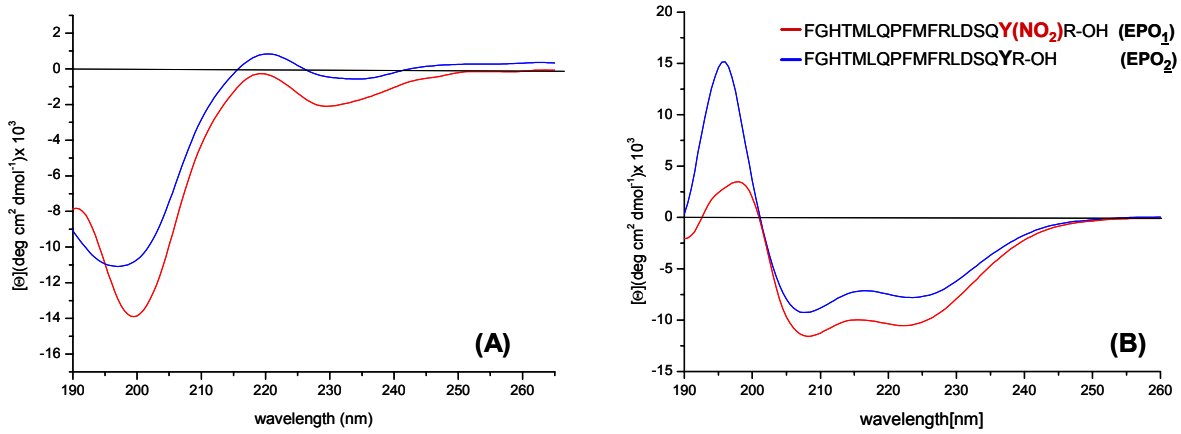

Figure 40: *CD spectra of the nitrated ($EPO_{\underline{1}}$) and non-nitrated ($EPO_{\underline{2}}$) peptides recorded in water (A) and 9:1 TFE: water mixtures (B) (v/v).*

In summary, a single nitrated tyrosine containing peptide was identified by HPLC-ESI mass spectrometry in the highly oxidized human eosinophil peroxidase isolated from hypereosinohilc patients. The selectivity of the specific nitration site is derived from the protein structure and folding and from the close vicinity of reactive nitrogen species production. These results confirm the hypothesis that Tyr nitration of the eosinophil granule proteins is exclusively mediated by EPO, which appears to nitrate itself via an autocatalytic mechanism that remains to be understood.

2.2.3 Identification of tyrosine nitration in human cationic eosinophil proteins

2.2.3.1 Structure and biological activity of human eosinophil granule proteins

Human eosinophil cationic protein (ECP) and eosinophil-derived neurotoxin (EDN) are major effector proteins located together with eosinophil peroxidase (EPO) in the eosinophil granule matrix, and their secretion is related to the pathogenesis of inflammatory diseases [189]. ECP and EDN belong to the ribonuclease A (RNase A, EC 3.1.27.5) superfamily (s. Figure 41) but the role of ribonuclease activity in the physiologic function of these proteins remains unclear. As in all members of the RNase A superfamily, the residues of the catalytic site are conserved (Gln^{14}, His^{15}, Lys^{38} and His^{128}). Molecular cloning of both ECP [190], [191] and EDN [192] defined the homology between these proteins (67% amino acid sequence identity) and confirm the relationship to human pancreatic ribonuclease A with limited homology (32 and 26 %, respectively) (Figure 42).

The RNase activity of ECP is known to be ca. 100 times lower than that of EDN (187). In addition to its weak RNase activity, ECP is involved in the immune response system exhibiting a number of properties: it has marked toxicity for a variety of helminth parasites, hemoflagellates and bacteria and promote degranulation of mast cells, and is toxic to single-stranded RNA viruses [193, 194]. The mechanisms of action of ECP has not been clarified but is believed to exert many of its effects by creating functional pores or channels that traverse the plasmalemma of target cells [195]. The antibacterial activity and parasitic toxicity of ECP are higher than those of EDN [194] and does not seem to be related to its RNase activity. The ECP level in biological fluids is currently used as a clinical tool for the quantitative estimation of inflammatory activity in asthma and other allergic diseases [196].

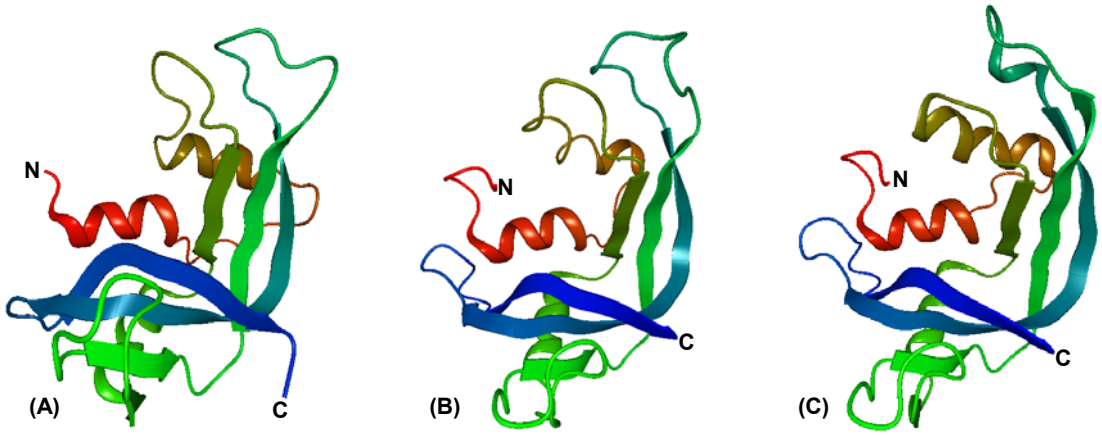

Figure 41: *Ribbon diagram of the human ribonuclease A (RNase A) based on the X-Ray crystal structure (PDB accession number 1E21), (B) Ribbon diagram of the human ECP (PDB accession number 1H1H) and (C) Ribbon diagram of the human EDN (PDB accession number 1GQV). All structures were processed in Ballview 1.1.1 molecular modelling program.*

Mature ECP and EDN are polypeptides of 133 and 134 amino acid, respectively; with four possible sites for tyrosine nitration. ECP is very basic due to a high content of arginine residues. The amino acid sequence of both ECP and EDN include three and five potential sites for asparagines-linked glycosylation, respectively (s. Figure 42).

ECP ^{1}RPPQFTRAQWFAIQHISLNPPRCTIAMRAINN^{33}YRWRCKNQNTFLRTTFA
EDN ^{1}KPPQFTWAQWFETQHINMTSQQCTNAMQVINN^{33}YQRRCKNQNTFLLTTFA

ECP ^{50}NVVNVCGNQSIRCPHNRTLNNCHRSRFRVPLLHCDLINPGAQNISNCR^{98}YA
EDN ^{50}NVVNVCGNPNMTCPSNKTRKNCHHSGSQVPLIHCNLTTPSPQNISNCR^{98}YA

ECP ^{100}DRPGRRF^{107}YVVACDNRDPRDSPR^{122}YPVVPVHLDTTI^{133}
EDN ^{100}QTPANMF^{107}YIVACDNRDQRRDPPQ^{123}YPVVPVHLDRII^{134}

Legend:
- possible sites for nitration
- common amino acids in both proteins
- possible sites for glycosylation
- **underline** trypsin - cleavage sites

Figure 42: *Structure based sequence alignment of mature ECP and EDN proteins taken from UniProtKB (as Swiss-Prot entry P12724 and P10153). ECP and EDN share 67% sequence homology exhibiting the same location for all four tyrosine residues.*

The identification of the specific tyrosine nitration site in Eosinophil peroxidase by mass spectrometry raised the hypothesis that secreted EPO from activated eosinophils using nitrite (NO_2^-) and H_2O_2 as co-substrate catalyzes the nitration in ECP and EDN, being located all together in the eosinophil crystalloid granule. This novel mechanism may have significant consequences concerning the innate immune defence towards parasites and possibly for host tissue destruction during parasite infection and disorders characterized by eosinophil cell activation.

2.2.3.2 Mass spectrometric peptide mapping of eosinophil cationic protein and eosinophil derived-neurotoxin

The mature eosinophil cationic protein (ECP) and eosinophil-derived neurotoxin (EDN) were isolated and purified from human eosinophil granule suspension, derived from hypereosinophilic patients exhibiting abnormal increased number of eosinophil in blood. After purification, eosinophil cationic protein and eosinophil-derived neurotoxin were separated by gel electrophoresis, the separated proteins transferred on to a nitrocellulose membrane, and the membrane was stained with a 3NT antibody (s. Figure 43). Due to the high sequence homology the intact ECP and EDN were observed as expected, at the same molecular mass ca. 16 kDa. It is known that eosinophl proteins are highly glycosylated and two additional bands at higher masses correspond to the glycosylated forms of these proteins. Western blot analyses shows intensive positive staining for ECP and less intensive stain for EDN at specific bands (ca. 16 kDa). The glycosylated forms of eosinophil proteins appear also to be nitrated, suggesting that glycosylation is remote from the nitrated tyrosine residue and can not create a steric effect for reactive nitrogen specie (RNS) (s. Figure 43).

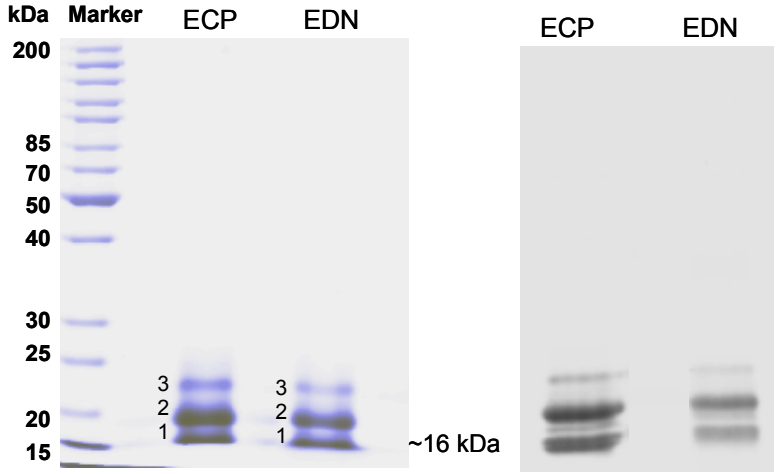

Figure 43: *SDS gel electrophoresis of ECP and EDN purified from human eosinophil granules and visualized by colloidal Coomassie (left) and Western blot using a monoclonal 3-nitro-tyrosine antibody.*

The protein bands which appear for both proteins at ~16 kDa (band 1) were excised, in-gel digested with trypsin, and the resulting tryptic peptides were extracted, and analysed by MALDI-TOF – MS. The measured tryptic peptide fragments were further used for Database search. Figure 44 shows the MALDI-TOF peptide mass fingerprinting for ECP. The protein band 1 was identified with very high probability (Top score of 93), as eosinophil cationic protein (RNase 3, Chain B, X-Ray crystal structure of ECP). 10 tryptic peptides were directly identified and covered 56 % of the protein sequence, comprising all four tyrosine residue. Using as variable modification entries (oxidation M, H, W) for Database search, only the single methionine residue (Met^{27}) of ECP was found to be oxidised to methionine sulfoxide.

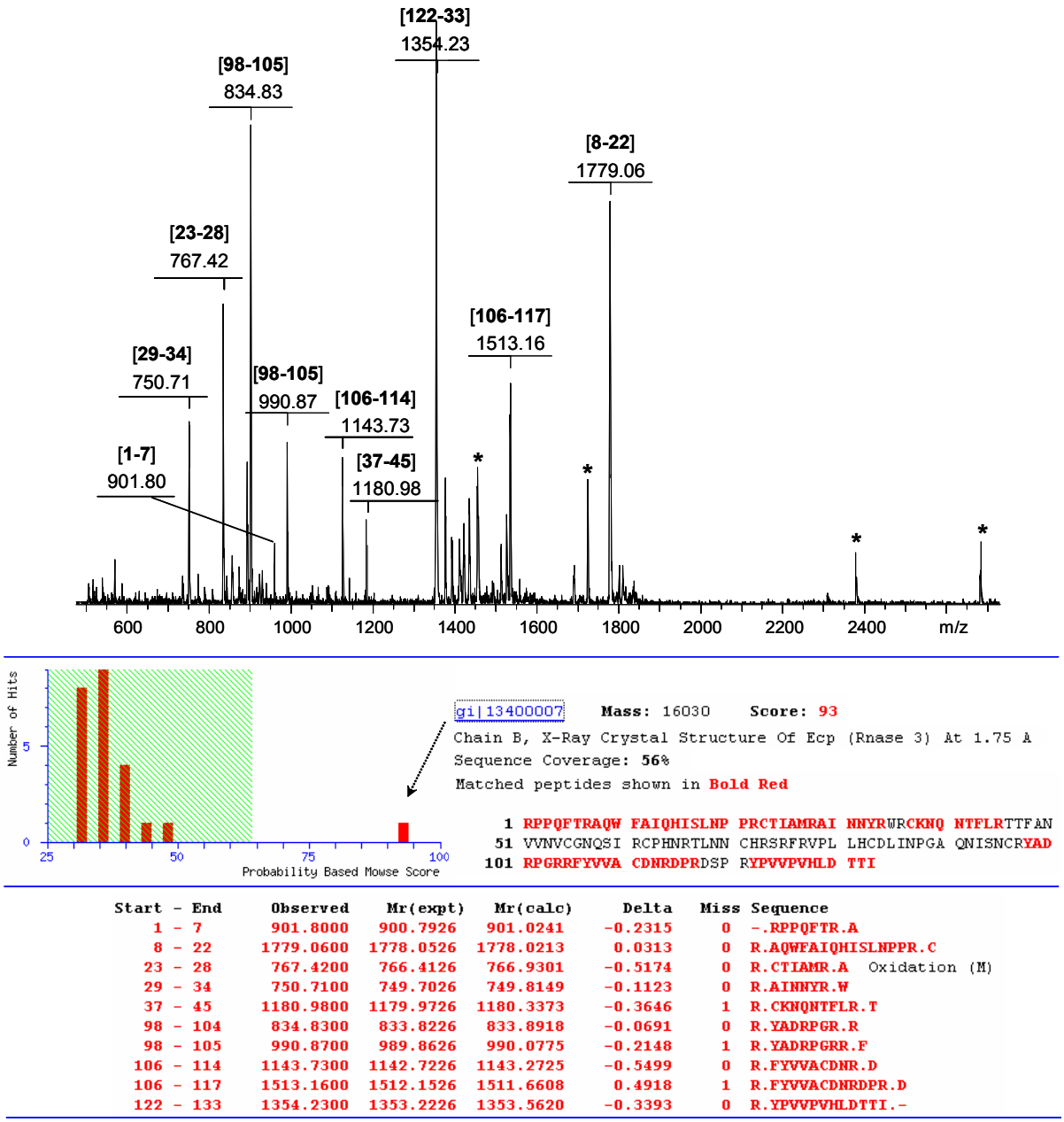

Start - End	Observed	Mr(expt)	Mr(calc)	Delta	Miss	Sequence
1 - 7	901.8000	900.7926	901.0241	-0.2315	0	-.RPPQFTR.A
8 - 22	1779.0600	1778.0526	1778.0213	0.0313	0	R.AQWFAIQHISLNPPR.C
23 - 28	767.4200	766.4126	766.9301	-0.5174	0	R.CTIAMR.A Oxidation (M)
29 - 34	750.7100	749.7026	749.8149	-0.1123	0	R.AINNYR.W
37 - 45	1180.9800	1179.9726	1180.3373	-0.3646	1	R.CKNQNTFLR.T
98 - 104	834.8300	833.8226	833.8918	-0.0691	0	R.YADRPGR.R
98 - 105	990.8700	989.8626	990.0775	-0.2148	1	R.YADRPGRR.F
106 - 114	1143.7300	1142.7226	1143.2725	-0.5499	0	R.FYVVACDNR.D
106 - 117	1513.1600	1512.1526	1511.6608	0.4918	1	R.FYVVACDNRDPR.D
122 - 133	1354.2300	1353.2226	1353.5620	-0.3393	0	R.YPVVPVHLDTTI.-

Figure 44: *Identification of eosinophil cationic protein (band 1) by MALDI-TOF peptide mass fingerprinting. The measured peptide masses of tryptic digested ECP were used for Database search using MASCOT search engine and NCBInr Database. 10 tryptic peptides were directly identified from MALDI-TOF mass data and they covered 56 % of the protein sequence (shown in red).*

The identification of ECP by MALDI-TOF peptide mass fingerprinting from ECP protein band 2 yielded a lower sequence coverage (16%) containing only two tyrosine residues, while for ECP protein band 3 the identification failed.

The corresponding EDN identification by MALDI-TOF peptide mass fingerprinting from protein band 1 is shown in Figure 45. The protein band 1 was identified with significant probability (Top score of 56), as nonsecretory ribonuclease precursor, EC 3.1.27.5 (Eosinophil derived neurotoxin). Only four tryptic peptides were directly identified and they covered 21 % of the protein sequence, comprising all three tyrosine residue at the C-terminal of EDN. The single oxidative modification in EDN observed in Database results is the methionine sulfoxide at the (Met^{107}) residue.

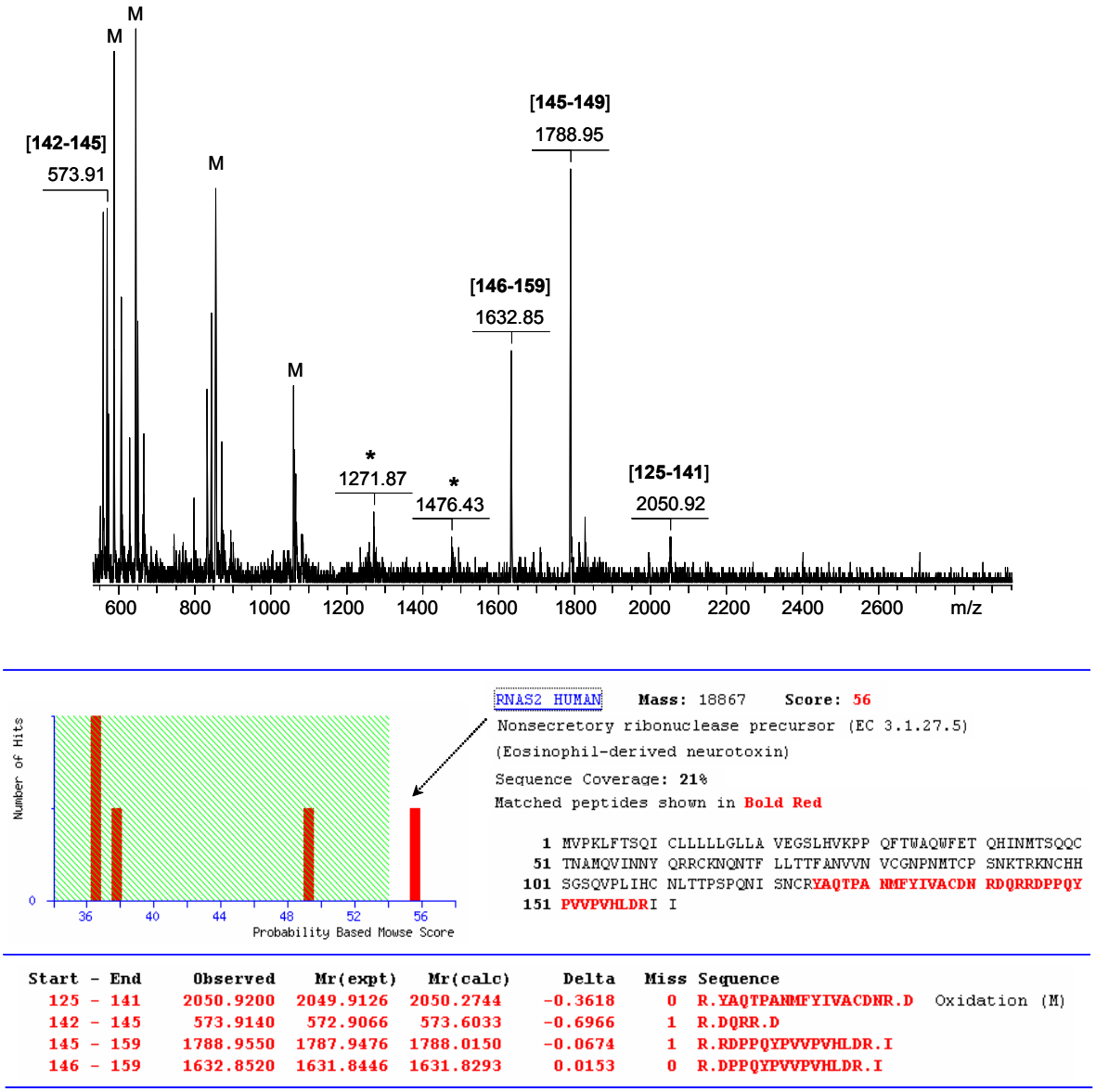

Figure 45: *Identification of eosinophil-derived neurotoxin (band 1) by MALDI-TOF peptide mass fingerprinting. The measured peptide masses of tryptic digested EDN were used for Database search using MASCOT search engine and NCBInr Database. 4 tryptic peptides were directly identified from MALDI-TOF mass data and they covered 21 % of the protein sequence (shown in red).*

Theoretical tryptic peptide fragments provided by the GPMAW program (s. Appendix 4) showed that due to low abundance of Arg and Lys residues in EDN the resulting peptides comprised masse only over 1600 Da, for which a low recovery from the gel matrix may result. The masses observed below 500 Da are usually covered by the most popular α-cyano-4-hydroxycinnamic acid (4-HCCA) matrix used for MALDI-TOF sample preparation which appears generally to give matrix-cluster peaks till the mass region covered by enzyme-digested peptides (i.e., m/z above ~ similar 1000) [197]. When an analyte mixture is very dilute and/or the sample contains a large amount of salts, ion peaks from matrix clusters can be quite intense, compared to peptide peaks. This matrix-cluster interference becomes more pronounced as the amount of analyte decreases (s. Figure 45).

2.2.3.3 Identification of *in vivo* nitration in Eosinophil cationic protein

The identification of nitrated tyrosine residue in ECP and EDN directly after SDS-PAGE separation using “bottom up” approach was found difficult and was hampered by low levels of modifications in eosinophil proteins. To provide specific structural identification of nitration in ECP and EDN, a new proteolytic affinity-mass spectrometric approach was developed as described in paragraph 2.1. The procedure is analogue to epitope extraction, as described in previous studies [122, 124].

For the identification of nitrated tyrosine site in ECP and EDN, a antibody against 3-nitrotyrosine was employed in a proteolytic affinity extraction-MS “PROFINEX” approach for direct identification of specific nitrated sites in eosinophil granule proteins (s. Figure 9). For this purpose, an immobilized antibody column was prepared. The monoclonal anti 3-NT antibody (dissolved in coupling buffer (0.2 M $NaHCO_3$, 0.5 M NaCl, pH 8.3) were added to dry NHS-activated 6-aminohexanoic acid-coupled Sepharose. After 2 h, the mixture was loaded into a microcolumn and extensive washing and blocking steps were carried out. Afterwards, the column was ready to be used for 3-nitrotyrosine peptide extraction experiments.

The specific binding of 3NT antibody (MAB5404, s. Experimental Part) employed in this study was previously proved (s. paragraph 2.4)

The first 6 ml of the wash fractions obtained after immobilization of the antibodies on NHS-activated Sepharose were collected in three different eppendorf tubes and lyophilised. After acetone precipitation for 4 hrs they were analysed by 1D-gel electrophoresis in order to check the possible loss of anti 3-nitro-tyrosine antibody by an incomplete coupling with NHS-activated Sepharose. 5 µg of 3-NT mAb stock solution were compared with the wash fraction divided in three parts. The fade band that can be distinguished in the wash 1 indicates that no significant 3NT antibody (>95%) remained unbound after immobilization on the Sepharose (s. Figure 46).

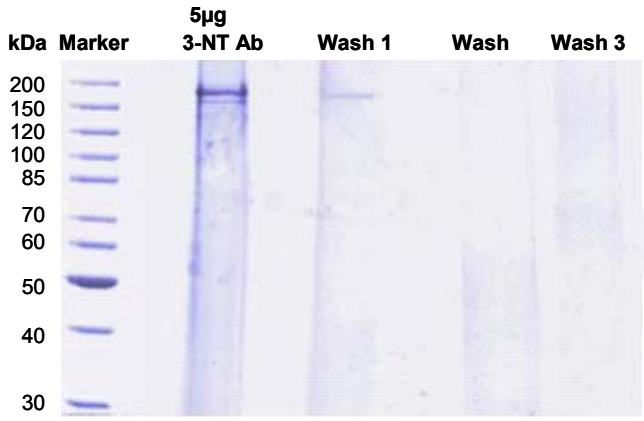

Figure 46: *SDS-PAGE of 3-NT mAb (MAB5404). 5µg stock solution of 3-NT mAb is compared with the first 6 ml of wash fraction collected after its immobilization on Sepharose.*

The specific binding of 3NT antibody (MAB5404, s. Experimental Part) employed in this study was previously proved (s. paragraph 2.4)

For the proteolytic affinity extraction-MS experiments, the isolated eosinophil cationic protein from patients with abnormal elevate number of eosinophil in blood, was first denatured in order to disrupt disulphide bonds by using DTT and IAA. In solution digested by trypsin was performed at 37^{o}C and after 4 hrs the reaction was quenched by adding 1mM HCl (hydrochloric acid). The tryptic peptides mixture was redisolved in PBS buffer and then added on the column. The column was incubated for 2 hrs at room temperature. Due to the high specificity of the 3NT antibody for the antigen,

only peptides containing the antigenic determinant (the 3-nitro-tyrosine) should interact with the antibody. In the next step the non-bound peptides were removed by washing the column using PBS buffer (supernatant fraction) and the immune complex was dissociated by addition of 0.1 % TFA. The supernatant, wash (last ml of wash) and elution fractions were collected, lyophilised and after desalting by using ZipTip C_{18} were analysed by mass spectrometry. The PROFINEX – MALDI-TOF mass spectrometric data is summarised in Figure 47. The unbound tryptic peptide contained in the supernatant fraction were analysed by MALDI-TOF (Figure 47A). All 4 tyrosine residues were found to be unmodified within the supernatant fraction (54% sequence coverage).

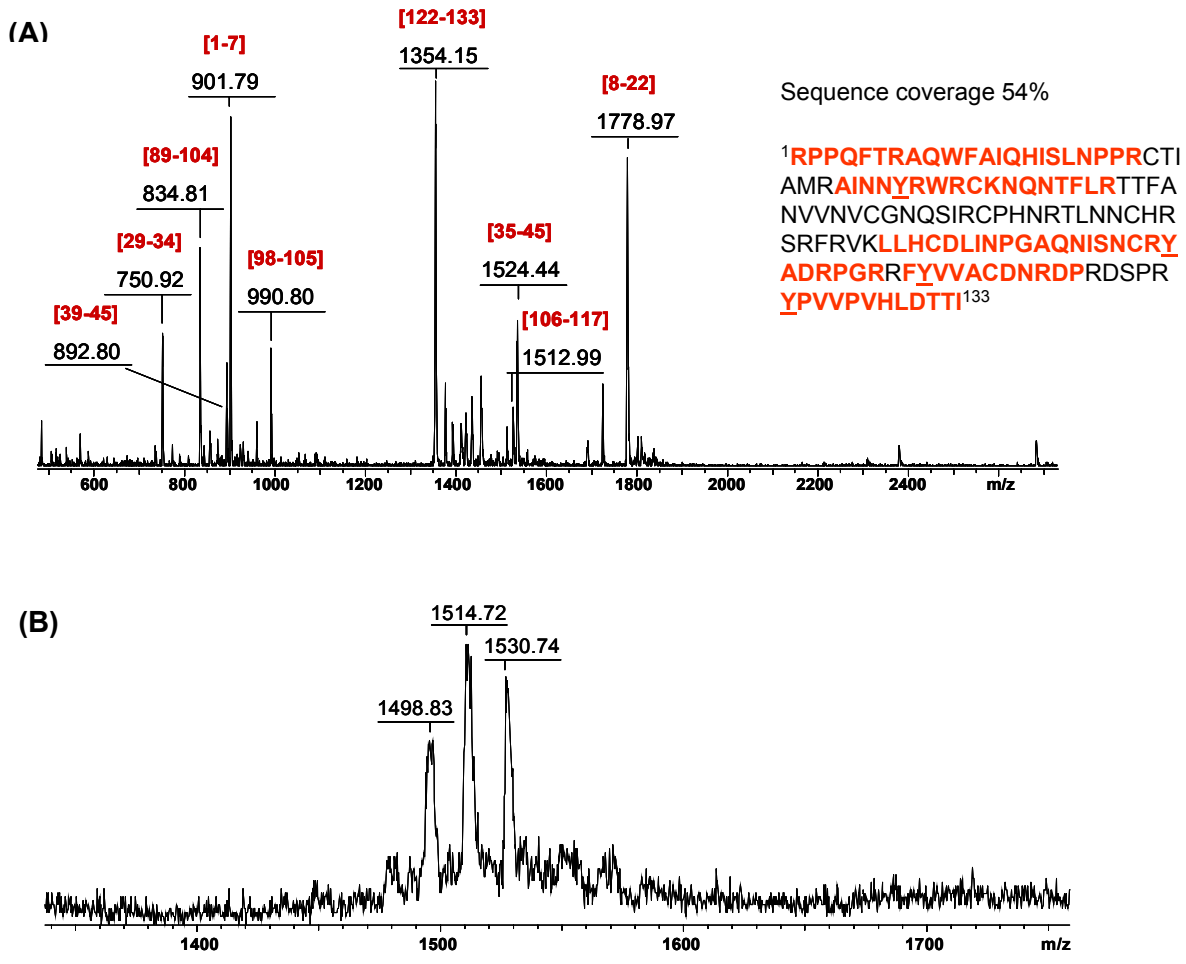

Figure 47: *PROFINEX-MALDI-TOF mass spectrometric data of (A) supernatant fraction and (B) elution fraction.*

Figure 47B shows the MALDI-TOF spectrum of the elution fraction which contained a nitrated peptide, ECP (23-34) tryptic peptide fragment, characterized by a specific photochemical decomposition using UV-MALDI laser radiation. Due to the low mass accuracy time of flight mass analyzer, the molecular ion mass could not be precisely ascertained by a comparison with the theoretical tryptic nitro-tyrosine containing peptide given in the GPMAW program. The unequivocal identification was obtained by high resolution nano-ESI-FT-ICR mass spectrometry. The corresponding mass spectrum of the eluted fraction is shown in Figure 48. The nano-ESI-FTICR spectrum yielded a major doubly protonated molecular ion at *m/z* 764.3618, corresponding to the eosinophil cationic protein ^{23}CTIAMRAINNY(NO$_2$)R^{34} peptide fragment, nitrated at Tyr-33. The monoisotopic mass of the singly charged molecular ion was determined after deconvolution of the ESI mass spectrum using the XMASS software and correspond to ECP (23-34) peptide fragment with a mass difference of 103 Da (45 Da for the nitro-group and 58 Da for Cys^{23} - carbamidomethyl formation).

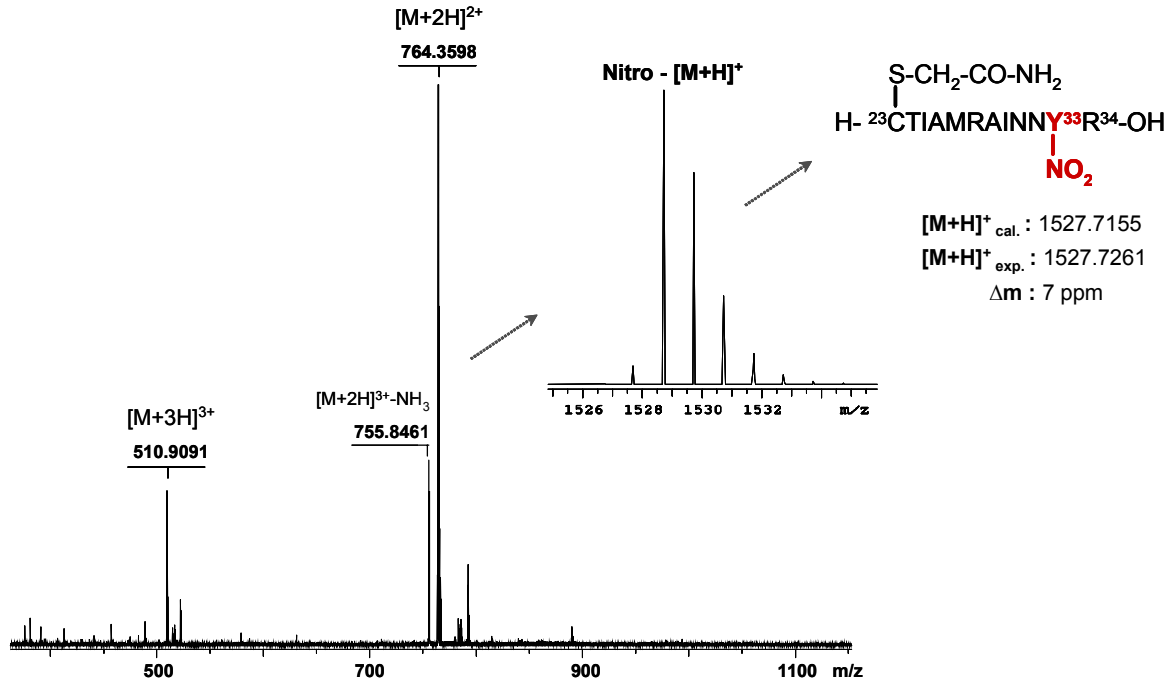

Figure 48: *Nano-ESI FTICR mass spectrum of the elution fraction containing the nitrated ECP (23-34) peptide fragment, with nitro-Tyr^{33} residue. The insert show the isotopic fine structure of the [M+H]$^+$ ion obtained by deconvolution.*

Additional proof for the nitrated (23-34) peptide sequence was obtained by MS/MS using infrared multiphoton dissociation (IRMPD) [198]. IRMPD fragmentation experiment was carried out after isolation of the most intensive doubly charged ion at m/z 764.3818. The b and y fragments ions obtained provided information about the unambiguous location of nitrated Tyr^{33} residue (s. Figure 49).

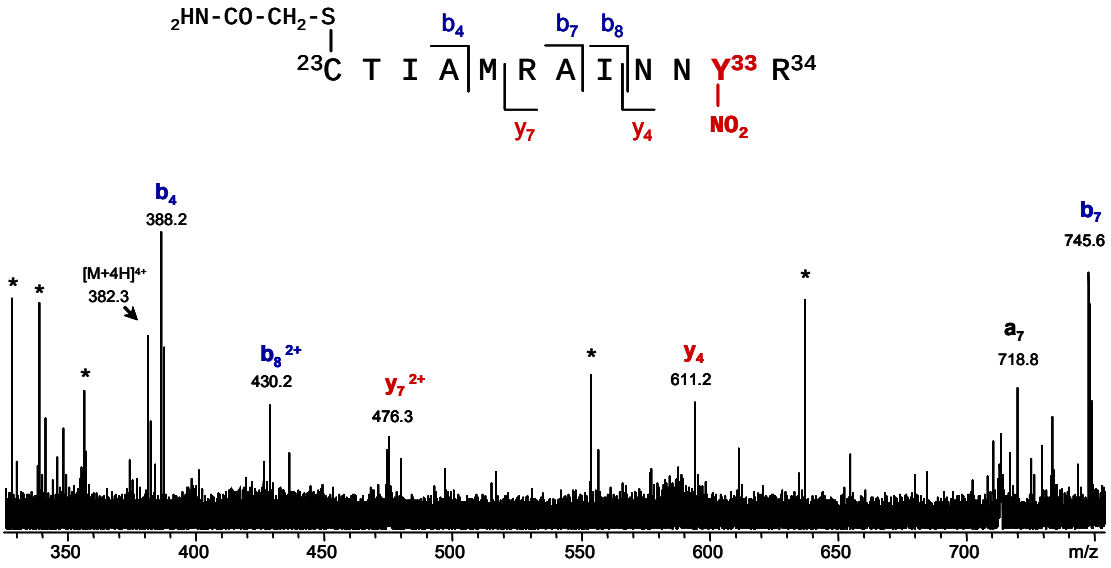

Figure 49: *ESI-FTICR-IRMPD tandem mass spectrum of $[M+2H]^{2+}$ ion corresponding to the nitrated ECP(23-34) peptide. The nitrated Tyr-33 residue was ascertained by y_4 and y_7 ions.*

The miss cleavage by Arg^{28} indicates that this arginine residue is part of an “epitope”-binding structure of eosinophil cationic protein only upon nitration of Tyr^{33}, since the same arginine residue was cleaved by trypsin in the non-nitrated Tyr^{33} containing ECP sequence (s. Figure 47A).

The spatial orientation of tyrosine residues in eosinophil cationic protein was deduced using its available crystal structure in Protein Data Bank (PBD accession number 1H1H) [199]. Using BallView 1.1.1 a molecular modelling program, the accessible surface area was rendering including different colours for tyrosine residues: yellow for Try^{33}, red Try^{98} Try^{107} Try^{122}, and green for all hydroxyl groups in

para position of the tyrosine residue (s. Figure 50). The solvent accessible surface (SAS) structure showed that Tyr^{33} residue of ECP has the highest surface accessibility, while the other three Tyr residues are embedded in the inner structure of the molecule. Moreover the hydroxyl group (-OH, in green) of theTry^{33} residue and implicit the two equivalent carbons CE1 and CE2 in the *ortho* position relative to the hydroxyl group, which are critical for allowing Tyrosine to be modified by nitration, extremely protrudes in the exterior space. The molecular SAS model shows that Try^{98} is completely orientate in the inner part and its hydroxyl group is not exposed to the surface, while for Try^{107} and Try^{122} the hydroxyl group and the two equivalents CE1 and CE2 appear relatively exposed to the surface.

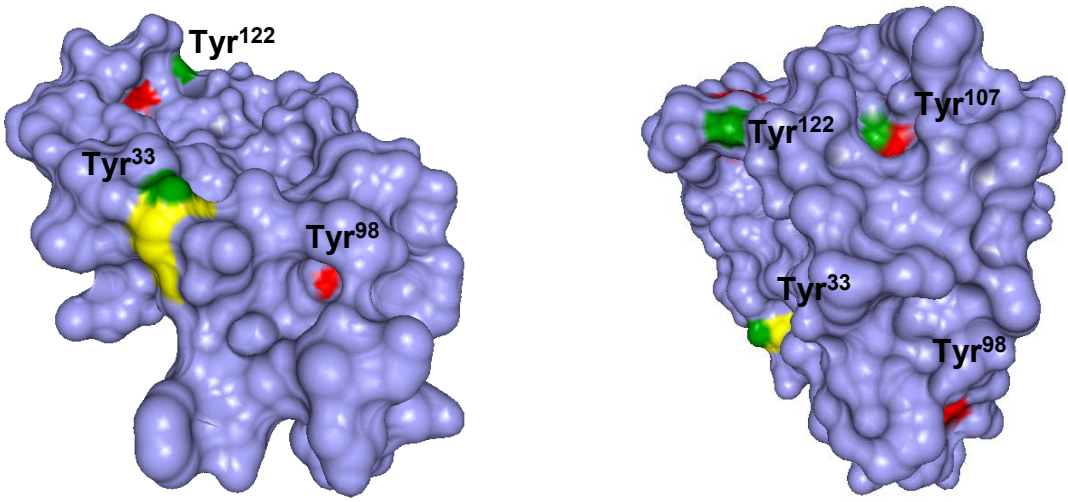

Figure 50: *Modelling structure of ECP indicating the accessible surface area of ECP .The model structures were rendered using BallView 1.1.1 program based on the available X-Ray crystal structure of the ECP (PDB entry 1H1H).The location of all four tyrosine residues are indicated by colours as follows yellow -Tyr^{33}, red - Tyr^{89}, Tyr^{107}, Tyr^{122}, green –OH groups of Tyr residues.*

.

2.2.3.3.1 Characterization of the nitrated ECP model peptides binding to the anti 3-nitrotyrosine antibody

Based on the results obtained by identification of the nitration site of eosinophil cationic protein, a major goal for further studies was to identify the factors which may determine the selectivity of the *in vivo* eosinophil nitration.

To this purpose, nitrated model peptides comprising all four tyrosine residues in ECP protein sequence were synthesized, purified and analyzed by mass spectrometric as described in the Experimental Part. Table 7 shows the analytical characteristics of synthetic ECP nitro-tyrosine peptides; the specific HPLC retention time and the molecular ions mass recoded by MALDI-TOF –MS. To investigate the binding of nitrated tyrosine containing peptide to the monoclonal anti 3-nitro tyrosine (MAB5404) antibody employed in the immunoaffinty - MS of ECP, an indirect ELISA method was developed. A detailed description of the experimental conditions of the ELISA using CovaLink plates is given in the Experimental part. CovaLink NH is a polystyrene surface grafted with secondary amino groups (– NH –) which serves as a matrix-ligand for covalent coupling.

Table 7: *RP-HPLC and MALDI-TOF-MS data of synthetic ECP peptides*

Peptide No.	Code	Sequence	Nitration site	HPLC R_t (min)[a]	$[M+H]^+$ calculated / found[b]
1	ECP_1	^{28}AINNYRWRCL^{38}	Nitro-Y^{33}	17.58	1367.65 / 1368.81
2	ECP_2	^{92}NISNCRYADR^{101}	Nitro-Y^{98}	15.57	1255.53 / 1256.75
3	ECP_3	^{101}RPGRRFYVVA^{110}	Nitro-Y^{107}	18.07	1265.68 / 1266.57
4	ECP_4	^{118} DSPRYPVVPVHL^{129}	Nitro-Y^{122}	14.25	1423.73 / 1424.61

[a] RP-HPLC column: Polymer -PLRP (250 x 4.6 mm, 300Å, 5µm); 365 nm.
[b] MALDI-TOF mass spectra were recorded with a Bruker Biflex™ linear TOF mass spectrometer equipped with an UV-MALDI source.

In the indirect ELISA, 3-nitrotyrosine ECP peptides were immobilised on CovaLink plates and then the monoclonal 3-NT antibody was added. A secondary peroxidase-conjugated antibody and OPD/H_2O_2 substrate were added and the absorbance was measured on a Wallac 1420 Victor^2 ELISA Plate Counter at 450 nm. To compare the binding of nitrated ECP peptides to the monoclonal anti 3-nitrotyrosine antibody, the maximum response was considered for all peptide as 100% and then the concentrations needed for obtaining an half maximum binding (OD_{450} = 50%) were determined. The ELISA data showed that nitro-Tyr^{33} containing peptide (ECP_1) bound to the monoclonal 3-NT antibody with higher affinity than the other nitro-tyrosine ECP-peptides, suggesting that the affinity differences between these peptides were due to the sequence environment of the nitrated tyrosine residue (s. Figure 51).

As shown in Figure 51A the highest binding intensity of nitrated EPC_1 peptide to the monoclonal anti 3-nitrotyrosine antibody correspond to 0.082 µM (lowest amount of peptide to obtain an OD_{450nm} = 50%. Figure 51B represent a zoom in of the region with maximum binging for the other nitro-tyrosine ECP peptides. The maximum binding responses of nitrated EPC_4 peptide and nitrated EPC_3 to the monoclonal anti 3NT antibody correspond to 0.31 µM and 0.85 µM respectively, while nitrated EPC_2 peptide corresponding Tyr^{98} which is completely buried in the protein structure give no significant interactions with the antibody.

The hypothesis from this study was that the anti 3-nitrotyrosine antibody recognises a specific sequence motif comprising several amino acids in the vicinity of the nitro-tyrosine residue.

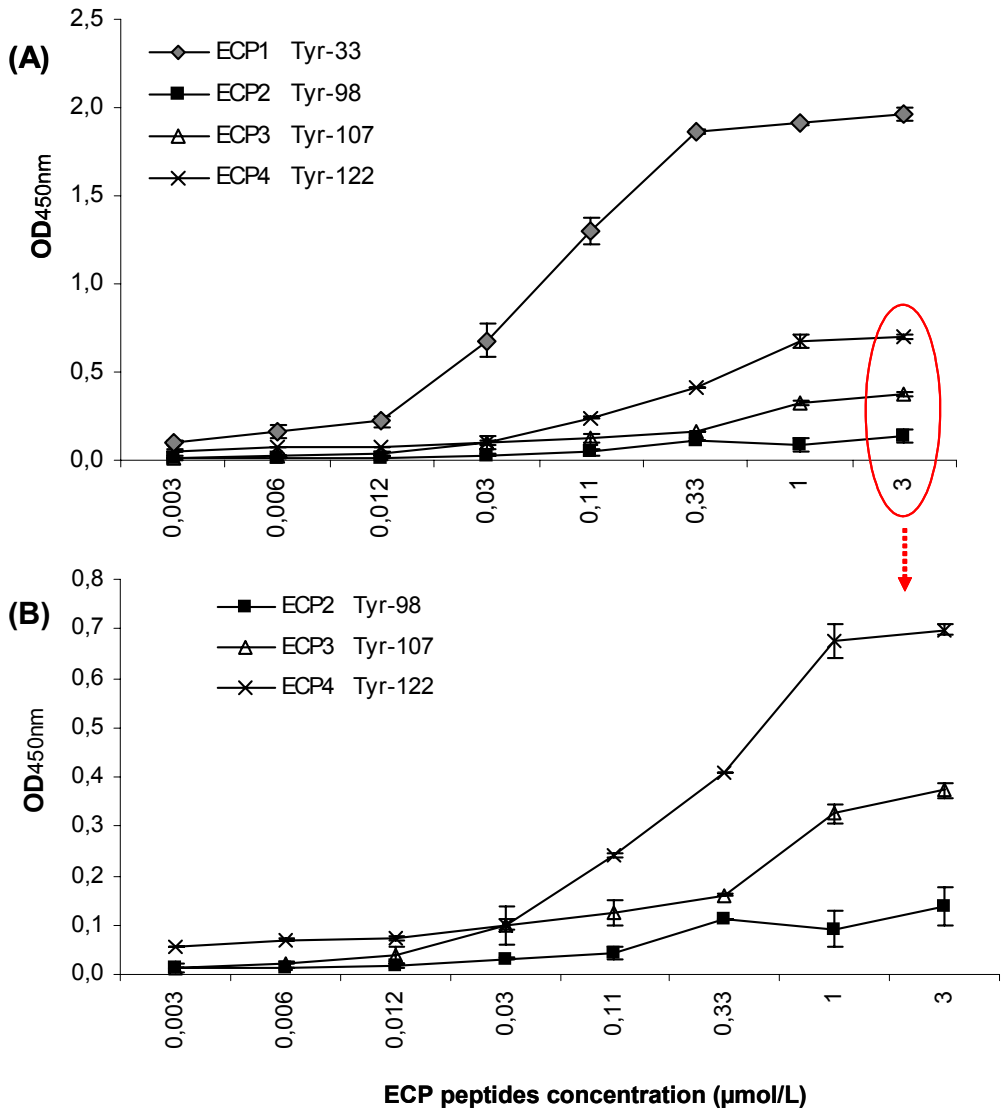

Figure 51: *Binding of ECP nitrated tyrosine–containing peptides to the m 3NT antibody (MAB5404) as measured by indirect ELISA. Background signals obtained by measuring the direct absorbance of 3NT antibody on the plate without using peptides antigen have been substracted.*

2.2.3.3.2 Conformational characterisation of nitrated ECP peptides by CD spectroscopy

It is known that antigen – antibody interactions are conformation-dependent, thus the determination of conformational preferences of a protein sequence that becomes nitrated at a tyrosine residue represents an important feature in their immunoaffinity characterization. From known X-Ray crystal structure (PDB accession number 1H1H) of eosinophil cationic protein, a ribbon structure was obtained using the BallView 1.1.1 program, and the four tyrosine residues are represented in the structure. The ribbon structure showed that Tyr^{33} and Tyr^{122} are located in a turn, while Tyr^{98} and Tyr^{107} are located on the same β-sheet. Moreover, the Tyr^{33} residue of ECP is surface exposed, while the other three tyrosine residues are oriented towards the inner structure of the molecule (s. Figure 52).

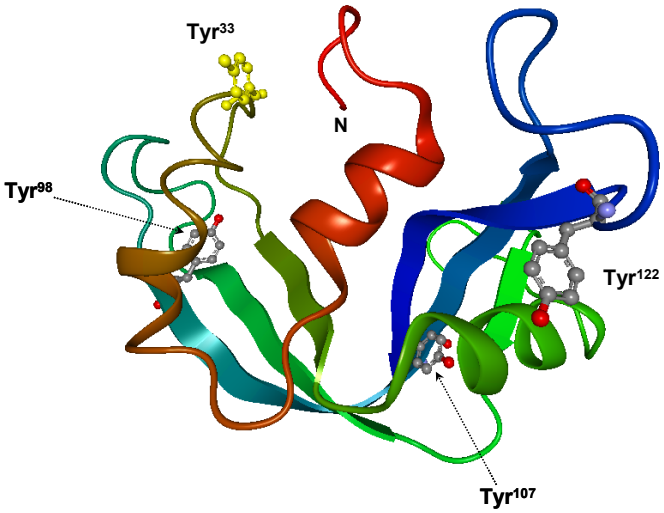

Figure 52: *Ribbon diagram of the human eosinophil cationic protein (ECP) based on the X-Ray crystal structure (PDB accession number 1H1H). The figure was rendered using the program BallView 1.1.1 and the localization of all four tyrosine residues within the secondary ECP structure is indicated.*

In order to obtain information about the structure of the synthetic nitrated ECP peptides, molecular dynamic simulations using the HyperChem 6.0 software were carried out. AMBER96 parameters were applied for the geometry optimization. The calculations were performed taking into account the presence of water molecules. The structures modelling of the nitrated ECP peptides are shown in Figure 53. According to these results the ECP_2 (B) and ECP_4 (D) peptides are more flexible molecules having an open structure, in comparison with ECP_1 (A) and ECP_3 (C) which are more compact.

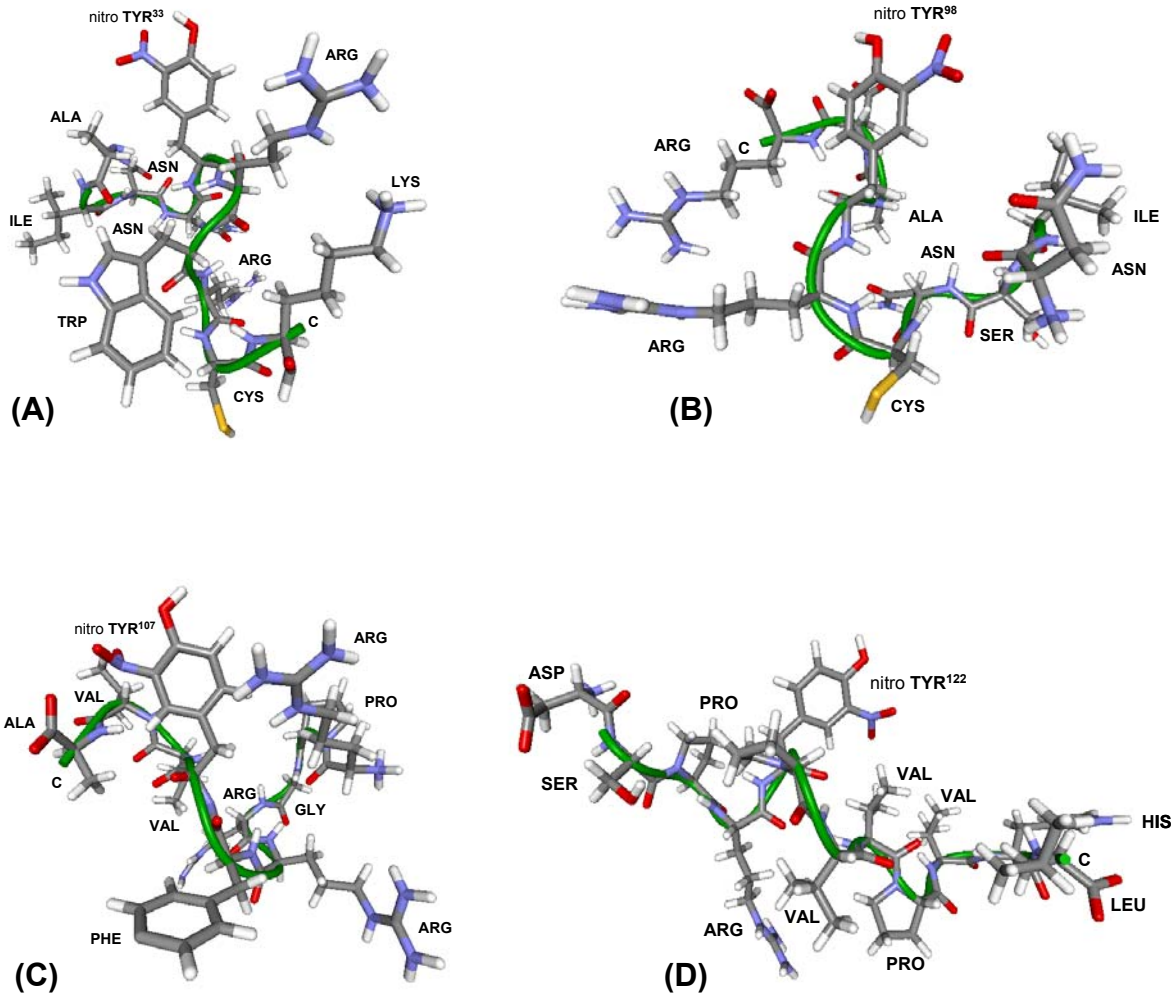

Figure 53: *Structural modelling of (A) ECP_1, (B) ECP_2, (C) ECP_3, (D) ECP_4 nitro-tyrosine peptides. The adopted nonregular secondary structure (random coil) of each peptide is indicated in green.*

The conformational preferences of the synthetic ECP nitrated tyrosine containing peptides were studied by CD spectroscopy. Spectra were recorded in water and in trifluoroethanol, which stabilizes peptide and proteins in ordered conformation (s. Figure 54). The CD spectra of nitro-Tyr ECP peptides in water are characterised by the presence of a negative band below 200 nm, and a less intensive positive band at approximative 220-225 nm, which are indicative for a random coil conformation (s. Figure 54A). The ECP_1- Tyr^{33} exhibits the lowest ellipticity in water. Interestingly, in TFE, the nitro-Tyr ECP peptides adopt different conformations (s. Figure 54B). The nitro-Tyr^{33} (ECP_1) peptide showed the most ordered conformation characterised by an intensive positive band at 188 nm and a broad negative band around 208 nm. In the presence of TFE, ECP_2 and ECP_3 peptides adopt an ordered structure, which is close to the theoretical helix shape, whit the positive band (π - $\pi^*_{perpendicular}$ transition) shifted to ~186 nm, the first negative band shifted (π - $\pi^*_{parallel}$ transition) around 200-204 nm and the second negative band (n - π^* transition) shifted toward higher wavelength (ca. 228 nm) and showed increased intensity. The ECP_4 peptide did not show any significant conformational changes in the presence of TFE; it adopts a random coil conformation in both water and TFE. The CD spectra in water demonstrates that the nitrated ECP peptides may not adopt the corresponding conformation as in the ECP protein sequence, while in TFE the peptides tend to mimic the natural conformation, demonstrating that TFE does not induce helix conformation arbitrarily, its just enhances the existing propensity.

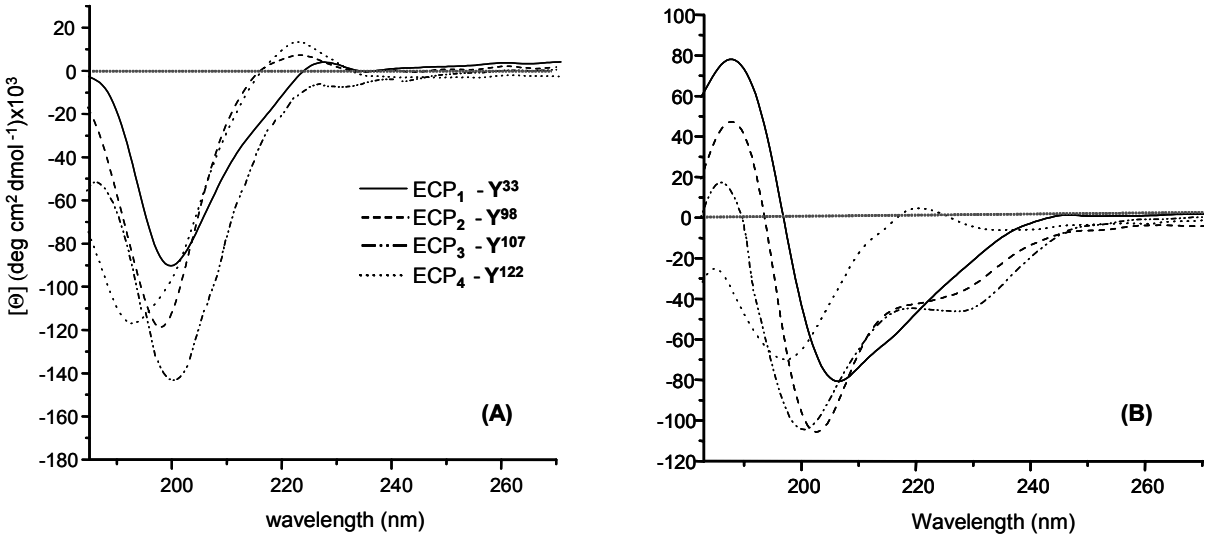

Figure 54: *CD spectra of synthetic nitro-tyrosine ECP peptides in MilliQ (A) and 100% trifluoroethanol (TFE) (B).*

In conclusion, major factors which direct the selectivity of protein nitration are specific primary structure and conformation. The Tyr^{33} is located (i) in a flexible sequence containing turn inducing residues, and (ii) no cysteine, histidine and methionine are in its close vicinity (s. Figure 53A), residues which may be alternative targets for the reaction with RNS, are two important factors which promotes specific nitration of Tyr^{33} in eosinophil cationic protein.

2.2.3.4 Identification of *in vivo* nitration in Eosinophil-derived neurotoxin

For the identification of nitrated tyrosine residue(s) in Eosinophil-derived neurotoxin (EDN) an identical immunoaffinity antibody column was employed as for the eosinophil cationic protein. The same immunoaffinity-MS approach was used for the identification of 3-nitrotyrosin residue in EDN, however trypsin was replaced by thermolysin due to the low number of Arg and Lys residues as shown in Figure 42 and Appendix 4. Thermolysin is a thermostable extracellular metallo-endopeptidase containing calcium and zinc as cofactors, which hydrolyzes peptide bonds at the N-terminal side of hydrophobic amino acid residues with low cleavage specificity;

therefore, it produces a number of short fragments that are suitable for MS and Edman sequencing. The pH optimum is 8.0 and the optimal temperature for activity is 70 °C. In order to obtain longer peptide fragments, the thermolysin digestion in solution was performed at 70°C for a shorter time (4 hrs) using an enzyme**:** substrate ratio of 1:50.

The digestion mixture was added to the Sepharose-3NT immobilised antibody and after removing the non-bound fragments by washing steps; the elution was performed with 0.1% TFA. The supernatant fraction (non-bound peptide fragments) was analysed by MALDI-TOF mass spectrometry (s. Figure 55). Database search using MALDI-TOF mass data could not be performed since thermolysin does not exist as an entry in the Database search. The resulted peptide fragments were compared with the theoretical EDN peptide masses using the GPMAW program, and 52% of the sequence was identified as shown in Figure 55.

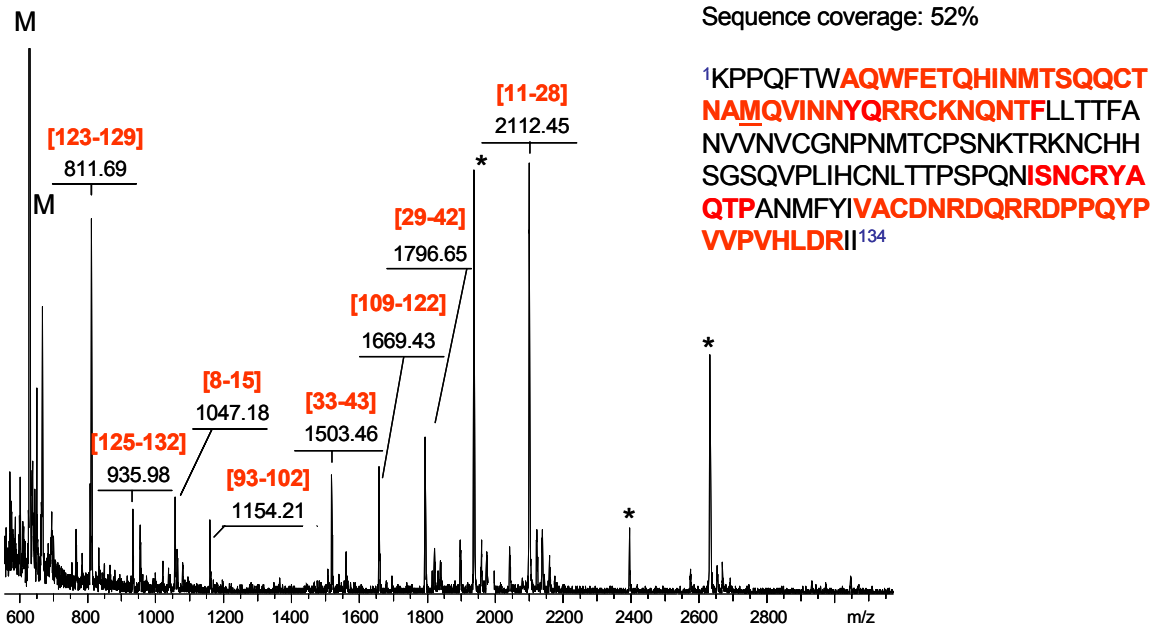

Figure 55: *MALDI-TOF mass spectrum of non-bound thermolysin peptides fragments (supernatant fraction) of eosinophil-derived neurotoxin-PROFINEX-experiment. The insert shows the thermolysin peptide fragments which covered 52% of EDN sequence. The sequence coverage was determined using the resulted peptides after a theoretical digestion in GPMAW program.*

The elution fraction was directly analyzed by nano-ESI-FTICR MS. The spectrum in Figure 56 showed a single peptide with most abundant multiply (doubly, triply and quadruply) protoneted molecular ions. The peptide was identified as EDN - ^{29}VINNY(NO_2)QRRCKNQNTF^{43} peptide fragment nitrated at Tyr^{33} residue. The monoisotopic mass of the singly charged molecular ion was determined after deconvolution of the ESI mass spectrum using XMASS software and correspond to EDN- (29-43) peptide fragment with addition of 45 Da for the nitro-group at Try^{33}, and 58 Da for carbamidomethyl derivatization of the Cys residue.

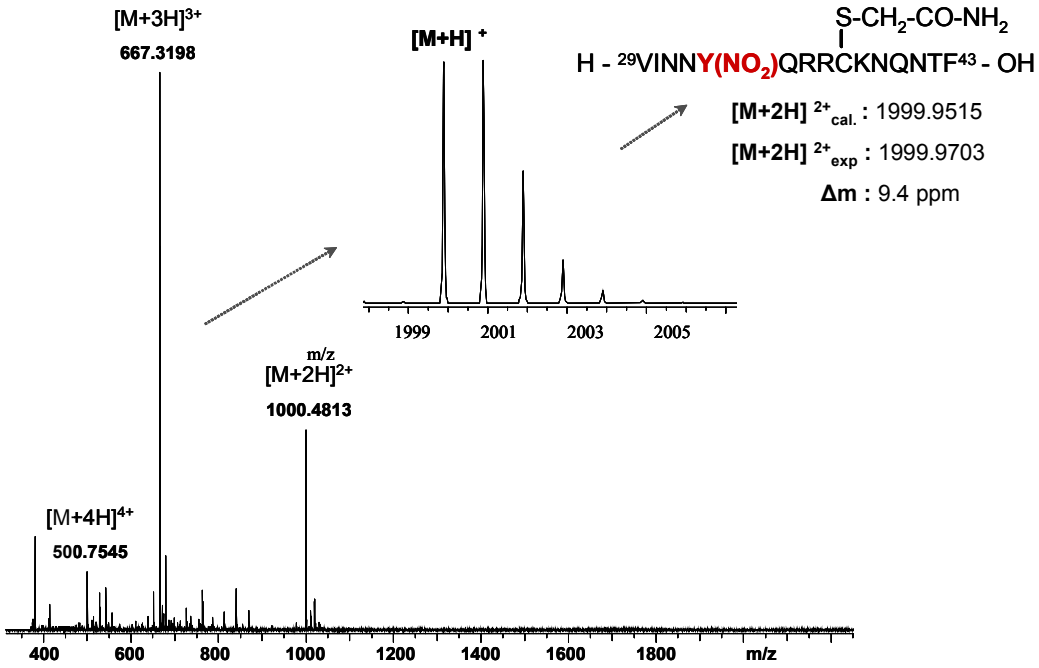

Figure 56: *Nano - ESI FTICR mass spectrum of the elution fraction containing the nitrated EDN (29-43) peptide fragmnent, with nitro-Tyr^{33} residue. The insert show the isotopic fine structure of the [M+H]$^+$ ion obtained by deconvolution.*

An alternative technique to identify the site of tyrosine nitration of EDN was Edman degradation (s. the Experimental section). A second PROFINEX –MS experiment was performed using 200 µg of EDN and the elution fraction was desalted and concentrated by ZipTip C18 pipette micro-tips and then subjected to N-terminal sequence analysis. The HPLC chromatograms of two PTH-amino acids released during Edman degradation of the elution fraction are shown in Figure 57. A standard

mixture of 19 PTH-amino acids (except cysteine and nitro-tyrosine) was injected onto the column for separation as the standard cycle of the sequencing run (s. Figure 57). The retention times of the amino acids from this chromatogram are used to identify the amino acids in the sequencing cycles. Unmodified cysteine cannot be analyzed by Edman sequencing due to the labile side chain and highly reactive sulfhydryl group which leads to a blank cycle where a cysteine should be and possible blockage of the N-terminal end. However, the sequencing of carbamidomethylated cysteine comprised in EDN (29-43) produces two products with the same retention time as Glu and Ser.

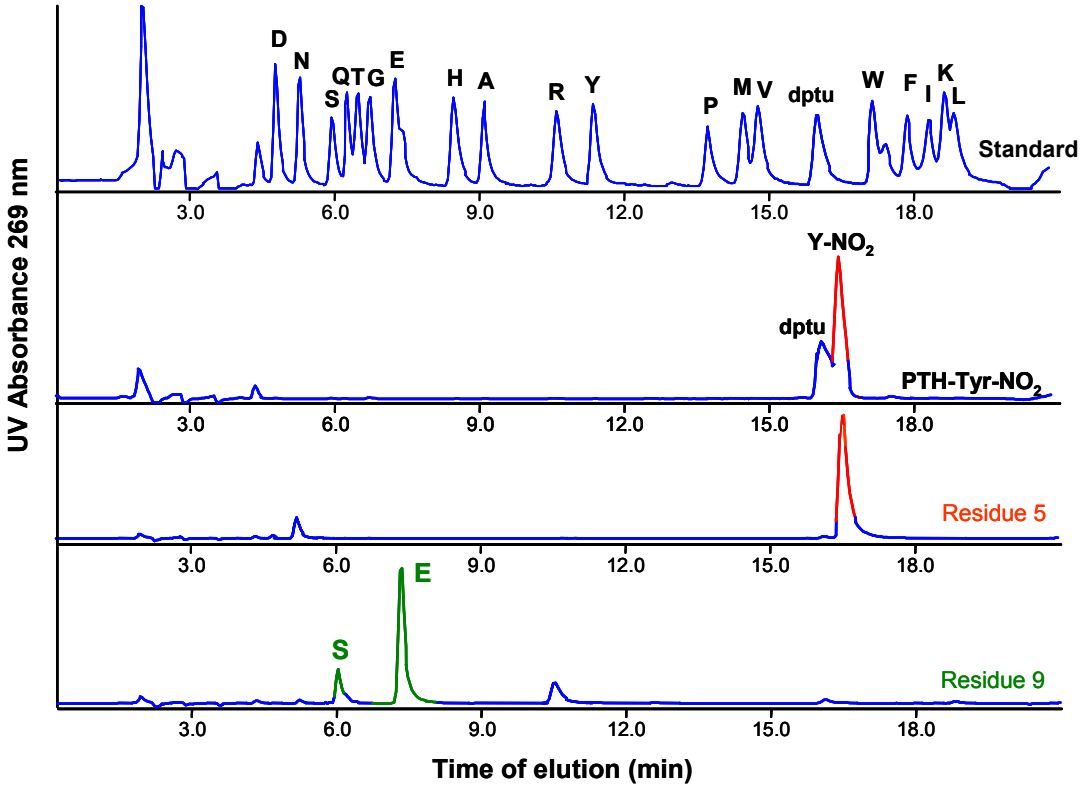

Figure 57: *Edman sequencing elution profiles of bound EDN (29-43) thermolysin peptide fragment (PROFINEX-elution fraction). (A) Standard amino acids, (B) PTH- 3-nitro-tyrosine amino acid, (C) Elution peak of residue number 5 correspond to 3-nitro-Tyr[33], (C) Elution peaks for residues number 9 (cysteine derivatized to carbamidomethyl) obtained as a mixture of components with the retention time of Ser, Glu.*

Since no nitro-tyrosine was included in the standard cycle, in order to identify the retention time of the PTH-nitro-tyrosine, the pure nitro-Tyr (440 pMol) was subjected to a separate sequencing run consisting of one single sequencing cycle (s. Figure 57). The fifth sequencing cycle corresponds to the nitro-tyrosine residue and the mixture of serine and glutamate was obtained for residue 9, the carbamidomethyl derivatized form of cysteine (s. Figure 57 C and D).

By means of Edman degradation followed by quantitative analysis of the PTH-derivatives amino acids was also possible to estimate the amount of the 3-nitro-tyrosine modification in EDN (s. Figure 58). The estimation of tyrosine nitration level was determined by analysis of the initial and repetitive yields in each sequencing cycle. The initial yield (typically 50-80%) refers to the quantity of amino acid recovered in the first cycle of the Edman chemistry and is expressed as a percentage of the total sample analyzed. The repetitive yield, typically 90-99%, represents the recovery of the PTH amino acid after each cycle of the chemistry, and is dependent on the instrumentation as well as the individual characteristics of the sample.

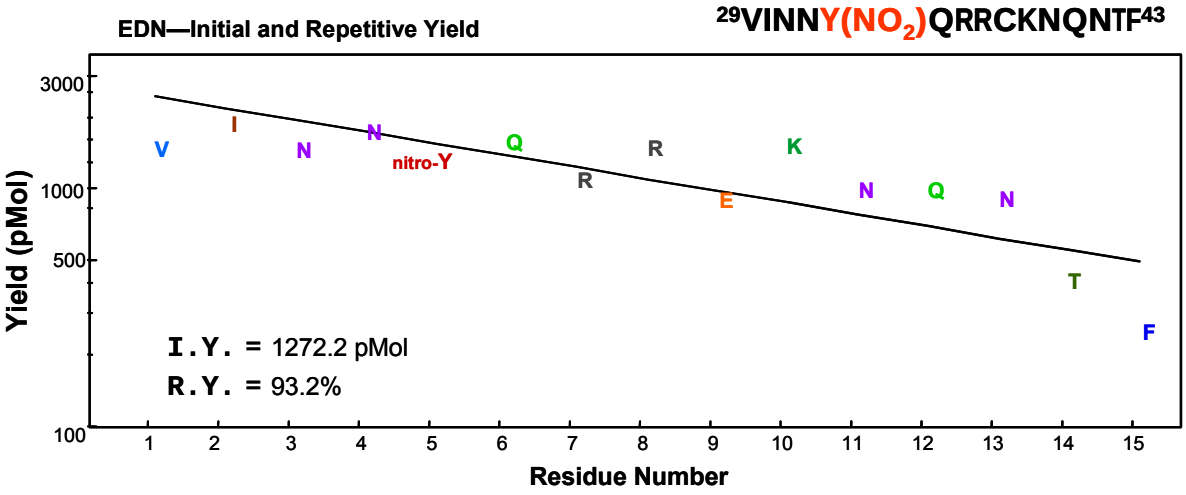

Figure 58: *Quantitative analysis of nitrated (29-43) EDN peptide using the initial and the repetitive yield by Edman sequencing.*

The apparent quantification was calculated from the amount of nitrated peptide sequenced by Edman degradation. Using 13 nM of EDN ca. 1.27 nM of nitrated Tyr^{33} peptide was determined by Edman sequencing; this represents approximative 10 %

nitration of the eosinophil – derived neurotoxin. For ECP a higher percent of 3-nitro tyrosine containing peptide was calculated, results which confirmed the western blot experiments, where the ECP showed much more intensive positive response than EDN.

Table 8: *Quantitative estimation of nitro-tyrosine containing peptides in ECP and EDN by Edman sequencing*

Nitrated Protein	Sequence	Nitration site	Amount of nitro-tyrosine peptide*
Eosinophil cationic protein	^{23}CTIAMRAINN**Y**R^{34}	*Tyr^{33}*	17
Eosinophil-derived neurotoxin	^{29}VINN**Y**QRRCKNQNTF^{43}	*Tyr^{33}*	10

** % of eosinophil proteins determined using the initial and the repetitive yield by Edman sequencing.*

For comparison with eosinophil cationic protein the spatial orientation of the tyrosine residues in eosinophil-derived neurotoxin protein was deduced using the crystal structure from Protein Data Bank (PBD accession number 1GQV). Due to only 67% sequence homology, the ribbon modelling structure shows that Tyr^{33} in EDN is part of a helix conformation, while the other three tyrosine residues remain at the same position (s. Figure 59). Using BallView 1.1.1 program, the accessible surface area was determined for all tyrosine residues (Try^{33}, red Try^{98} Try^{107} Try^{122}). The solvent accessible surface (SAS) structure showed that Tyr^{33} residue with its hydroxyl group (-OH, in green) and the two equivalent carbons CE1 and CE2, as in ECP, has the highest surface accessibility, followed by Try^{123} and Try^{98}. The Try^{107} is completely embedded in the inner protein structure.

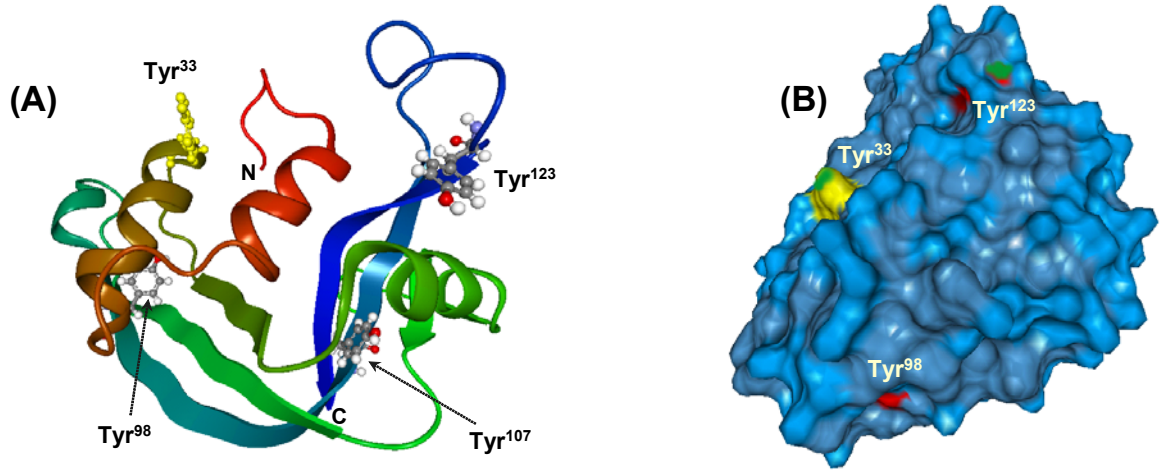

Figure 59: *Modelling structure of EDN indicating the location of all four tyrosine residues. (A) Ribbon diagram of eosinophil-derived neurotoxin. (B) Solvent surface accessibility (SAS) of EDN; the location of surface exposed tyrosine residues are indicated by colours as follows: yellow for Tyr^{33}, red for Tyr^{98} and Tyr^{123} and green for hydroxyl group of tyrosine. The model structures were rendered using BallView 1.1.1 program based on the available X-Ray crystal structure of the EDN (PDB entry 1GQV)*

In summary, the proteolytic affinity-mass spectrometry approach was shown as a highly efficient tool for the molecular identification of nitration sites in eosinophil proteins. Edman sequencing analysis confirmed all results and provided a quantitative estimation for the nitro-tyrosine modification in Eosinophil toxins.

2.3 Synthesis and mass spectrometric characterization of nitrated peptides

2.3.1 Solid phase peptide synthesis of nitrated tyrosine peptides

Following the identification of tyrosine nitration (Tyr-430 residue) in vicinity of the catalytic site of bovine Prostacyclin synthase, model peptides comprising the sequence LKNY were constructed. Several model peptides containing both unmodified tyrosine and 3-nitro-tyrosine residues were synthesized by solid-phase peptide synthesis (SPPS) using 9-fluorenylmethoxycarbonyl (Fmoc), a base labile α-amino protecting group and the standard side chain protection chemistry [200], [201].

The first peptide synthesised by SPPS using Fmoc chemistry was the nitrated PCS ^{427}LKN**Y**$(NO_2)^{430}$ peptide fragment. This peptide was synthesised on a semi-automated peptide synthesiser on NovaSyn® TGR resin (s. Figure 60 A) with a capacity of 0.27 mmol/g using the following N-α-protected amino acids Fmoc-Leu-OH, Fmoc-3-nitro-Tyr-OH and the side chain protected amino acids derivatives: Fmoc-Lys(Boc)-OH, Fmoc-Asn(Trt)-OH. NovaSyn® TGR resin is prepared from NovaSyn® TG amino resin by derivatization with the modified Rink linker, which is designed to release peptide amides upon the final cleavage.

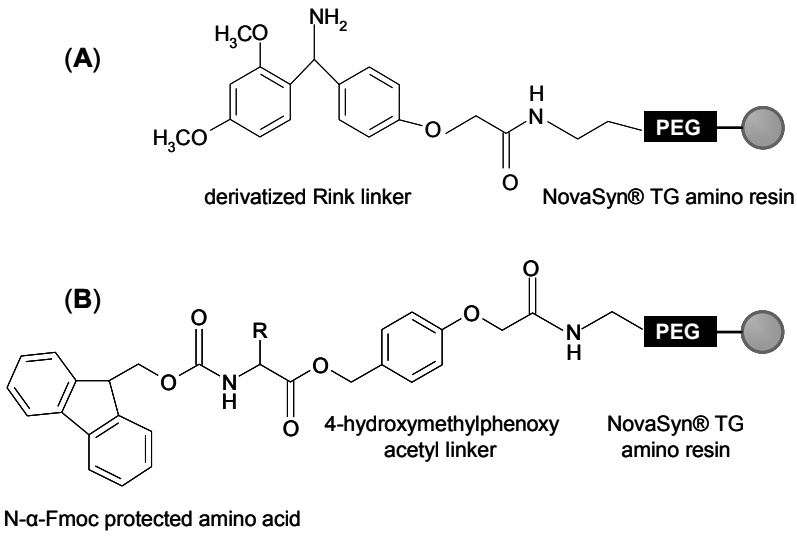

Figure 60: *Schematic representation of resins used for peptide synthesis (A) NovaSyn® TGR resin and (B) N-α-Fmoc protected amino acids preloaded NovaSyn® TGA resin.*

The C-terminal amino acid residue of the target peptide was first activated to an active ester species using PyBOP (benzotriazol-1-yl-oxy-tris-pyrrolidinophosphonium hexafluorophosphate) in the presence of NMM (*N*-methylmorpholine) and then attached to the resin via its carboxylic group. To begin each further coupling, the Fmoc group on the resin bound amino acid was removed with 20% piperidin in N, N-dimethyl formamide (DMF). It was then rinsed and an N-α-protected amino acid preactivated at its *alpha* carboxyl group was added onto the reaction column. The activated amino acid and the resin bound amino acid were allowed to react in the presence of base to form a new peptide bond. The deprotection / coupling cycles were repeated four times for each new amino acid until the desired peptide sequence was assembled at the resin. Extensive washing with DMF was performed after each step in order to remove excess of reagents and by-products. Once the peptide sequence was complete a final N-α-Fmoc deprotection was performed in order to release an N-terminal free (-NH_2) peptide. The peptide was then ready to be cleaved from the resin simultaneously with the removal of the side chain protecting groups. This reaction was accomplished using a mixture of trifluoroacetic acid (TFA) and scavangers such as triisopropylsilane (TIS), or ethanedithiol (EDT), which serve to neutralize all the cations formed during the removal of the side chain protecting groups.

After cleavage from the resin, the nitrated ^{427}LKN**Y**(**NO_2**)^{430} (**1**) was precipitated with *t*-butylmethyl-ether, washed with diethyl ether and dissolved in 5 % acetic acid prior to freeze-drying. Crude products were characterized by analytical RP-HPLC and MALDI-TOF and if necessary purified by preparative (RP-HPLC) (s. Table 9 and Figure 61).

Table 9: *RP-HPLC and MALDI-TOF-MS data of synthetic PCS peptides fragments.*

No.	Peptide code	Sequence	RP-HPLC Rt (min) [c]	MALDI-TOF $[M+H]^+_{cal./exp.}$ [d]
1	PCS_1[a]	H-LKN**Y(NO$_2$)-**NH_2	14.25	581.30/582.97
2	PCS_2-Y[a]	H-DFYKDGKRLKN**Y**SL-OH	15.27	1746.91 / 1747.72
3	PCS_2-Y-NO_2[a]	H-DFYKDGKRLKN**Y(NO$_2$)**SL-OH	16.08	1791.90 / 1792.96
4	PCS_2-(RR)[b]	H-DF**Y(NO$_2$)**KDG**R**RLKNYSL-OH	18.37	1819.90 / 1822.13
5	PCS_2-(Ala)[a]	H-DFYKDGKR**AAA**Y(NO$_2$)**A**L-OH	19.05	1633.79 / 1634.71
6	PCS_2-F[a]	H-DFYKDGKRLKN**F**SL-OH	18.52	1730.92 / 1732.71

[a] Tyr-430 of Prostacyclin synthase

[b] Tyr-421 of Prostacyclin synthase, Lys^{425} was replaced by an Arg

[c] RP-HPLC column: Vydac C_{18} (250x4 mm, 300Å, 5µm); 365nm for nitro-Tyr and 220nm for Tyr/Phe containing peptides

[d] MALDI-TOF mass spectra were recorded with a Bruker Biflex™ linear TOF mass spectrometer equipped with an UV-MALDI source

The analytical RP-HPLC chromatogram of nitrated PCS (**1**) peptide showed a major peak at 14.25 min. retention time, which was collected, lyophilized and then analysed by MALDI-TOF - MS. Besides Na^+ and K^+ adducts formation, two additional peaks with lower masses (-16 Da and -32 Da) than the intact molecular ion $[M+H]^+$ of nitrated peptide (**1**) were observed.

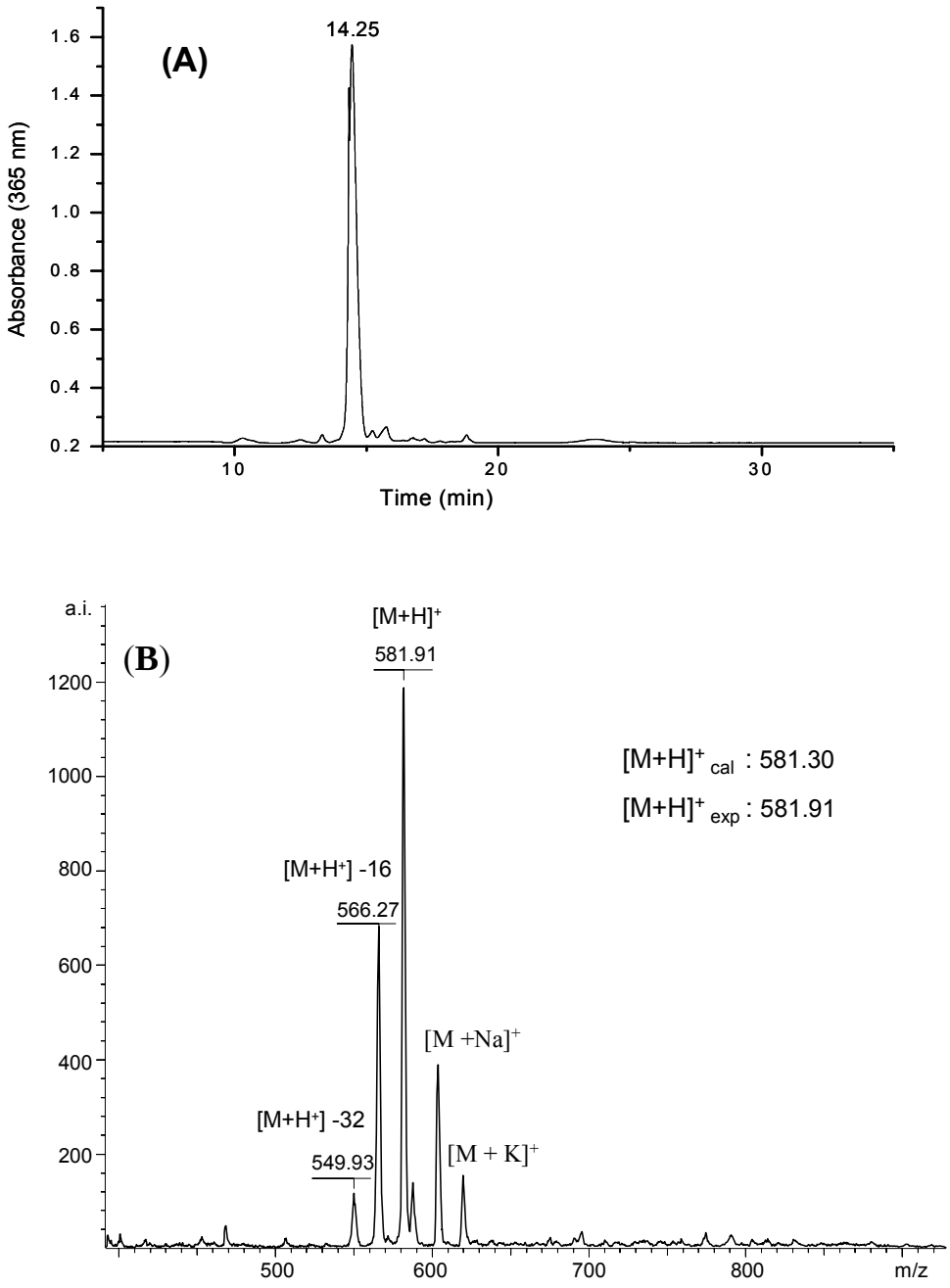

Figure 61: *Analytical RP-HPLC profile monitored at 365 nm (A) and UV-MALDI-TOF mass spectrum (B) of nitrated PCS (**1**) peptide.*

A series of nitro-tyrosine, tyrosine and phenylalanine containing peptides, corresponding to the PCS (419-432) sequence were synthesized using the same procedure as described previously on a preloaded NovaSyn® TGA resin (s. Figure 60). Since the first C-terminal amino acid was already coupled to the resin the first step of the synthesis was deprotection of the Fmoc N-α- amino acid - TGA resin. The

following steps were performed as described before until completion of the peptide sequence, and after final cleavage using TFA and scavenger, C-terminal (-COOH) synthetic peptides were obtained. The use of 3-nitrotyrosine within the standard Fmoc and side-chain protection chemistry (t-butyl, *t*-Boc, trityl,) allowed high coupling yields and homogeneities already for crude peptides after deprotection. Upon precipitation, all peptides were characterized by analytical RP-HPLC and MALDI-TOF mass spectrometry (s. Table 9). The HPLC profiles and the MALDI-TOF mass spectrum of non-nitrated PCS (**2**) and nitrated PCS (**3**) peptides are compared in Figure 62.

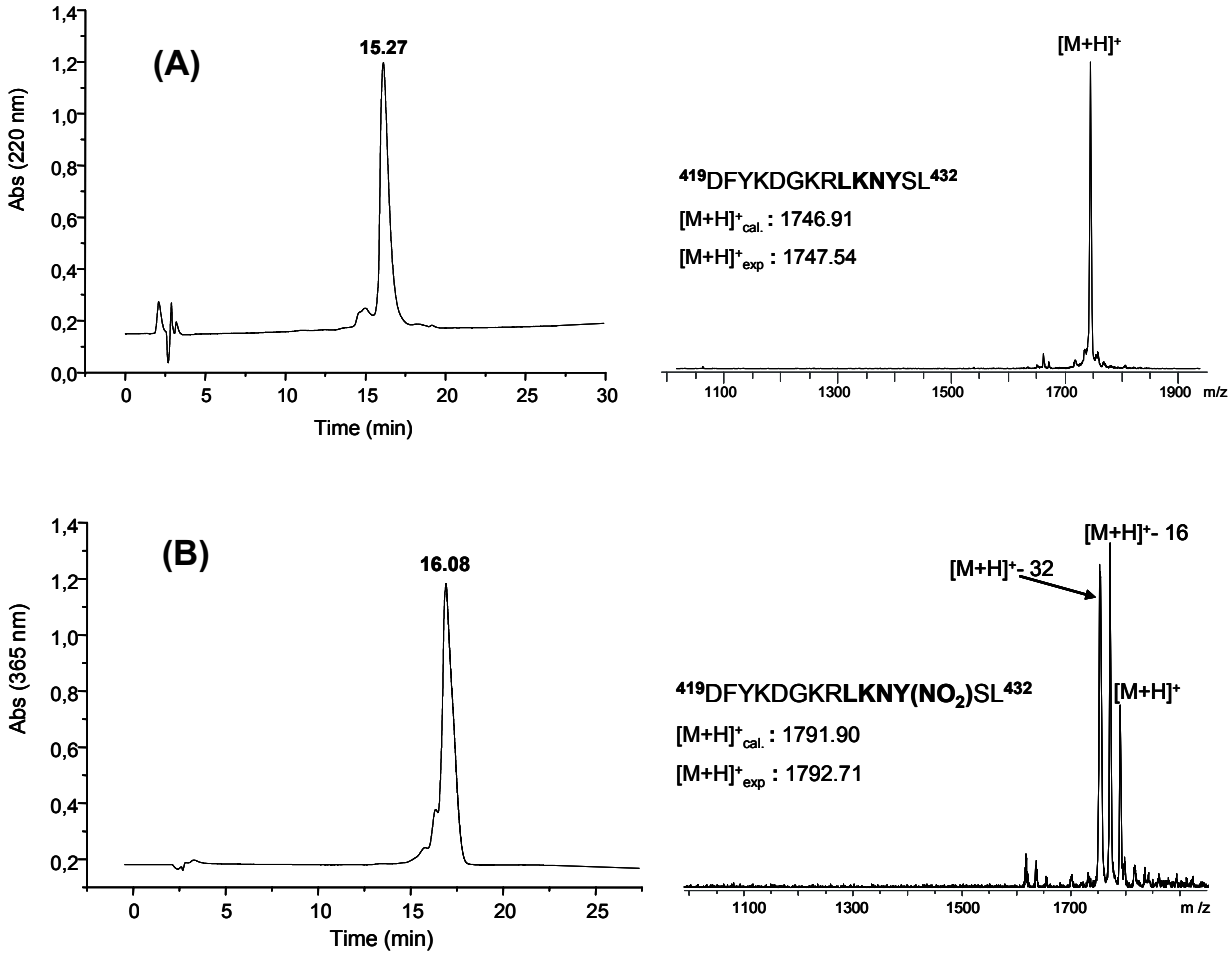

Figure 62: *Analytical RP-HPLC chromatograms and MALDI-TOF mass spectrum of (A) non-nitrated PCS (2) and (B) nitrated PCS (3) peptides.*

The MALDI-TOF mass spectrum of non-nitrated PCS (**2**) peptide showed a single intact molecular $[M+H]^+$ ion at 1747.57, while a characteristic addition of +45 Da to the molecular ion of the nitro-substituted tyrosine group in PCS (**3**) at 1792.71 was observed. During MALDI-TOF MS analysis, the 3-nitrotyrosine residue undergoes specific fragmentation to major fragments $[M+H]^+$ -16 and $[M+H]^+$ -32 (s. Figure 62). To clarify this possible fragmentation pathway, the nitro-tyrosine peptides were analysed by high resolution and high mass accuracy using MALDI-FT-ICR MS.

2.3.2 High resolution mass spectrometric characterization of synthetic nitro-tyrosine peptides

Recently, high resolution Fourier transform ion-cyclotron resonance mass spectrometry (FTICR-MS) has been established as a powerful tool for the mass spectrometric structure determination of protein modification, using both electrospray (ESI) and MALDI ionisation [202-204]. The feasibility and advantage of FT-ICR-MS have been demonstrated by elucidation of a specific nitration at the Tyr-430 residue of the catalytic site of bovine Prostacyclin synthase (PCS) [205].

The synthetic, nitrated and non-nitrated PCS peptides were characterised by nano-ESI-FTICR and UV/IR-MALDI-FTICR mass spectrometry as shown in Table 10.

Table 10: *nano-ESI, UV-and IR-MALDI-FTICR mass spectrometric data of PCS synthetic peptides.*

		Nano-ESI-FTICR		**UV-MALDI-FTICR**		**IR-MALDI-FTICR**	
No.	**Peptide code**	**m/z exp.**	**Δm [ppm]**	**m/z exp.**	**Δm [ppm]**	**m/z exp.**	**Δm [ppm]**
1	PCS_1	581.3043	0.17	581.3044	0.34	581.3051	1.5
2	PCS_2-Y	1746.9183	0.6	1746.9188	0.86	1746.9191	1.1
3	PCS_2-Y-NO_2	1791.9073	2.6	191.9043	1.0	1791.9068	2.4
4	PCS_2-(RR)	1819.9117	1.7	1819.9115	1.6	1819.9125	2.1

The nano-ESI-FTICR spectra of all Tyr-nitrated peptides showed most abundant multiply (mainly doubly and triply) protonated molecular ions without detectable fragmentation with mass determination accuracies in the low ppm range, as illustrated in Figure 63 by the peptide PCS (**3**), (419-432) fragment of bovine Protacyclin synthase, nitrated at the active site Tyr-430 residue. A comparative molecular modelling study of some Tyr-nitrated and non-nitrated model peptides did not indicate significant structural changes upon nitration, beyond the somewhat exposed structure of the 3-nitro group (s. insert in Figure 63).

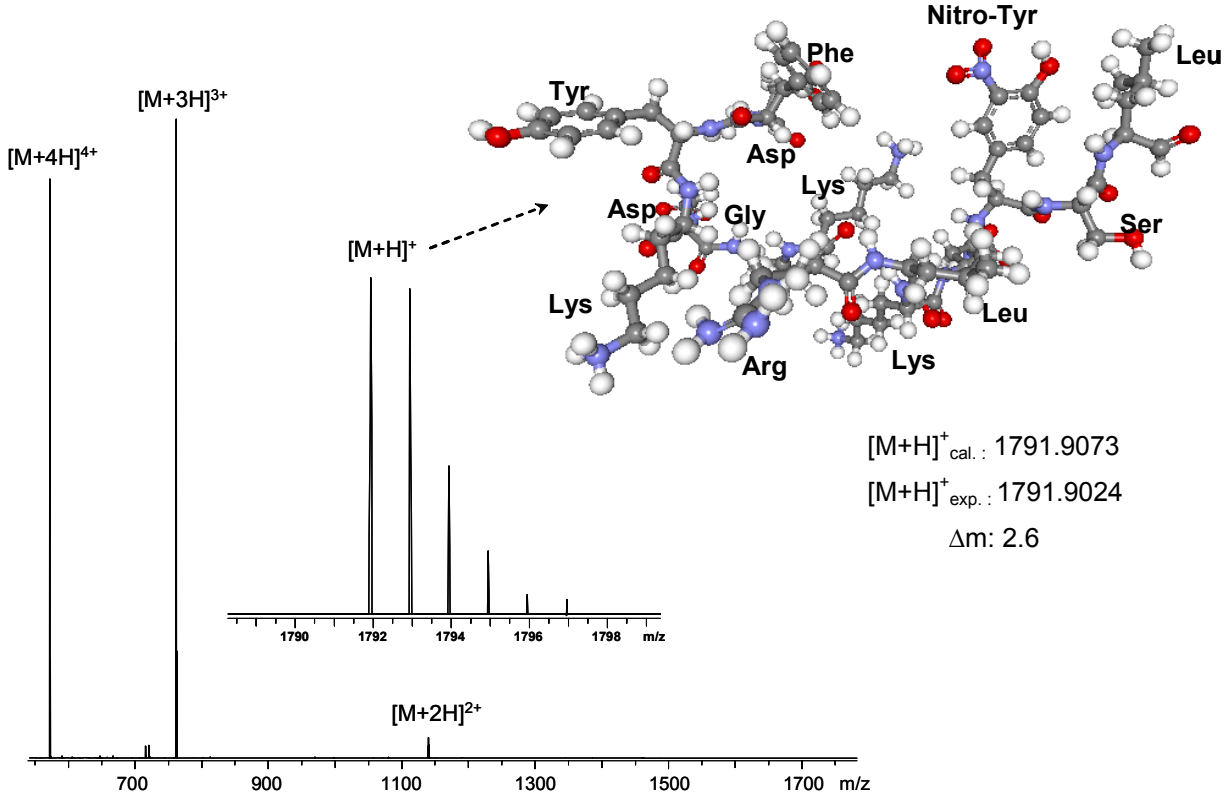

Figure 63: *nano-ESI-FTICR mass spectrum of synthetic PCS (**3**) peptide. The inserts show the isotopic fine structure of the $[M+H]^+$ ion obtained by deconvolution of the most abundant triply charged ion $[M+3H]^{3+}$, and a structure model of the peptide with the Tyr-430 residue using the Hyperchem III programme.*

In addition, the synthetic nitro-Tyr^{430} PCS peptide (**3**) was analyzed using electrospray ionization on an Esquire 3000plus ion trap mass spectrometer. This mass spectrometer allowed detailed structure information of peptides by specific fragmentations using the *collision-induced dissociation* (CID) technique [206].

The spectrum in Figure 64A shows exclusively the doubly, triply and quadruply charged peptide ions, indicating the molecular homogeneity of the PCS peptide. The amino acid sequence was confirmed by isolation and fragmentation of the doubly charged precursor ion of m/z 896.3 (Figure 64B). The CID mass spectrum contains the characteristic b and y fragment ions and the experimental molecular weight of 1792.12 ($MW_{cal.}$ = 1790.89), which are consistent with the indicated amino acid sequence PCS-(419-432). The details of the identification of b and y ions in CID spectra are presented in Appendix 4. The base peak ion in this spectrum is y_{13}^{2+} at m/z 838.8, indicating that the loss of the aspartic acid from the N-terminus with retention of retention of both charges on the remaining C-terminal peptide fragment represents the dominating decomposition pathway. The nitrated tyrosine was unambiguously assigned at the residue 430 of the peptide, as indicated by the fragment ion y_2 (m/z 219.0) and y_3 (m/z 427) which are separated by 207 amu; the shift in mass results from the presence of the nitro-group at Tyr^{430} (addition of 45 amu to the of a non-modified tyrosine residue). In addition, the immonium ion at m/z 180.9 is indicated for nitro-tyrosine and may be used for selective identification of nitrated tyrosine residues in complex mixture (s. Figure 64C) [107].

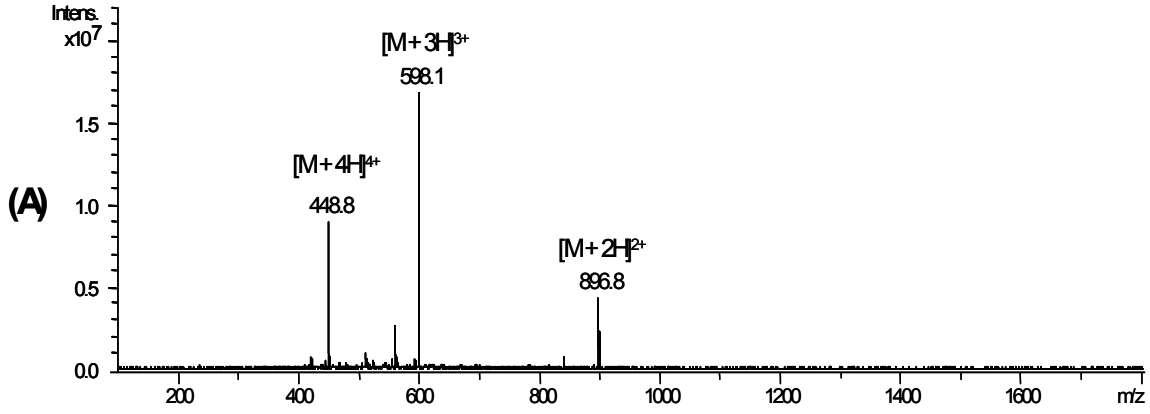

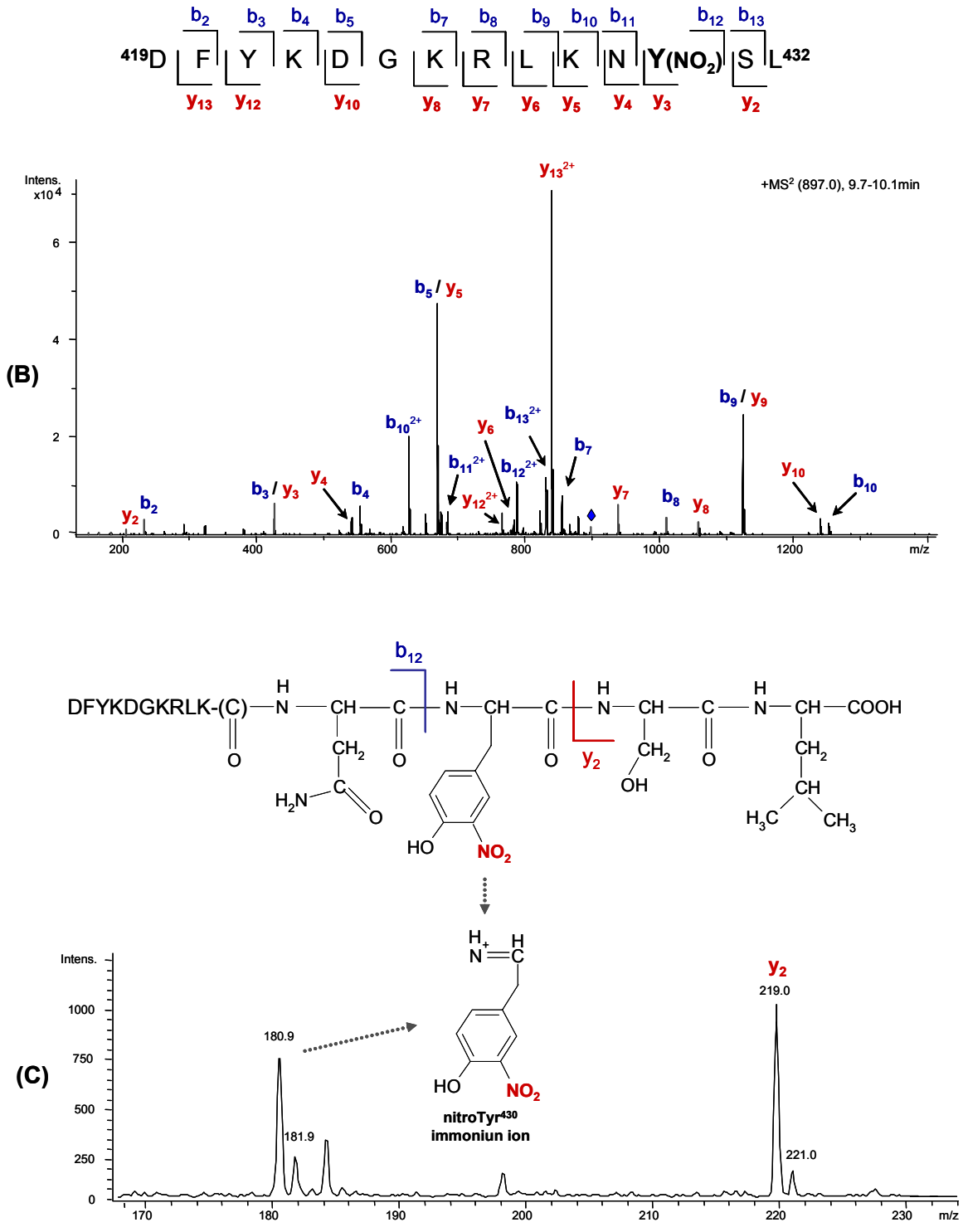

Figure 64: *ESI-Ion trap MS of the synthetic PCS (**3**) peptide, (A) ESI-mass spectrum showing doubly, triply and quadruply charged peptide ions. (B) CID mass spectrum of the doubly protonated precursor ion at m/z 896.8. The observed b and y fragment ions are indicated in blue and red, respectively; (C) Zoom of the CID mass spectrum in the lower mass range showing the specific immonium ion for nitro-Tyr^{430}. The insert shows the partial chemical structure of nitrated PCS peptide (**3**) and the immonium ion formation.*

The tyrosine- nitrated and non- nitrated peptides were further analysed by UV- and IR-MALDI-FT-ICR-MS, using the perpendicular UV-nitrogen at 337 nm and a 2.97μm Er: YAG infrared laser systems and identical DHB-matrix and sample preparations on the sample target of the Scout-100 MALDI source (s. Figure 65). The IR absorption, even though a factor of at least 10 weaker than those encountered in the UV, leads to enough deposition of energy into the sample to make plausible the desorption of molecules [207]. Moreover, IR-MALDI having 5-10 μm desorption depth, consumed much more material than UV-MALDI with 0.1-1μm, and only a few spectra could be obtained from the same spot in IR-MALDI analysis [93, 208].

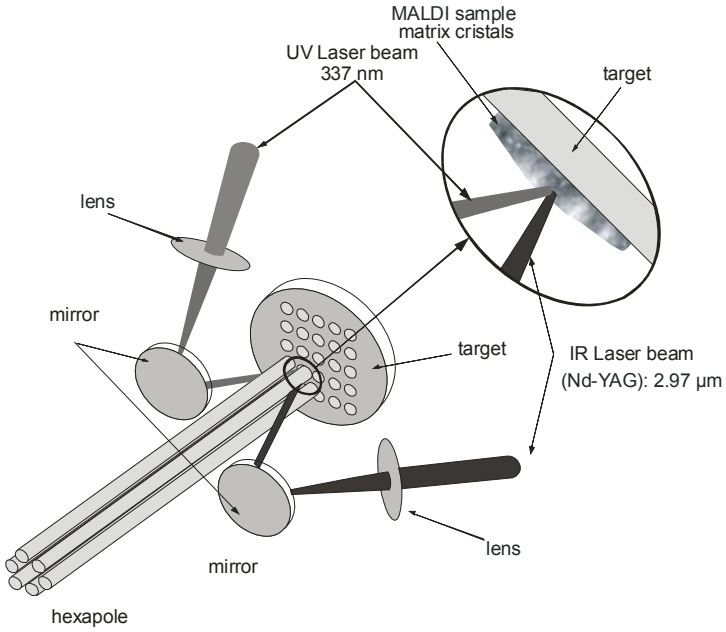

Figure 65: *Scheme of the IR-MALDI source attached to the Bruker ApexII FT-ICR- mass spectrometer equipped with the Scout 100- UV- MALDI source.*

Comparable mass determination accuracies (typically 1-5 ppm) of protonated molecular ions were observed in both cases (s. Table 10). As previously reported [106] the UV-MALDI spectra showed a series of specific photochemical fragmentations for the nitrated peptides which were not observed for the unmodified peptides, with major fragment ions at $[M+H-16]^+$, $[M+H\ 30]^+$ and $[M+H\ 32]^+$. This specific fragmentation of the 3-nitro-tyrosyl residues in peptides, corresponds to the loss of one oxygen to form a 3-nitroso-Tyr derivative [Tyr(NO)], loss of two oxygens

to form a nitrene-type fragment [Tyr (**:**N**:**)], and reduction of the nitro group to formally yield an amine [Tyr (NH_2)] (s. Figure 66). The high mass resolution and accuracies provided by FT-ICR-MS directly ascertain the fragmentation pattern reported by Sarver *et al*., thus excluding other possible fragment ion types. A possible photochemical mechanism underlying this fragmentation has been previously discussed [106].

Although the UV-MALDI-induced fragmentation still provided the analysis of intact molecular ions of the synthetic 3-nitrotyrosyl- model peptides in this study, their unequivocal detection and molecular weight assignments of tyrosine nitrations in proteome analyses of proteolytic peptides mixture by low resolution UV-MALDI-MS might be significantly hampered, particularly by the possible difficulties to distinguish the $[M+H -30]^+$ and $[M+H- 32]^+$ ions. This problem may be further substantiated in the case of low nitration levels that are typically encountered in the study of cellular nitrated proteins [34, 205].

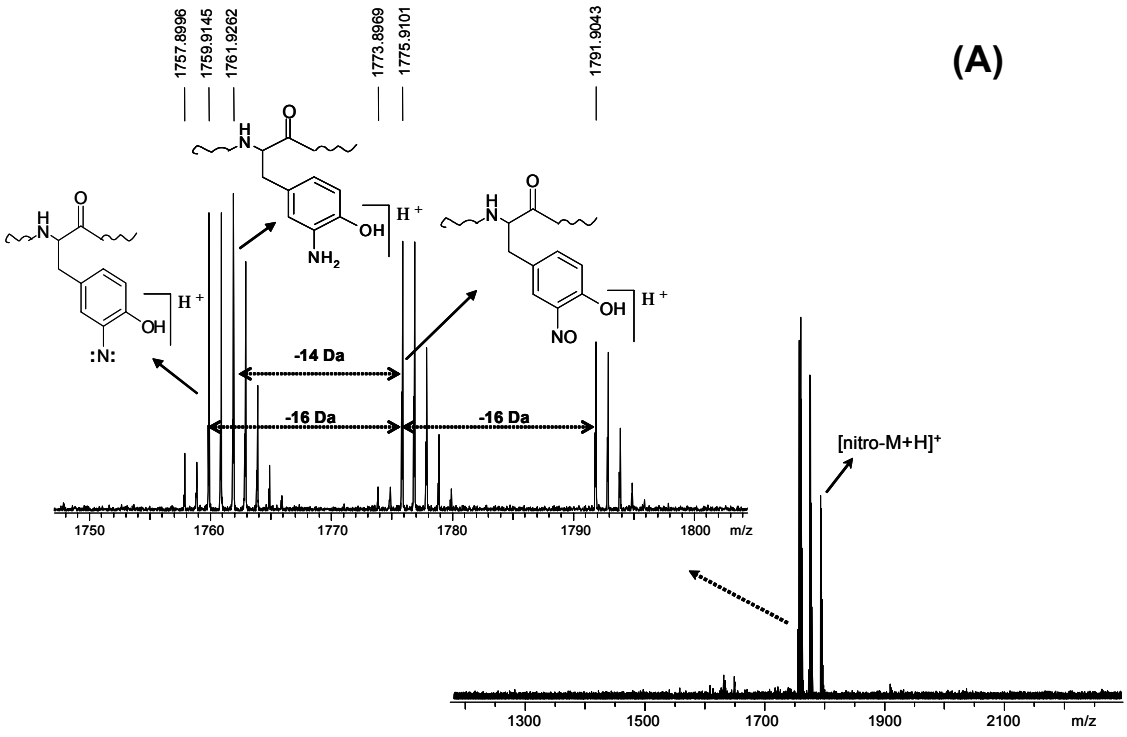

Figure 66: *UV- MALDI-FT-ICR mass spectrum of PCS (**3**) peptide. Monoisotopic ion mass is given in* Table 10*. The upper insert shows the photochemical fragmentation and major products identified by accurate mass determination.*

In contrast, IR-MALDI-FTICR-MS analyses of a series of 3-nitrotyrosine containing peptides provided $[M+H]^+$ ions of high intensities without any photochemical fragmentation (Table 10, Figure 67). The stability under IR-MALDI conditions is illustrated by the spectrum of the PCS (**3**), (419-432) fragment of Prostacyclin synthase which showed a most abundant $[M+H]^+$ ion at m/z 1791.9068. Using the identical DHB matrix as in UV-MALDI-FTICR-MS, the loss of water at higher laser energy was observed as the only fragmentation in IR-MALDI-FTICR spectra.

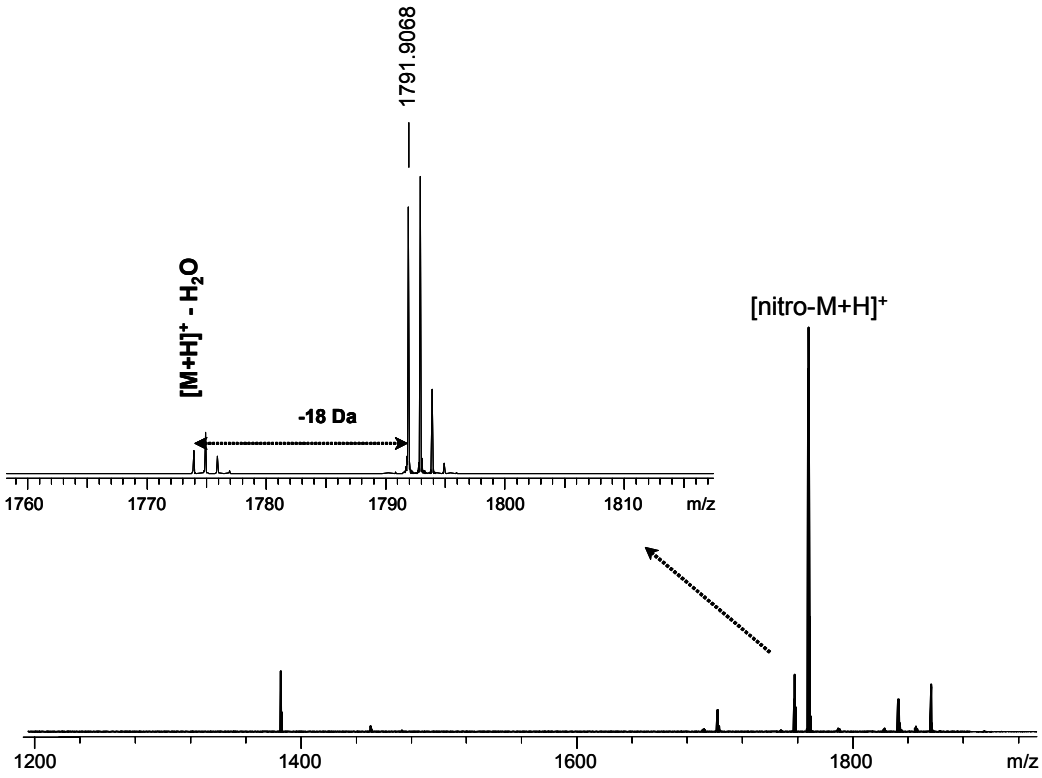

Figure 67: *IR- MALDI-FT-ICR mass spectrum of PCS (**3**). The upper insert shows the loss of H_2O at the high laser energy.*

In conclusion, the ESI-MS^n analysis of 3-nitrotyroeine-conatining peptides yields unambiguous results, where the introduction of the nitro group increases the molecular weight of the original peptide by + 45 atomic mass units (amu). Moreover the IR-MALDI results demonstrate the stability of 3-nitrotyrosyl peptides under infrared laser conditions, thus indicating the advantages of IR-MALDI-MS for the identification of 3-nitro-tyroisne modification in proteins/ peptides mixture.

2.4 Elucidation of recognition specificity of anti 3-NT antibodies with nitro-tyrosine peptides

2.4.1 Structural principles of IgG antibodies

Antibodies are immune-system-related proteins called immunoglobulins (Ig) that normally function to recognize and bind to the foreign molecules on the surface of pathogens. Antibodies are divided into five major classes, IgM, IgG,IgA, IgD and IgE, based on their constant region structure, immune function and types of B-cell secretors. Immunoglobulin G (IgG) accounts for 75-80 % of the total immunoglobulin pool in normal blood serum. The basic antibody molecule is depicted as a Y-shaped structure consisting of four polypeptides chains: two identical heavy (H) chains (50-75 kDa) and two identical light (L) chains (25 kDa) (s. Figure 68A). Each heavy chain is linked to a light chain by a cysteinyl-bond, and the two heavy chains are bound to each other by disulfide bridges and non-covalent interactions. The first X-ray crystal structure of an intact mouse IgG revealed that an antibody molecule is globular in structure and heavy and light chains have repeating substructures called domains comprising ~ 110 amino acids (PDB accession number 1IGT) [209]. The domains at the N-terminal ends are called the variable domains (V_H and V_L) because their amino acid sequences were found to vary greatly among different antibody. The other domains are called constant region (C_H and C_L) because they do not differ to the same extent from antibody to antibody.

The parts of the antibody molecule that bind to antigen are called the antigen-binding fragments (Fabs) and are located in the variable domains of the H-and L- chains. More detailed analysis shows that the variability is confined to three connecting loops regions (5-15 amino acids in length), called the hyper-variable regions (HV). The HV loops directly contact a portion of the antigen's surface and are also referred to as complementarity determining regions (CDRs) [210]. The amino acid residues involved in the interaction with the antigen form the paratope [211].

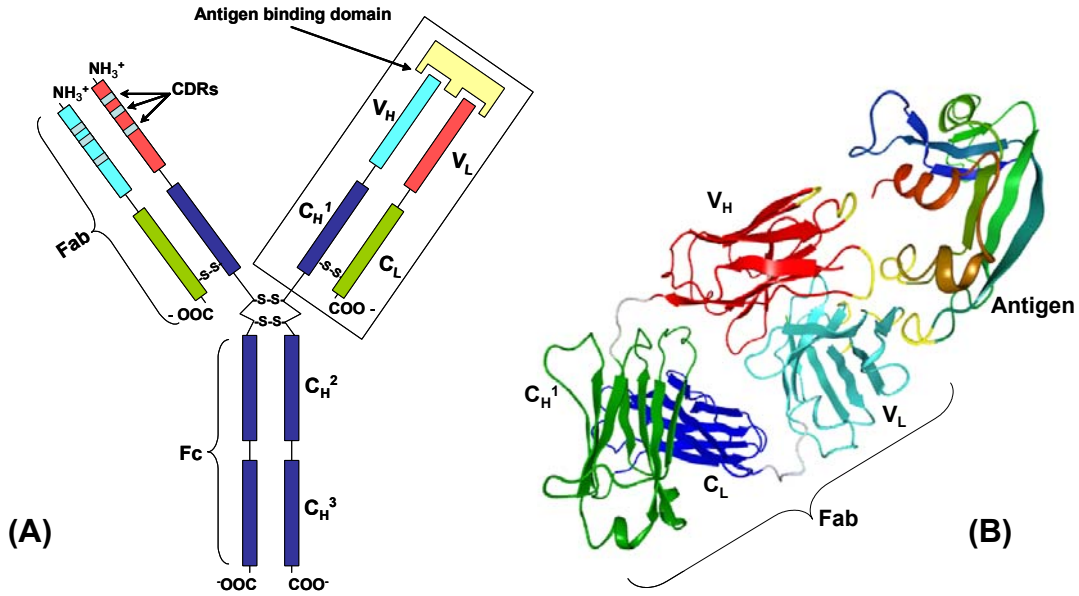

Figure 68: *Schematic representation of the immunoglobulin G and the antigen binding site. a) Two heterodimers made of a heavy and light chain are linked to form the IgG molecule. The heavy chain consists of 3 constant domains (C_H) and a variable domain (C_V) and is linked through a disulfide bridge to a light chain composed of a constant (C_L) and a variable (V_L) domain. b) Ribbon diagram of Fab fragment from the crystal structure of the IgG monoclonal antibody (PDB accession number 1IGT). The hypervariable regions (CDRs) located on the variable domains of the heavy (red) and light (turquoise) chain form the binding cleft which interacts with the antigen are shown in yellow.*

Antigens are usually proteins or polypeptides but may also be polysaccharides or, less commonly, lipids or nucleic acids. Generally an antibody does not bind to the complete antigen; but binds specific a part called epitope or antigenic determinant. Epitopes can be linear, formed by a continuous sequence of 8 to 15 amino acids, or discontinuous, formed by a specific folding structure of the antigen protein. To form an immune complex, noncovalent interactions (hydrogen bonds, ionic bonds, hydrophobic interactions, Van der Waals interactions) are established between the surfaces of the two molecules, complementary in their topology [212].

The ability to induce a humoral immune response is called immunogenicity and depends on the capacity of the immune system to distinguish between self and nonself agents, molecular size of a foreign agent, its chemical composition and heterogeneity. The immunogens are molecules that interact specifically with the

immunoglobulins and elicit an immune response. Antibodies are produced in the white blood cells, called B lymphocyte which makes copies of its own unique antibody and displayed them on its outer surface. Each B-cell clone interacts with a different sequence of amino acids on the surface of the immunogen and will secrete a specific antibody for this sequence. The affinity separation of the IgG molecules interacting with the immunogen produces a purified polyclonal antibody. In contrast, by fusion of an activated, antibody-producing B cell with a myeloma cell (a cancerous plasma cell) a hybrid cell is formed, called a hybridoma, which possesses the immortal-growth properties of the myeloma cell and secretes only the antibody produced by the activated B cell. The affinity separation of the IgG molecules using the immobilized immunogen will lead to a purified monoclonal antibody. The high degree of specificity of monoclonal antibodies and their specific uniformity make them ideal for pharmaceutical applications [213].

2.4.2 Comparison of molecular recognition specificity of two anti-nitro-tyrosine antibodies

In this study two commercially available antibodies raised against different immunogens containing 3-nitrotyrosine were characterized with regard to their recognition specificities and affinities to synthetic Tyr-nitrated peptides of Prostacyclin synthase. Affinity bindings of tyrosine- nitrated and non-nitrated PCS peptides to 3-NT antibodies were compared using (i), conventional dot blot and ELISA, and (ii), a newly developed immunoaffinity – mass spectrometric approach. The synthetic Prostacyclin synthase peptides and their chemical characteristics are summarized in Table 11 and the characteristics of anti nitro-tyrosine antibodies employed in this study as given by the manufacturers are summarized in Table 12 .

Table 11: *Mass spectrometric characterization of synthetic PCS peptides*

No.	Peptide code	Sequence	MALDI-TOF [c] m/z $[M+H]^+_{calc/exp}$
1	PCS-Y[a]	DFYKDGKRLKN**Y**SL-OH	1746.91 / 1747.72
2	PCS-NO_2[a]	DFYKDGKRLKN**Y(NO_2)**SL-OH	1791.90 / 1792.96
3	PCS-NO_2(RR)[b]	DF**Y(NO_2)**KDG**R**RLKNYSL-OH	1819.90 / 1822.13
4	PCS-NO_2(Ala)[a]	DFYKDGKR**AAA**Y(NO_2)**A**L-OH	1633.79 / 1634.71
5	PCS-F[a]	DFYKDGKRLKN**F**SL-OH	1730.92 / 1732.71
6	PCS[a]	LKN**Y(NO_2)**-NH_2	581.64/582.97

[a] Tyr-430 of Prostacycline synthase

[b] Tyr-421 of Prostacycline synthase, Lys^{425} was replaced by an Arg.

[c] MALDI-TOF mass spectra were recorded with a Bruker Biflex™ linear TOF mass spectrometer

Table 12: *Characteristic of monoclonal antibodies against 3-nitro-tyrosine*

Supplier	Antibody details
Chemicon International **(1), (3)**	Mouse Anti-Nitrotyrosine Monoclonal Antibody **(MAB5404)** **Concentration:** 1 µg/µl **Immunogen:** Nitrated KLH (Keyhole-limpet hemocyanin)
Santa Cruz **(2)**	Mouse Monoclonal Nitrotyrosine **(39B6)** **Concentration:** 0.2 µg/µl **Immunogen:** 3-(2-(4-hydroxy-3-nitrophenyl)acetamido) propionic acid-bovine serum albumin conjugate

2.4.2.1 Binding of anti 3-NT antibodies to PCS peptides by Dot blot

Dot blot is a straightforward, simple technique for peptide and protein detection in which the samples are spotted directly onto a membrane through circular templates. The method is based on the antigen-antibody recognition by using a first antibody against the membrane- immobilized antigen, and a second label-conjugated antibody for detection of the first antibody (s. Figure 69). The PCS peptides were spotted on a

nitrocellulose membrane, and the unspecific sites were blocked with Roti®-Block solution. After washing steps with PBS-Tween buffer, the membrane was incubated with anti-3-NT antibody for 1 hr at room temperature. After further washing steps, a second enzyme-conjugated antibody (horse radish peroxidase (HRP) goat anti-mouse IgG) which recognizes the Fc (crystallisable fragment) fragment of the first antibody was added and incubated for 45 min. A mixture of ECL-solutions was added in order to develop the membrane and expose it on a film.

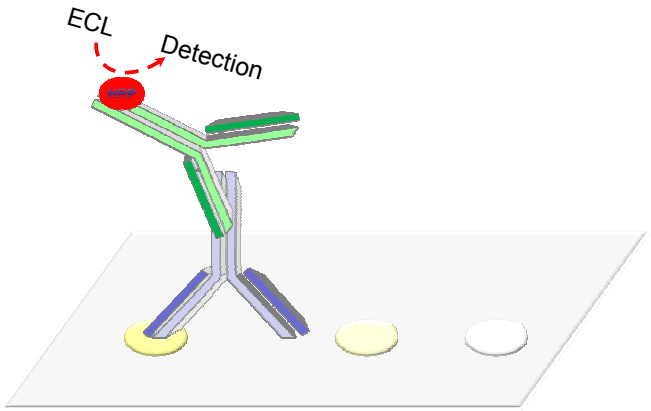

Figure 69: *Schematic representation of an immuno Dot blot experiment*

Figure 70 shows the dot blot binding responses of the 3-NT- antibodies to different PCS peptides. The MAB5404 (Chemicon; **1**) gave an intense positive response only for the authentic Tyr-430 –nitrated peptide containing the actual Tyr-nitration site in PCS (s. Figure 70A); the 39B6 antibody (Santa Cruz; **2**) gave an intense response for the same peptide, however additional weaker positive responses were observed for the PCS peptide nitrated at Tyr-421 (**3**) and for the peptide (**4**) in which the amino acid residues around the nitrated Tyr-430 were replaced by alanine residues (s. Figure 70B). Since no response was observed for the two non-nitrated Tyr- and Phe-containing peptides (**1**, **5**) of PCS (419-432) fragment, it can be concluded that both antibodies show high specificity for nitro-tyrosine.

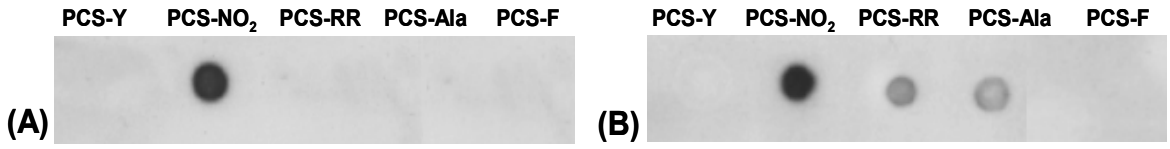

PCS-Y (1) ^{419}DFYKDGKRLKN**Y**SL^{432}
PCS-NO$_2$ (2) ^{419}DFYKDGKRLKN**Y(NO$_2$)**SL^{432}
PCS-RR (3) ^{419}DF**Y(NO$_2$)**KDG**RR**LKNYSL^{432}
PCS-Ala (4) ^{419}DFYKDGKR**AAAY(NO$_2$)A**L^{432}
PCS-F (5) ^{419}DFYKDGKRLKN**F**SL^{432}

Figure 70: *Dot blots analysis of (A) MAB5404 (Chemicon) antibody (**1**) and (B) 39B6 (Santa Cruz) antibody (**2**) to synthetic PCS (419-432) peptides.*

2.4.2.2 Binding of anti 3-NT antibodies to PCS peptides by affinity-mass spectrometry

In order to ascertain the results of the dot blot experiments by a molecular recognition response, the 3-NT-antibody interactions were characterised by using immuno-affinity – mass spectrometry as illustrated in Figure 71. The affinity - MS procedure is based on the binding of antigen- peptides to an antibody immobilized on a micro-column; upon removal of unbound material by washings steps, the affinity-bound peptides are specifically dissociated from the column by acidification and analyzed by MS.

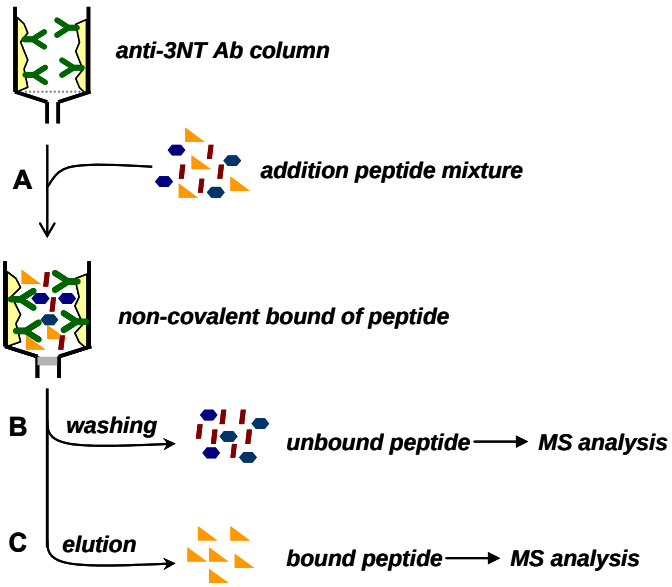

Figure 71: *Schematic representation of immunoaffinity–MS experiment using an immobilized antibody column.(A) Binding of peptides to the immobilized Ab column; (B) removal of unbound peptides; (C) dissociation of the antigen-antibody complex followed by washing steps and storage*

Two antibody columns were prepared by coupling the mouse antibody MAB5404 (**1**) and the mouse antibody 39B6 (**2**) to NHS-activated Sepharose, as described in Experimental part. The PCS peptides were dissolved in PBS buffer, pH 7.4 and added to the antibody columns. After 2 hrs incubation, the unbound peptides were removed, the column was washed several times with PBS buffer, and the peptide-antibody complexes were dissociated using 0.1 % TFA. The first washing fractions containing unbound peptides, and the elution fractions which contain the peptides specifically bound to the 3-NT antibody column were collected, lyophilized and analysed by mass spectrometry.

Corresponding binding results for a mixture of the PCS (Y-430) (**1**) and the PCS-(Y(NO_2)-430) peptide (**2**) to the monoclonal MAB5404 (Chemicon) antibody column (**1**) are shown in Figure 72. The affinity-mass spectrometric data showed that only the Tyr-430- nitrated PCS- peptide bound to the MAB5404 (Chemicon) antibody column. In contrast, affinity–MS experiments performed with several PCS (419-432) peptides that (i), contained a nitration site at Tyr-421, or (ii) contained an alanine sequence adjacent to the Tyr-430 residue did not show binding affinity. These results

suggest high recognition specificity for this nitration site that had been shown previously to cause specific inactivation of Prostacyclin synthase upon treatment with peroxynitrite [205].

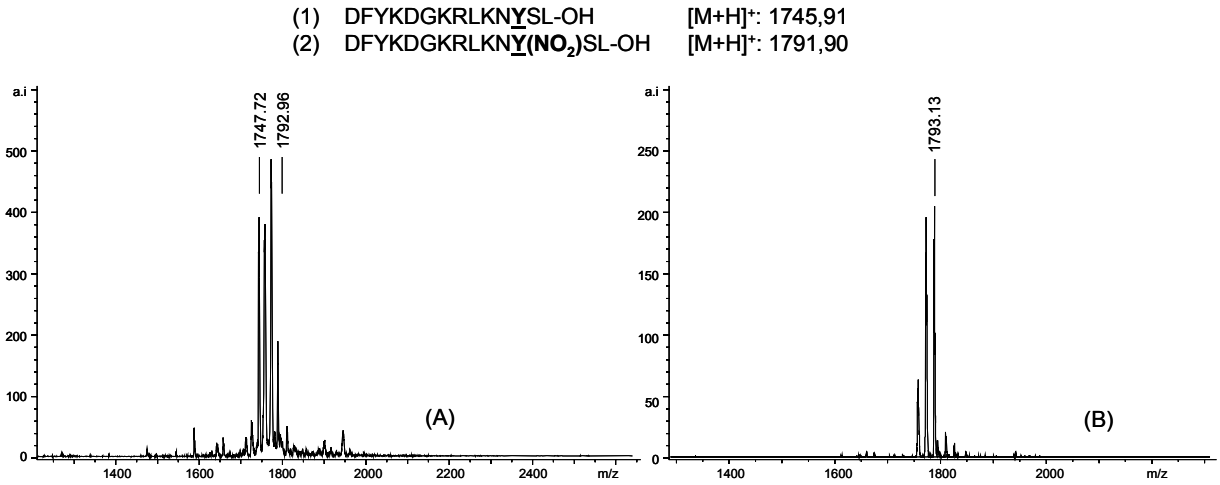

Figure 72: *Affinity-mass spectrometry analysis of PCS (419-432) peptides 1 and 2 (nitrated at Tyr^{430}) with the monoclonal antibody MAB5404 (1); MALDI-TOF-MS of the washing (A) and elution (B) fractions.*

Furthermore, these results indicate that the affinity of the MAB5404 antibody (**1**) (raised against nitrated keyhole limpet hemocyanin carrier protein) is not merely directed by a nitrated tyrosine residue, but also by a recognition sequence encompassing amino acid adjacent to the nitration site.

Somewhat different results regarding a possible sequence-specific motif for recognition of nitro-Tyrosine were obtained for the 39B6 (Santa Cruz) antibody (**2**). The affinity-mass spectrometry data for this antibody generally showed binding affinity for the nitrated PCS peptides, consistent with the results obtained by the dot blot experiments. In order to compare the binding in affinity-MS analyses, equimolar mixtures (200 µmol) of nitrated PCS peptides were applied to the 3-NT antibody column. The MALDI - mass spectrum of the elution fraction of the equimolar mixture of nitrated Tyr-430 PCS peptides **2** and **4** (s. Figure 73) showed affinity for both peptides, albeit with lower affinity for the peptide containing the alanine-sequence mutation adjacent to the nitration site. Similar results with the 39B6 antibody (**2**) column were obtained by affinity-MS of PCS peptides nitrated at different Tyr

residues, such as using peptide **3**. Thus, the elution fraction of an equimolar mixture of nitrated Tyr-430 PCS-Ala (**4**) and nitrated PCS-RR (**3)**; nitro-Tyr-421) indicate comparable affinities for both peptides (s. Figure 73). The binding affinity observed was significantly lower than that of the Tyr-430 nitrated peptide **2**; however, due to the photochemical decomposition of the nitro group in Tyr-nitrated peptides under UV-MALDI-MS conditions, no quantitative determination was carried out from the mass spectrometric data.

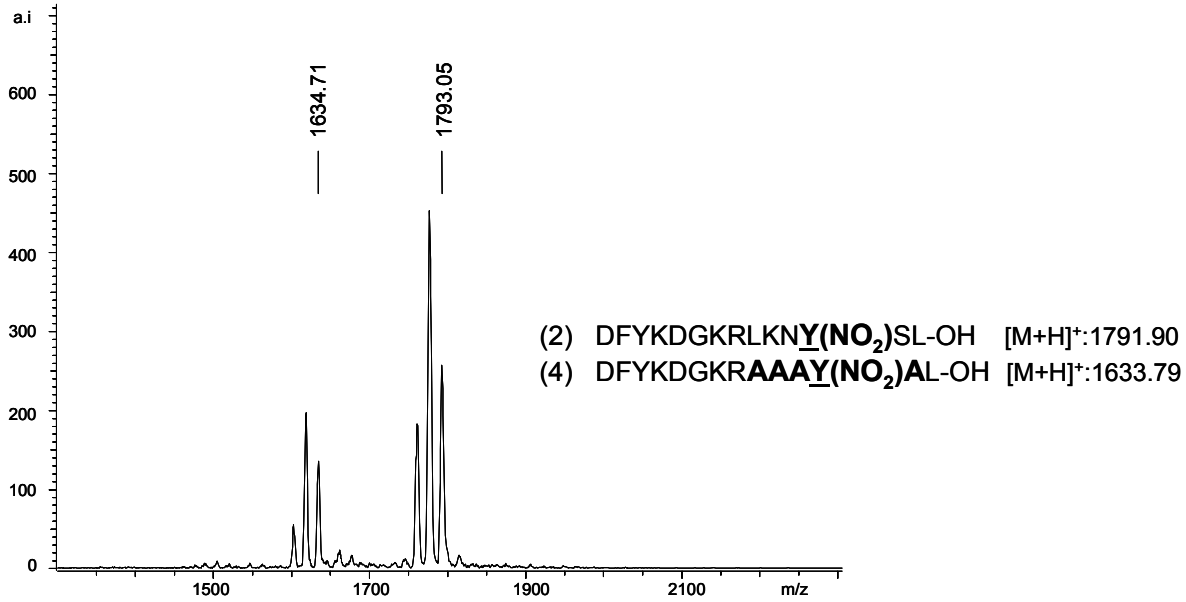

Figure 73: *Affinity-mass spectrometry analysis: (MALDI-TOF-MS of elution fraction) of the nitrated Tyr-430 PCS- peptides 2 and 4 to the 39B6 antibody (2).*

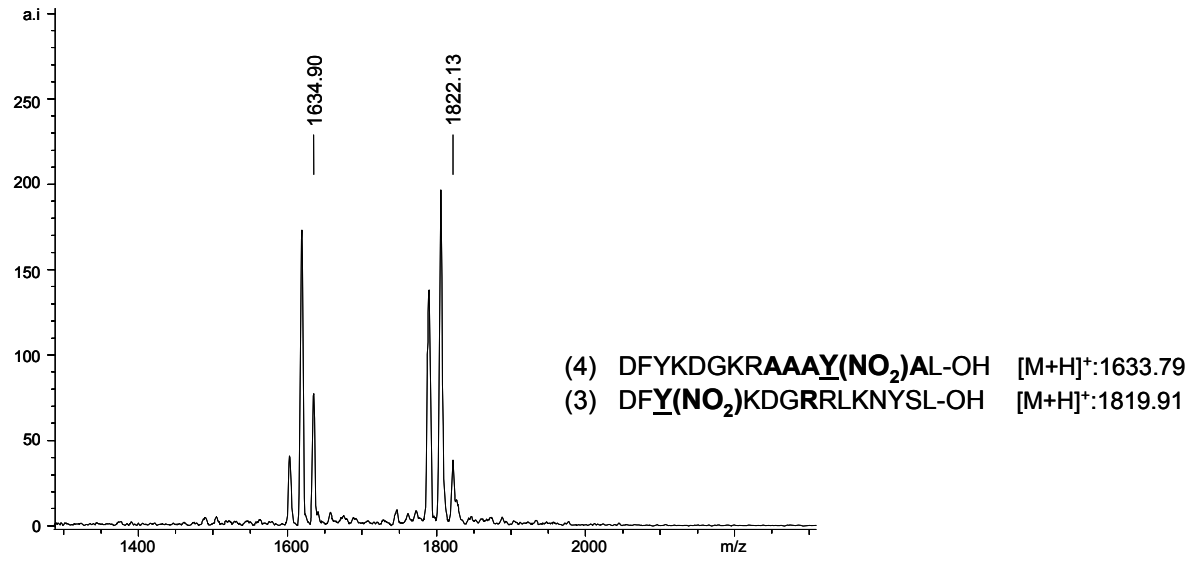

Figure 74: *Affinity-mass spectrometry analysis: (MALDI-TOF-MS of elution fraction) of the mutated Tyr-nitrated peptides PCS-Ala (4) and nitrated Tyr-421 containing peptide, PCS-RR (3) with the 39B6 antibody (2).*

2.4.2.3 Binding of anti 3-NT antibodies to PCS peptides by ELISA

A quantitative estimation of the bindining affinities of the PCS peptides was performed by indirect ELISA as an established technique for comparison of biomolecular affinities. In this study, only a comparative semi-quantitative analysis was aimed at, with regard to the observation that antibody binding may be influenced by a hindered of access of 3-nitrotyrosine residues, and by the structural environment of a nitro-tyrosine motif [214]. Due to the substantial differences in surface adsorption of small peptides, and to minimize unspecific adsorption, covalent attachment was employed with CovaLink-NH plates [215], in which a polystyrene surface is grafted with secondary amino groups to orientate the immobilized peptide on the surface in order to expose the epitope. In the first step of the ELISA determination, the NH-linker was activated using disuccinimidyl suberate (DSS). DSS is a bifunctional linker which activates secondary amine group of the plate and free N-terminal group of the peptide (s. Figure 75). An excess of DSS was used to prevent coupling of both DSS ends to the CovaLink surface.

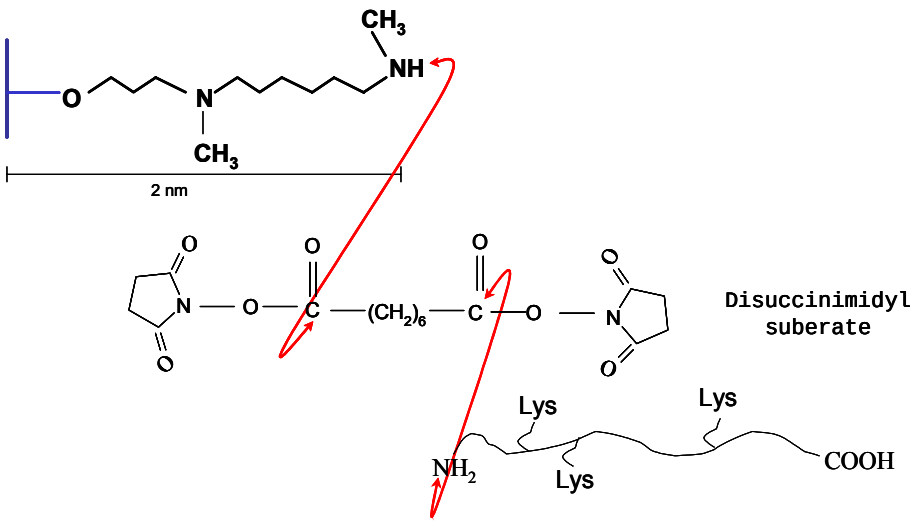

Figure 75: *Schematic representation of disuccinimidyl suberate (DSS) CovaLink activation and its coupling to primary amino groups of peptides.*

Upon activation of CovaLink plate surface the diluted peptides solution was added and incubated overnight. After suitable washing and blocking steps, the CovaLink-NH plate was then incubated with the anti- 3-NT antibody, and horse radish peroxidase

(HRP) goat anti-mouse IgG was used as a detection antibody with OPD/H_2O_2 used as the substrate for HRP as described in Materials and Methods. The absorbance was measured added and the absorbance was measured on a Wallac 1420 Victor^2 ELISA Plate Counter at λ = 450 nm (s. Figure 76).

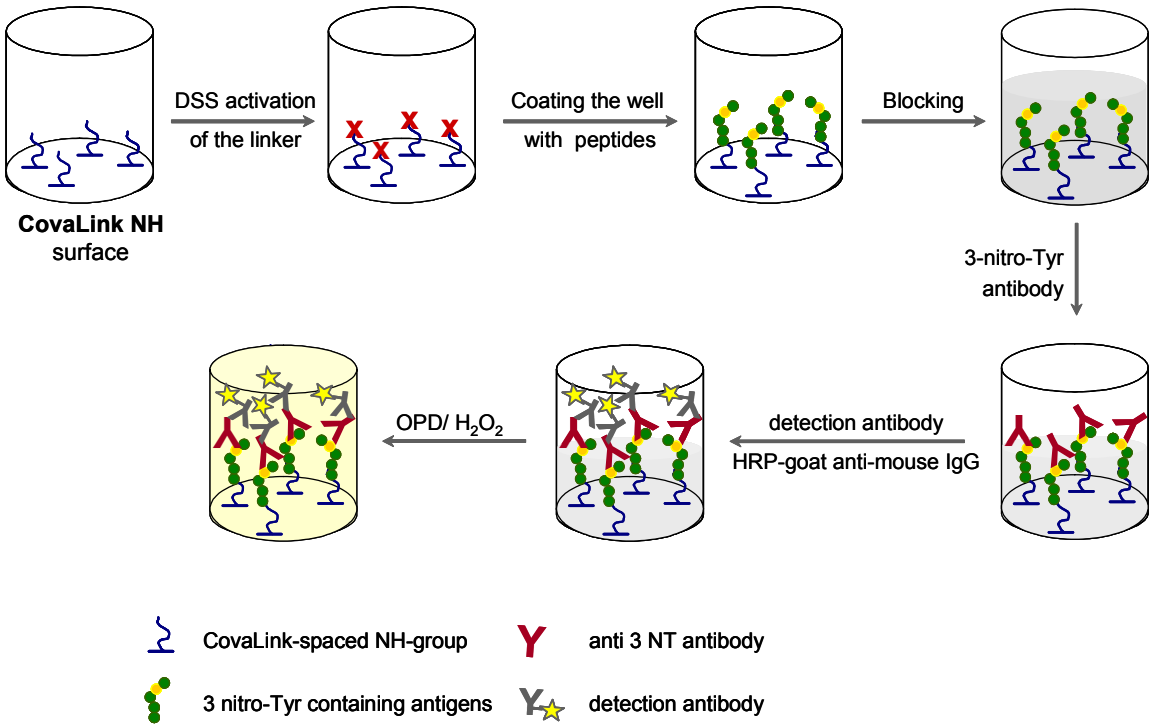

Figure 76: *Schematic representation of indirect ELISA method*

Corresponding ELISA experiments with the two anti nitro-tyrosine antibodies are compared in Figure 6 for the series of nitrated PCS peptides. For comparison of the affinities of the PCS peptides, the concentrations needed for obtaining an OD_{450} =1 were determined (s. Figure 77).

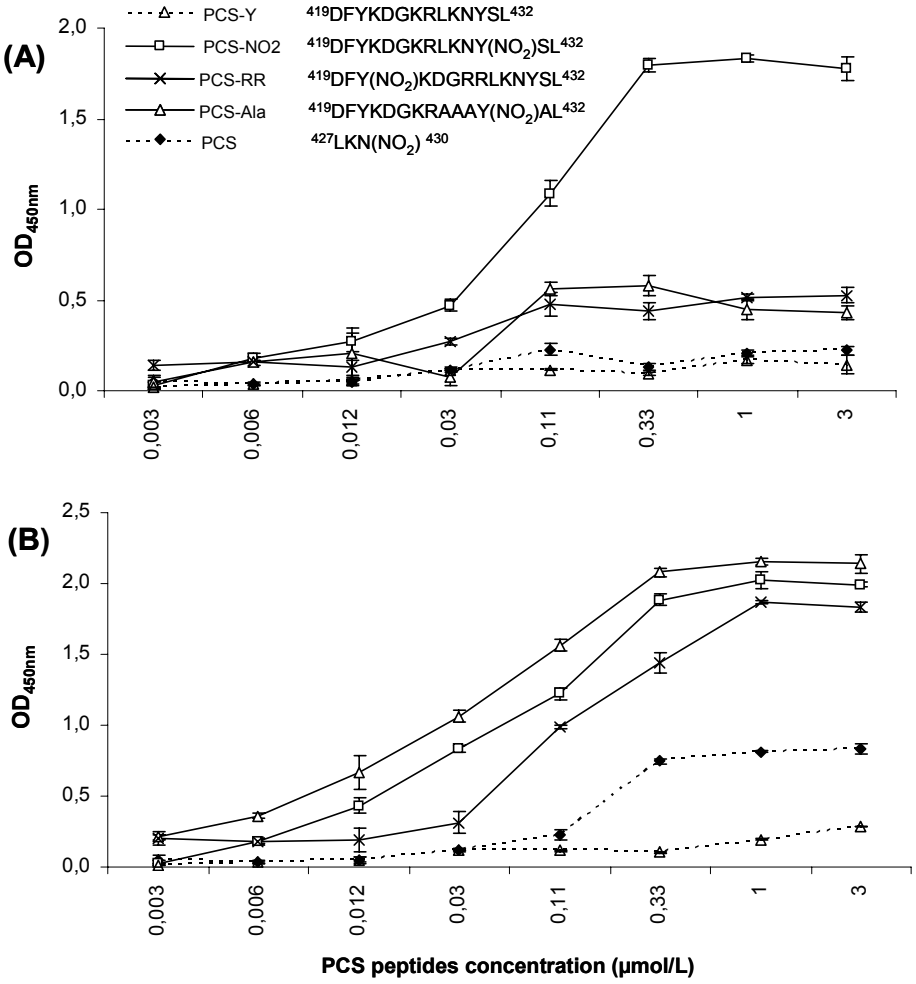

Figure 77: *ELISA determination of the binding of the MAB5404 (Chemicon) antibody (A) and the 39B6 (Santa Cruz) antibody (B) to synthetic Prostacyclin synthase peptides.*

According to the ELISA data with the MAB5404 antibody (s. Figure 77A), only the Tyr-430 nitrated PCS - peptide **2** showed significant affinity to this antibody (lowest amount of PCS-NO_2 peptide to obtain an OD_{450} =1: 0.1 µM). This result is consistent with the affinity-MS data and confirmed the requirement of a specific sequence motif around the 3-nitrotyrosine for antibody interaction. Thus, sequence mutation by alanine residues adjacent to the Tyr-430 nitration site, and change of the nitration position (Tyr-421), resulted in drastically diminished antibody binding. In contrast, the 39B6 antibody revealed significant binding for all nitrated PCS peptides (s. Figure 77 B). The results of the ELISA determinations revealed some differences to the affinity-mass spectrometric analyses in which the Tyr-430 nitrated PCS-peptide (**2**) showed

lower affinity than the alanine mutated peptide (**4**) (lowest amount of PCS-NO_2 peptide to obtain an OD_{450} =1: 0.07 µM)**.** This effect might be explained by the increase in hydrophobicity introduced by the alanine mutation causing increased exposure of the nitrated Tyr-430. In the ELISA determination with the 39B6 antibody (**2**), significant affinity was also found for the short, nitrated PCS tetra-peptide, PCS (427-430) fragment which was not detected with the MAB5404 antibody (**1**).

The differences found in binding affinities of Tyr-nitrated peptides by affinity-mass spectrometry in comparison to dot blot and ELISA determinations, may be attributed to the different types of antigens used for producing the anti-3-NT antibodies have been raised. Thus, the 39B6 antibody (Santa Cruz) was raised against a 3-(2-(4-hydroxy-3-nitrophenyl) acetamido) propionyl-bovine serum albumin conjugate in which the (4-hydroxy)-3-nitrophenyl group is more exposed and freely accessible, compared to the nitrotyrosine residue in the polypeptide chain of the nitrated KLH (Keyhole-limpet hemocyanin) carrier protein, employed as antigen for the MAB5404 (Chemicon) antibody. Hence, the 39B6 antibody showed generally high affinity to single 3-nitrotyrosine amino acid residues, in contrast to the epitope-peptide sequence motif determining the recognition specificity of the MAB5404 antibody. This recognition motif has been recently characterised in our laboratory to require a set of positively charged residues (Lys, Arg) at the N-terminal adjacent to the nitro-tyrosine residue [216].

2.4.3 Affinity binding of nitro-tyrosine peptides to unspecific 3-NT antibodies

Usually, antibodies directed against 3-nitrotyrosine provide some qualitative information of protein nitration [114]. Unfortunately, quantitative immunochemical analysis is cumbersome and subject to variability due to both antibody specificity and affinity. These features may become important with the development of monoclonal anti-3-nitro-tyrosine antibodies and their employment by immunological techniques.

To achieve the identification and characterization of 3-NT-containing proteins, commercial monoclonal antibodies were employed in this work. Several anti 3-NT antibodies were characterised as having low specificity against to 3-nitro-tyrosine containing sequences. Eosinophil peroxidase model peptides were used as substrates in Dot blot experiments, as primary test for determining the antibody selectivity. Figure 78 shows the dot blot binding responses of the 3-NT- antibodies to different EPO peptides. The MAB5404 (Chemicon, **3**) gave intense positive responses for the authentic Tyr-349 –nitrated peptide containing the actual Tyr-nitration site in EPO.

1. **EPO – NO_2** **FGHTMLQPFMFRLDSQY(NO_2)R- OH**
2. **EPO** **FGHTMLQPFMFRLDSQYR- OH**
3. **EPO – F** **FGHTMLQPFMFRLDSQFR- OH**
4. **Aβ 1 – 40** **DEAFRHDSGYEVHHQKLVFFAEDVGSNKGAIIGLMVGGVV- NH_2**

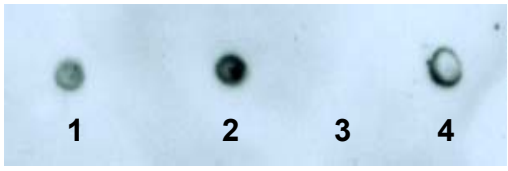

Figure 78: *Dot blots analysis of (A) MAB5404 (Chemicon) antibody (**2**) to synthetic EPO (419-432) and amyloid Aβ peptides.*

However, a positive response was obtained in the case of, the β-amyloid peptide (Aβ 1-40) which is the main constituent of amyloid plaques in Alzheimer's disease. This

peptide contained only one tyrosine residue and a glutamic acid residue adjacent right next to the tyrosine residue which mimics a negative charged of a nitro-group attached to tyrosine (s. Figure 79).

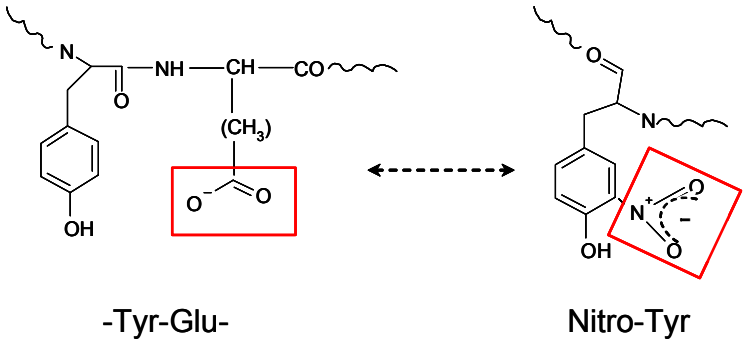

Figure 79: *Chemical structures of 3-nitro-tyrosinecontaining peptide and –Tyr-Glu – in Aβ peptide.*

The monoclonal antibody MAB5404 (Chemicon; **3**) was employed in an immunoaffinity-mass spectrometric experiment in order to prove the low specificity to synthetic EPO peptides. For the immunoaffinity-MS experiment EPO 1, 2 and 3 were bound to the anti-3NTAb **3** The MALDI-TOF mass spectra of the unbound excess mixture showed the [M+H]+ ion of all three peptides (s. Figure 80A). After washing steps until no MS spectra (Figure 80B), bound peptides were dissociated by acidification, and MALDI-TOF spectrum of the elution fraction showed the presence of all nitrated EPO peptides (Figure 80C). These results confirm that the anti-3NTAb **3** was not specific for nitrated peptides. Thus, in conclusion, the immuno-analytical detection of protein nitration critically depends on antibody specificity, and evaluation by affinity-mass spectrometry is needed.

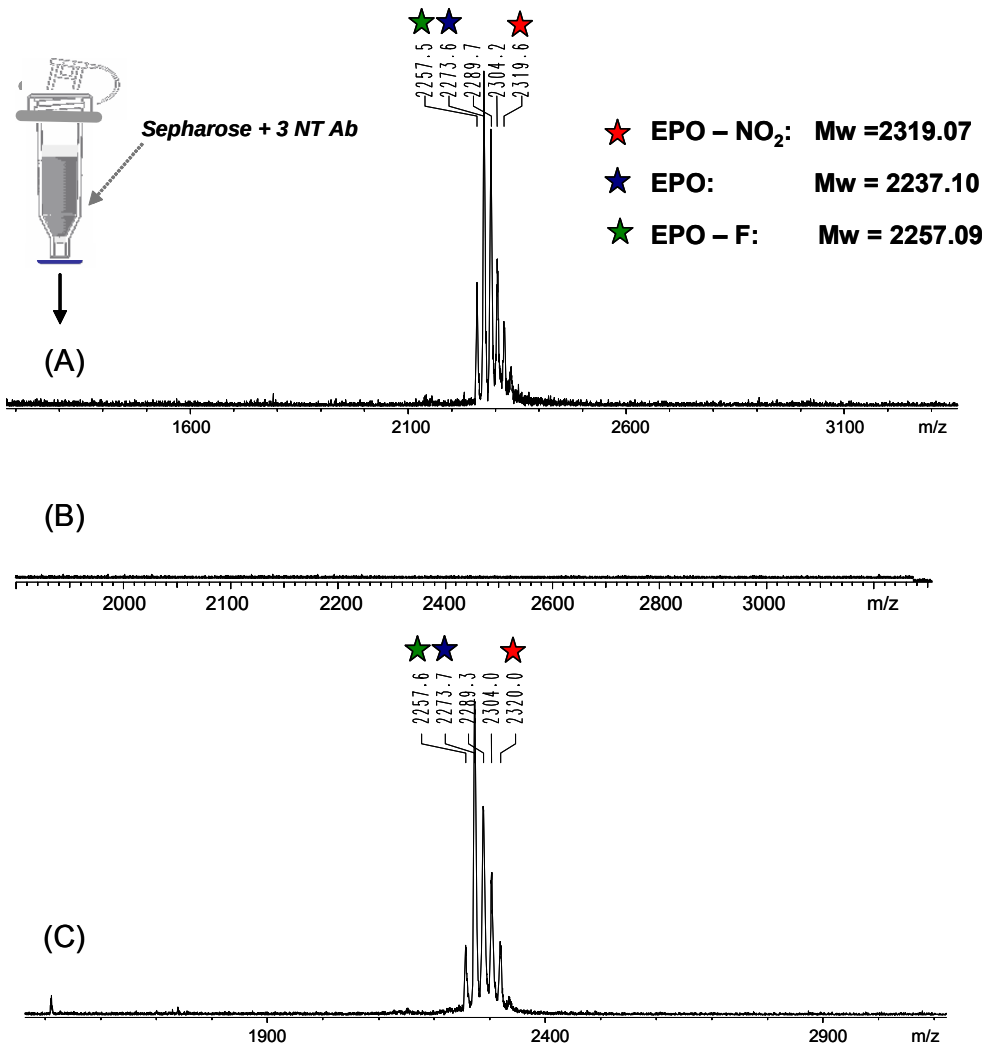

Figure 80: *Binding of Eosinophil peroxidase synthetic peptides to monoclonal 3NTAb **3**. MALDI-TOF mass spectrum of (A) supernatant (unbound peptides) washing (B) and elution (bound peptides) (C) fractions*

3 EXPERIMENTAL PART

3.1 Materials and reagents

The following commercially available reagents were used in this work: Urea, DL-Dithiothreitol (DTT), TEMED, Coomassie Brilliant Blue G250, activated CH-Sepharose 4B, polyoxyethylen-sorbitanmonolaureat (Tween20), 2,2,2-trifluoroethanol (TFE), dimethylsulfoxide (DMSO), α-cyano-4-hydroxicinnamic acid (HCCA), iodoacetamide, Ponceau S dye, were purchased from **Sigma**. Acrylamide/bis solution (30% acrylamide, sodium dodecyl sulfate (SDS), trichloroacetic acid (TCA), acetonitrile (MeCN), tris-(hydroxymethyl)-aminomethane (Tris) and ethanol were purchased from **Roth**. Iodoacetamide, Bromophenol Blue, t-butylmethylether, N-methylmorpholine (NMM), piperidine, trifluoroacetic acid (TFA), triethylsilane, dihydroxy benzoic acid (DHB) were purchased from **Fluka Chemie**. CHAPS and D-(+)-Biotin was obtained from **Calbiochem**. N-α-Fmoc protected amino acids, NovaSyn TGR, N-α-Fmoc protected amino acids attached to NovaSyn TGA, Benzotriazole-1-yl-oxy-tris-pyrrolidino-phosphonium hexafluoro-phosphate (PyBOP) were purchased from **NovaBiochem**. Fmoc-3-nitro-Tyr-OH was purchased from **Bachem**. N, N-dimethylformamide (DMF) was purchased from **Acros Organics**. Disodium hydrogen phophate-2-hydrate (Na_2HPO_4) was from **Riedel-de Haen**. The enhanced chemiluminescence (ECL) kit and nitrocellulose transfer membranes (Hybond C, pore size 0.5 µm) were purchased from **Amersham Biosciences**.

The reagents and solvents were of analytical grade, or highest available purity.

3.2 Enzymes, Antibodies and Proteins

Human angiotensin II, human bradykinin, human angiotensin I, human neurotensin,human adrenocorticotropic hormone (ACTH), bovine insulin ß-chain oxidized, bovine insulin, bovine serum albumin: **Sigma.**

Sequence grade TPCK-modified trypsin, Porcine: was purchased from **Promega**, Pronase from Streptomyces griseus was obtained from **Roche Molecular Diagnostics**. Thermolysin, type X from Bacillus thermoproteolyticus rokko was purchased from **Sigma**.

Mouse anti-3 nitrotyrosine monoclonal antibodies were from different companies as summarize in Table 13. A rabbit polyclonal antibody against PGI_2 synthase was produced according to Siegle et al [217]. Horse radish peroxidase (HRP) goat anti-mouse IgG and HRP-anti-biotin antibody were purchased from **Jackson Immunoresearch.** HRP- goat anti-rabbit IgG was obtained from **Pierce** (stock solutions 0.8 mg/ml).

Table 13: *monoclonal 3-nitro-tyroine antibodies employed in the present work*

Company	Antibody details
Chemicon International	Mouse Anti-Nitrotyrosine Monoclonal Antibody (MAB5404) **Concentration:** 1mg/ml **Immunogen:** Nitrated KLH **Applications :** Western blot: 1-100-1:1000
Upstate Biotechnology	Anti-Nitrotyrosine, clone 1A6 **Concentration:** 1mg/ml **Immunogen:** Nitrated KLH **Applications :** Immunocytochemistry: 5-10µg/ml
Santa Cruz	Mouse Monoclonal Nitrotyrosine (39B6) **Concentration:** 0.2mg/ml **Immunogen:** 3-(2-(4-hydroxy-3-nitrophenyl)acetamido) propionic acid-bovine serum albumin conjugate **Applications :** Western blot 1:200-1:2500

3.2.1 Isolation and preparation of proteins

3.2.1.1 Preparation of bovine aortic microsomes

Endothelial and smooth muscle layers from 8 to 10 freshly received bovine aorta were isolated by dissection at 4 °C, rapidly frozen in liquid nitrogen, and stored at 70°C. Frozen strips were homogenized at 0–4 °C in a Waring blender in 100 mM potassium-phosphate buffer, pH 7.5, containing 1 mM EDTA, 0.1 mM dithiothreitol, 0.1 mM butylated hydroxytoluene, and 44 mg/L phenylmethylsulfonyl fluoride. The microsomal fraction was obtained by centrifugation as described by Ullrich *et al.* [218] to a final volume of 75–100 ml, with a protein concentration of 10–20 mg/ml. The homogenization buffer contained 50 mM K_2HPO_4, pH 7.5, without additional protease inhibitors. (These experiments were performed by P. Schmidt and M. Bachschmid in the Laboratory of Biological Chemistry, University of Konstanz).

3.2.1.1.1 Peroxynitrite treatment of bovine aortic microsomes

PN was a gift from Dr. Koppenol (ETH Zürich, Switzerland) and was synthesized from NO and potassium superoxide according to Kissner *et al*. [219]. Reaction with PN was carried out with microsomes because active enzyme is required for nitration and further purification steps involving denaturating detergents partially inactivate the protein. PN (10 µl) at a defined concentration was quickly added by thorough Vortex mixing to an ice-cold microsomal suspension (990 µl, total protein concentration 1 mg/ml in 50 mM potassium-phosphate buffer, pH 7.5). Controls were treated with decomposed PN (24 h at room temperature) (The PN reaction was performed by M. Bachschmid in the Laboratory of Biological Chemistry, University of Konstanz).

3.2.2 Isolation and purification of eosinophil proteins

All three eosinophil proteins were isolated from four patients with hypereosinophilia; abnormal elevate number of eosinophil in blood, using standardized protocols previously described [132, 162]. All samples were obtained according to approved protocols by the ethic committee of Mayo Clinic Laboratories in Rochester, and upon informed consent of patients. Pure eosinophil samples at an estimated concentration were provided by Prof. Döring and M. Ulrich, Institute of Medical Microbiology and Hygiene, Universitätsklinikum Tübingen,

3.3 Solid phase peptide synthesis (SPPS)

The peptide sequences described in this work were synthesized by SPPS according to Fmoc/tBu strategy using a semiautomated peptide synthesizer EPS 221 (Abimed, Germany). The peptide synthesizer is based on a pipetting robot operated from a keypad controller with a disc drive. Separate software allows the modification of the program on a standard PC according to the scale of the synthesis and the sequence-related difficulties of the peptide to be synthesized.

The general procedure of SPPS employed is shown in Figure 81.

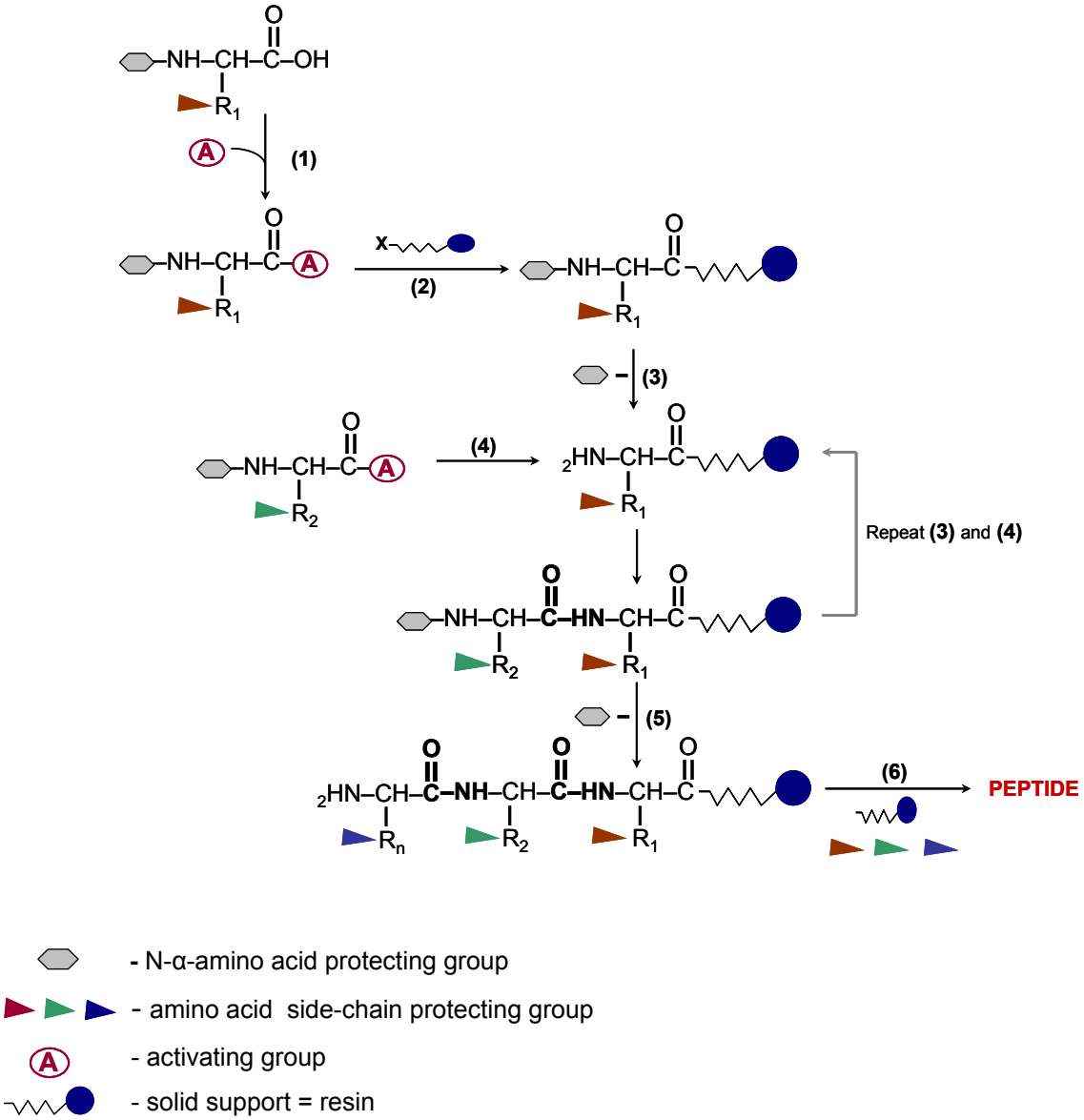

Figure 81: *Schematic representation of the solid phase peptide synthesis according to the Fmoc strategy*

A single peptide was synthesized on NovaSyn TGR resins which contain an acide-labile Rink amide linker providing amidated carboxy-terminal at the peptide after cleavage Different pre-loaded NovaSyn TGA resins (N-α-Fmoc protected amino acids attached to NovaSyn TGA) have been used in order to obtain after the final cleavage free carboxy-terminal at the peptide (Figure 60). Before beginning the synthesis the resin is washed with 30 ml of DMF followed by 10 minutes incubation time. This step ensures a good solvation and accessibility of the growing peptide chains.

The amino acids used were N-(α)-fluorenylmethyloxycarbonyl (Fmoc) protected. The side-chain protecting groups are described in the appendix 3. For the synthesis, the amino acids were weighted considering a fivefold molar excess relative to the amount of resin.

Using a NovaSyn TGR resin the initial step of the synthesis is the activation of N-α - Fmoc protected amino acid followed by an immediate coupling reaction on the DMF-swelled-resin. Whereas using pre-loaded NovaSyn TGA resin which contains already the first N-α - Fmoc protected amino attached to the resin, the initial step of the synthesis is deprotection of Fmoc group in order to release free N-terminal group which will react with the second activated amino acid.

Deprotection of the protected N (α)-amino group: Fmoc group removal occurs via base-induced β-elimination and is achieved by a short treatment (5 min) addition of 20% piperidine in DMF. As a result dibenzofulvene and carbon dioxide are split off (Figure 82). In general this treatment is repeated and slightly prolonged (15 min) and under these conditions complete deblocking is attained in most cases.

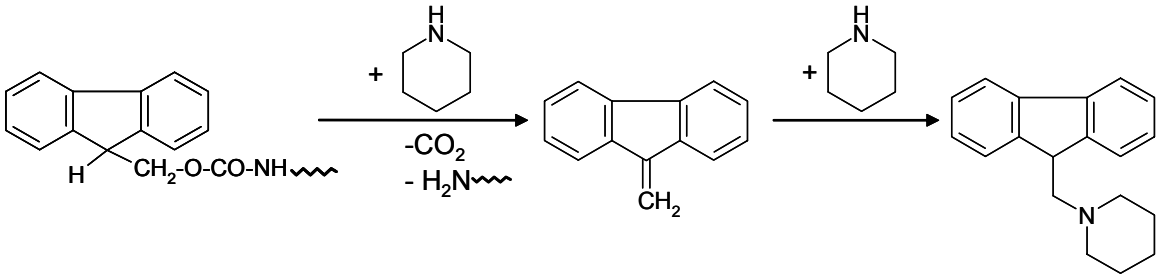

Figure 82 : *Schematic representation of Fmoc removal (deprotection step).*

Activation and coupling of a side chain protected amino acid: The amino acid is activated by addition of PyBOP (benzotriazol-1-yl-oxy-tris-pyrrolidinophosphonium hexafluorophosphate) in presence of a catalytic base, NMM (N-methyl morpholine). Both reagents are used as stock solutions with a concentration of: 0.9 mmol/ml PyBOP and 4 mmol/ml NMM. PyBOP is used in tandem with a tertiary amine base which abstracts the acidic carboxyl proton. The generated carboxylate anion attacks the positively charged phosphorous atom, substituting for the benzotriazolyl group. The benzotriazolyl anion itself acts as a nucleophile at the acyl centre. In the

resulting substitution reaction the OBt ester and a phosphonamide are formed (s. Figure 83).

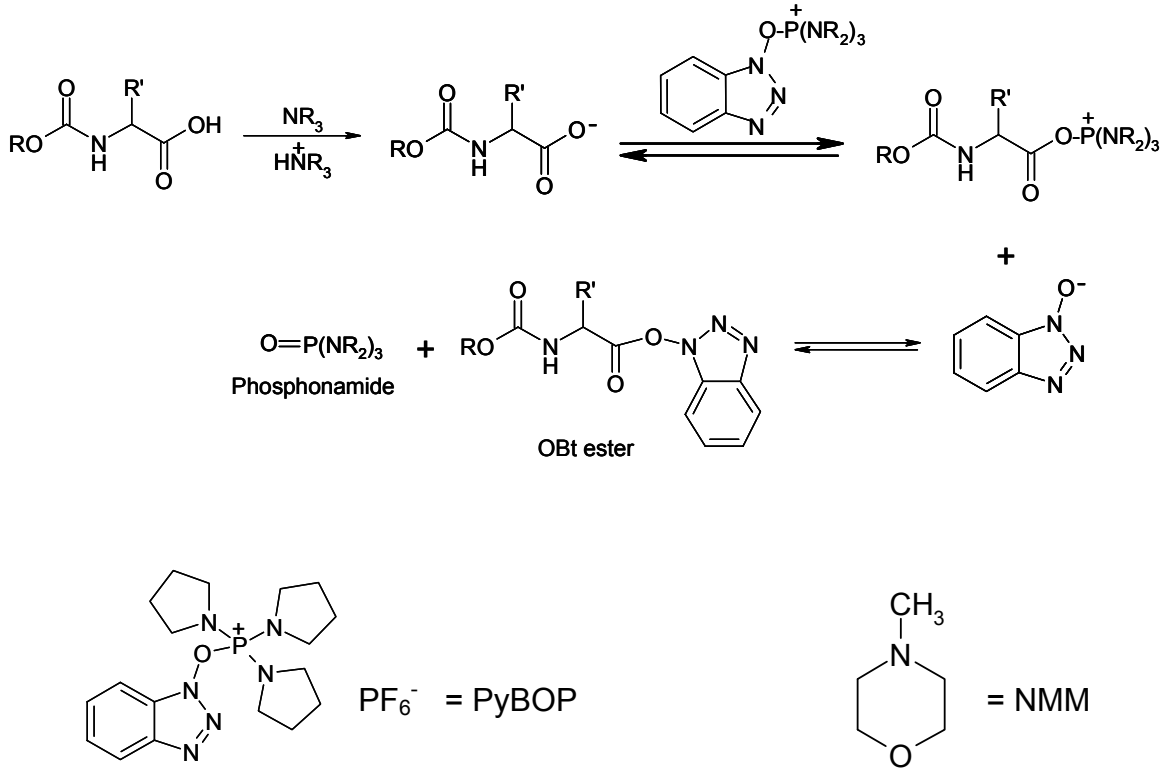

Figure 83: *Schematic representation of the activation of amino acids by PyBOP in presence of NMM.*

The solubilized and activated amino acid is added to the resin and incubated for 30 min. Depending on the amino acid sequence; a double coupling procedure might be employed by solubilization of a second cartridge containing the same amino acid followed by addition to the resin and incubation.

Cleavage of the peptide from the resin: Optimum cleavage conditions are very much dependent on the individual amino acid residue present, the side chain protecting groups and the type of linker attached to the resin. For majority of peptide, it cleavage from the resin may be performed with TFA as cleavage reagent, triethylsilan and deionized water as scavengers (95: 2.5: 2.5). The reaction takes place 2-3 hours at room temperature in the darkness. After cleavage the resulted mixture was precipitated with cold *t*-butylmethylether (10 ml ether/ml cleavage

cocktail) over night at -28 ^{o} C. Then the precipitate was filtered off, washed several times with diethylether up to the elimination of TFA and scavengers. After the last filtration, the peptide was solubilized in 5% acetic acid (aqueous solution) prior to freeze-drying.

3.4 Chromatographic and electrophoretic separation methods

3.4.1 Reverse-Phase High Performance Liquid Chromatography

High-performance liquid chromatography (HPLC) is used frequently in biochemistry and analytical chemistry to separate components of a mixture by using a variety of chemical interactions between the substances being analyzed (analyte) and the chromatography column. Molecules that posses some degree of hydrophobic character, such as proteins and peptides, can be separated by reverse phase chromatography with excellent recovery and resolution. RP-HPLC operates on the principle of hydrophobic interactions, which result from repulsive forces between a polar eluent, the relatively non-polar analyte, and the non-polar stationary phase.

The sample to be analysed is introduced into the HPLC column via a manual injector in a small volume directly into the stream of mobile phase and is retarded by specific chemical or physical interactions with the stationary phase as it traverses the length of the column. The silanol groups of the support are chemically derivatized with hydrophobic alkyl chains (C4, C8, and C18) that interact with the hydrophobic moieties of the analyte. Polypeptides are eluted from the reverse phase column with aqueous solvents containing an ionic modifier to adjust the pH and an organic modifier to displace and elute the peptide. An increasing gradient in the organic modifier is applied by using a two-phase mobile system:

Solvent A: 0.1 % (v/v) TFA in MilliQ
Solvent B: 80% (v/v) acetonitrile, 0.1% (v/v) TFA in MilliQ

The solutions were thoroughly deaerated prior to use by vacuum combined with sonication. The sample was dissolved in solvents that are compatible with the mobile

phase (usually the components of the gradient starting point) to avoid precipitation in the pores of the column packing. To prevent column contamination and damage the sample was centrifuged before injection.

Analytical RP-HPLC was performed on a Bio-Rad system (Bio-Rad Laboratories, Richmond, CA) using different columns, depending on the hydrophobicity of the sample to be analyzed: (i) analytical Nucleosil 300-7 C_{18} column (250x4 mm, 300 Å, 7 µm) (Macherey-Nagel, Düren, Germany); (ii) PLRP-S column (250 x 4.6mm, 300 Å, 5µm) contain rigid macroporous spherical particles of polystyrene/divinylbenzene (Polymer Laboratories, Darmstadt, Germany). Linear gradient elution (0 min 10% B; 5 min 10% B; 55 min 60% B) with eluent A (0.1% TFA in water) and eluent B (0.1% TFA in acetonitrile-water (80:20 v/v)) was used at a flow rate of 1 mL/min. The samples were dissolved in eluent A and the peaks were detected at two different wavelengths λ=365 nm for nitrated peptides and λ= 220 nm for non-nitrated peptides. The purification of polypeptides was carried out on a Knauer system (Bad Homburg, Germany) using a preparative C_{18} column (GROM-SIL 120 ODS-4 HE, 10 µm, 250x20 mm, pore size 120 Å; Herrenberg-Kayh, Germany) The same eluents as described above with appropriate linear gradients were applied. Flow rate was 10 mL/min for preparative HPLC. Peaks were detected at 365 nm and 220 nm.

3.4.2 Sodium dodecyl sulphate - polyacrylamide gel electrophoresis

Gel electrophoresis is the most commonly used method for determining the size and amount of protein chains. SDS-PAGE, sodium dodecyl sulfate polyacrylamide gel electrophoresis, is a technique used in biochemistry, genetics and molecular biology to separate proteins according to their electrophoretic mobility (a function of length of polypeptide chain or molecular weight as well as higher order protein folding, posttranslational modifications and other factors). The solution of proteins to be analyzed is first mixed with SDS, an anionic detergent which denatures secondary and non–disulfide–linked tertiary structures, and applies a negative charge to each protein in proportion to its mass. Polyacrylamide gel separates protein molecules according to both size and charge. It is a synthetic gel, thermo-stable, transparent, strong, and relatively chemically inert, can be prepared with a wide range of average

pore sizes; can withstand high voltage gradients, and is feasible to various staining and destaining procedures.

SDS-PAGE was performed according to Laemmli [220] using the Mini-Protean II gel or the Mini-Protean 3 electrophoresis system (BioRad, München, Germany). SDS-polyacrylamide gels were cast between two glasses plates and the dimensions of the each resulted gel were 90 x 60 x 1 mm.

SDS-PAGE is performed as a discontinuous (DISC) electrophoresis utilizing gels of different pore sizes namely stacking gel (spacer gel) which is pour over the top of the separating gel (resolving gel). When proteins migrate from one gel to the other they become concentrated into sharp bands, which produce higher resolution. The size of the pores created in the gel is inversely related to the amount of acrylamide used. Gels with a low percentage of acrylamide are typically used to resolve large proteins and high percentage gels are used to resolve small proteins. Table 14 provides recipes for preparing gels with different acrylamide concentrations.

Table 14: *Composition of SDS-polyacrylamide gels according to Laemmli protocol.*

Monomer concentration (%T, 2.6% C)	**Stacking gel**	**Separating gel**		
	5%	**10%**	**12%**	**15%**
4 x Stacking gel buffer [a]	2.5 ml	-	-	-
4 x Separating gel buffer [b]	-	6 ml	6 ml	6 ml
MilliQ water	5.8 ml	10 ml	8.4 ml	6 ml
Acrylamide/bis solution [c] (30.8% T, 2.6% C)	1.7 ml	8 ml	9.6 ml	12 ml
APS [d]	85 µl	125 µl	125 µl	125 µl
TEMED [e]	20 µl	20 µl	20 µl	20 µl

[a] 0.5 M Tris-HCl, 0.4% SDS (w/v), pH 6.8

[b] 1.5 M Tris-HCl, 0.4% SDS (w/v), pH 8.8

[c] 30% (w/v) Acrylamide, 0.8% (w/v) N, N'- Methylenebisacrylamide

[d] 10% (w/v) Ammonium persulfate

[e] N, N, N', N'- tetramethylethylenediamine

The proteins are solubilizpupued and denatured using the stock solution of SDS reducing buffer (50 mM Tris-HCl, 4 % (w/v) SDS, 12 % (w/v) Glycerol, 100 mM DTT, 0.02 % (w/v) bromophenol blue, pH 6.8) and boiled for 5 min at 57 °C. The electrode (running) buffer was composed of 25 mM Tris, 192 mM Glycin and 0.1% SDS. Gel electrophoresis was carried out using a Power/PAC 1000 power supply (Bio-Rad, München, Germany) at 50 V for ca. 30 min until the tracking dye went into the separating gel, and at 100 V for ca. 2 h until the tracking dye reached the anodic end of the separating gel.

The molecular weights of unknown proteins were estimated by running standard proteins of known molecular weights in a separate lane of the same gel. In the present work two different molecular weight markers were employed: PS-101, protein molecular weight marker from Jena Bioscience (Jena, Germany) (s. Table 15) and PageRuler^{TM} unstained protein ladder (SM0661) from Fermentas Life Science (St. Leon-Rot, Germany) [221].

Table 15: *Protein molecular weight marker for SDS-PAGE-analysis (PS-101, Jena Bioscience)*

Molecular weight marker proteins	Molecular weight (Da)
Phosphorylase b	97,400
Bovine serum albumin	66,200
Alcohol dehydrogenase	37,600
Carbonic anhydrase	28,500
Myoglobin	18,400
Lysozyme	14,400

The gels were scanned using a GS-710 Calibrated Imaging Densitometer and image analysis was carried out using the MultiAnalyst software (BioRad, Richmond, CA, USA).

3.4.2.1 Sensitive colloidal Coomassie staining

This protocol is a modification of the method of Neuhoff et al. [222] ,which involves the binding of Coomassie Blue G250 to proteins. In acidic solution Coomassie® Brilliant Blue G-250 has an absorbance maximum at 465 nm. After the addition of protein, hydrophobic amino acid residues and arginine residues bind to the dye and produce a very low background due to colloidal properties of the stain. As a result, the absorbance maximum of the dye shifts from 465 nm to 595 nm (Figure 84). Coomassie Blue binds roughly stoichiometrically to proteins, so this staining method is well suited for densitometric determinations. The proteins are detected as blue bands on a clear background, after fixing the gel with TCA for obtaining maximum sensitivity.

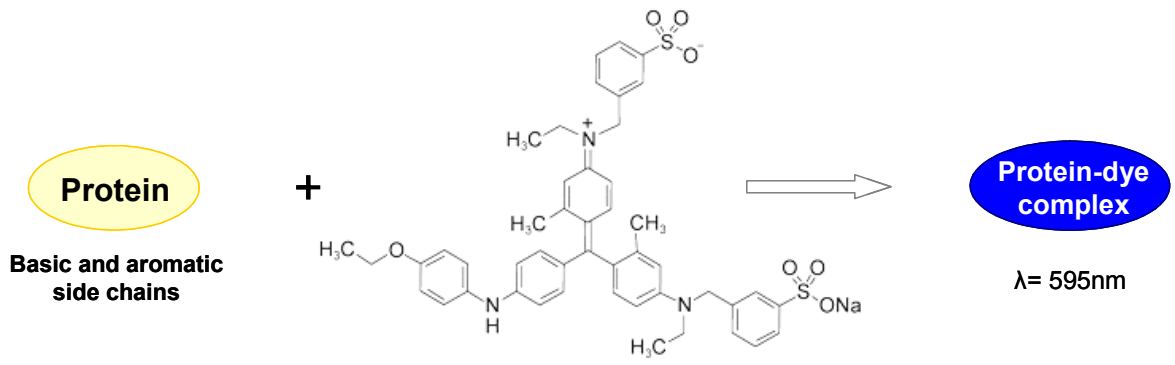

Figure 84: *Scheme of protein staining by Coomassie® Brilliant Blue G-250*

The detailed protocol is described below:

1. Fix the gel with gentle agitation for at least 1 hour in 12% (w/v) TCA
2. Prepare the colloidal Coomassie stain by mixing 200 ml solution of 10% (w/v) ammonium sulfate and 2% phosphoric acid in MilliQ water with 2 ml of 5% Coomassie Blue G250 dissolved in MilliQ water. Shake strongly this solution for several minutes and then add 50 ml methanol. Shake again the new solution (colloidal Coomassie stain) for several minutes prior to use.
3. Remove the fixative and place the gel in the freshly prepared colloidal Coomassie stain. Stain the gel overnight with gentle agitation.

4. Wash the gel with 25% methanol in MilliQ water for 1 hour.
5. Wash the gel with MilliQ water and repeat washing step until the protein bands are at the desired contrast against the background of the gel.

3.5 Chemical modification reaction and enzymatic fragmentation of proteins

The aim of in gel digestion protocols is to obtain sufficient cleavage to extract enough peptides from the gel matrix in such a way, so that these are compatible with subsequent MS analysis. A series of enzymes with different cleavage specificities were used for the proteolytic digestion studies.

3.5.1 Reduction and alkylation of disulfide bonds in solution

Prior to the digestion of highly pure (> 90%) protein solution the reduction of disulfide bonds was performed in two simple steps. The protein was first dissolved to a concentration of 1µg/µl in 10 mM NH_4HCO_3 (pH 8) and than DTT in 10 mM NH_4HCO_3 (50-fold excess, relating to the -S-S-bound in protein) was added. The reduction was carried out for 1h at 56°C under gentle shaking. After cooling to room temperature a solution of IAA in MilliQ was added in 2.2 fold excess relating to DTT amount and the reaction was performed for 45 min at ambient temperature in the dark with occasional vortexing. After lyophilization the sample were digested by using different enzymes.

Carboxymethylation may be carried out without prior reduction in order to modify only the cysteine residues that are not involved in disulfide bridges.

3.5.2 Proteolytic digestion of proteins in solution using trypsin

Peptides and proteins to be proteolytically digested were solubilized in 10 mM NH_4HCO_3, pH=8, at a concentration of 0.5-1 µg/µL. Stock solutions of the sequence grade TPCK-modified porcine trypsin 1 µg/µl in 50 mM acetic acid were stored at -28°C. Trypsin was added to the sample at an enzyme to substrate ratio of 1:20 (w/w) or 1:50 (w/w) and the digestion was carried out at 37°C [223]. The reaction was monitored in time by removal of sample aliquots, quenching by freezing in liquid nitrogen. The resulting peptide mixtures were analyzed directly by mass spectrometry or were used for immuno- affinity experiments.

3.5.3 Proteolytic digestion of proteins in solution using thermolysin

Stock solutions of thermolysin 1 µg/µl were prepared in 50 mM Tris, pH 8.0, containing 5 mM $CaCl_2$. The solution was stored at -28°C as frozen aliquots for 1 month. For protein digestion a ratio of 1:50 (w/w) thermolysin: protein was used. The digestion was performed for 6 hours, at 60ºC in 50 mM Tris, pH 8.0, 5 mM $CaCl_2$, and 10% (v/v) ACN. The reaction was quenched by freezing the sample with liquid nitrogen.

3.5.4 In-gel trypsin digestion procedure of Coomassie Brilliant Blue stained proteins

Before excising the bands, the gel was washed in MilliQ for 15 min. The spot of interest was cut out from the gel, into 1-2 mm^2 pieces, placed in a siliconized eppendorf tube. After washing for 15 min with 100 µl MilliQ, the liquid was discarded and the gel pieces were dehydrated by incubation for 30 min in 100 µl of 60% ACN. The liquid was discarded and the gel pieces were dried using a centrifugal vacuum evaporator. The pieces are rehydrated with 100 µl 50 mM NH_4HCO_3 for 15 min and dehydrated with 60% ACN. This step is repeated until the gel pieces are destained. The gel pieces are lyophilized to complete dryness. For digestion, an enzyme solution containing 25 mM NH_4HCO_3 and 12.5 ng/µl trypsin is prepared on ice. The

gel pieces are allowed to rehydrate for 45 min on ice or at 4°C, in the appropriate volume of enzyme solution needed to completely swell the gel. The excess of enzyme solution is removed by several washing steps; the gel pieces are covered with 25 mM NH_4HCO_3 and incubated overnight at 37°C. Proteolytic peptides are extracted by incubating gel pieces with 3:2 ACN/ 0.1%TFA (v/v) for 2 h at room temperature. The solution is collected and the step is repeated 2 times.

3.5.5 Reduction and alkylation of disulfide bonds in gel matrix

After destaining a volume of 10 mM dithiotreitol (DTT) in 25 mM NH_4HCO_3 sufficient to cover the gel pieces was added, and the proteins were reduced for 1 h at 56 °C. After cooling to room temperature, the DTT solution was replaced with roughly the same volume of 55 mM iodoacetamide in MilliQ. After 45 min incubation at ambient temperature in the dark with occasional vortexing, the gel pieces were washed with 50-100 μL of 25 mM NH_4HCO_3 for 10 min, and shrunk again by addition of the same volume of acetonitrile. The liquid phase was removed, and the gel pieces were completely dried in a vacuum centrifuge.

3.5.6 In gel thermolysin digestion of nitrated PGI_2 synthase

After destaining the shrinked gel pieces were reswollen for 1 h in 200 µl of digest solution containing 50 mM Tris, pH 8.0, 5 mM $CaCl_2$, 10% (v/v) acetonitrile, and 25 ng/µl thermolysin. Then the supernatant was removed and the proteolytic digestion was carried out for 24 h at 50 °C under gentle shaking. Peptides were extracted several times with 3:2 ACN/ 0.1%TFA (v/v) for 24 h, lyophilized to dryness, and analyzed on the above described HPLC system. Peptide fragments were detected at 220 and 365 nm; peaks showing a strong absorption at 365 nm were collected and lyophilized for further mass spectrometric analysis.

3.6 Circular Dichroism Spectroscopy (CD)

CD spectroscopy measures differences in the absorption of left-handed polarized light versus right-handed polarized light which arise due to structural asymmetry of a substance. CD spectroscopy has been extensively applied to the structural characterization of peptides and proteins such as (a) monitoring conformational changes (e.g., monomer-oligomer, substrate binding, denaturation processes) and (b) prediction of secondary structural content. Specifically, peptide/protein secondary and tertiary structure can be monitored by the peptide transitions in the far UV (~180-220 nm-were the chromophore in the peptide bond) and by the aromatic side chain transitions in the near UV (~ 250-300 nm). CD spectra can then be analyzed for the different secondary structural types: e.g. alpha helix, beta sheet or turns) (Figure 85).

The spectral features of each secondary structural type are summarized below:

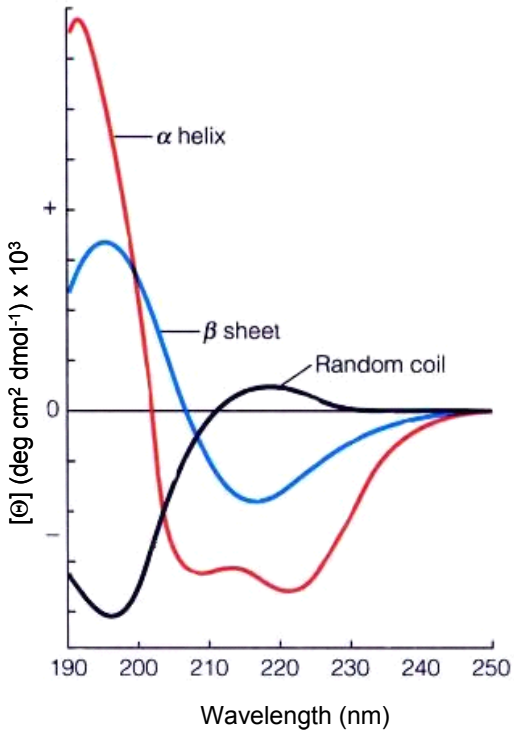

Far UV-CD of random coil:

- negative band below 200 nm ($\pi \rightarrow \pi^*$)

Far UV-CD of β-Sheet:

- negative band at218 nm ($\pi \rightarrow \pi^*$)
- positive band at 195 nm ($n \rightarrow \pi^*$)

Far UV-CD of α-helix

- negative bands at
  - 208 nm ($\pi_{parallel} \rightarrow \pi^*$)
  - 222 nm ($n \rightarrow \pi^*$)
- positive band at 190 nm($\pi_{perpendicular} \rightarrow \pi^*$)

Figure 85: *Circular dichroism spectra of poly-L-lysine in various conformations. In red 100% helix, in blue 100% β-sheet and in black 100% random coil.*

The simplest method of extracting secondary structure content from CD data is to assume that a spectrum is a linear combination of CD spectra of each contributing secondary structure type (e.g., "pure" alpha helix, "pure" beta strand etc.) weighted by its abundance in the polypeptide conformation. The major drawback of this approach is that there are no standard reference CD spectra for "pure" secondary structures. Synthetic homopolypeptides used to obtain reference spectra are in general poor models for the secondary structures found in proteins.

Circular dichroism (CD) spectra were recorded on a Jasco spectropolarimeter; model J-715, equipped with a Xe lamp. The measurements were carried out at 25°C in quartz cells of 0.05 cm path-length; under constant nitrogen flush. The instrument was calibrated with 0.06% (w/v) ammonium-d-camphor-10-sulfonate in water. In order to improve the signal to noise ratio, the spectra were averages of five scans between λ=270 and 180-190 nm. Results were expressed in terms of ellipticity, molar ellipticity or mean residue ellipticity (deg cm^2 $dmol^{-1}$) after subtraction of the solvent (PBS, MilliQ or TFE) baseline.

3.7 Desalting and concentration of the peptide and protein samples prior to mass spectrometric analysis

3.7.1 ZipTip cleanup procedure

The ZipTip cleanup procedure was performed using $ZipTip_{C18}$ pipette tips from Millipore. A ZipTip pipette tip is a micro-column with the resin prepacked into the narrow end of a 10 µl pipette tip. ZipTip pipette tips contain C_{18} or C_4 reversed-phase media for concentrating and purifying peptide and protein samples. $ZipTip_{C18}$ pipette tips are most applicable for peptides and low molecular weight proteins, while $ZipTip_{C4}$ pipette tips are most suitable for low to intermediate molecular weight proteins. The ZipTip method consists mainly in five steps: wetting and equilibration of the ZipTip pipette tip, binding of the peptides and/or proteins to ZipTip pipette tip, washing and elution. Table 16outlines the solutions required for use with ZipTip pipette tips containing C_{18} media.

Table 16: *Solutions required for use with ZipTip pipette tips containing C_{18} media.*

Solution	ZipTip$_{C18}$ Pipette Tips
Wetting solution	100% acetonitrile (ACN)
Sample preparation	0.5% trifluoroacetic (TFA) in MilliQ water; final sample solution pH < 4
Equilibration solution	0.1% TFA in MilliQ water
Wash solution	0.1% TFA in MilliQ water
Elution solution*	0.1% TFA/50% ACN with or without matrix

*For electrospray, elute with 2% acetic acid /50% methanol

3.7.2 Desalting and concentration of peptide samples using Microcon centrifugal filter devices

Microcon centrifugal filter devices offer a fast, convenient and reproducible means to concentrate, desalt, and purify microsamples of peptides and proteins. Samples of up to 500 µL can be rapidly reduced to as little as 5 µL. These easy-to-use, disposable units incorporate a low-binding YM regenerated cellulose membrane and an inverted spin sample transfer method which delivers outstanding recoveries (Figure 86). A deadstop feature avoids risk of spinning the sample to dryness. A wide range of ultrafiltration cut-offs is available, devices with cut-off 10000 (YM-10) being used in this work.

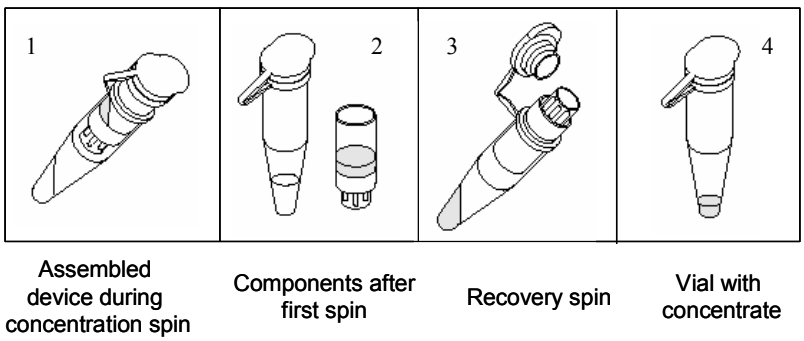

Figure 86: *Schematic representation of the Microcon centrifugal filter device.*

3.8 Immuno-analytical methods

3.8.1 Dot blot assay

1-2 µl peptides solution (1µg/µl) in PBS (pH= 7.4) were spotted on nitrocellulose (NC) membrane and dried for 5 min at room temperature. NC membranes were blocked for 2 hrs by using Roti®-Block solution in MilliQ. Membranes were then probed 1h with mouse monoclonal antibody against 3-nitro-tyrosine (1:2500) in PBS-Tween buffer. The membranes were then washed three times in PBS-Tween buffer and probed again with a goat anti-mouse horseradish peroxidase conjugate (1:5000, Sigma) in PBS-Tween for 45 min. After washing the membrane five times in wash buffer the immuno-positive spot were visualised by using ECL- Plus system (Amersham Pharmacia). The ECL- kit consists of two reagents, a luminol solution and an oxidizing solution which are added to react with the labelled secondary antibody.

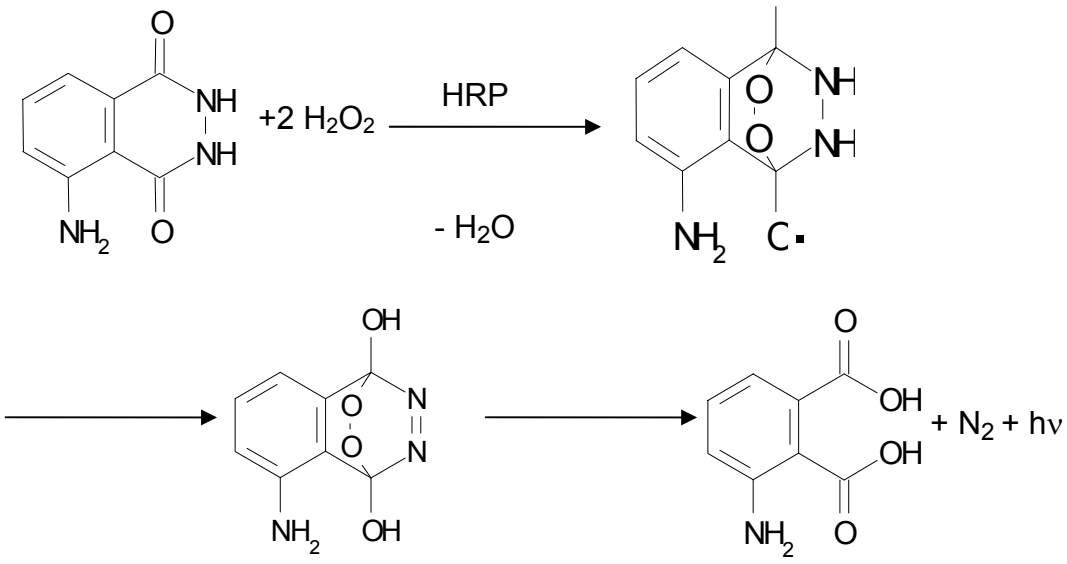

Figure 87: *Reaction scheme of Luminol detection in Dot-Blot- or Western-Blot-experiments*

The principle of detection procedure is that HRP-catalyzed oxidation of luminol by hydroperoxide ion in aprotic media generates an excited state product, 3-aminophtharate*, which emits blue luminescent lights of 425-510 nm as it decays to

the ground state. The antigen bound with HRP-labeled antibody shows a corresponding band on the X-ray film.

3.8.2 Western blot

The term “blotting” refers to the transfer of biological samples from a gel to a membrane and their subsequent detection on the surface of the membrane. Western blotting (also called immunoblotting because antibodies are used to specifically detect their antigen) was introduced by Towbin, *et al*. in 1979 [224].

After separation of EPO, ECP and EDN by 12% (v/v) SDS-PAGE (100V, 2h) the proteins were transferred onto a nitrocellulose membrane by a semidry blot procedure as shown in Figure 88.

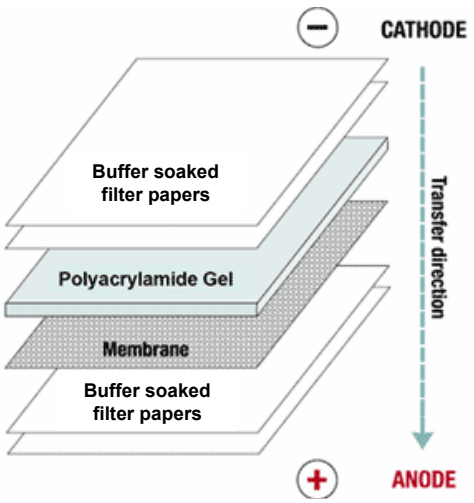

Figure 88: *Schematic representation of protein blotting with a semi-dry transfer unit.*

The transfer was performed using a constant current of 34 mA for 90 min. The blotting buffer contained 25 mM Tris, 152 mM glycine, 20% (v/v) methanol, pH 8.3. Transfer efficiency of proteins was examined by staining the membrane for 2 min with 0.1% Ponceau S in 5% (v/v) acetic acid. Ponceau S is an anionic dye that binds to the basic amino groups of proteins in acid solution and produces a vivid red colour with as little as ~ 0.05 g protein.

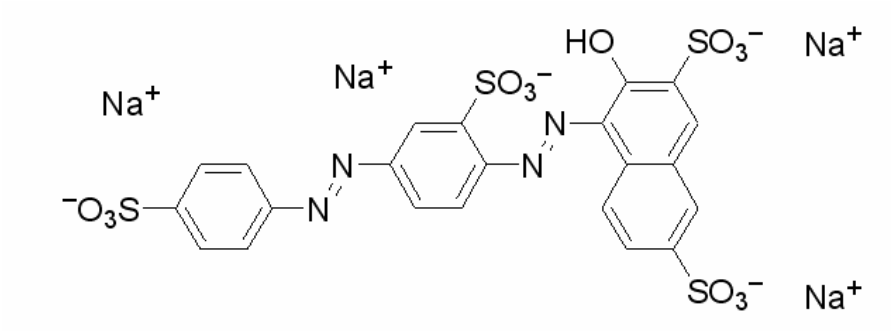

Figure 89: *Chemical structure of Ponceau S: 3-Hydroxy-4-(2-sulfo-4-[4-sulfophenylazo] phenylazo)-2,7-naphthalenedisulfonic acid sodium salt*

After destaining in PBS, the membrane was blocked with 5% Roti®-block (v/v) (Carl Roth GmbH + Co Karlsruhe, Germany) for 2 h at room temperature. The membrane was then incubated for 2 h with a mouse monoclonal antibody against 3-nitro–Tyrosine (1:2500). After repeated washing with PBS/0.1% Tween 20 the membrane was incubated for 45 min with a HRP-conjugated goat anti-mouse antibody at a dilution of 1:10000 for 45 min, and ECL (Amersham Biosciences, England) was used for detection of antibody binding according to the manufacturer's instruction.

3.8.3 Enzyme-Linked Immunosorbent Assay (ELISA)

96-well CovaLink ELISA plates (Nunc GmbH & Co. KG, Wiesbaden, Germany) were activated at room temperature with 100 µL/well DSS for one hour. After two washing steps with distilled water the wells were coated overnight at room temperature with 100 µL/well of peptides (12 serial dilutions of peptides in a concentration range between 0.003 and 3 µM) were prepared in PBS buffer which contains 5 mM Na_2HPO_4 and 150 mM NaCl, pH 7.5). The wells were washed four times with 200 µL/well of 0.05% Tween-20 v/v in PBS, pH 7.5, then the non-specific adsorption sites were blocked with 200 µL/well of 5% BSA w/v in PBS (2 hrs at RT). The anti 3-nitrotyrosine mAb c=1 µg/µL was diluted 2500 times in 5% BSA and added to each well (100 µL/well). After incubation at room temperature for one hour and washing steps, 100 µL of peroxidase labelled goat anti-mouse IgG diluted 10000 times in 5% BSA was added to each well. After an additional incubation for one hour and washing

three times with 200 µL/well PBS-T and two times with 200 µL/well 0.05 M sodium phosphate-citrate buffer, pH 5, 100 µL of *o*-phenylenediamine dihydrochloride in sodium phosphate-citrate buffer, pH 5, at c=1 mg/mL and 2 µL of 30% hydrogen-peroxide per 10 mL of substrate buffer was added. After 5-10 minutes, the absorbance at λ=450 nm was measured on a Wallac 1420 Victor^2 ELISA Plate Counter (PerkinElmer, Boston, MA).

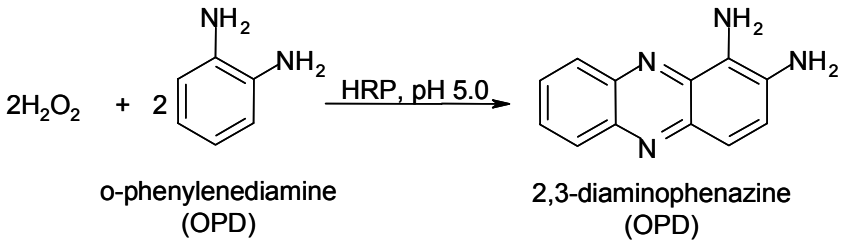

Figure 90: *Schematic representation of the reaction catalysed by horseradish peroxidase. The oxidation product of o-phenylenediamine produced by horseradish peroxidase is 2,3-diaminophenazine. This product is orange-brown in colour and can be read spectrophotometrically at 450 nm.*

In order to compare the binding intensities of different peptides, the concentration of peptides which was necessary for obtaining half maximum binding ($OD_{450\ nm}$ of ½) was calculated.

3.8.4 Immuno-affinity chromatography

3.8.4.1 Preparation of monoclonal anti 3NT antibody affinity column

100 µg of monoclonal anti 3-nitro-tyrosine antibody was dissolved in coupling buffer (0.2 M $NaHCO_3$, 0.5 M NaCl, pH 8.3). The solution was added to the appropriate amount of dry NHS-activated Sepharose (Sigma, FRG), (1 g sepharose swells in approximately 3 mL of coupling buffer) and incubated at room temperature under vigorous stirring. NHS-activated Sepharose is an excellent matrix for immobilizing antibodies, peptides or proteins. Accessible amine groups present on the N-terminal

or on (ε –amine group) of lysine residues react with NHS-ester forming a very stable amide bond, releasing N-hydroxysuccinimide (s. Figure 91).

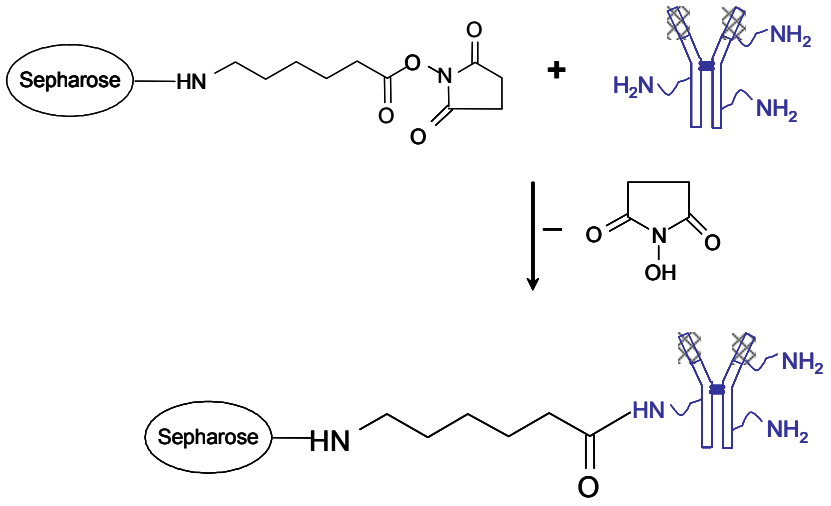

Figure 91: *Reaction of immobilizing antibodies on the N-hydroxysuccinimide-activated 6-Aminohexanoic acid - Sepharose. The reaction takes place at the free amino-terminus of the antibody molecule with the elimination of the N-hydroxysuccinimide. The new formed amide bond is chemically very stable and allows the use of different buffer systems for the affinity chromatography.*

Coupling was completed after 2-4 hrs, and the Sepharose-coupling product was loaded into a 0.8 mL micro-column (Mobitec, Germany) providing the possibility of extensive washing without significant loss of material. The washing steps are given below: 10 mL blocking buffer (0.1 M Ethanolamine, 0.5 M NaCl, pH 8.3), 10 mL washing buffer (0.2 M NaOAc, 0.5 M NaCl, pH 4.0). The washing steps were repeated four times for each buffer. The column was kept 1 h at room temperature and then washed again as described before. At the end the column was washed with 10 mL PBS buffer and stored at 4° C.

3.8.4.2 Study of antigen-antibody binding by affinity method

After the immobilization of 3-NTantibody on the NHS-activated Sepharose the column was ready to be used for the affinity experiments. For this the antigen peptides solution (prepared in PBS buffer, pH 7.4) was bound to the antibody column and reacted for 2h. The non–bound peptides were removed by washing steps using PBS buffer. The immune complex was dissociated by addition of 0.1 % TFA (aqueous solution, pH=2) on the column. The wash and elution fractions were collected, lyophilized, redissolved in 0.1% TFA and desalted by using ZipTip procedure before MALDI-TOF analysis.
For the comparison of differences in affinity binding of different peptides to 3-NT antibody an equimolar mixture, 200 µmol of each peptide was used in a normal affinity experiment.

3.8.4.3 Proteolytic affinity peptide extraction – PROFINEX

The proteolytical in solution generated ECP and EDN peptides fragments were added onto the micro-3-NT-antibody column and incubated under gently shaken for 2 hours at room temperature. The non-bound peptides fragments (supernatant fraction) were removed by blowing out the column almost to complete dryness of the affinity matrix using a 10 mL syringe. The matrix was subsequently washed with 100-200 mL PBS buffer for removal of unbound peptides. The immune complex between nitrated peptide and 3-NT antibody was dissociated by addition of 0.1% TFA.The collected fractions were analyzed by MALDI-TOF and nano-ESI FT-ICR-MS.

3.9 Mass spectrometric methods

3.9.1 Time of flight mass spectrometry

For MALDI-TOF MS analysis of proteins and peptides, samples are co-crystallized with an excess of organic matrix that absorbs at a specific wavelength (usually 337 nm). Typically, sinapinic acid (SA) is the matrix of choice for large proteins, whereas α-cyano-4-hydroxy-cinnamic acid (HCCA) is the preferred matrix for peptide mapping. Following a short laser pulse (3 ns), analytes are desorbed and ionized into the gas phase, and their m/z values are determined in a TOF mass analyzer. In TOF analyzers the mass-to-charge ratio of an ion is determined by measuring their flight time. After acceleration of the ions in the source to a fixed kinetic energy, they pass a field free drift tube with a velocity proportional to $(m_i/z_i)^{-1/2}$ (m_i/z_i is the mass-to-charge ratio of a particular ion species). Due to their mass-dependent velocities, ions are separated during their flight. A detector at the end of the flight tube produces a signal for each ion species. Typical flight times are between a few microseconds and several 100 µs. Mass accuracy determinations vary from 0.01% to 0.1% depending on the sample preparation technique and the method used for calibration. A schematic drawing of the TOF mass spectrometer set up with MALD ionization is given in Figure 92.

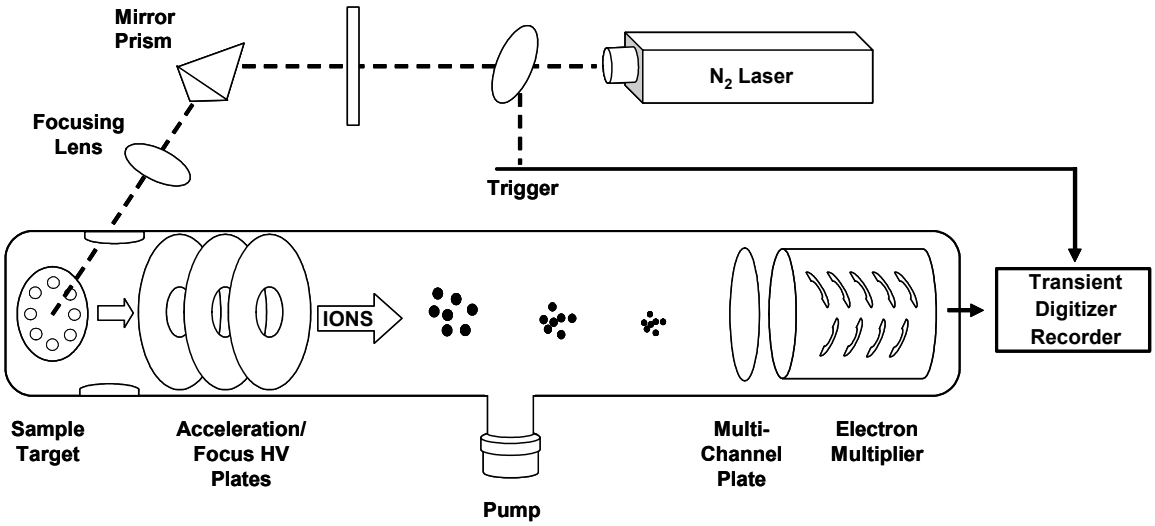

Figure 92: *Schematic representation of a linear time-of-flight matrix-assisted laser desorption mass spectrometer.*

MALDI-TOF MS analysis was carried out with a Bruker Biflex linear TOF mass spectrometer (Bruker Daltonik, Bremen, Germany) equipped with a nitrogen UV laser (λ_{max}=337 nm) and a delayed extraction system, a dual channel plate detector, a 26-sample SCOUT source, a video system and a XMASS data system for spectra acquisition and instrument control. For measurement 1µl of a freshly prepared saturated solution of α-cyano-4-hydroxy-cinnamic acid (HCCA) in acetonitrile/0.1% TFA (2:1) was applied onto the dry stainless steel MALDI target and 1µl of the sample solution was added. Desalting and concentration of the samples was achieved by using ZipTip$_{C18}$™ pipette tips (Millipore) as described before. Acquisition of spectra was carried out at an acceleration voltage (V_{acc}) of 20 kV and a detector voltage of 1.5 kV. Fifty to 200 single shots were accumulated into a final spectrum. External calibration was carried out using the average masses of singly protonated ion signals of standard peptide mixture.

Table 17: *Mass spectrometric characterisation of Peptides in standard mixture*

Peptides	pmol/ml*	$[M+H]^+$ Monoisotopic**	$[M+H]^+$ Average**
Angiotensin II	0.8	1046.5418	1047.20
Bradikynin	0.7	1060.5687	1061.23
Angiotensin I	1.2	12 96.6848	1297.50
Neurotensin	0.8	1672.9176	1673.95
Insulin bovine	1.3	5730.6081	5734.58
Additional peptides ions			
Insulin bovine	$[M+2H]^{2+}_{av.}$: 2867.78		
Insulin bovine-oxidized	$[M+H]^{+}_{av.}$: 3496.95		

** Peptide concentration in fin al solution*

*** m/z values indicated are calculated*

3.9.2 Fourier-transform Ion-Cyclotron Resonance mass spectrometry

FT-ICR mass spectrometric analysis was performed with a Bruker APEX II FT-ICR instrument equipped with an actively shielded 7T superconducting magnet (Magnex, Oxford, UK), a cylindrical infinity ICR cell. The ICR cell consists of 3 opposing pair of plates placed in the homogeneous region of the magnet. The analyte ions are trapped inside the cell by a low potential (1V) applied to the trapping plates. In a strong magnetic field along the z-direction the ions are constrained to move in circular orbits in the xy-plane referred as cyclotron motion. The frequency of the ion cyclotron motion is identical for all ions of the same m/z and is independent of their velocity as it can be seen in the cyclotron equation:

$$\omega = zB/m$$

The excitation is accomplished by applying an alternating voltage to one opposing pair of plates oriented parallel to the electric field. If the frequency of the alternating electric field equals the cyclotron frequency of the ions of a particular m/z, then the cyclotron motion of these ions will be coherently excited. After excitation these ions move as a single ion packet on an orbit with increased radius.

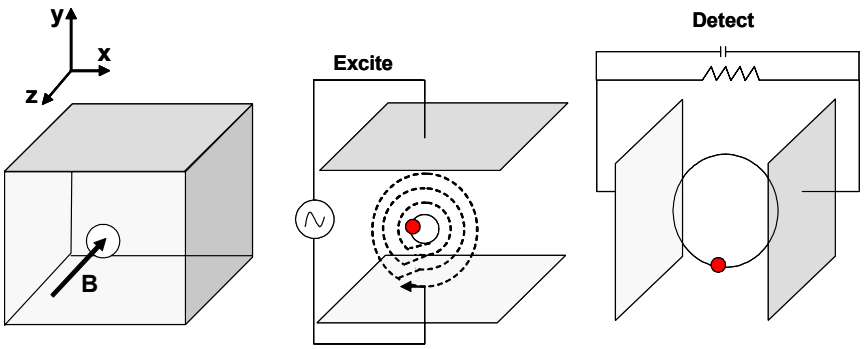

Figure 93: *Schematic representation of an ICR cell used in FTMS*

The rotating ion packet induces an alternating charge in the detection plates of an ICR cell and an alternating voltage across this conductor, which is amplified and registered as transient or time domain signal. After its acquisition, the time domain data is stored and subsequently Fourier transformed yielding the cyclotron frequency spectrum, which is converted to the mass spectrum. A very good vacuum (10^{-9}) is required to avoid collisions of the ion packet in the cell with neutral molecules that could lead to a decrease of the radius.

3.9.2.1 MALDI-FT-ICR mass spectrometry

MALDI-FT-ICR mass spectrometry was performed with the Bruker APEX II FT-ICR mass spectrometer using and an external Scout 100 fully automated X-Y target stage MALDI source with pulsed collision gas. A schematic representation of the APEX II FT-ICR mass spectrometer equipped with MALDI source is depicted in the Figure 94. The MALDI target is a circular steel plate with 25 or 49 sample placement spots. This plate is placed on the end of a cylindrical target manipulation rod and held in place by a magnet. The rod can be inserted into or removed from the mass spectrometric vacuum system. In the inserted position, the target plate is fixed at 1 mm distance from the hexapole ion guide. The pulsed nitrogen laser was operated at 337 nm and ions generated in the MALDI process were cooled with the pulsing collision gas and directly captured into the hexapole ion guide. Ions generated by 20-30 laser shots were accumulated in the hexapole for 0.5-1s at 30V and extracted at -15V.

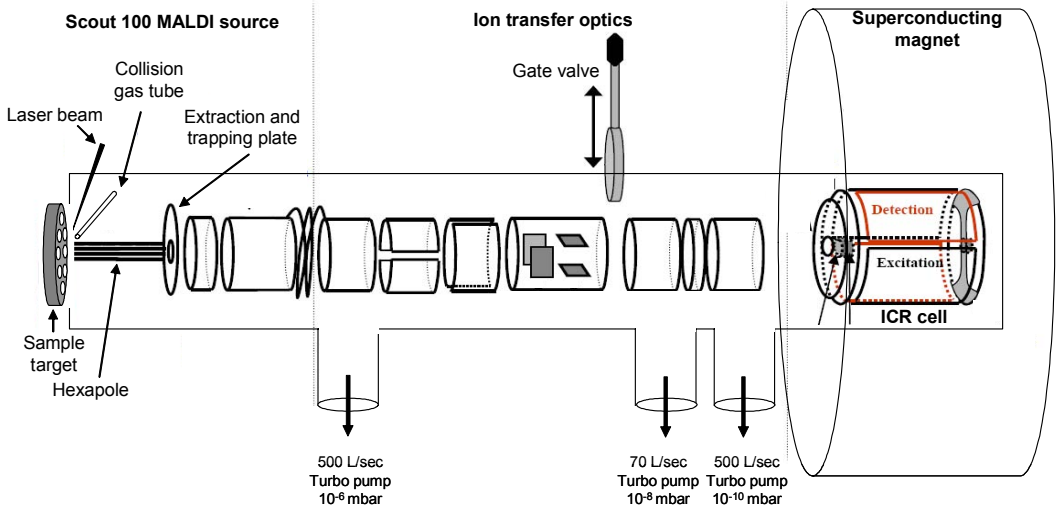

Figure 94: *Schematic representation of Bruker APEX II FT-ICR mass spectrometer equipped with MALDI source*

Trapping of the ions into the analyzer cell was performed applying a small, symmetric positive voltage (1-1.2 V for positive ions) to the trapping plates. In order to detect the trapped ions, they were excited applying an oscillating electrical field. The image current generated by the coherent motion of the ions in the ICR cell was detected, amplified and digitized yielding a time domain signal or transient. After its acquisition, the time domain data was stored and subsequently Fourier transformed yielding the cyclotron frequency spectrum, which was then converted to the mass spectrum.

A 100 mg ml^{-1} solution of 2,5-dihydroxybenzoic acid (DHB) in acetonitrile:0.1% trifluoroacetic acid in water (2:1) was used as the matrix. 0.5µl of matrix solution and 0.5 µl of sample solution were mixed on the stainless steel MALDI target and allowed to dry in ambient air. External calibration was performed prior to each measurement using the monoisotopic masses of singly protonated ion from the standard peptide mixture (s. Table *17*). Acquisition and processing of spectra were performed with XMASS software (Bruker Daltonik, Bremen, Germany).

3.9.2.2 Nano-ESI-FT-ICR mass spectrometry

3.9.2.2.1 Production of gold-coated nanospray capillaries

Nanospray capillaries were manufactured using borosilicate glass capillaries of the type GC120F-10 from Clark Electromedical Instruments (Pangbourne, UK), which were pulled with a microcapillary puller P-97 from Sutter Instrument Co. (Novato, CA, USA)) in a two step cycle. The parameters for the first step were: heat: 315, pull strength: 100, velocity: 10, cooling time: 200, and for the second step: heat: 295, pull strength: 200, velocity: 30, cooling time: 225. The nanospray capillaries were then coated with gold using a Polaron SC7610 Sputter-Coater (VG Microtech, Uckfield, UK).

3.9.2.2.2 Nano-ESI-FTICR MS analysis

The nanospray capillary was loaded with 0.5–5 µL of sample solution using a GELoader tip or by dipping the capillary tip into the sample solution, in order to avoid plugging due to solvent impurities. The loaded nanospray capillary was fixed in the metal mounting of the x,y,z-nanospray system and then placed in front of the glass capillary entrance of the 7T Bruker Daltonik APEX II FTICR mass spectrometer. The voltage at the capillary tip was manually adjusted to 700–1200 V. The mass spectra were obtained by collecting 32-128 single scans. Experimental conditions: capillary exit voltage (ΔCS): 45-70 V; setting of skimmer 1: 10; setting of skimmer 2: 7; RF amplitude: 500; ionisation pulse time: 2500 ms; ionisation delay time: 0.001 s; excitation sweep pulse: 1.2 ms; excitation sweep attenuation 1: 2.16 dB. Acquisition and processing of spectra were performed with XMASS software (Bruker Daltonik, Bremen, Germany). External calibration was carried out using monoisotopic masses of angiotensin I fragment ions formed by in-source fragmentation (ΔCS = 150V).

3.9.3 Tandem mass spectrometry

Structure information by specific fragmentation of gas-phase ions of biomolecules can be obtained by several MS/MS techniques. Tandem MS consists of activation of a primary precursor ion by addition of excess internal energy to this ion, dissociation, followed by mass analysis of the product ion.

FTICR, Ion trap and Triple quadrupole MS, provides multistage MS^n, simultaneous detection of a wide mass range of ions, and offers different excitation and fragmentation methods (CID, SORI, IRMPD, ECD). The choice of a protein fragmentation path depends on the purpose of the fragmentation and the already known characteristics of the protein. Fragmentation pattern for a given protein is highly reproducible and specific.

The types of fragment ions observed in an MS/MS spectrum depend on many factors including primary structure, internal energy, how the energy was introduced, and charge state. A generally accepted nomenclature for fragment ions is the system proposed by Roepstorff and Fohlman [225]. Fragments can only be detected if they carry at least one charge. The cleavage pattern of a bond in the peptide chain backbone can occur in either of three types of bonds Cα-C, C-N, or N-Cα, which yields six types of fragments that are labelled a_n, b_n, c_n, when the positive charge is kept on the N-terminal part and x_n, y_n, z_n, when the positive charge is kept on the C-terminus part [226].

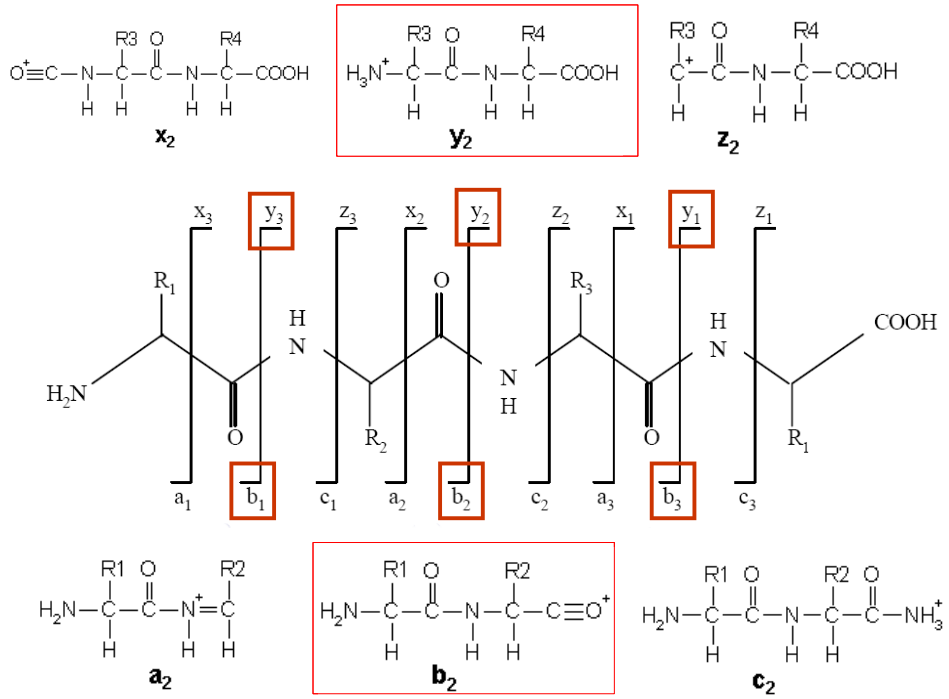

Figure 95: *Peptide cleavage nomenclature proposed by Roepstorff and Fohlman. Peptide ions fragment at the peptide backbone to produce major series of fragment ions. Fragment ions from N-terminus are called a, b, c, and fragment ions from the C-terminus are called x, y, z ions. The ions obtained by IRMPD and CID are mostly b and y ions and are marked with a red square.*

3.9.3.1 FT-ICR MS/MS analysis

Once ions have been formed (by either MALDI or ESI ionization methods) and trapped in the analyzer cell, isolation of a precursor ion was achieved by ejecting from the cell all ions of higher and lower masses through the application of suitable excitation pulses with the appropriate frequencies and amplitudes. Parameters used for isolation of precursor ions were: correlated sweep attenuation: 8-10 dB, ejection safety belt: 500 -1000 Hz.

Infrared multiphoton dissociation (IRMPD) provides a greater selectivity than collision induced dissociation and appears to dissociate more stable ions [227]. With this method typically *b* and *y*-ions are observed (s. Figure 24). The technique involves

firing a relatively high powered IR laser through the center of the cell and, slowly increasing the dissociation ladder. For a typically applied CO_2 (IR) laser (10.6 μm), the steps in energy are 0.12 eV. The laser power was set to 50% and the laser irradiation time to 50-200 msec.

3.9.3.2 nano-ESI-triple-quadrupole-linear ion trap MS/MS analysis

MS/MS analysis was conducted on an Applied Biosystems/MDS SCIEX QTRAP™, a hybrid triple-quadrupole – ion trap mass spectrometer equipped with a Flow NanoSpray™ source. This instrument is based on a triple quadrupole ion path and is capable of all conventional tandem quadrupole scan modes as well as several high sensitivity ion trap mass spectrometer scans using the final quadrupole as a linear ion trap (LIT) MS. The enhanced scan modes (Enhanced Product Ion, Enhanced Resolution and Enhanced MS) use the “trap” capabilities of the instrument to improve sensitivity, resolution, and mass accuracy.

Enhanced Product Ion (EPI) scan is performed when a precursor ion that is resolved through the first quadrupole (Q1) collides with nitrogen gas in the quadrupole collision cell (Q2). The product ions are transferred to Q3 where they are trapped by the Q2-Q3 interquad lens and an exit lens after Q3. After the Q3 LIT has been filled, the ions are resonantly ejected through the exit lens to the ion detector. Scan speeds available are 250, 1000 and 4000 Da/s. Best resolutions are achieved at 250 Da/s scan speeds. A schematic representation of the hybrid triple-quadrupole-linear ion trap mass spectrometer working in the EPI scan mode is shown in Figure 96.

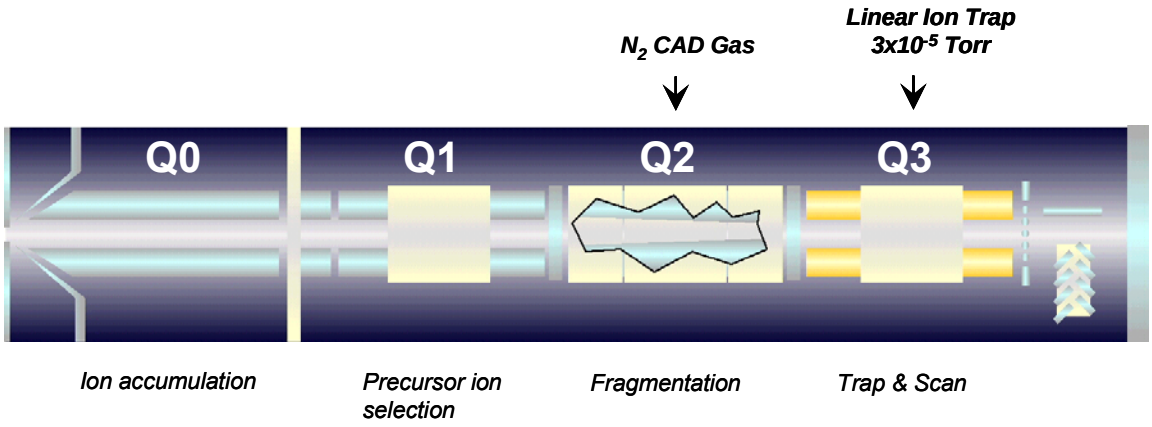

Figure 96: *Schematic representation of the hybrid triple-quadrupole ion trap mass spectrometer working in Enhanced Product Ion (EPI) scan mode.*

Enhanced Resolution (ER) scan is a narrow range scan used to determine charge states and accurate monoisotopic masses of precursor ions for MS/MS. In Enhanced Resolution scan mode, selected ions are filtered through Q1 and passed through Q2 without fragmentation. They are then trapped in the Q3 LIT, scanned slowly out of the trap (250 Da/s scan speed) and detected. In *Enhanced MS (EMS)* scan mode the ions are passed through Q1 and Q2 without fragmentation, trapped in the Q3 LIT for a specified time and then scanned out and detected.

Gold-coated nanospray capillaries were manufactured as described before. The nanospray capillary was loaded with 4 µL of desalted sample solution using a GELoader tip. The loaded capillary was fixed in the metal mounting of the NanoSpray source and then pushed forward into the ion source region. The voltage at the capillary tip was manually adjusted to 900 V. Automated MS/MS analysis was performed utilizing the Information Dependent Acquisition (IDA) feature of Analyst® software 1.3.2. For each cycle of IDA experiment, a survey spectrum was first acquired using Enhanced MS, and then m/z values of three most abundant ion peaks were automatically selected and measured in Enhanced Resolution scan mode (to get the charge state and accurate monoisotopic mass). MS/MS analysis of these three ions was then performed using Enhanced Product Ion scan mode. After each cycle, the analysed *m/z* values were automatically added to a dynamic exclusion list. Finally, all MS/MS spectra acquired were batch processed and submitted to MASCOT search engine for protein identification.

3.9.3.3 ESI -Ion Trap MS/MS mass analysis

The API-ESI (Atmospheric Pressure Interface-ElectroSpray Ionization) generates ions, focuses and transports them into the ion trap mass analyser. The spray chamber is outside the vacuum manifold. The ion transport and focusing components are located inside the vacuum manifold. The pressure differential between the spray chamber and the ion focusing and transport region pushes the ions through the capillary. The operator controls the high voltage electrostatic gradient, the temperature and flow of the drying gas and the pressure of the nebulizer gas. This control is all done by means of the system software.

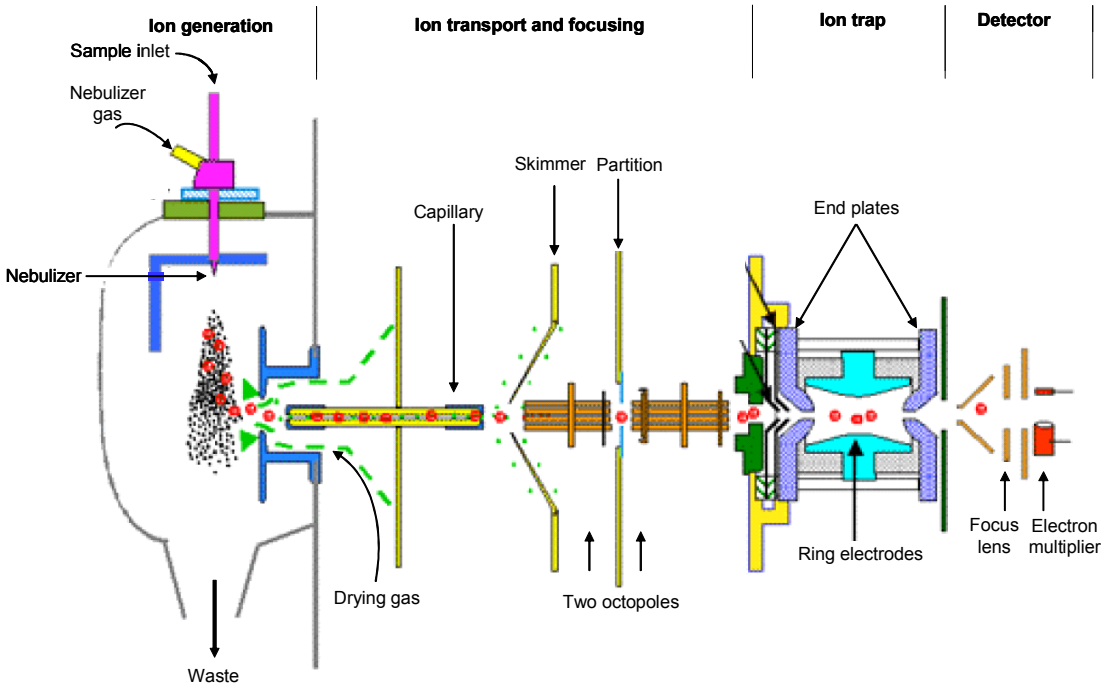

Figure 97: *Schematic representation of the Bruker Esquire 3000 ion trap mass spectrometer*

ESI-MS and MS/MS spectra were acquired in the positive ion mode on an Esquire 3000plus ion trap instrument (Bruker Daltonik, Bremen, Germany), equipped with a syringe pump operated at a flow rate of 3 uL/min. The peptides were dissolved at a concentration of 0.01 ug/uL in 50% acetonitrile in 0.1% formic acid. The source parameters employed were as follow: capillary voltage -3.5 kV, end plate offset 500V, capillary exit 120V, nebuliser gas 10 psi, dry gas 7L/min. The precursor ions for

MS/MS experiments were isolated using an m/z window of 2 Da, and the fragmentation amplitude was optimized within the range 0.5-1.3 V, depending on the fragmentation efficiency of each individual peptide precursor ion.

3.10 N-terminal sequence analysis

Automated amino acid sequence analysis was performed on an Applied Biosystems Model 494 Procise Sequencer attached to a Model 140C Microgradient System and a 785A Programmable Absorbance Detector. All solvents and reagents used were of sequencing grade purity (Applied Biosystems).

The elution fraction (3:2 ACN /0.1% TFA) was applied on a glass fibre filter (Applied Biosystems) in aliquots of 5 uL, each application followed by drying under a stream of argon. The sequencing was carried out using the standard pulsed liquid method. The sequencing data were analysed with the Model 610 A Data Analysis.

To identify the elution position of nitro-tyrosine the pure amino acid (20 uL, 22pMol/uL in 20%ACN, 1%TFA) was subjected to one sequencing cycle.

3.11 Computer Programs

3.11.1 GPMAW

For the molecular weight determination of peptides and proteins and the proteolytic fragments obtained after protease digestion, the GPMAW 5.0 (General Protein/ Mass Analysis for Windows) (Lighthouse Data, Denmark) program was used. This program enables the calculation of the monoisotopic and average masses of the peptides or proteins, also the simulation of the proteolytic digestion of peptides and proteins, followed by searching for different fragments having a known mass. Using this program is possible to introduce different modifications at certain amino acid positions. One can obtain the average and the monoisotopic values for $[M+H]^+$-ions

and also the values of fragment ions having different charges. GPMAW 5.0 program may predict the secondary structure and the hydrophobicity of a given protein or peptide sequence.

3.11.2 BALLView 1.1.1

BALLView is an open source software [196, 197] employed in this work for the visualization and modeling of molecular structures. The program is able to import structures from the most common molecular structure formats (PDB, MOL, MOL2 and SD). Structures can be visualized with all standard graphical models and coloring methods. Different parts of a molecule can be freely visualized and selected for special tasks.

3.11.3 HyperChem 6.0

HyperChem 6.0 software was used for the molecular dynamic simulation of polypeptides. AMBER96 parameters were applied for the geometry optimization and the calculations were performed taking into account the presence of water molecules.

3.11.4 Search engines for identifying proteins

Most of the identification and characterization programs compare user-submitted data with information archived in one or more databases. The identification and characterization of the proteins separated on 1D-gel and visualized by Coommassie blue staining was achieved by proteolytic digestion of the proteins using trypsin, mass spectrometric molecular weight determination of the fragments resulted and sequence assignment by database search [195].

The search was carried out within the NCBInr protein database using the MASCOT search engine (ref website). Established in 1988 as a national resource for molecular biology information, NCBI is a comprehensive, non-identical protein database which

creates public databases, conducts research in computational biology, develops software tools for analyzing genome data, and disseminates biomedical information - all for the better understanding of molecular processes affecting human health and disease. The entries have been compiled from a variety of sources including GenBank (National Institutes of Health genetic-sequence database), PIR (International Protein Sequence Database), SWISS-Prot, PRF (Protein Research Foundation) and PDB (Brookhaven Protein Data Bank).

MASCOT search options against NCBInr database were 1-4 missing tryptic cleavage, monoisotopic mass search with error tolerance between 5 and 30 ppm in case of using FT-ICR-MS and 1-2 Da for TOF-MS, carbamidomethyl derivatization of cysteine as fixed modification, oxidized methionine, tryptophan, histidine and deamidation (NQ) as variable modifications.

4 SUMMARY

Protein nitration is a posttranslational modification which may occur under physiological conditions, but may be substantially enhanced under various pathological conditions associated with oxidative stress. For the molecular correlation of protein nitration with pathogenic mechanisms of human diseases and with animal or cellular models of diseases it is essential to identify the protein targets of nitration and the specific individual modification sites. In this work the development of analytical and immunological methodologies allowed the identification and the quantitative estimation of tyrosine nitrated proteins. Specific nitrated tyrosine structures in given proteins may be of importance as oxidative biomarkers. Therefore, the identification of nitrated tyrosine residues in proteins represents an important task.

The development of new immunoanalytical methods and their mass spectrometric applications in “in vivo” and “in vitro” studies were the major goals of the present dissertation.

In the first part of the thesis, the Tyr-nitration in Prostacyclin synthase (PCS) upon treatment of bovine aortic microsomes by peroxynitrite (PN) was identified at Tyr-430 residue using a combination of proteolytic fragmentation, HPLC detection and nano-ESI-FTICR mass spectrometry. The identified nitrated tetra peptide (PCS - 427-430) resulted from an unpredicted thermolysine cleavage. The low accessibility of Tyr-430 hampered the identification of the nitration site. According to the proposed X-ray structure of Prostacyclin synthase the Tyr-430 and heme bound-Cys-441 form a loop around the heme and this structure is embedded in a tightly folded conformation. This structure explains the high resistance to proteases, and the difficulties for obtaining reproducible identification of nitrated PCS by Western blots, caused by protein refolding on the blotting membrane.

A second part of the dissertation was focused on the identification of physiological tyrosine nitration in human eosinophil granule proteins (EPO, ECP, EDN) isolated from patients with hypereosinophilia, elevate eosinophil numbers in blood. The close

relationship between eosinophilia and nitro-tyrosine formation suggested that the eosinophil peroxidase (EPO) itself is an important factor in promoting protein nitration. First evidence for nitration of all three eosinophil proteins was obtained from Western blot analysis using an anti 3-nitrotyrosine antibody. The site-selective nitration at Tyr^{349} in eosinophil peroxidase was identified using HPLC-ESI-MS with specific UV detection for 3-nitrotyrosine containing peptides. A molecular modelling investigation showed that the Tyr^{349} is present in a highly flexible loop region, in a weak, parallel stacking interaction with Tyr^{555}. Upon nitration at Tyr^{349}, the flexibility of this loop is lost due to steric hindrance and the net electronegativity of the nitrated tyrosine residue likely prevents the stacking interactions with Tyr^{555}, forcing the nitro group of Tyr^{349} to be permanently surface exposed.

Due to a low level of nitrated proteins in the biological eosinophil samples, the identification is often very difficult. A new method was developed to specifically identify tyrosine nitration by a proteolytic affinity extraction (PROFINEX) approach combined with high resolution mass spectrometry. This method, analog to the highly efficient epitope – identification – MS methods was found to be sensitive and specific to identify tyrosine nitrations in biological samples. Using this approach specific tyrosine nitrations were identified at Tyr^{33} for human eosinophil cationic protein (ECP) and eosinophil-derived neurotoxin (EDN). By mean of tandem MS/MS analysis additional proof for the modified structure at Tyr^{33} was obtained. Furthermore, a combination of the proteolytic affinity peptide extraction and Edman sequencing provided quantitative information of the endogenous nitration in eosinophil granule proteins. Conformation studies of nitrated peptides by circular dichroism (CD) and molecular modeling studies indicated that the Tyr^{33} is located on a flexible, random coil structure which exposes the tyrosine residue to the surface of eosinophil proteins.

In a further part of this thesis, tyrosine and nitro-tyrosine – containing peptides were synthesized by solid-phase peptide synthesis accordingly to Fmoc strategy. The use of 3-nitrotyrosine within the standard Fmoc and side-chain protection chemistry (t.-butyl, trityl) provided high coupling yields and homogeneities already of crude peptides after deprotection. The synthetic peptides were characterized by mass spectrometry and used for immuno-analytical studies. ESI-MS provided

unambiguous identification of 3-nitrotyrosine peptide by addition of 45 Daltons which correspond to $+NO_2$ and –H at the tyrosine residue. Collision-induced dissociation in electrospray tandem mass spectrometry produces an immonium ion (*m*/*z* 181.06) which characterise the presence of a nitro-tyrosine modification. Using UV-MALDI-MS, 3-nitrotyrosine peptides were found to undergo extensive photochemical fragmentation at the nitro-phenyl group, which may hamper or prevent the unequivocal identification of Tyr-nitration in cellular proteins. The application of IR-MALDI-FTICR-MS was shown as a useful method for analysis of 3-nitrotyrosine containing peptides which undergo photochemical fragmentation under UV-MALDI conditions but were stable under IR – MALDI laser radiation.

In complementing the conventional immunoanalytical techniques such as Dot blot and ELISA, affinity- mass spectrometry was shown in the last part of the dissertation as a powerful tool for characterising recognition specificities of different antibodies. The comparison of the three methods provided consistent results to reveal differences in binding affinities and specificities by the anti nitro-tyrosine antibodies, showing that antibody binding is influenced by the peptide structure adjacent to the nitro-tyrosine modification. The capability of anti nitro-tyrosine antibodies to discriminate between nitro-tyrosine in different environments in proteins may be useful for producing antibodies to specific motifs containing tyrosine residues, and for the development of highly specific biomarkers.

5 ZUSAMMENFASSUNG

Die Nitrierung von Proteinen ist eine posttranslationale Modifikation, die in jüngster Zeit unter physiologischen Bedingungen nachgewiesen wurde und Interesse gefunden hat, und die unter pathophysiologischen Bedingungen als „oxidative Stress“ – Modifizierung verstärkt auftritt. Zur Ermittlung von molekularen Beziehungen zwischen Protein-Nitrierung und pathogenen Mechanismen von Erkrankungen beim Menschen sowie in Tiermodellen ist die Identifizierung von infizierten Targetproteinen und die Aufklärung der modifizierten Strukturen von entscheidender Bedeutung. In der vorliegenden Dissertation ermöglichte die Entwicklung von neuen analytischen und immunologischen Methoden die Identifizierung und quantitative Bestimmung von Tyrosin-nitrierten Proteinen. Spezifische, Tyrosin-nitrierte Proteinstrukturen sind als mögliche „oxidative Biomarker“ von Bedeutung. Die Entwicklung und Anwendung von neuen immun-analytischen und massenspektrometrischen Methoden zu entsprechenden Untersuchungen *in vitro* und *in vivo* waren zentrale Zielsetzungen der Dissertation.

Im ersten Teil der Dissertation wurde die Tyrosin-Nitrierung der Prostacyclin-Synthase (PCS) aus Rinderaorta- Mikrosomen nach Oxidation durch Peroxynitrit untersucht. Durch eine Kombination von proteolytischem Abbau, HPLC und Nano-ESI- FTICR - Massenspektrometrie wurde eine spezifische Nitrierung von Tyr-430 nachgewiesen. Das identifizierte nitrierte Tetrapeptid PCS (427-430) wurde durch eine ungewöhnliche Spaltung mit Thermolysin erhalten, was Hinweise auf eine geringe Zugänglichkeit der Modifizierungsstelle lieferte. Der Vergleich mit der Röntgenkristallstruktur der PCS bestätigt, dass der modifizierte Tyr-430- Rest in dem eng gefalteten, wenig zugänglichen katalytischen Zentrum der PCS liegt, und somit die hohe Resistenz dieser Domäne gegenüber Proteasen erklärt.

In einem zweiten Teil der Dissertation wurde die *physiologische* Tyr-Nitrierung in menschlichen Eosinophil-Proteinen untersucht. In den Proteinen Eosinophil-Peroxidase (EPO), Eosinophil-Kationisches Protein (ECP) und „Eosinophil-derived neurotoxin“ (EDN) konnten Tyr-nitrierte Strukturen erstmals unter physiologischen Bedingungen nachgewiesen werden. Erste Hinweise auf Nitrierung der Eosinophil-

Proteine wurden aus Westernblot-Daten mit anti-Nitrotyrosin- Antikörpern erhalten. Für die Eosinophil-Peroxidase wurde eine spezifische Nitrierung von Tyr-349 durch HPLC-Tandem-MS mit strukturspezifischer UV-Detektion nachgewiesen. Dabei zeigten Molekülmodellstudien, dass der Tyr-349- Rest in einem flexiblen Loop-Bereich liegt, dessen Flexibilität durch sterische- und Ladungs-Effekte aufgrund der Nitrierung verlorengeht; die ohne Modifizierung vorliegende Wechselwirkung mit dem Tyr-555 Rest geht dadurch verloren und die Niro-Tyr-349 wird an der Proteinoberfläche exponiert.

Die meist sehr geringe Nitrierungsrate von Proteinen erschwert die Identifizierung von Tyr- Nitrierungen. In der vorliegenden Arbeit wurde eine neue, hochempfindliche und spezifische Methode zur Identifizierung von Tyr-Nitrierungen aus biologischem Material durch Kombination von proteolytischer Affinitätsextraktion und Massenspektrometrie entwickelt (PROFINEX-MS). Die Anwendung dieser Methode ermöglichte erstmals die Aufklärung der Nitrierungen von Tyr-33 des ECP- Proteins, sowie des analogen Tyr-33 Rests des EDN-Proteins aus menschlichen Eosinphilen. Die Strukturen der Modifizierungen wurden zusätzlich durch Tandem-MS Analyse der Fragmentpeptide gesichert. Mit Hilfe der Affinitäts-MS Methode sowie Edman-Sequenzanalyse wurden erstmals auch quantitative Abschätzungen der Nitrierungsraten erhalten, die für die Eosinophilproteine ECP und EDN bei ca. 10-15 % liegen. Konformationsuntersuchungen der Tyr- nitrierten Peptide mittels CD-Spektroskopie zeigen hohe Flexibilität und ungeordnete Struktur des Nitrotyrosinrests.

In einem weiteren Teil der Arbeit wurden Nitrotyrosin-haltige Modellpeptide durch Festphasensynthese synthetisiert, massenspektrometrisch und immunanalytisch charakterisiert. Die Darstellung der nitrierten Peptide gelang mit der Fmoc- Methode in hoher Ausbeute und Reinheit. Vergleichende Untersuchungen mittels ESI-MS und MALDI-MS zeigten, dass Nitrotyrosin-Peptide unter MALDI-Bedingungen mit Stickstoff-UV-Laser eine charakteristische photochemische Fragmentierung der Nitro-Tyr-Gruppe eingehen; dagegen wurden mit der IR- MALDI-MS stabile Molekülionen ohne Zersetzung erhalten.

In Ergänzung und Erweiterung der standardmäßigen immunoanalytischen Methoden,

Dotblot und ELISA, wurde die Affinitäts- Massenspektrometrie im letzten Teil der Arbeit zur molekularen Charakterisierung der Spezifität von Anti-Nitrotyrosin-Antikörpern angewendet. Die Ergebnisse zeigen unterschiedliche Erkennungsspezifitäten von kommerziell erhältlichen Antikörpern, die zur Entwicklung von spezifischem Biomarkern der Tyrosin-Nitrierung genutzt werden können. Mit Hilfe der Affinitäts-MS konnte ein spezifisches Epitopmotiv der Erkennung von Nitrotyrosin- Peptidsubstraten identifiziert werden.

6 LITERATURE

1. Schoneich, C., Reactive oxygen species and biological aging: a mechanistic approach. *Exp Gerontol*, 1999. **34**(1): p. 19-34.

2. Khidekel, N. and L.C. Hsieh-Wilson, A 'molecular switchboard'--covalent modifications to proteins and their impact on transcription. *Org Biomol Chem*, 2004. **2**(1): p. 1-7.

3. Sies, H., Biochemistry of Oxidative Stress. *Angew. Chem. Int. Ed. Engl.*, 1986. **25**: p. 1058-1071.

4. Baskin, S.I. and H. Salem, eds. *Oxidants, Antioxidants, and Free Radicals*. 1997, Tylor & Francis.

5. Stadtman, E.R. and B.S. Berlett, Reactive oxygen-mediated protein oxidation in aging and disease. *Chem Res Toxicol*, 1997. **10**(5): p. 485-94.

6. Malencik, D.A. and S.R. Anderson, Dityrosine as a product of oxidative stress and fluorescent probe. *Amino Acids*, 2003. **25**(3-4): p. 233-47.

7. Perna, A.F., D. Ingrosso, and N.G. De Santo, Homocysteine and oxidative stress. *Amino Acids*, 2003. **25**(3-4): p. 409-17.

8. Ullrich, V. and R. Kissner, Redox signaling: bioinorganic chemistry at its best. *J Inorg Biochem*, 2006. **100**(12): p. 2079-86.

9. Holliday, R., Understanding Ageing. 1995.

10. Halliwell, B., Free radicals, antioxidants, and human disease: curiosity, cause, or consequence? *Lancet*, 1994. **344**(8924): p. 721-4.

11. Sies, H., Strategies of antioxidant defense. *Eur J Biochem*, 1993. **215**(2): p. 213-9.

12. Beckman, J.S., Y.Z. Ye, S.R. Anderson, J. Chen, M.A. Accavitti, and C.R. White, Extensive nitration of protein tyrosines in human atherosclerosis detected by immunohistochemistry. *biol Chem Hoppe Seyler*, 1994. **375**: p. 81-88.

13. Cromheeke, K.M., M.M. Kockx, G.R. De Meyer, J.M. Bosmans, H. Bult, W.J. Beelaerts, C.J. Vrints, and A.G. Herman, Inducible nitric oxide synthase colocalizes with signs of lipid oxidation/peroxidation in human atherosclerotic plaques. *Cardiovasc Res*, 1999. **43**(3): p. 744-54.

14. Haddad, I.Y., G. Pataki, P. Hu, C. Galliani, J.S. Beckman, and S. Matalon, Quantitation of nitrotyrosine levels in lung sections of patients and animals with acute lung injury. *J Clin Invest*, 1994. **94**(6): p. 2407-13.

15. Hanazawa, T., S.A. Kharitonov, and P.J. Barnes, Increased nitrotyrosine in exhaled breath condensate of patients with asthma. *Am J Respir Crit Care Med*, 2000. **162**(4 Pt 1): p. 1273-6.

16. Kharitonov, S.A. and P.J. Barnes, Biomarkers of some pulmonary diseases in exhaled breath. *Biomarkers*, 2002. **7**(1): p. 1-32.

17. Beckman, J.S., J. Chen, J.P. Crow, and Y.Z. Ye, Reactions of nitric oxide, superoxide and peroxynitrite with superoxide dismutase in neurodegeneration. *Prog Brain Res*,

1994. **103**: p. 371-80.

18. Teunissen, C.E., J. de Vente, H.W. Steinbusch, and C. De Bruijn, Biochemical markers related to Alzheimer's dementia in serum and cerebrospinal fluid. *Neurobiol Aging*, 2002. **23**(4): p. 485-508.

19. Giasson, B.I., J.E. Duda, I.V. Murray, Q. Chen, J.M. Souza, H.I. Hurtig, H. Ischiropoulos, J.Q. Trojanowski, and V.M. Lee, Oxidative damage linked to neurodegeneration by selective alpha-synuclein nitration in synucleinopathy lesions. *Science*, 2000. **290**(5493): p. 985-9.

20. Cuzzocrea, S., B. Zingarelli, D. Villari, A.P. Caputi, and G. Longo, Evidence for in vivo peroxynitrite production in human chronic hepatitis. *Life Sci*, 1998. **63**(2): p. PL25-30.

21. Garcia-Monzon, C., P.L. Majano, I. Zubia, P. Sanz, A. Apolinario, and R. Moreno-Otero, Intrahepatic accumulation of nitrotyrosine in chronic viral hepatitis is associated with histological severity of liver disease. *J Hepatol*, 2000. **32**(2): p. 331-8.

22. Ceriello, A., F. Mercuri, L. Quagliaro, R. Assaloni, E. Motz, L. Tonutti, and C. Taboga, Detection of nitrotyrosine in the diabetic plasma: evidence of oxidative stress. *Diabetologia*, 2001. **44**(7): p. 834-8.

23. Kamisaki, Y., K. Wada, K. Bian, B. Balabanli, K. Davis, E. Martin, F. Behbod, Y.C. Lee, and F. Murad, An activity in rat tissues that modifies nitrotyrosine-containing proteins. *Proc Natl Acad Sci U S A*, 1998. **95**(20): p. 11584-9.

24. Irie, Y., M. Saeki, Y. Kamisaki, E. Martin, and F. Murad, Histone H1.2 is a substrate for denitrase, an activity that reduces nitrotyrosine immunoreactivity in proteins. *Proc Natl Acad Sci U S A*, 2003. **100**(10): p. 5634-9.

25. Turko, I.V. and F. Murad, Protein nitration in cardiovascular diseases. *Pharmacol Rev*, 2002. **54**(4): p. 619-34.

26. Beckman, J.S., T.W. Beckman, J. Chen, P.A. Marshall, and B.A. Freeman, Apparent hydroxyl radical production by peroxynitrite: implications for endothelial injury from nitric oxide and superoxide. *Proc Natl Acad Sci U S A*, 1990. **87**(4): p. 1620-4.

27. Radi, R., J.S. Beckman, K.M. Bush, and B.A. Freeman, Peroxynitrite oxidation of sulfhydryls. The cytotoxic potential of superoxide and nitric oxide. *J Biol Chem*, 1991. **266**(7): p. 4244-50.

28. Radi, R., J.S. Beckman, K.M. Bush, and B.A. Freeman, Peroxynitrite-induced membrane lipid peroxidation: the cytotoxic potential of superoxide and nitric oxide. *Arch Biochem Biophys*, 1991. **288**(2): p. 481-7.

29. Yermilov, V., Y. Yoshie, J. Rubio, and H. Ohshima, Effects of carbon dioxide/bicarbonate on induction of DNA single-strand breaks and formation of 8-nitroguanine, 8-oxoguanine and base-propenal mediated by peroxynitrite. *FEBS Lett*, 1996. **399**(1-2): p. 67-70.

30. Szabo, C. and H. Ohshima, DNA damage induced by peroxynitrite: subsequent biological effects. *Nitric Oxide*, 1997. **1**(5): p. 373-85.

31. Kennedy, L.J., K. Moore, Jr., J.L. Caulfield, S.R. Tannenbaum, and P.C. Dedon, Quantitation of 8-oxoguanine and strand breaks produced by four oxidizing agents. *Chem Res Toxicol*, 1997. **10**(4): p. 386-92.

32. Ischiropoulos, H. and A.B. al-Mehdi, Peroxynitrite-mediated oxidative protein modifications. *FEBS Lett*, 1995. **364**(3): p. 279-82.

33. Eiserich, J.P., R.P. Patel, and V.B. O'Donnell, Pathophysiology of nitric oxide and related species: free radical reactions and modification of biomolecules. *Mol Aspects Med*, 1998. **19**(4-5): p. 221-357.

34. Beckman, J.S., Oxidative damage and tyrosine nitration from peroxynitrite. *Chem Res Toxicol*, 1996. **9**(5): p. 836-44.

35. Kooy, N.W., J.A. Royall, Y.Z. Ye, D.R. Kelly, and J.S. Beckman, Evidence for in vivo peroxynitrite production in human acute lung injury. *Am J Respir Crit Care Med*, 1995. **151**(4): p. 1250-4.

36. Balint, B., S.A. Kharitonov, T. Hanazawa, L.E. Donnelly, P.L. Shah, M.E. Hodson, and P.J. Barnes, Increased nitrotyrosine in exhaled breath condensate in cystic fibrosis. *Eur Respir J*, 2001. **17**(6): p. 1201-7.

37. Saleh, D., P. Ernst, S. Lim, P.J. Barnes, and A. Giaid, Increased formation of the potent oxidant peroxynitrite in the airways of asthmatic patients is associated with induction of nitric oxide synthase: effect of inhaled glucocorticoid. *Faseb J*, 1998. **12**(11): p. 929-37.

38. Li, X., P. De Sarno, L. Song, J.S. Beckman, and R.S. Jope, Peroxynitrite modulates tyrosine phosphorylation and phosphoinositide signalling in human neuroblastoma SH-SY5Y cells: attenuated effects in human 1321N1 astrocytoma cells. *Biochem J*, 1998. **331 (Pt 2)**: p. 599-606.

39. Zhang, Y.J., Y.F. Xu, Y.H. Liu, J. Yin, H.L. Li, Q. Wang, and J.Z. Wang, Peroxynitrite induces Alzheimer-like tau modifications and accumulation in rat brain and its underlying mechanisms. *Faseb J*, 2006. **20**(9): p. 1431-42.

40. Zou, M.H., M. Leist, and V. Ullrich, Selective nitration of prostacyclin synthase and defective vasorelaxation in atherosclerotic bovine coronary arteries. *Am J Pathol*, 1999. **154**(5): p. 1359-65.

41. Pacher, P. and C. Szabo, Role of peroxynitrite in the pathogenesis of cardiovascular complications of diabetes. *Curr Opin Pharmacol*, 2006. **6**(2): p. 136-41.

42. Chen, X.L., W.B. Li, A.M. Zhou, J. Ai, and S.S. Huang, Role of endogenous peroxynitrite in pulmonary injury and fibrosis induced by bleomycin A5 in rats. *Acta Pharmacol Sin*, 2003. **24**(7): p. 697-702.

43. Crow, J.P. and J.S. Beckman, Reactions between nitric oxide, superoxide, and peroxynitrite: footprints of peroxynitrite in vivo. *Adv Pharmacol*, 1995. **34**: p. 17-43.

44. Pfeiffer, S., A.C. Gorren, K. Schmidt, E.R. Werner, B. Hansert, D.S. Bohle, and B. Mayer, Metabolic fate of peroxynitrite in aqueous solution. Reaction with nitric oxide and pH-dependent decomposition to nitrite and oxygen in a 2:1 stoichiometry. *J Biol Chem*, 1997. **272**(6): p. 3465-70.

45. Ramezanian, M.S., S. Padmaja, and W.H. Koppenol, Nitration and hydroxylation of phenolic compounds by peroxynitrite. *Chem Res Toxicol*, 1996. **9**(1): p. 232-40.

46. Crow, J.P., C. Spruell, J. Chen, C. Gunn, H. Ischiropoulos, M. Tsai, C.D. Smith, R. Radi, W.H. Koppenol, and J.S. Beckman, On the pH-dependent yield of hydroxyl

radical products from peroxynitrite. *Free Radic Biol Med*, 1994. **16**(3): p. 331-8.

47. Alvarez, B. and R. Radi, Peroxynitrite reactivity with amino acids and proteins. *Amino Acids*, 2003. **25**(3-4): p. 295-311.

48. Swaim, M.W. and S.V. Pizzo, Methionine sulfoxide and the oxidative regulation of plasma proteinase inhibitors. *J Leukoc Biol*, 1988. **43**(4): p. 365-79.

49. Stadtman, E.R., Metal ion-catalyzed oxidation of proteins: biochemical mechanism and biological consequences. *Free Radic Biol Med*, 1990. **9**(4): p. 315-25.

50. Crow, J.P., J.S. Beckman, and J.M. McCord, Sensitivity of the essential zinc-thiolate moiety of yeast alcohol dehydrogenase to hypochlorite and peroxynitrite. *Biochemistry*, 1995. **34**(11): p. 3544-52.

51. Uchida, K., Histidine and lysine as targets of oxidative modification. *Amino Acids*, 2003. **25**(3-4): p. 249-57.

52. Beckman, J.S. and W.H. Koppenol, Nitric oxide, superoxide, and peroxynitrite: the good, the bad, and ugly. *Am J Physiol*, 1996. **271**(5 Pt 1): p. C1424-37.

53. Sawa, T., T. Akaike, and H. Maeda, Tyrosine nitration by peroxynitrite formed from nitric oxide and superoxide generated by xanthine oxidase. *J Biol Chem*, 2000. **275**(42): p. 32467-74.

54. Zou, M.H., T. Klein, J.P. Pasquet, and V. Ullrich, Interleukin 1beta decreases prostacyclin synthase activity in rat mesangial cells via endogenous peroxynitrite formation. *Biochem J*, 1998. **336 (Pt 2)**: p. 507-12.

55. Pietraforte, D., A.M. Salzano, G. Marino, and M. Minetti, Peroxynitrite-dependent modifications of tyrosine residues in hemoglobin. Formation of tyrosyl radical(s) and 3-nitrotyrosine. *Amino Acids*, 2003. **25**(3-4): p. 341-50.

56. Lehnig, M., Radical mechanisms of the decomposition of peroxynitrite and the peroxynitrite-CO(2) adduct and of reactions with L-tyrosine and related compounds as studied by (15)N chemically induced dynamic nuclear polarization. *Arch Biochem Biophys*, 1999. **368**(2): p. 303-18.

57. Ischiropoulos, H., Biological tyrosine nitration: a pathophysiological function of nitric oxide and reactive oxygen species. *Arch Biochem Biophys*, 1998. **356**(1): p. 1-11.

58. Berlett, B.S., R.L. Levine, and E.R. Stadtman, Carbon dioxide stimulates peroxynitrite-mediated nitration of tyrosine residues and inhibits oxidation of methionine residues of glutamine synthetase: both modifications mimic effects of adenylylation. *Proc Natl Acad Sci U S A*, 1998. **95**(6): p. 2784-9.

59. Zou, M.H., A. Daiber, J.A. Peterson, H. Shoun, and V. Ullrich, Rapid reactions of peroxynitrite with heme-thiolate proteins as the basis for protection of prostacyclin synthase from inactivation by nitration. *Arch Biochem Biophys*, 2000. **376**(1): p. 149-55.

60. Quijano, C., D. Hernandez-Saavedra, L. Castro, J.M. McCord, B.A. Freeman, and R. Radi, Reaction of peroxynitrite with Mn-superoxide dismutase. Role of the metal center in decomposition kinetics and nitration. *J Biol Chem*, 2001. **276**(15): p. 11631-8.

61. Souza, J.M., E. Daikhin, M. Yudkoff, C.S. Raman, and H. Ischiropoulos, Factors determining the selectivity of protein tyrosine nitration. *Arch Biochem Biophys*, 1999. **371**(2): p. 169-78.

62. Blanchard-Fillion, B., J.M. Souza, T. Friel, G.C. Jiang, K. Vrana, V. Sharov, L. Barron, C. Schoneich, C. Quijano, B. Alvarez, R. Radi, S. Przedborski, G.S. Fernando, J. Horwitz, and H. Ischiropoulos, Nitration and inactivation of tyrosine hydroxylase by peroxynitrite. *J Biol Chem*, 2001. **276**(49): p. 46017-23.

63. Zhang, H., J. Joseph, J. Feix, N. Hogg, and B. Kalyanaraman, Nitration and oxidation of a hydrophobic tyrosine probe by peroxynitrite in membranes: comparison with nitration and oxidation of tyrosine by peroxynitrite in aqueous solution. *Biochemistry*, 2001. **40**(25): p. 7675-86.

64. MacMillan-Crow, L.A., J.P. Crow, and J.A. Thompson, Peroxynitrite-mediated inactivation of manganese superoxide dismutase involves nitration and oxidation of critical tyrosine residues. *Biochemistry*, 1998. **37**(6): p. 1613-22.

65. Fukuyama, N., Y. Takebayashi, M. Hida, H. Ishida, K. Ichimori, and H. Nakazawa, Clinical evidence of peroxynitrite formation in chronic renal failure patients with septic shock. *Free Radic Biol Med*, 1997. **22**(5): p. 771-4.

66. Kamisaki, Y., K. Wada, K. Nakamoto, Y. Kishimoto, M. Kitano, and T. Itoh, Sensitive determination of nitrotyrosine in human plasma by isocratic high-performance liquid chromatography. *J Chromatogr B Biomed Appl*, 1996. **685**(2): p. 343-7.

67. Crowley, J.R., K. Yarasheski, C. Leeuwenburgh, J. Turk, and J.W. Heinecke, Isotope dilution mass spectrometric quantification of 3-nitrotyrosine in proteins and tissues is facilitated by reduction to 3-aminotyrosine. *Anal Biochem*, 1998. **259**(1): p. 127-35.

68. Frost, M.T., B. Halliwell, and K.P. Moore, Analysis of free and protein-bound nitrotyrosine in human plasma by a gas chromatography/mass spectrometry method that avoids nitration artifacts. *Biochem J*, 2000. **345 Pt 3**: p. 453-8.

69. Greis, K.D., S. Zhu, and S. Matalon, Identification of nitration sites on surfactant protein A by tandem electrospray mass spectrometry. *Arch Biochem Biophys*, 1996. **335**(2): p. 396-402.

70. Yi, D., G.A. Smythe, B.C. Blount, and M.W. Duncan, Peroxynitrite-mediated nitration of peptides: characterization of the products by electrospray and combined gas chromatography-mass spectrometry. *Arch Biochem Biophys*, 1997. **344**(2): p. 253-9.

71. Jiao, K., S. Mandapati, P.L. Skipper, S.R. Tannenbaum, and J.S. Wishnok, Site-selective nitration of tyrosine in human serum albumin by peroxynitrite. *Anal Biochem*, 2001. **293**(1): p. 43-52.

72. Aulak, K.S., M. Miyagi, L. Yan, K.A. West, D. Massillon, J.W. Crabb, and D.J. Stuehr, Proteomic method identifies proteins nitrated in vivo during inflammatory challenge. *Proc Natl Acad Sci U S A*, 2001. **98**(21): p. 12056-61.

73. Castegna, A., V. Thongboonkerd, J.B. Klein, B. Lynn, W.R. Markesbery, and D.A. Butterfield, Proteomic identification of nitrated proteins in Alzheimer's disease brain. *J Neurochem*, 2003. **85**(6): p. 1394-401.

74. Kanski, J., S.J. Hong, and C. Schoneich, Proteomic analysis of protein nitration in aging skeletal muscle and identification of nitrotyrosine-containing sequences in vivo

by nanoelectrospray ionization tandem mass spectrometry. *J Biol Chem*, 2005. **280**(25): p. 24261-6.

75. Sultana, R., T. Reed, M. Perluigi, R. Coccia, W.M. Pierce, and D.A. Butterfield, Proteomic identification of nitrated brain proteins in amnestic mild cognitive impairment: a regional study. *J Cell Mol Med*, 2007. **11**(4): p. 839-51.

76. ter Steege, J.C., L. Koster-Kamphuis, E.A. van Straaten, P.P. Forget, and W.A. Buurman, Nitrotyrosine in plasma of celiac disease patients as detected by a new sandwich ELISA. *Free Radic Biol Med*, 1998. **25**(8): p. 953-63.

77. Heijnen, H.F., E. van Donselaar, J.W. Slot, D.M. Fries, B. Blachard-Fillion, R. Hodara, R. Lightfoot, M. Polydoro, D. Spielberg, L. Thomson, E.A. Regan, J. Crapo, and H. Ischiropoulos, Subcellular localization of tyrosine-nitrated proteins is dictated by reactive oxygen species generating enzymes and by proximity to nitric oxide synthase. *Free Radic Biol Med*, 2006. **40**(11): p. 1903-13.

78. Ye, Y.Z., M. Strong, Z.Q. Huang, and J.S. Beckman, Antibodies that recognize nitrotyrosine. *Methods Enzymol*, 1996. **269**: p. 201-9.

79. Turko, I.V., L. Li, K.S. Aulak, D.J. Stuehr, J.Y. Chang, and F. Murad, Protein tyrosine nitration in the mitochondria from diabetic mouse heart. Implications to dysfunctional mitochondria in diabetes. *J Biol Chem*, 2003. **278**(36): p. 33972-7.

80. ter Steege, J., W. Buurman, J.W. Arends, and P. Forget, Presence of inducible nitric oxide synthase, nitrotyrosine, CD68, and CD14 in the small intestine in celiac disease. *Lab Invest*, 1997. **77**(1): p. 29-36.

81. Hinson, J.A., S.L. Michael, S.G. Ault, and N.R. Pumford, Western blot analysis for nitrotyrosine protein adducts in livers of saline-treated and acetaminophen-treated mice. *Toxicol Sci*, 2000. **53**(2): p. 467-73.

82. Duda, J.E., B.I. Giasson, Q. Chen, T.L. Gur, H.I. Hurtig, M.B. Stern, S.M. Gollomp, H. Ischiropoulos, V.M. Lee, and J.Q. Trojanowski, Widespread nitration of pathological inclusions in neurodegenerative synucleinopathies. *Am J Pathol*, 2000. **157**(5): p. 1439-45.

83. Pignatelli, B., C.Q. Li, P. Boffetta, Q. Chen, W. Ahrens, F. Nyberg, A. Mukeria, I. Bruske-Hohlfeld, C. Fortes, V. Constantinescu, H. Ischiropoulos, and H. Ohshima, Nitrated and oxidized plasma proteins in smokers and lung cancer patients. *Cancer Res*, 2001. **61**(2): p. 778-84.

84. Franze, T., M.G. Weller, R. Niessner, and U. Poschl, Enzyme immunoassays for the investigation of protein nitration by air pollutants. *Analyst*, 2003. **128**(7): p. 824-31.

85. Morrissey, B.M., K. Schilling, J.V. Weil, P.E. Silkoff, and D.M. Rodman, Nitric oxide and protein nitration in the cystic fibrosis airway. *Arch Biochem Biophys*, 2002. **406**(1): p. 33-9.

86. Good, P.F., A. Hsu, P. Werner, D.P. Perl, and C.W. Olanow, Protein nitration in Parkinson's disease. *J Neuropathol Exp Neurol*, 1998. **57**(4): p. 338-42.

87. Smith, M.A., P.L. Richey Harris, L.M. Sayre, J.S. Beckman, and G. Perry, Widespread peroxynitrite-mediated damage in Alzheimer's disease. *J Neurosci*, 1997. **17**(8): p. 2653-7.

88. Steiner, R., S. Albaugh, and M.-C. Kilhoffer, *Distribution of separations between groups in an engineered calmodulin*, in *Journal of Fluorescence*. 1991. p. 15-22.

89. Rischel, C., P. Thyberg, F. Rigler, and F.M. Poulsen, Time-resolved fluorescence studies of the molten globule state of apomyoglobin. *J Mol Biol*, 1996. **257**(4): p. 877-85.

90. De Filippis, V., R. Frasson, and A. Fontana, 3-Nitrotyrosine as a spectroscopic probe for investigating protein protein interactions. *Protein Sci*, 2006. **15**(5): p. 976-86.

91. Fenn, J.B., M. Mann, C.K. Meng, S.F. Wong, and C.M. Whitehouse, Electrospray ionization for mass spectrometry of large biomolecules. *Science*, 1989. **246**(4926): p. 64-71.

92. Karas, M. and F. Hillenkamp, Laser desorption ionization of proteins with molecular masses exceeding 10,000 daltons. *Anal Chem*, 1988. **60**(20): p. 2299-301.

93. Hillenkamp, F., M. Karas, R.C. Beavis, and B.T. Chait, Matrix-assisted laser desorption/ionization mass spectrometry of biopolymers. *Anal Chem*, 1991. **63**(24): p. 1193A-1203A.

94. Tanaka, K., The origin of macromolecule ionization by laser irradiation (Nobel lecture). *Angew Chem Int Ed Engl*, 2003. **42**(33): p. 3860-70.

95. Enke, C.G., A predictive model for matrix and analyte effects in electrospray ionization of singly-charged ionic analytes. *Anal Chem*, 1997. **69**(23): p. 4885-93.

96. Kebarle, P., Ho, Y., *Electrospray Ionisation Mass Spectrometry*. 1997, New York: Wiley.

97. Smith, R.D., J.A. Loo, C.G. Edmonds, C.J. Barinaga, and H.R. Udseth, New developments in biochemical mass spectrometry: electrospray ionization. *Anal Chem*, 1990. **62**(9): p. 882-99.

98. Gaskell, S.J., Electrospray: Principles and Practice. *J. Mass Spectrom.*, 1997. **32**: p. 677-688.

99. Emmett, M.R., F.M. White, C.L. Hendrickson, S.D. Shi, and A.G. Marshall, Application of micro-electrospray liquid chromatography techniques to FT-ICR MS to enable high-sensitivity biological analysis. *J Am Soc Mass Spectrom*, 1998. **9**(4): p. 333-40.

100. Wilm, M. and M. Mann, Analytical properties of the nanoelectrospray ion source. *Anal Chem*, 1996. **68**(1): p. 1-8.

101. Gobry, V., J. van Oostrum, M. Martinelli, T.C. Rohner, F. Reymond, J.S. Rossier, and H.H. Girault, Microfabricated polymer injector for direct mass spectrometry coupling. *Proteomics*, 2002. **2**(4): p. 405-12.

102. Rossier, J., F. Reymond, and P.E. Michel, Polymer microfluidic chips for electrochemical and biochemical analyses. *Electrophoresis*, 2002. **23**(6): p. 858-67.

103. Karas, M., Hillenkamp, F. in *AIP Conf. Proc.* 1993.

104. Glocker, M.O., S.H. Bauer, J. Kast, J. Volz, and M. Przybylski, Characterization of specific noncovalent protein complexes by UV matrix-assisted laser desorption

ionization mass spectrometry. *J Mass Spectrom*, 1996. **31**(11): p. 1221-7.

105. Willard, B.B., C.I. Ruse, J.A. Keightley, M. Bond, and M. Kinter, Site-specific quantitation of protein nitration using liquid chromatography/tandem mass spectrometry. *Anal Chem*, 2003. **75**(10): p. 2370-6.

106. Sarver, A., N.K. Scheffler, M.D. Shetlar, and B.W. Gibson, Analysis of peptides and proteins containing nitrotyrosine by matrix-assisted laser desorption/ionization mass spectrometry. *J Am Soc Mass Spectrom*, 2001. **12**(4): p. 439-48.

107. Petersson, A.S., H. Steen, D.E. Kalume, K. Caidahl, and P. Roepstorff, Investigation of tyrosine nitration in proteins by mass spectrometry. *J Mass Spectrom*, 2001. **36**(6): p. 616-25.

108. Miyagi, M., H. Sakaguchi, R.M. Darrow, L. Yan, K.A. West, K.S. Aulak, D.J. Stuehr, J.G. Hollyfield, D.T. Organisciak, and J.W. Crabb, Evidence that light modulates protein nitration in rat retina. *Mol Cell Proteomics*, 2002. **1**(4): p. 293-303.

109. Kanski, J., M.A. Alterman, and C. Schoneich, Proteomic identification of age-dependent protein nitration in rat skeletal muscle. *Free Radic Biol Med*, 2003. **35**(10): p. 1229-39.

110. Nikov, G., V. Bhat, J.S. Wishnok, and S.R. Tannenbaum, Analysis of nitrated proteins by nitrotyrosine-specific affinity probes and mass spectrometry. *Anal Biochem*, 2003. **320**(2): p. 214-22.

111. Zhang, Q., W.J. Qian, T.V. Knyushko, T.R. Clauss, S.O. Purvine, R.J. Moore, C.A. Sacksteder, M.H. Chin, D.J. Smith, D.G. Camp, 2nd, D.J. Bigelow, and R.D. Smith, A method for selective enrichment and analysis of nitrotyrosine-containing peptides in complex proteome samples. *J Proteome Res*, 2007. **6**(6): p. 2257-68.

112. Halliwell, B., K. Zhao, and M. Whiteman, Nitric oxide and peroxynitrite. The ugly, the uglier and the not so good: a personal view of recent controversies. *Free Radic Res*, 1999. **31**(6): p. 651-69.

113. Franze, T., M.G. Weller, R. Niessner, and U. Poschl, Comparison of nitrotyrosine antibodies and development of immunoassays for the detection of nitrated proteins. *Analyst*, 2004. **129**(7): p. 589-96.

114. Viera, L., Y.Z. Ye, A.G. Estevez, and J.S. Beckman, Immunohistochemical methods to detect nitrotyrosine. *Methods Enzymol*, 1999. **301**: p. 373-81.

115. van der Vliet, A., J.P. Eiserich, H. Kaur, C.E. Cross, and B. Halliwell, Nitrotyrosine as biomarker for reactive nitrogen species. *Methods Enzymol*, 1996. **269**: p. 175-84.

116. Crow, J.P. and H. Ischiropoulos, Detection and quantitation of nitrotyrosine residues in proteins: in vivo marker of peroxynitrite. *Methods Enzymol*, 1996. **269**: p. 185-94.

117. Yamakura, F., H. Taka, T. Fujimura, and K. Murayama, Inactivation of human manganese-superoxide dismutase by peroxynitrite is caused by exclusive nitration of tyrosine 34 to 3-nitrotyrosine. *J Biol Chem*, 1998. **273**(23): p. 14085-9.

118. Viner, R.I., D.A. Ferrington, T.D. Williams, D.J. Bigelow, and C. Schoneich, Protein modification during biological aging: selective tyrosine nitration of the SERCA2a isoform of the sarcoplasmic reticulum Ca2+-ATPase in skeletal muscle. *Biochem J*, 1999. **340 (Pt 3)**: p. 657-69.

119. Sharov, V.S., N.A. Galeva, T.V. Knyushko, D.J. Bigelow, T.D. Williams, and C. Schoneich, Two-dimensional separation of the membrane protein sarcoplasmic reticulum Ca-ATPase for high-performance liquid chromatography-tandem mass spectrometry analysis of posttranslational protein modifications. *Anal Biochem*, 2002. **308**(2): p. 328-35.

120. Kuhn, D.M., M. Sadidi, X. Liu, C. Kreipke, T. Geddes, C. Borges, and J.T. Watson, Peroxynitrite-induced nitration of tyrosine hydroxylase: identification of tyrosines 423, 428, and 432 as sites of modification by matrix-assisted laser desorption ionization time-of-flight mass spectrometry and tyrosine-scanning mutagenesis. *J Biol Chem*, 2002. **277**(16): p. 14336-42.

121. MacMillan-Crow, L.A., J.P. Crow, J.D. Kerby, J.S. Beckman, and J.A. Thompson, Nitration and inactivation of manganese superoxide dismutase in chronic rejection of human renal allografts. *Proc Natl Acad Sci U S A*, 1996. **93**(21): p. 11853-8.

122. Suckau, D., J. Kohl, G. Karwath, K. Schneider, M. Casaretto, D. Bitter-Suermann, and M. Przybylski, Molecular epitope identification by limited proteolysis of an immobilized antigen-antibody complex and mass spectrometric peptide mapping. *Proc Natl Acad Sci U S A*, 1990. **87**(24): p. 9848-52.

123. McLaurin, J., R. Cecal, M.E. Kierstead, X. Tian, A.L. Phinney, M. Manea, J.E. French, M.H. Lambermon, A.A. Darabie, M.E. Brown, C. Janus, M.A. Chishti, P. Horne, D. Westaway, P.E. Fraser, H.T. Mount, M. Przybylski, and P. St George-Hyslop, Therapeutically effective antibodies against amyloid-beta peptide target amyloid-beta residues 4-10 and inhibit cytotoxicity and fibrillogenesis. *Nat Med*, 2002. **8**(11): p. 1263-9.

124. Macht, M., A. Marquardt, S.O. Deininger, E. Damoc, M. Kohlmann, and M. Przybylski, "Affinity-proteomics": direct protein identification from biological material using mass spectrometric epitope mapping. *Anal Bioanal Chem*, 2004. **378**(4): p. 1102-11.

125. Stefanescu, R., R.E. Iacob, E.N. Damoc, A. Marquardt, E. Amstalden, M. Manea, I. Perdivara, M. Maftei, G. Paraschiv, and M. Przybylski, Mass spectrometric approaches for elucidation of antigenantibody recognition structures in molecular immunology. *Eur J Mass Spectrom (Chichester, Eng)*, 2007. **13**(1): p. 69-75.

126. Macht, M., W. Fiedler, K. Kurzinger, and M. Przybylski, Mass spectrometric mapping of protein epitope structures of myocardial infarct markers myoglobin and troponin T. *Biochemistry*, 1996. **35**(49): p. 15633-9.

127. Papac, D.I., J. Hoyes, and K.B. Tomer, Epitope mapping of the gastrin-releasing peptide/anti-bombesin monoclonal antibody complex by proteolysis followed by matrix-assisted laser desorption ionization mass spectrometry. *Protein Sci*, 1994. **3**(9): p. 1485-92.

128. Fiedler, W., C. Borchers, M. Macht, S.O. Deininger, and M. Przybylski, Molecular characterization of a conformational epitope of hen egg white lysozyme by differential chemical modification of immune complexes and mass spectrometric peptide mapping. *Bioconjug Chem*, 1998. **9**(2): p. 236-41.

129. Jeyarajah, S., C.E. Parker, M.T. Summer, and K.B. Tomer, Matrix-assisted laser desorption ionization/mass spectrometry mapping of human immunodeficiency virus-gp120 epitopes recognized by a limited polyclonal antibody. *J Am Soc Mass Spectrom*, 1998. **9**(2): p. 157-65.

130. Hochleitner, E.O., M.K. Gorny, S. Zolla-Pazner, and K.B. Tomer, Mass spectrometric characterization of a discontinuous epitope of the HIV envelope protein HIV-gp120 recognized by the human monoclonal antibody 1331A. *J Immunol*, 2000. **164**(8): p. 4156-61.

131. Yu, L., S.J. Gaskell., and J.L. Brookman., *Epitope mapping of monoclonal antibodies by mass spectrometry: identification of protein antigens in complex biological systems*, in *J Am Soc Mass Spectrom*. 1998. p. 208-15.

132. Ulrich. M, Petre. A, Youhnovski.N, Prömm. F, Schirle. M, Schumm. M, Pero. R, Doyle. A, Checkel. J, Kita. H, Acharya. R, Simon. H, Schwarz. H, Przybylskiand. M, and Döring. G, *Post-translational tyrosine nitration of eosinophil granule toxins mediated by eosinophil peroxidase*, in *JBC in press*. 2008.

133. Parker, C.E., L.J. Deterding, C. Hager-Braun, J.M. Binley, N. Schulke, H. Katinger, J.P. Moore, and K.B. Tomer., *Fine definition of the epitope on the gp41 glycoprotein of human immunodeficiency virus type 1 for the neutralizing monoclonal antibody 2F5*, in *J Virol.* 2001. p. 10906-11.

134. Daiber, A., S. Herold, C. Schoneich, D. Namgaladze, J.A. Peterson, and V. Ullrich, Nitration and inactivation of cytochrome P450BM-3 by peroxynitrite. Stopped-flow measurements prove ferryl intermediates. *Eur J Biochem*, 2000. **267**(23): p. 6729-39.

135. Zou, M., C. Martin, and V. Ullrich, Tyrosine nitration as a mechanism of selective inactivation of prostacyclin synthase by peroxynitrite. *Biol Chem*, 1997. **378**(7): p. 707-13.

136. Huie, R.E. and S. Padmaja, The reaction of no with superoxide. *Free Radic Res Commun*, 1993. **18**(4): p. 195-9.

137. Zou, M.H. and V. Ullrich, Peroxynitrite formed by simultaneous generation of nitric oxide and superoxide selectively inhibits bovine aortic prostacyclin synthase. *FEBS Lett*, 1996. **382**(1-2): p. 101-4.

138. Chiang, C.W., H.C. Yeh, L.H. Wang, and N.L. Chan, Crystal structure of the human prostacyclin synthase. *J Mol Biol*, 2006. **364**(3): p. 266-74.

139. Deng, H., A. Huang, S.P. So, Y.Z. Lin, and K.H. Ruan, Substrate access channel topology in membrane-bound prostacyclin synthase. *Biochem J*, 2002. **362**(Pt 3): p. 545-51.

140. Mehl, M., A. Daiber, S. Herold, H. Shoun, and V. Ullrich, Peroxynitrite reaction with heme proteins. *Nitric Oxide*, 1999. **3**(2): p. 142-52.

141. Deeb, R.S., G. Hao, S.S. Gross, M. Laine, J.H. Qiu, B. Resnick, E.J. Barbar, D.P. Hajjar, and R.K. Upmacis, Heme catalyzes tyrosine 385 nitration and inactivation of prostaglandin H2 synthase-1 by peroxynitrite. *J Lipid Res*, 2006. **47**(5): p. 898-911.

142. Spisni, E., C. Griffoni, S. Santi, M. Riccio, R. Marulli, G. Bartolini, M. Toni, V. Ullrich, and V. Tomasi, Colocalization prostacyclin (PGI2) synthase--caveolin-1 in endothelial cells and new roles for PGI2 in angiogenesis. *Exp Cell Res*, 2001. **266**(1): p. 31-43.

143. Zou, M., A. Yesilkaya, and V. Ullrich, Peroxynitrite inactivates prostacyclin synthase by heme-thiolate-catalyzed tyrosine nitration. *Drug Metab Rev*, 1999. **31**(2): p. 343-9.

144. Padmaja, S. and R.E. Huie, The reaction of nitric oxide with organic peroxyl radicals.

Biochem Biophys Res Commun, 1993. **195**(2): p. 539-44.

145. Katusic, Z.S., Superoxide anion and endothelial regulation of arterial tone. *Free Radic Biol Med*, 1996. **20**(3): p. 443-8.

146. Daiber, A., C. Schoneich, P. Schmidt, C. Jung, and V. Ullrich, Autocatalytic nitration of P450CAM by peroxynitrite. *J Inorg Biochem*, 2000. **81**(3): p. 213-20.

147. Petre, B.A., N. Youhnovski, J. Lukkari, R. Weber, and M. Przybylski, Structural characterisation of tyrosine-nitrated peptides by ultraviolet and infrared matrix-assisted laser desorption/ionisation Fourier transform ion cyclotron resonance mass spectrometry. *Eur J Mass Spectrom (Chichester, Eng)*, 2005. **11**(5): p. 513-8.

148. Duguet, A., H. Iijima, S.Y. Eum, Q. Hamid, and D.H. Eidelman, Eosinophil peroxidase mediates protein nitration in allergic airway inflammation in mice. *Am J Respir Crit Care Med*, 2001. **164**(7): p. 1119-26.

149. Rothenberg, M.E. and S.P. Hogan, The eosinophil. *Annu Rev Immunol*, 2006. **24**: p. 147-74.

150. Gleich, G.J., E.A. Ottesen, K.M. Leiferman, and S.J. Ackerman, Eosinophils and human disease. *Int Arch Allergy Appl Immunol*, 1989. **88**(1-2): p. 59-62.

151. Slungaard, A., G.M. Vercellotti, G. Walker, R.D. Nelson, and H.S. Jacob, Tumor necrosis factor alpha/cachectin stimulates eosinophil oxidant production and toxicity towards human endothelium. *J Exp Med*, 1990. **171**(6): p. 2025-41.

152. Eiserich, J.P., M. Hristova, C.E. Cross, A.D. Jones, B.A. Freeman, B. Halliwell, and A. van der Vliet, Formation of nitric oxide-derived inflammatory oxidants by myeloperoxidase in neutrophils. *Nature*, 1998. **391**(6665): p. 393-7.

153. Brennan, M.L., W. Wu, X. Fu, Z. Shen, W. Song, H. Frost, C. Vadseth, L. Narine, E. Lenkiewicz, M.T. Borchers, A.J. Lusis, J.J. Lee, N.A. Lee, H.M. Abu-Soud, H. Ischiropoulos, and S.L. Hazen, A tale of two controversies: defining both the role of peroxidases in nitrotyrosine formation in vivo using eosinophil peroxidase and myeloperoxidase-deficient mice, and the nature of peroxidase-generated reactive nitrogen species. *J Biol Chem*, 2002. **277**(20): p. 17415-27.

154. Sampson, J.B., Y. Ye, H. Rosen, and J.S. Beckman, Myeloperoxidase and horseradish peroxidase catalyze tyrosine nitration in proteins from nitrite and hydrogen peroxide. *Arch Biochem Biophys*, 1998. **356**(2): p. 207-13.

155. Wu, W., Y. Chen, and S.L. Hazen, Eosinophil peroxidase nitrates protein tyrosyl residues. Implications for oxidative damage by nitrating intermediates in eosinophilic inflammatory disorders. *J Biol Chem*, 1999. **274**(36): p. 25933-44.

156. Burner, U., P.G. Furtmuller, A.J. Kettle, W.H. Koppenol, and C. Obinger, Mechanism of reaction of myeloperoxidase with nitrite. *J Biol Chem*, 2000. **275**(27): p. 20597-601.

157. Monzani, E., R. Roncone, M. Galliano, W.H. Koppenol, and L. Casella, Mechanistic insight into the peroxidase catalyzed nitration of tyrosine derivatives by nitrite and hydrogen peroxide. *Eur J Biochem*, 2004. **271**(5): p. 895-906.

158. Olsen, R.L., K. Syse, C. Little, and T.B. Christensen, Further characterization of human eosinophil peroxidase. *Biochem J*, 1985. **229**(3): p. 779-84.

159. Ten, R.M., L.R. Pease, D.J. McKean, M.P. Bell, and G.J. Gleich, Molecular cloning of the human eosinophil peroxidase. Evidence for the existence of a peroxidase multigene family. *J Exp Med*, 1989. **169**(5): p. 1757-69.

160. Thomsen, A.R., L. Sottrup-Jensen, G.J. Gleich, and C. Oxvig, The status of half-cystine residues and locations of N-glycosylated asparagine residues in human eosinophil peroxidase. *Arch Biochem Biophys*, 2000. **379**(1): p. 147-52.

161. Munoz, N.M. and A.R. Leff, Highly purified selective isolation of eosinophils from human peripheral blood by negative immunomagnetic selection. *Nat Protoc*, 2006. **1**(6): p. 2613-20.

162. Abu-Ghazaleh, R.I., S.L. Dunnette, D.A. Loegering, J.L. Checkel, H. Kita, L.L. Thomas, and G.J. Gleich, Eosinophil granule proteins in peripheral blood granulocytes. *J Leukoc Biol*, 1992. **52**(6): p. 611-8.

163. Shevchenko, A., O.N. Jensen, A.V. Podtelejnikov, F. Sagliocco, M. Wilm, O. Vorm, P. Mortensen, H. Boucherie, and M. Mann, Linking genome and proteome by mass spectrometry: large-scale identification of yeast proteins from two dimensional gels. *Proc Natl Acad Sci U S A*, 1996. **93**(25): p. 14440-5.

164. PERE_HUMAN and (P11678). http://www.expasy.org.

165. Potter, S.M., W.J. Henzel, and D.W. Aswad, In vitro aging of calmodulin generates isoaspartate at multiple Asn-Gly and Asp-Gly sites in calcium-binding domains II, III, and IV. *Protein Sci*, 1993. **2**(10): p. 1648-63.

166. Orpiszewski, J., N. Schormann, B. Kluve-Beckerman, J.J. Liepnieks, and M.D. Benson, Protein aging hypothesis of Alzheimer disease. *Faseb J*, 2000. **14**(9): p. 1255-63.

167. Aylin, F., S. Konuklar, and V. Aviyente, Modelling the hydrolysis of succinimide: formation of aspartate and reversible isomerization of aspartic acid via succinimide. *Org Biomol Chem*, 2003. **1**(13): p. 2290-7.

168. Laurer, J.I., C.G. Fields, and G.B. Fields, *Sequence dependence of aspartimide formation during 9-fluorenylmethoxycarbonyl solid-phase peptide synthesis*, in *letters in Peptide Science*. 1994. p. 197-205.

169. http://www.abrf.org/index.cfm/dm.home?AvgMass=all.

170. Urbanavicius, A., *Free Radical Damages In Proteins -internet*.

171. Ayala, A. and R.G. Cutler, The utilization of 5-hydroxyl-2-amino valeric acid as a specific marker of oxidized arginine and proline residues in proteins. *Free Radic Biol Med*, 1996. **21**(1): p. 65-80.

172. Turell, L., H. Botti, S. Carballal, G. Ferrer-Sueta, J.M. Souza, R. Duran, B.A. Freeman, R. Radi, and B. Alvarez, Reactivity of sulfenic acid in human serum albumin. *Biochemistry*, 2008. **47**(1): p. 358-67.

173. Michalek, R.D., K.J. Nelson, B.C. Holbrook, J.S. Yi, D. Stridiron, L.W. Daniel, J.S. Fetrow, S.B. King, L.B. Poole, and J.M. Grayson, The requirement of reversible cysteine sulfenic acid formation for T cell activation and function. *J Immunol*, 2007. **179**(10): p. 6456-67.

174. Ishii, T., O. Sunami, H. Nakajima, H. Nishio, T. Takeuchi, and F. Hata, Critical role of sulfenic acid formation of thiols in the inactivation of glyceraldehyde-3-phosphate dehydrogenase by nitric oxide. *Biochem Pharmacol*, 1999. **58**(1): p. 133-43.

175. van Spronsen, F.J., D.J. Reijngoud, G.P. Smit, G.T. Nagel, F. Stellaard, R. Berger, and H.S. Heymans, Phenylketonuria. The in vivo hydroxylation rate of phenylalanine into tyrosine is decreased. *J Clin Invest*, 1998. **101**(12): p. 2875-80.

176. Nair, U.J., J. Nair, M.D. Friesen, H. Bartsch, and H. Ohshima, Ortho- and meta-tyrosine formation from phenylalanine in human saliva as a marker of hydroxyl radical generation during betel quid chewing. *Carcinogenesis*, 1995. **16**(5): p. 1195-8.

177. Hasslacher, C., H.G. Kopischke, E. Burklin, F. Gechter, and R. Reichenbacher, In vivo studies on basement membrane synthesis in diabetic and nondiabetic rats. *Res Exp Med (Berl)*, 1982. **181**(3): p. 245-51.

178. Sogut, S., H. Ozyurt, F. Armutcu, L. Kart, M. Iraz, O. Akyol, S. Ozen, S. Kaplan, I. Temel, and Z. Yildirim, Erdosteine prevents bleomycin-induced pulmonary fibrosis in rats. *Eur J Pharmacol*, 2004. **494**(2-3): p. 213-20.

179. Biggio, G., G.U. Corsini, F. Fadda, G. Ligouri, and G.L. Gessa, [Role of tryptophan in the physiological regulation of brain serotonin synthesis (author's transl)]. *S Ta Nu*, 1975. **5**(4): p. 219-22.

180. Rafii, M., J.M. McKenzie, S.A. Roberts, G. Steiner, R.O. Ball, and P.B. Pencharz, In vivo regulation of phenylalanine hydroxylation to tyrosine, studied using enrichment in apoB-100. *Am J Physiol Endocrinol Metab*, 2008. **294**(2): p. E475-9.

181. Zhu, G., M. Okada, S. Yoshida, S. Hirose, and S. Kaneko, Both 3,4-dihydroxyphenylalanine and dopamine releases are regulated by Ca2+-induced Ca2+ releasing system in rat striatum. *Neurosci Lett*, 2004. **362**(3): p. 244-8.

182. Morin, B., M.J. Davies, and R.T. Dean, The protein oxidation product 3,4-dihydroxyphenylalanine (DOPA) mediates oxidative DNA damage. *Biochem J*, 1998. **330 (Pt 3)**: p. 1059-67.

183. Hager, J.W., *A new linear ion trap mass spectrometer*, in *Rapid Commun. Mass Spectrom.* 2002. p. 512-26.

184. Ong, S.E. and M. Mann, Mass spectrometry-based proteomics turns quantitative. *Nat Chem Biol*, 2005. **1**(5): p. 252-62.

185. Fiedler, T.J., C.A. Davey, and R.E. Fenna, X-ray crystal structure and characterization of halide-binding sites of human myeloperoxidase at 1.8 A resolution. *J Biol Chem*, 2000. **275**(16): p. 11964-71.

186. McGaughey, G.B., M. Gagne, and A.K. Rappe, pi-Stacking interactions. Alive and well in proteins. *J Biol Chem*, 1998. **273**(25): p. 15458-63.

187. Buck, M., Trifluoroethanol and colleagues: cosolvents come of age. Recent studies with peptides and proteins. *Q Rev Biophys*, 1998. **31**(3): p. 297-355.

188. Nelson, J.W. and N.R. Kallenbach, Stabilization of the ribonuclease S-peptide alpha-helix by trifluoroethanol. *Proteins*, 1986. **1**(3): p. 211-7.

189. Gleich, G.J., C.R. Adolphson, and K.M. Leiferman, The biology of the eosinophilic

leukocyte. *Annu Rev Med*, 1993. **44**: p. 85-101.

190. Barker, R.L., D.A. Loegering, R.M. Ten, K.J. Hamann, L.R. Pease, and G.J. Gleich, Eosinophil cationic protein cDNA. Comparison with other toxic cationic proteins and ribonucleases. *J Immunol*, 1989. **143**(3): p. 952-5.

191. Rosenberg, H.F., S.J. Ackerman, and D.G. Tenen, Human eosinophil cationic protein. Molecular cloning of a cytotoxin and helminthotoxin with ribonuclease activity. *J Exp Med*, 1989. **170**(1): p. 163-76.

192. Rosenberg, H.F., D.G. Tenen, and S.J. Ackerman, Molecular cloning of the human eosinophil-derived neurotoxin: a member of the ribonuclease gene family. *Proc Natl Acad Sci U S A*, 1989. **86**(12): p. 4460-4.

193. Gleich, G.J., D.A. Loegering, M.P. Bell, J.L. Checkel, S.J. Ackerman, and D.J. McKean, Biochemical and functional similarities between human eosinophil-derived neurotoxin and eosinophil cationic protein: homology with ribonuclease. *Proc Natl Acad Sci U S A*, 1986. **83**(10): p. 3146-50.

194. Rosenberg, H.F., The eosinophil ribonucleases. *Cell Mol Life Sci*, 1998. **54**(8): p. 795-803.

195. Young, J.D., C.G. Peterson, P. Venge, and Z.A. Cohn, Mechanism of membrane damage mediated by human eosinophil cationic protein. *Nature*, 1986. **321**(6070): p. 613-6.

196. Zapalka, M., F. Kopriva, and J. Szotkowska, Monitoring of serum eosinophil cationic protein (ECP) level and its clinical value in paediatric practice. *Acta Univ Palacki Olomuc Fac Med*, 1998. **141**: p. 21-3.

197. Keller, B.O. and L. Li, Discerning matrix-cluster peaks in matrix-assisted laser desorption/ionization time-of-flight mass spectra of dilute peptide mixtures. *J Am Soc Mass Spectrom*, 2000. **11**(1): p. 88-93.

198. Little, D.P., J.P. Speir, M.W. Senko, P.B. O'Connor, and F.W. McLafferty, Infrared multiphoton dissociation of large multiply charged ions for biomolecule sequencing. *Anal Chem*, 1994. **66**(18): p. 2809-15.

199. Mohan, C.G., E. Boix, H.R. Evans, Z. Nikolovski, M.V. Nogues, C.M. Cuchillo, and K.R. Acharya, The crystal structure of eosinophil cationic protein in complex with 2',5'-ADP at 2.0 A resolution reveals the details of the ribonucleolytic active site. *Biochemistry*, 2002. **41**(40): p. 12100-6.

200. Fields, G.B. and R.L. Noble, Solid phase peptide synthesis utilizing 9-fluorenylmethoxycarbonyl amino acids. *Int J Pept Protein Res*, 1990. **35**(3): p. 161-214.

201. Carpino, L.A. and G.Y. Han, *J. Am. Chem. Soc.*, 1970(92): p. 5748.

202. Bai, Y., D. Galetskiy, E. Damoc, C. Paschen, Z. Liu, M. Griese, S. Liu, and M. Przybylski, High resolution mass spectrometric alveolar proteomics: identification of surfactant protein SP-A and SP-D modifications in proteinosis and cystic fibrosis patients. *Proteomics*, 2004. **4**(8): p. 2300-9.

203. Damoc, E., N. Youhnovski, D. Crettaz, J.D. Tissot, and M. Przybylski, High resolution proteome analysis of cryoglobulins using Fourier transform-ion cyclotron resonance

mass spectrometry. *Proteomics*, 2003. **3**(8): p. 1425-33.

204. Fligge, T.A., K. Bruns, and M. Przybylski, Analytical development of electrospray and nanoelectrospray mass spectrometry in combination with liquid chromatography for the characterization of proteins. *J Chromatogr B Biomed Sci Appl*, 1998. **706**(1): p. 91-100.

205. Schmidt, P., N. Youhnovski, A. Daiber, A. Balan, M. Arsic, M. Bachschmid, M. Przybylski, and V. Ullrich, Specific nitration at tyrosine 430 revealed by high resolution mass spectrometry as basis for redox regulation of bovine prostacyclin synthase. *J Biol Chem*, 2003. **278**(15): p. 12813-9.

206. Yang, Y.S., A.D. Marshall, P. McPhie, W.X. Guo, X. Xie, X. Chen, and W.B. Jakoby, Two phenol sulfotransferase species from one cDNA: nature of the differences. *Protein Expr Purif*, 1996. **8**(4): p. 423-9.

207. Berkenkamp, S., M. Karas, and F. Hillenkamp, Ice as a matrix for IR-matrix-assisted laser desorption/ionization: mass spectra from a protein single crystal. *Proc Natl Acad Sci U S A*, 1996. **93**(14): p. 7003-7.

208. Nordhoff, E., A. Ingendoh, R. Cramer, A. Overberg, B. Stahl, M. Karas, F. Hillenkamp, and P.F. Crain, Matrix-assisted laser desorption/ionization mass spectrometry of nucleic acids with wavelengths in the ultraviolet and infrared. *Rapid Commun Mass Spectrom*, 1992. **6**(12): p. 771-6.

209. Harris, L.J., S.B. Larson, K.W. Hasel, and A. McPherson, Refined structure of an intact IgG2a monoclonal antibody. *Biochemistry*, 1997. **36**(7): p. 1581-97.

210. MacCallum, R.M., A.C. Martin, and J.M. Thornton, Antibody-antigen interactions: contact analysis and binding site topography. *J Mol Biol*, 1996. **262**(5): p. 732-45.

211. Sundberg, E.J. and R.A. Mariuzza, Molecular recognition in antibody-antigen complexes. *Adv Protein Chem*, 2002. **61**: p. 119-60.

212. Braden, B.C. and R.J. Poljak, Structural features of the reactions between antibodies and protein antigens. *Faseb J*, 1995. **9**(1): p. 9-16.

213. Davies, D.R., E.A. Padlan, and S. Sheriff, Antibody-antigen complexes. *Annu Rev Biochem*, 1990. **59**: p. 439-73.

214. Khan, J., D.M. Brennand, N. Bradley, B. Gao, R. Bruckdorfer, and M. Jacobs, 3-Nitrotyrosine in the proteins of human plasma determined by an ELISA method. *Biochem J*, 1998. **330 (Pt 2)**: p. 795-801.

215. www.nuncbrand.com.

216. Dragusanu, M., B.A. Petre, and M. Przybylski, *Epitope- motif structure of an anti-nitrotyrosyl-antibody in 3-nitrotyrosine-peptides elucidated by proteolytic excision-mass spectrometry and immnoanalytical methods*, in *J.Pep. Chem -submitted*. 2008.

217. Siegle, I., R. Nusing, R. Brugger, R. Sprenger, R. Zecher, and V. Ullrich, Characterization of monoclonal antibodies generated against bovine and porcine prostacyclin synthase and quantitation of bovine prostacyclin synthase. *FEBS Lett*, 1994. **347**(2-3): p. 221-5.

218. Ullrich, V., M.H. Zou, and M. Bachschmid, New physiological and pathophysiological

aspects on the thromboxane A(2)-prostacyclin regulatory system. *Biochim Biophys Acta*, 2001. **1532**(1-2): p. 1-14.

219. Kissner, R., T. Nauser, P. Bugnon, P.G. Lye, and W.H. Koppenol, Formation and properties of peroxynitrite as studied by laser flash photolysis, high-pressure stopped-flow technique, and pulse radiolysis. *Chem Res Toxicol*, 1997. **10**(11): p. 1285-92.

220. Laemmli, U.K., Cleavage of structural proteins during the assembly of the head of bacteriophage T4. *Nature*, 1970. **227**(5259): p. 680-5.

221. http://www.fermentas.com/catalog/electrophoresis.

222. Neuhoff, V., N. Arold, D. Taube, and W. Ehrhardt, Improved staining of proteins in polyacrylamide gels including isoelectric focusing gels with clear background at nanogram sensitivity using Coomassie Brilliant Blue G-250 and R-250. *Electrophoresis*, 1988. **9**: p. 255-262.

223. Olsen, J.V., S.E. Ong, and M. Mann, Trypsin cleaves exclusively C-terminal to arginine and lysine residues. *Mol Cell Proteomics*, 2004. **3**(6): p. 608-14.

224. ZipTip pipete tips. *http://www.millipore.com/catalogue.nsf/docs/C5737*.

225. Towbin, H., T. Staehelin, and J. Gordon, Electrophoretic transfer of proteins from polyacrylamide gels to nitrocellulose sheets: procedure and some applications. *Proc Natl Acad Sci U S A*, 1979. **76**(9): p. 4350-4.

226. Roepstorff, P. and J. Fohlman, Proposal for a common nomenclature for sequence ions in mass spectra of peptides. *Biomed Mass Spectrom*, 1984. **11**(11): p. 601.

227. Whitehouse, C.M., R.N. Dreyer, M. Yamashita, and J.B. Fenn, Electrospray interface for liquid chromatographs and mass spectrometers. *Anal Chem*, 1985. **57**(3): p. 675-9.

7 APPENDIX

7.1 Appendix 1

Abbreviation

ACN	Acetonitrile
Ab	Antibodies
Aß	ß-amyloid peptide
amu	atomic mass units
APS	Ammoniumperoxodisulfat
Calc.	Calculated
CD	Circular dichroism
CDR	Complementary determining region
CID	Collision induced dissociation
Da	Dalton
DHB	Dihydroxybenzoic acid
DMF	Dimethylformamide
DTT	1,4-DL Dithiothreitol
ECP	Eosinophil cationic protein
EDN	Eosinophil derived-neurotoxin
ELISA	Enzyme linked immunosorbent assay
EPO	Eosinophil peroxidase
E: S	Enzyme: Substrate-Ratios (w/w)
ESI-MS	Electrospray / Ionisations- Mass spectrometry
Exp.	Experimental
Fab	Antigen-binding fragment
FT ICR	Fourier transform ion cyclotron resonance
Fmoc	9-Fluorenylmethoxycarbonyl-Rest
HCCA	4-Hydroxy-α-cynamic acid
HPLC	High performance liquid chromatography
IAA	Iodoacetamide
IgG	γ-Immunglobulins
IR	Infrared

KLH	keyhole limpet hemocyanin
m Ab	monoclonal antibody
MALDI-MS	Matrix-assisted Laser desorptions-/Ionisations-Mass spectrometry
MBP	Major basic protein
min	minute
m/z	mass over charge ratio
NCBI	National center for biothechnology Information
NT	3-nitro-tyrosine
OD	Optical density
OPD	*o*-phenylenediamine dihydrochloride
PBS	phosphate buffered saline
PGI_2	Prostacycline synthase
pH	negative logarithmus of H_3O^+-iones concentration
ppm	parts per million
PyBOP	Benzotriazol-1-yloxy-tris-pyrrolidinophosphonium-PF_6^-Salt
RP	Reversed phase
PCS	prostacycline synthase
SDS-PAGE	Sodiumdodecylsulfat-Polyacrylamid-Gel electrophoresis
T	Tesla
TCA	Trichloroacetic acid
TEMED	N,N,N',N'-Tetramethylethylendiamine
TFA	Trifluoracetic acid
TIC	Total ion chromatogram
TOF	time of flight
Tris	Tris-(hydroxymetyl-) aminomethane
Tween	Polyoxyethylen Sorbitan Monolaurat
UV	Ultraviolet
V	Volt
XIC	eXtracted ion current
°C	Grad Celsius

7.2 Appendix 2

Amino acid	Chemical structure of oxidized products		
Cysteine	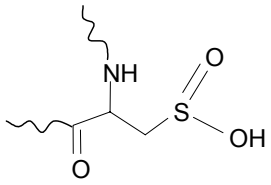	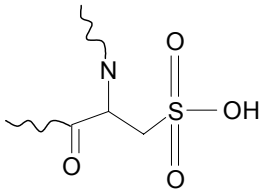	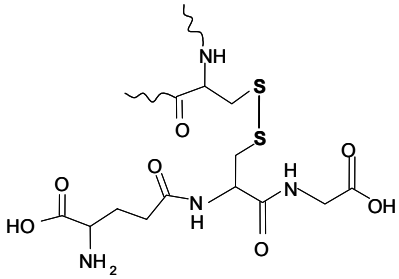
	protein-sulphinic acid	**protein-sulphonic acid**	**protein-Cys-S-S-glutathione**
Methionine / **Histidine**	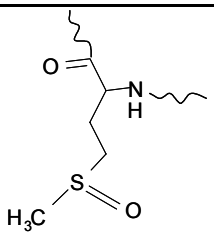	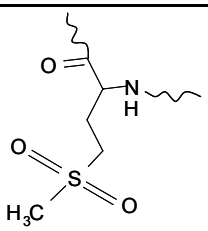	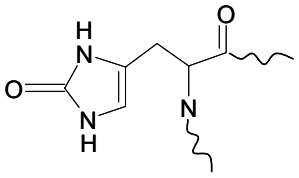
	methionine sulfoxide	**methionine sulfone**	**2-oxo-histidine**
Lysine / **Arginine**	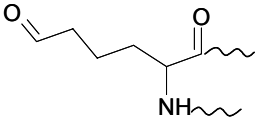	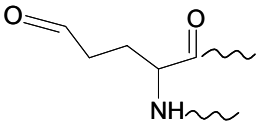	
	α-aminoadipic-δ-semialdehyde (allysine)	**glutamic semialdehyde from Arg**	
Proline	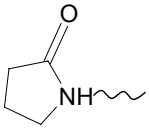	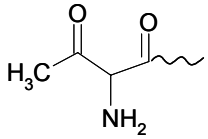	
Threonine	**2-pyrrolidone from Pro**	**2-amino-3-Ketobutyrate from Thr**	
Phenylalanine	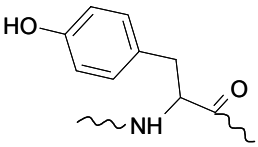	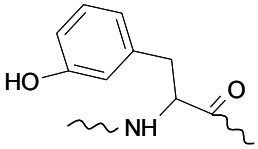	
	***ortho*-tyrosine**	***meta*-tyrosine**	
Tryptophan	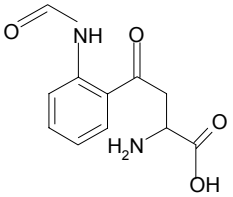	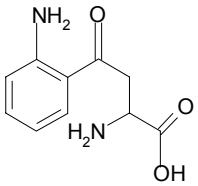	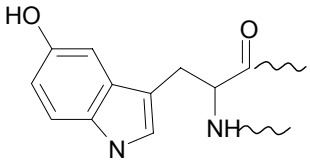
	***N*-formyl-kynurenine**	**kynurenine**	**5-hydroxytryptophan**
Tyrosine	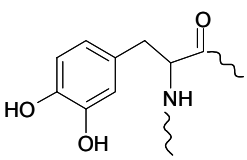	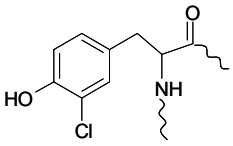	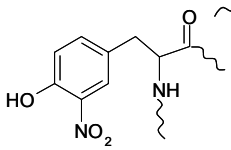
	3-hydroxy-tyrosine	**3-chloro-tyrosine**	**3-nitro-tyrosine**
			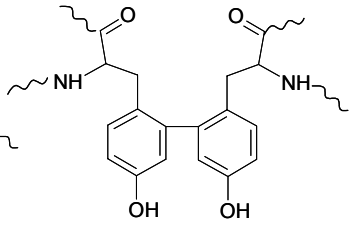
			di-tyrosine

7.3 Appendix 3

7.3.1 N-α-Fmoc amino acid derivatives

N-α-Fmoc-L-Alanine (*Fmoc-Ala-OH*)

N-α-Fmoc-N^G-2,2,4,6,7-pentamethyldihydrobenzofuran-5-sulfonyl-L-Ariginine (*Fmoc-Arg(Pbf)-OH*)

N-α-Fmoc-N-β-trityl-L-Asparagine (*Fmoc-Asn(Trt)-OH*)

N-α-Fmoc-L-Aspartic acid β-*t*-butyl ester (*Fmoc-Asp(OtBu)-OH*)

N-α-Fmoc-S-trityl-L-Cysteine (*Fmoc-Cys(Trt)-OH*)

N-α-Fmoc-N-γ-trityl-L-Glutamine (*Fmoc-Gln(Trt)-OH*)

N-α-Fmoc-L-Glutamic acid γ-*t*-butyl ester (*Fmoc-Glu(OtBu)-OH*)

N-α-Fmoc-L-Glycine (*Fmoc-Gly-OH*)

N-α-Fmoc-N-im-trityl-L-Histidine (*Fmoc-His(Trt)-OH*)

N-α-Fmoc-L-Isoleucine (*Fmoc-Ile-OH*)

N-α-Fmoc-L-Leucine (*Fmoc-Leu-OH*)

N-α-Fmoc-N-ε-*t*-Boc-L-Lysine (*Fmoc-Lys(Boc)-OH*)

N-α-Fmoc-L-Methionine (*Fmoc-Met-OH*)

N-α-Fmoc-L-Phenylalanine (*Fmoc-Phe-OH*)

N-α-Fmoc-L-Proline (*Fmoc-Pro-OH*)

N-α-Fmoc-O-*t*-butyl-L-Serine (*Fmoc-Ser(tBu)-OH*)

N-α-Fmoc-O-*t*-butyl-L-Threonine (*Fmoc-Thr(tBu)-OH*)

N-α-Fmoc-N-in-*t*-Boc-L-Tryptophan (*Fmoc-Trp(Boc)-OH*)

N-α-Fmoc-O-*t*-butyl-L-Tyrosine (*Fmoc-Tyr(tBu)-OH*)

N-α-Fmoc-L-Valine-OH (*Fmoc-Val-OH*)

7.3.2 Amino acids

Name	One letter code	Three letters code	Mass increment
Alanin	A	Ala	71.08
Arginin	R	Arg	156.19
Asparagin	N	Asn	114.10
Aspartic acid	D	Asp	115.09
Cystein	C	Cys	103.14
Glutamin	Q	Gln	128.13
Glutamic acid	E	Glu	129.12
Glycin	G	Gly	57.05
Histidin	H	His	137.14
Isoleucin	I	Ile	113.16
Leucin	L	Leu	113.16
Lysin	K	Lys	128.17
Methionin	M	Met	131.20
Phenylalanin	F	Phe	147.18
Prolin	P	Pro	97.12
Serin	S	Ser	87.08
Threonin	T	Thr	101.11
Tryptophan	W	Trp	186.21
Tyrosin	Y	Tyr	163.18
3-nitro-Tyrosine	Y-NO_2	Tyr-NO_2	208.19
Valin	V	Val	99.13

7.4 Appendix 4

Table 1: *Theoretical tryptic peptides fragments of Eosinophil-derived neurotoxin (Swiss Prot entry P12724) obtained using GPMAW program*

GPMAW 6.11 [Default] - [[1] Trypsin -> Eosinophil-derived neurotoxin (Swiss-Prot entry P10153)]

Mo. S ½ Alt i Low | Trypsin [/K/R-\P] - p2 | Sync. windows

Num	From-To	MH+	HPLC	pI	Sequence
6	69- 69	147.11	1,09	9,47	K
2	36- 36	175.12	1,41	10,76	R
10	118-118	175.12	1,41	10,76	R
12	133-134	245.19	13,83	6,97	II
5	67- 68	276.17	1,72	10,80	TR
3	37- 38	307.14	7,24	9,30	CK
17[1]	67- 69	404.26	1,86	11,51	TRK
9	115-117	418.20	3,06	7,04	DQR
14[1]	36- 38	463.24	8,11	9,80	RCK
21[1]	115-118	574.31	4,17	10,99	DQRR
11	119-132	1631.85	18,78	5,12	DPPCYPVVPVHLDR
22[1]	118-132	1787.96	18,92	7,49	RDPPCYPVVPVHLDR
23[1]	119-134	1858.02	23,17	5,12	DPPCYPVVPVHLDRII
33[2]	118-134	2014.12	23,19	7,49	RDPPCYPVVPVHLDRII
8	98-114	2033.92	22,08	6,07	YAQTPANMFYIVACDNR
32[2]	115-132	2187.14	19,43	7,81	DQRRDPPCYPVVPVHLDR
20[1]	98-117	2433.11	22,39	6,22	YAQTPANMFYIVACDNRDQR
31[2]	98-118	2589.21	22,50	8,63	YAQTPANMFYIVACDNRDQRR
4	39- 66	3155.47	22,10	8,14	NQNTFLLTTFANVVNVCGNPNMTCPSNK
7	70- 97	3228.48	25,86	7,94	NCHHSGSQVPLIHCNLTTPSPQNISNCR
18[1]	69- 97	3356.58	25,72	8,46	KNCHHSGSQVPLIHCNLTTPSPQNISNCR
16[1]	39- 68	3412.62	22,29	8,77	NQNTFLLTTFANVVNVCGNPNMTCPSNKTR
15[1]	37- 66	3443.60	23,90	8,58	CKNQNTFLLTTFANVVNVCGNPNMTCPSNK
27[2]	39- 69	3540.71	22,20	9,61	NQNTFLLTTFANVVNVCGNPNMTCPSNKTRK
25[2]	36- 66	3599.70	24,03	8,96	RCKNQNTFLLTTFANVVNVCGNPNMTCPSNK
28[2]	67- 97	3613.73	25,82	9,02	TRKNCHHSGSQVPLIHCNLTTPSPQNISNCR
26[2]	37- 68	3700.75	24,06	9,44	CKNQNTFLLTTFANVVNVCGNPNMTCPSNKTR
1	1- 35	4326.01	31,05	8,61	KPPQFTWAQWFETQHINMTSQQCTNAMQVINNYQR
13[1]	1- 36	4482.11	31,10	9,51	KPPQFTWAQWFETQHINMTSQQCTNAMQVINNYQRR
24[2]	1- 38	4770.23	32,37	9,48	KPPQFTWAQWFETQHINMTSQQCTNAMQVINNYQRRCK

Table 2: *Product ion (MS/MS) spectra details of the doubly charged precursor ions m/z 896.3*

Amino acid	**b - ion**	**$b_{calc.}$**	**$b_{exp.}$**	**Δm (Da)**	**y - ion**	**y_{calc}**	**$Y_{exp.}$**	**Δm (Da)**
^{419}Asp	b_1^+	116.03	-	-	y_{14}^{2+}	*	*	*
Phe	b_2^+	263.10	262.87	0.87	y_{13}^{2+}	838.94	838.81	0.16
Tyr	b_3^+	426.16	426.08	0.18	y_{12}^{2+}	765.40	765.26	0.18
Lys	b_4^+	554.26	554.15	0.19	y_{11}^{2+}	1366.74	-	-
Asp	b_5^+	669.28	669.17	0.16	y_{10}^+	1238.64	1238.44	0.16
Gly	b_6^+	726.31	-	-	y_9^+	1123.62	1123.41	0.18
Lys	b_7^+	854.40	854.23	0.2	y_8^+	1066.60	1066.37	0.21
Arg	b_8^+	1010.50	1010.31	0.19	y_7^+	938.50	938.32	0.19
Leu	b_9^+	1123.59	1123.41	0.16	y_6^+	782.40	782.18	0.28
Lys	b_{10}^+	1251.68	1251.44	0.19	y_5^+	669.20	669.17	0.04
	b_{10}^{2+}	626.34	626.26	0.13				
Asn	b_{11}^+	683.87	683.27	0.86	y_4^+	541.22	541.12	0.18
nitro-Tyr	b_{12}^{2+}	787.39	787.26	0.16	y_3^+	427.18	426.08	0.18
Ser	b_{13}^{2+}	830.90	830.73	0.2	y_2^+	219.13	219.01	0.5
^{432}Leu	b_{14}^{2+}	*	*	*	y_1^+	-	-	-

-ions not observed (b_1^+, b_6^+, b_{11}^+, y_1^+)

* ions may not be formed (b_{14}^+, y_{14}^+)